SEPTEMBER 2019 M.Sc. in Mechanical Engineering HAZIM ABDULRIDHA INTEEK AL SADOON

REPUBLIC OF TURKEY
GAZİANTEP UNIVERSITY
GRADUATE SCHOOL OF NATURAL & APPLIED SCIENCES

COMPARATIVE MERITS OF ACCELERATION AND ACOUSTIC EMISSION DATA IN THE PREVENTIVE MAINTENANCE OF ANTIFRICTION BEARINGS

M.Sc. THESIS
IN
MECHANICAL ENGINEERING

BY
HAZIM ABDULRIDHA INTEEK AL SADOON
SEPTEMBER 2019

COMPARATIVE MERITS OF ACCELERATION AND ACOUSTIC EMISSION DATA IN PREVENTIVE MAINTENANCE OF ANTIFRICTION BEARINGS

M.Sc. Thesis
in
Mechanical Engineering
Gaziantep University

Supervisor
Prof. Dr. Sedat BAYSEÇ

by
Hazim Abdulridha Inteek AL SADOON
September 2019

REPUBLIC OF TURKEY
GAZİANTEP UNIVERSITY
GRADUATE SCHOOL OF NATURAL & APPLIED SCIENCES
MECHANICAL ENGINEERING

Name of the Thesis: Comparative Merits of Acceleration and Acoustic Emission Data In Preventive Maintenance of Antifriction Bearings

Name of the Student: Hazim Abdulridha Inteek AL SADOON

Exam Date: 12.09.2019

Approval of the Graduate School of Natural and Applied Sciences

Prof. Dr. A. Necmeddin YAZICI
Director

I certify that this thesis satisfies all the requirements as a thesis for the degree of Master of Science.

Prof. Dr. Melda ÇARPINLIOĞLU
Head of Department

This is to certify that we have read this thesis and that in our consensus/majority opinion it is fully adequate, in scope and quality, as a thesis for the degree of Master of Science.

Prof. Dr. Sedat BAYSEÇ
Supervisor

Examining Committee Members:	Signature
Prof. Dr. Zafer Savaş DOĞANTAN	…..………………..
Prof. Dr. Sadettin KAPUCU	……...…………..
Prof. Dr. Sedat BAYSEÇ	……...…………..

I hereby declare that all information in this document has been obtained and presented in accordance with academic rules and ethical conduct. I also declare that, as required by these rules and conduct, I have fully cited and referenced all material and results that are not original to this work.

Hazim Abdulridha Inteek AL SADOON

ABSTRACT

COMPARATIVE MERITS OF ACCELERATION AND ACOUSTIC EMISSION DATA IN THE PREVENTIVE MAINTENANCE OF ANTIFRICTION BEARINGS

AL SADOON, Hazim Abdulridha Inteek
M.Sc. in Mechanical Engineering
Supervisor: Prof. Dr. Sedat BAYSEÇ
September 2019
137 pages

It is an ages long art that engineers and machine operators get clues from the sound produced by any machine on whether the machine is operating properly or not. Drivers listen to the sound of their engine and doctors listen to the heart beats and pulmonary sounds. In machinery, well being of anti-friction bearings is extremely important as a bearing breaking into pieces may generate irreparable damage. Although life time of antifriction bearings are estimable from the working conditions and statistical data, these are never accurate. Therefore it is very important to be able to detect a bearing moving towards a failure. Old bearings have greater clearance due to wear, yet, fatigue generates pittings of various sizes on the tracks where rolling elements move. These effects generate vibration and sound. Actually vibration and sound are almost synonymous in this respect, as sound is generated by the vibration of the machine. Sound and vibration recordings can be done by microphones and accelerometers, but the task of differentiation of the relevant data from the others is great. Some of the vibration certainly decays in the material of the machine components, whereas sound they produce may be beyond the threshold of the microphones. Both microphones and accelerometers add their own dynamic problems onto the recorded signal. This dissertation makes a survey on the use of acceleration and acoustic emission data in this respect. Then data taken from a test rig which contains a purposefully indented ball bearing under load and how they interpret the known fault is examined by using routines from Labview® Toolbox. Lastly, a comparison of the advantages and disadvantages of both are presented.

Key Words: Preventive Maintenance, Acoustic Emission, Vibration, Accelerometer, Antifriction Bearings

ÖZET

SÜRTÜNMESİZ YATAKLARIN ÖNLEYİCİ BAKIMINDA İVME VE AKUSTİK YAYINIM BİLGİLERİNİN KARŞILAŞTIRMALI ÜSTÜNLÜKLERİ

AL SADOON, Hazim Abdulridha Inteek
Yüksek Lisans Tezi, Makine Mühendisliği
Danışman: Prof. Dr. Sedat BAYSEÇ
Eylül 2019
137 sayfa

Mühendisler ve makine operatörlerinin herhangi bir makinenin sesini dinleyerek normal çalışıp çalışmadığı hakkında fikir edinmeleri çok eski bir gelenektir. Sürücüler motorlarının seslerini dinler, doktorlar kalp seslerini ve göğüsten gelen sesleri aynı sebeple dinler. Makinelerde sürtünmesiz yatakların iyi durumda olması bu yataklar dağıldığında çak daha önemli ve tamir Kabul etmeyecek arızalara sebep olabildiği için çok önemlidir. Sürtünmrsiz yatakların ömürleri hizmet şartları ve istatistik bilgiler kullanarak tahmin edilebilir ancak bu sonuçlar hiçbir şekilde kesin değildir. Bu sebeple bir sürtünmesiz yatağın tam olarak ne zaman değiştirilmesi gerektiğinin bilinmesi çok önemlidir. Yıpranmış yataklarda aşınmadan dolayı boşluklar fazladır. Bununla birlikte, malzeme yorulması yuvarlanma elemanlarının içinde çalıştığı oluklarda karıncalanmalar oluşturur. Bu etkenler fazladan ses ve titreşim oluştururlar. Ses titreşimden oluştuğu için gerçekte ses ve titreşim bilgileri birbiri ile eşdeğerdir. Ses ve titreşim ölçümleri mikrofon ve akselerometre ile yapılır, ancak arıza habercisi bilgilerin diğerlerinden ayırt edilmesi zor bir iştir. Meydana gelen titreşimlerin bazıları makinenin malzemesi içinde tabiiki sönümlenir. Ayrıca sönümlenmiş bir titreşimin ürettiği ses te mikrofonon duyu eşiğinin berisinde kalabilir. Mikrofon ve akselerometreler kendi dinamiklerini ölçtükleri sinyallere ekledikleri için ayrıca işi zorlaştırırlar. Bu çalışmada önleyici bakımda mikrofon ve akselerometre kullanımı üzerine bir araştırma yapılmıştır. Daha sonra özellikle üzerie bir delik delinerek bozulmuş ve yük altında çalışan bir bilyalı yatağın ses ve ivme ölçümleri alınarak bilinen hatayı nasıl ortaya koydukları araştırılmıştır. Sinyal analizinde Labview® Toolbox ta mevcut yazılımlar kullanılmıştır. Sonuç olarak hatalı veya arızalanmaya doğru ilerleyen bir sürtünmesiz yatağın belirlenmesinde ivme ve ses ölçümlerinin karşılaştırmalı avantaj ve dezavantajları verilmiştir.

Anahatr Kelimeler: Önleyici Bakım, Ses Yayınım Bilgisi, Titreşimler, Akselerometre, Sürtünmesiz Yataklar.

To my Parents and Family.

ACKNOWLEDGEMENTS

I am greatly indebted to my supervisor, Prof. Dr. Sedat Bayseç, for his continued support and encouragement throughout my graduate education. Without his continuous guidance, the completion of this thesis would not have been possible. I also want to thank Assoc. Prof. Necla Togun, for her continuous support and insightful comments since the very beginning of the research process. I wish to thank many people who helped me during this research process.

I would like to thank Dr. Alaa Abdulhady Jaber for his guidance. I very much appreciate many discussions I had with him on the research at hand.

I am aware of the help I have received from my dear friends, most of all. I am indebted to Dr.Hamed, Mr. Mohammed Al-Moula, Mr. Hassan Al-Moula, Mr. Osama. .

Finally, I would like to express my deepest gratitude to my family for all their love, support and encouragement throughout my life to this point. All of them stood by me to overcome the difficulties of life. I especially want to thank my dearest parents and my lovely wife for their encouragement and patience that have provided through inspiring me to be more than I am.

TABLE OF CONTENTS

Page

LIST OF TABLES

Page

LIST OF FIGURES

Page

LIST OF SYMBOLS

D_P	Pitch diameter
D_o	Outer diameter of bearing
D_i	Inner diameter of bearing
B	Bearing width
d	Ball diameter
f	Frequency of rotational speed
F_s	Sampling rate frequency
T	Total acquisition time
f_c	Frequency of cage
f_i	Frequency of inner race
f_o	Frequency of outer race
r_c	Radius of cage
r_i	Radius of inner race
r_o	Radius of outer race
θ	Contact angle of load in radial plane
ω_c	Angular velocity of a cage
ω_i	Angular velocity of an inner race
ω_o	Angular velocity of an outer race
v_c	Linear speed of cage
v_i	Linear speed of inner race
v_o	Linear speed of outer race
N_b	Number of balls
N	Number of samples
x_i	Amplitude of individual sample
μ	Mean value of samples
σ	Standard deviation
Δf	Frequency interval

LIST OF ABBREVIATIONS

AE	Acoustic Emission
BCM	Bearing Condition Monitoring
DAQ	Data Acquisition
BSF	Ball Span Frequency
BPFI	Ball Pass Frequency Of Bearing Inner Race
BPFO	Ball Pass Frequency Of Bearing Outer Race
FTF	Fundamental Train Frequency
NDT	Nondestructive Testing
PAC	Physical Acoustics Corporation
FFT	Fast Fourier Transform
RMS	Root Mean Square
P0	Load Level 0 Kg
P1	Load Level 5 Kg
P2	Load Level 10 Kg
DFT	Discrete Fourier Transform
MED	Minimum Entropy Deconvolution
ANN	Artificial Neural Network
SVM	Support Vector Machine
LLE	Largest Lyapunov Exponent
STFT	Sort-Time Frequency Domain
HFRT	High Frequency Resonance Technique

CHAPTER 1

INTRODUCTION

1.1 Introduction

1.1.1 Background to Condition Monitoring of Antifriction Bearings

A long time ago, rolling bearings have been a source of concern for technicians. Rolling bearings often cause rotary machines to breakdown or suddenly stopped, resulting in a loss of continuity of production and may result in high-risk operational accidents. It is often difficult to detect a deterioration in the condition of a bearing or wear of its parts in the early stages of its inception.

To prevent these faults and keep the bearings in good condition, there are several methods including non-destructive testing (NDT) that are part of preventive maintenance.

Indeed, these methods are used for the detection and diagnosis of bearings defects by using vibration, acoustic emission and external bearing temperature . Actually, many scientific publications have devoted to the detection and diagnosis of bearing defects. Most of these studies have focused on monitoring by using traditional vibration analysis methods. As a result of its effectiveness, this approach plays a very important role in the implementation of preventive maintenance. The most important features of this approach are that it allows to monitor the condition of rotating machines without having stopped. In this thesis, there are two methods of vibration analysis: time domain analysis and frequency domain analysis [1].

1.2 Condition Monitoring

Rolling element bearings are critical components in most machinery and failure in these parts may cause catastrophic incidents. Defects in rolling bearings can actually occur in the production process or due to fatigue, periodic loads, installation problems or due to improper lubrication .Therefore, bearing condition monitoring (BCM) techniques must be used to avoid any unexpected failure and breakdown [2].

BCM is a technique or method that offers a maintenance decision based on data collected during the operation. Several methods can be used to collect data such as: Acoustic emission (AE), vibration analysis, temperature measurement, and wear debris analysis, etc.

To effectively bearings condition monitoring, detect faults, diagnose accurately and reliably, more than one technique should be used to estimate the life of the bearings, rather than adopting one method. Such as statistical technique to be an indicator of predictive maintenance, It will be insufficient due to changing operating conditions, especially load and speed changes. These are resulting in misleading and unrealistic results, especially if the actual case of bearing is unknown. Therefore, because of the frequent use and more research in condition monitoring as a maintenance tool have led to the development of many techniques of faults detection and diagnosis, which will be discussed in this chapter. The most popular and used techniques are vibration and acoustic emission [3].

1.3 Bearing

A bearing is a power transmission element that constrains relative motion to the required movement and limits the friction between moving parts that result in loss of power whenever the components of the machine are turned on.

Or in other words, bearings are tribological components that carry the load when they are in contact with another part and are moving relative to it. The movement can be sliding or rotating. The main functions of bearings are:

1- Minimizes friction between Surfaces of rotary parts.

2- Support rotary parts of machines by supporting radial and axial load.

There are two main types of bearings according to the mechanism of friction between contact surfaces: plain bearings and roller bearings.

1.3.1 Plain Bearings

Indeed, a plain bearing is the simplest form of bearing, for surfaces rub against each other for this movement to be possible with minimal resistance. Friction between surfaces should be kept as little as possible by making the contact surfaces smooth enough and keeping the appropriate lubrication film between them continuously.

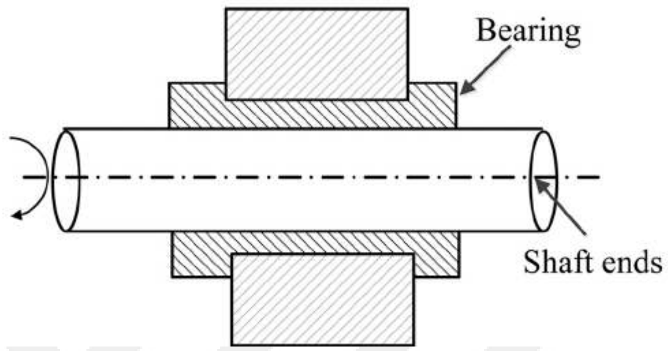

Figure 1.1 Example of a plain bearing [3].

The plain bearing material is generally softer than shaft or slider material. This allows the plain bearing to be as a victim instead of shaft or slider because of its design, relatively low cost and ease of replacing in a short time.

1.3.2 Rolling Element Bearings

Rolling element bearings or rolling bearings include all shapes of bearings that use rolling elements (balls, rollers or needles) to ensure minimal friction of constrained motion of one body relative to another. It supports the shafts (axially, radially or combination) and consists of bearing races or discs, cage and rolling elements, which can be spherical, cylindrical, tapered or barrel-shaped as shown in Figure 1.2, where these elements reduce the sliding friction of the contacting surfaces as less as possible because of its rolling. This type of bearings has been widely used as a power transmission element in rotating machines.

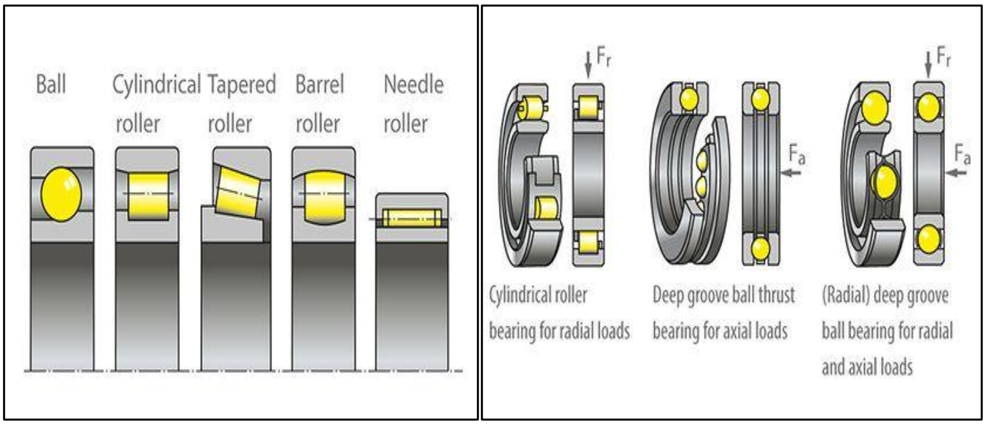

Figure 1.2 Examples of rolling element bearings [4].

Bearing selection is sometimes tricky as there are so many types of bearing are available in the markets like deep groove ball bearing, angular contact ball bearings, self - aligning ball bearings, spherical roller bearings, cylindrical roller bearings, taper roller bearings and thrust ball bearings, etc.

The selection of ball and roller bearings for a given installation depends upon load, load nature, rotational speed of shaft, expected life and nature of the environment where the bearing is working.

Based on the above factors, generally ball bearings are suitable for small machines running at high speeds, where the contact point between the ball and the outer race is very small due to the spherical shape of balls. This helps the ball to spin very smoothly.

Since the contact point is so small, the bearing can become overloaded at a specific point causing the ball bearing to become deformed. The rolling elements of the roller bearing are cylindrical, then point of contact between the roller and the race is a straight line rather than a point, so any type of rolling bearing is suitable for heavy-duty machines, where the load is distributed over a larger area and allows the bearing to withstand greater loads, as shown in Figure 1.3.

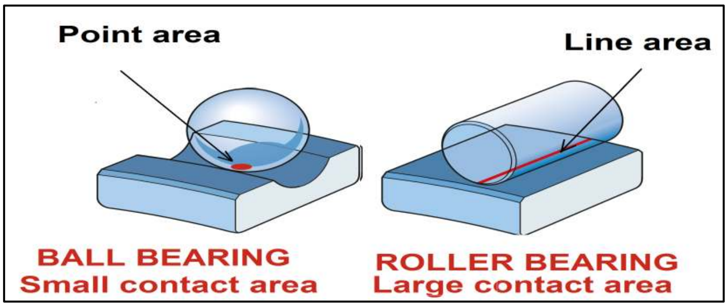

Figure 1.3 Examples of contact points [5].

1.4 Bearing Life

Rating life of a group of apparently identical ball or roller bearings is defined as the number of revolution's or hours of run at a given constant speed, that the 90% of a group of bearings will complete or exceed before a failure criteria develops in any of the bearing elements.

The term "life" can be given as the period of service for bearings, which ends with the phenomenon of fatigue. The fatigue occurs due to periodic stress, Which are generated by surfaces that are in continuous contact after a long time of running. Its beginning depends on the magnitude of the load during rotation. The fatigue begins as a crack and over time develops into a Flaking or Spalled area on the contact surfaces that carry the load [6].

1.5 Lubrication

One of the important considerations for smooth bearing operation is the lubrication. Lubricating oil is used to reduce friction between contact surfaces, where the sliding friction between the rolling bodies on the one hand and the raceways and cage on the other. When the bearing is in operation, the contact loads are high, but the bearing geometry is such that hydrodynamic lubrication can be reached during rotation, and a thin layer of lubricant can be maintained continuously [3].

1.6 Bearing Failures

The rolling bearing cannot work forever. It has a certain service life, where it is determined by the number of contact rolling cycles and the load applied during rotation on the raceways by rolling elements [7].

Studies show that ball rolling. For example, electrical motors as a case study, The distribution of faults show that 41 percent of the total number of faults refers to ball bearings, while 37 percent relates to stator faults, 10 percent to rotor faults and 12 percent to other malfunctions [8]. In addition, when analyzing the failure mode of wind generators, it was shown that in medium generators, 70 percent of failures are related to bearings, in large generators, 50 percent of errors related to bearings. Figure 1.4 illustrates the distribution of the faults for these examples [9].

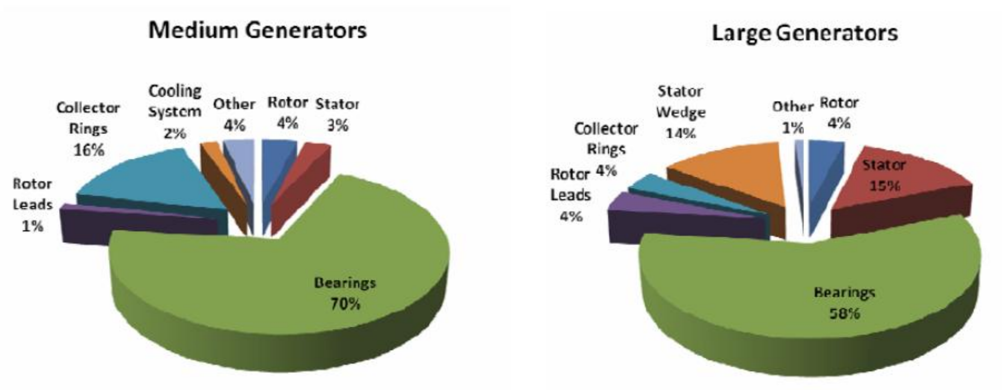

Figure 1.4 The faults distribution in the wind turbine generators [9].

1.7 Common Maintenance Management Strategies

The prime objective of a maintenance management strategy is to achieve the optimum balance between equipment performance, availability and cost of maintenance. Reducing the spend on maintenance can have serious consequences to production.

1.7.1 Breakdown Maintenance

Run-to-failure maintenance; assets are operated until they breakdown, at which point maintenance is performed. There is no maintenance performed before then. The simplest approach to maintenance, where the result of failure and the cost of machine parts is low. It is effective in this case.

1.7.2 Preventive (Scheduled) Maintenance (PM)

Preventive maintenance is the regular maintenance of machines to reduce the likelihood of their failure. This is done when machine is still working so that it does not break unexpectedly. This is scheduled for a time or depending on the triggers of the usage for machine. Thus reducing downtime and preventing delays in production and accidents compared to emergency shutdown maintenance, as well as reducing the cost of investments in technology compared to more complex systems [10].

1.7.3 Predictive Maintenance (PdM)

The predictive maintenance (PdM) is one of the modern maintenance management methods that have been applied in industrial countries in the late 1970s and early 1980s. It is a development in traditional maintenance methods. Predictive maintenance depends primarily on condition monitoring of machine and tracking the changes obtained to predict the possibility of malfunction. Know the type and the approximate date of its occurrence to save money, effort and time. This can be done by visual inspection, temperature, oil analysis of the equipment or any other condition-based monitoring (such as vibration or acoustic emission analysis) to evaluate asset performance in real-time [10].

There are many PdM technologies that can be implemented in the industry, including:

1. Vibration analysis: vibration analysis can detect imbalance, misalignment, belt failure, electrical problems and more. By measuring machine vibration.
2. Infrared thermography (IR): infrared thermal radiation is a method that detects infrared energy emitted by an object, transforms it and displays it as an image of the temperature distribution. Captures the temperature distribution on the surface and can be displayed as visual information. The temperature in real-time can be measured at a distance without contact with the object. Infrared thermal imaging is used for many mechanical or electrical equipment.
3. Ultrasound: an acoustical analysis at an ultrasonic level to identify problems that people usually do not hear. Such as gas, steam or air leakages.
4. Tribology: failure are detected by analyzing the foreign particles found in liquids that are considered an indicator of mechanical wear.
5. Motor circuit analysis (MCA): which can helps to prevent motor failures, and improve the energy efficiency of motor systems. Where measures motor condition by detecting electrical insulation and imbalances. It can be used to measure defects in rotors, cables or windings.

6. Laser alignment: assist in the alignment of rotating equipment, such as couplings, pulleys and belts. By using one of these technologies above, you can implement a PdM strategy while machines are running, which means virtually no downtime will occur. Figure 1.5 is the I-P-F Curve shows ultrasound and vibration as being the first technologies that detects a mechanical failure such as early-stage bearing wear, subsurface bearing fatigue [10].

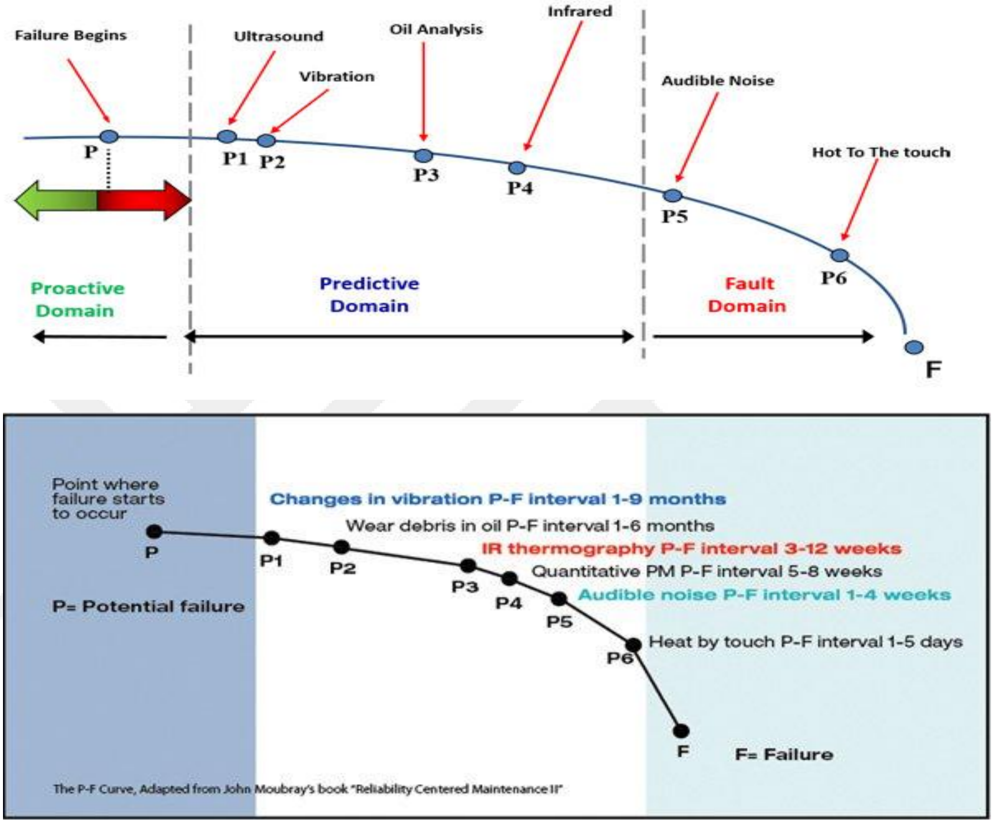

Figure 1.5 The I-P-F Curve showing ultrasound and vibration as an early indicators of a potential problem in bearings and rotating equipment [11].

CHAPTER 2

LITERATURE REVIEW

2.1 Introduction

Acoustic emission and vibration signal analysis are become common techniques for fault detection of rotating machinery, where they provide very important information about the abnormal formation of internal structures. An information that obtained through sound and vibration analysis enables us to plan the maintenance process. Studies have been previously conducted to use vibration and acoustic emissions for bearing condition monitoring. And there are many monitoring methods reported. A review of the performance and application of these methods is considered to be beneficial. Based on the analysis methods of the signal. Vibration and acoustic emission signals analysis can be performed in one of three fields: time domain, frequency domain and time-frequency domain.

2.2 Acoustic Emission Analysis Technology

Balerston [12] reported the first document on Acoustic Emission Technology (AET). Interestingly, this is probably one of the first applications related to condition monitoring.

Yoshioka and Fujiwara [13] studied the diagnosis of bearing faults by placing the sensor directly on the outer ring of the defective bearing and modulating the high-frequency burst of acoustic emission signal on the outer ring defect frequency.

Bangoli et al. [14] concluded that the sound intensity was low in the absence of defects in the rotating machine.

Rao and Ratnam [15] A comparison between vibration analysis and acoustic emission (AE) methods is described to predict the severity of defects in rolling bearings (as the size of the defect increases). The experimental investigation centered on seeded defect of same type with gradual increase of its size on the outer race of radially loaded cylindrical roller bearings and running the defective bearing at different speeds and loads. Data acquired through AE and vibration probes simultaneously for better diagnosis. Comparisons between AE and vibration over a range of speed and load conditions at gradual increase of defect size are presented, and from them, it is concluded that AE method is superior to identify the severity of defect.

Mba [16] study focused on applying standard acoustic emission (AE) parameters to a radially loaded bearing and establishing a suitable threshold for AE counting. The experimental setup was designed to allow for the presence of detectable defects on the inner and outer cage. It is concluded that, regardless of the rotational speed, radial load and the high background noise, simple AE parameters, such as RMS value and AE count, showed signs of a bearing defect.

2.3 Vibration Analysis Technology

The researchers used two methods to create local defects on the bearings to study the vibration response. The first is to run the bearing until a fault occurs and observe the change in the vibration response. The fault is usually accelerated by overload, over speed or by making the bearings unlubricated. Another method is to deliberately seed defects in the bearing, measure the vibration response, and compare it to a good quality bearing. The first method of life testing takes a long time. On the other hand, bearings with simulated defects are much faster to test, but special techniques are required to prepare defective bearings. A variety of techniques have been applied to measure and analyze the vibration response of bearings with local defects. These technologies are not completely independent. On the contrary, in many cases, they complement each other. Most of these technologies are performed in one of three areas: time domain, frequency domain, and time-frequency domain [17].

Butler [18] early work in this field investigated the use of shock pulse technique to detect damage to rolling element bearings by vibrational signals generated due to defects. He thought that when the rolling element passes over the damaged area in the bearing, it will produce a mechanical shock. It moves through the bearing structure to other parts, where it can be monitored using accelerometers by placing them on bearing housing. He concluded from experiments that shock pulse meters provide quantitative and reliable results. This method is effective, but has the disadvantage that when there are multiple faults in the machine, the pulse repetition will not correspond to a single fault, resulting in an erroneous diagnosis.

2.4 Time Domain Analysis Approach

The simplest method in the time domain is the statistical approach for measuring the overall root mean square level and the crest factor, the ratio of the peak value of the acceleration to the RMS value. This method has been applied with limited success for the detection of localized defects [19].

Collacott [20] have proposed some statistical parameters such as probability density and kurtosis for bearing defect detection. It has been suggested that the acceleration probability density of a bearing in good condition has a Gaussian distribution, and because the number of high acceleration levels is relatively increased, the damaged bearing leads to a non-Gaussian distribution with a dominant tail.

Dyer and Stewart [21] first proposed the use of kurtosis to detect bearing defects. For a healthy bearing with a Gaussian distribution, the kurtosis value is close to 3, and the kurtosis greater than 3 is itself considered a sign of an impending failure and does not require any prior history. However, one drawback is that when one disadvantage is that when the defect is done well, the kurtosis value will drop to the level of the healthy bearing. Therefore, it is recommended to measure the kurtosis of the selected frequency band. White [22] studied the effectiveness of kurtosis feature under a simulated condition.

Rush [23] shows the effectiveness of kurtosis in bearing defect detection, but in some cases, this method does not effectively detect incipient faults. The kurtosis has not yet become a very popular method of monitoring bearing conditions in the industry.

Springer [24] proposed a technique for detecting the local defects in the time domain based on the display of a vibration signal on an oscilloscope or by drawing a vibration signal on a graph recorder and observing the resulting periodic peaks due to defects in the rolling elements. Gustafsson and Tallian [25] proposed a defect detection method based on the number of peaks exceeding a preset voltage level.

Kim [26] reported that the shock pulse method can successfully detect faults in rolling bearings and is therefore widely recognized in the industry. While, Tandan and Nakra [19] stated that this method does not effectively detect faults at low speed. However, Butler [18] successfully used the shock pulse method to discover the defects in low-speed balls in papermaking lines.

Bhende et al. [27] developed an algorithm that usesd acoustic emission techniques to diagnose faults while the bearings are running. It was developed to handle various signals generated by different bearing defects. Time-domain analysis is used in conjunction with combined low-frequency analysis techniques such as Fast Fourier Transform and High-Frequency Envelope Detection. Envelope detection uses two methods, the Hilbert transform and the order analysis. Statistical parameters showed good results in increasing the severity condition of the defect. The RMS and crest factor are the most reliable parameters as they show a linear trend. Results of order analysis showed better results in detection of the severity of bearing defect than Hilbert transform.

2.5 Frequency-Domain Approach

Frequency domain or spectral analysis of vibration signals is probably the most widely used method for bearing defect detection. Especially after the advent of modern Fast Fourier Transform (FFT) analysis equipment, it becomes easier and more efficient to obtain narrowband spectrum. The low-frequency range and high-frequency range of the vibration spectrum are important when evaluating bearing conditions.

2.6 Related Work on Acoustic Emission and Vibration Analysis

Rogers [28] used the sound technology to monitor slow-rotating anti-friction slewing bearings on cranes used in natural gas production, and achieved some encouraging results compared to vibration monitoring technology.

Heng and Nor [29] presented a study using sound pressure and vibration signals to detect defects in rolling bearings using statistical analysis methods. It concluded that due to the sensitivity of the housing assembly to longitudinal vibration, the statistical parameters are affected by the shaft speed, which stimulates the retaining ring that holds the test bearing in its position. Under ideal conditions, statistical methods can be used to identify different types of defects present in the bearing. In addition, the results also showed that there is no significant advantage in using beta function parameters compared to using kurtosis and crest factors to detect and identify rolling bearing defects from sound and vibration signals.

Chaudhry and Tandon [17] identified defects that were seeded in bearings of various sizes in the speed range of 500 to 1500 rpm. Also they found that the count feature of healthy bearings was low and increased with increasing speed of damaged and undamaged bearings. The increase in load did not result in any significant change in the count feature of fault-free bearing and faulty bearing.

Kaewkongka [3] used the acceleration and the acoustic emission (AE) signals to monitor the condition of the bearings as a multi-sensor system; to increase reliability as well as to allow for a successful monitoring of a wider range of rotational speeds. If one sensor does not work properly, the other sensor can still provide the appropriate monitoring. The study concluded that the vibration method is suitable for high rotation speeds, whereas acoustic emission methods are suitable for low rotational speeds.

Al-Ghamed and Mba [30] compared AE and vibration analysis under a range of speed and load conditions. Besides, the main source of AE activity caused by seed defects was investigated. They concluded that AE provides earlier fault detection and improved recognition capabilities than vibration analysis. In addition, AE technology can also indicate the size of the defect so that the user can monitor the degradation rate of the bearing, unachievable with vibration analysis.

Kim et al. [31] conducted out a comparative experimental study on the application of the ultrasound technique for condition monitoring of low speed rolling element bearings and conventional vibration measurements with seeded faults on inner-race defects. Where statistical parameters extracted from the time domain and coated spectra were used in the frequency domain. Results revealed that the ultrasound technique is more effective in detecting low-speed bearings failure than that of the vibration measurement.

Roque at el. [32] explained why the deviation between the theoretically calculated values and the measured frequencies emitted by the device is usually deviated when using theoretical mathematical models to calculate the frequencies corresponding to the faulty bearings. The results showed that the cause of this indicated deviation was the effect of the rotation frequency of the bearing cage.

Saruhan at el. [33] studied vibration analysis for defects of rolling element bearings. They reached conclusions that led to the identification of the defects that were artificially seeded, their severity and location.

Van et al. [34] proposed a new diagnostic approach that combines envelope analysis, time synchronization and spectral averaging of vibration signals to extract a condition indicator for diagnosing rolling bearing faults. The proposed technique was tested using a vibration output of a steel bearing with seed defects on a bearing test rig. The result is an effective method that has been proven to diagnose all four bearings defects in the inner ring, outer ring, ball and cage.

Freitas et al. [35] have compared the results obtained from vibration and acoustic signals at an average speed of rotation. The selected methods for this comparison relate to semi-automatic processing based on envelope analysis, also a comparative analysis of the benefits of using different methods to obtain key statistical characteristics in the time domain to characterize the fault. Study showed that the benefits of pre-treatment techniques are not significant and their application efficiency may be related to the complexity of the device. In the case of acoustic emission signals, MED did not provide any benefits but the cepstral editing technique helped enhance the fault for all the features except for Kurtosis and Crest Factor. These last two features do not provide any interesting information to help identify the damage. It has also been verified that many features are related, and it may be important to consider applying feature selection algorithms to suggest pattern recognition.

Praveenkumar et al. [36] conducted a comparative study based on the analysis of vibration, sound and motor current for diagnosing gearbox malfunctions under various conditions of simulated gears and bearings. Statistical characteristics were extracted from the raw data of these three converter signals, and the best characteristics were selected from the extracted features. Then, the selected functions were set as input for artificial neural network (ANN) classifiers and support vector machine (SVM), and their characteristics were compared.

Caesarendra and Tjahjowidodo [37] presented an empirical study of features extraction methods for the application of low-speed slew bearing condition monitoring and find the proper features that represent the degradation condition of slew bearing rotating at very low speed with naturally defect. Feature extraction methods or algorithms in a wide range of applications such as vibration analysis, time series analysis and biomedical signal processing, was discussed. The selected features such as impulse factor, margin factor, approximate entropy and largest Lyapunov exponent (LLE) showed obvious changes in bearing condition from normal condition to final failure.

Kim et al. [38] an advanced condition monitoring system using acoustic emission and vibration analysis techniques for low and high-speed machines was studied. It concludes that acoustic emission technology is more sensitive than vibration technology when the AE sensor is far away from the object and it recommended that acoustic emission can successfully monitor crack propagation, insufficient lubrication, poor sealing, and shock signals such as bearing or gear peeling.

Hebrard [39] studied a combination of vibration analysis and acoustic emission techniques that provide different types of information in different frequency bands on test bearings with seed defects. The correlation between the low-frequency signal and the high-frequency signal is introduced by a signal acquisition strategy different from the signal processing step. Real-time transient analysis with real-time features extraction is performed in parallel with stream acquisition of two signals. The duration of the completion is continuously monitored to provide information about the absence of steady-state and settling time. Features extraction of defective and defect-free rolling bearings is compared at various speeds and load levels. They founded that in seeded defect testing, the basic source of AE is due to material protrusions above the average surface roughness. Besides, the maximum amplitude of AE is more sensitive to the occurrence and growth of defects than vibration measurements.

CHAPTER 3

ACOUSTIC EMISSION AND VIBRATION SIGNAL ANALYSIS

3.1 Vibration Analysis

As global production competition intensifies and pressures to use machines more efficiently, The importance of effective condition monitoring methods for the failure detection of rotating machines became apparent in the 1970s. Therefore, vibration monitoring has been successfully used to monitoring in dynamic field. The vibration-based approach has been widely accepted as an appropriate maintenance strategy in various industries to maintain expensive equipment, ensure continuity of production and minimize maintenance cost. The fact that all machines that contain moving components may vibrate, the cyclical excitation forces transmitted to adjacent components within machines can give rise to motion (vibration). Therefore, the nature and magnitude of the vibrations on a component of the machine can give valuable information for its mechanical condition. The waveforms of vibration signals from rotating machinery are often recorded and analyzed by processing the data using various techniques. Each different technique gives some information about the condition of the machine [3].

3.1.1 Sources of Vibration and Noise in Ball Bearings

Vibration is generated due to several reasons, operating alone or in combination as a result of the vibration of the main or auxiliary equipment.

1. Surface defects of the bearing.
2. Changes in ball bearing stiffness, where rolling bearing stiffness is characterized by the amount of elastic deformation (deflection). Rolling bearings have a higher stiffness than ball bearings.
3. Random shocks occur due to imperfect geometry.

Defects can also be divided into two groups of localized defects and distributed defects. Distributed defects are due to manufacturing errors and varying surface roughness. while the localized defects are the result of cracking and fatigue. As soon as a defect interacts with the bearing elements, a sudden change in surface creates a shock wave that can be monitored to detect bearing failure.

To implement a series of experimental studies on a ball bearing, there are two methods. First, operate the ball bearing under conditions similar to normal operating conditions, until it reaches the failure stage. But this is a very laborious method that will not produce results in a reasonable time. Or by removing the lubricant or increasing the load beyond the operating instructions to create a defect.
The second method is to seeding a certain defects on ball bearing components (balls, inner race, outer race) artificially by using the electric discharge mechanism (EDM). as was done in this study [10].

3.2 Acoustic Emission (AE)

The work of Joseph Kaiser marked the launch of Acoustic Emission (AE) technology in 1950. In the decades of the 1950s and 1960s, the study of the fundamental principles of acoustic emission attracted great interest, leading to the rapid development of instruments for characterizing AE behaviour in many materials [40][2000]. In the 1970s, acoustic emission was widely recognized for its unique function as a non-destructive test (NDT) for monitoring dynamic processes. Its use has been growing steadily in various industrial fields. In the 1980s, computers provided basic and powerful components for instrumentation and data analysis [3].

To be able to use acoustic emission as an effective condition monitoring technique, it is necessary to understand the acoustic emission source. The next section will introduce different acoustic emission sources.

3.2.1 Sources of Acoustic Emission

Acoustic emission occurs in the form of transient bursts that correspond to a localized micro failure within the body of the material. They are inherently broadband and contain frequencies from DC to the MHz region. In addition, source mechanism relating to the crack extension and plastic deformation, active in defect growth such as fatigues, is of high-frequency stress waves source [41].

Typically the frequencies lie within the range of 20 kHz to 1 MHz. In the case of a growing crack, arguably the most important acoustic emission source, the formation of new crack faces must be accompanied by sudden changes in stress and displacement of material in the vicinity of the crack [42]. Varying stresses and strains must, by definition, act as sources of stress (elastic) waves as shown in Figure 3.1.

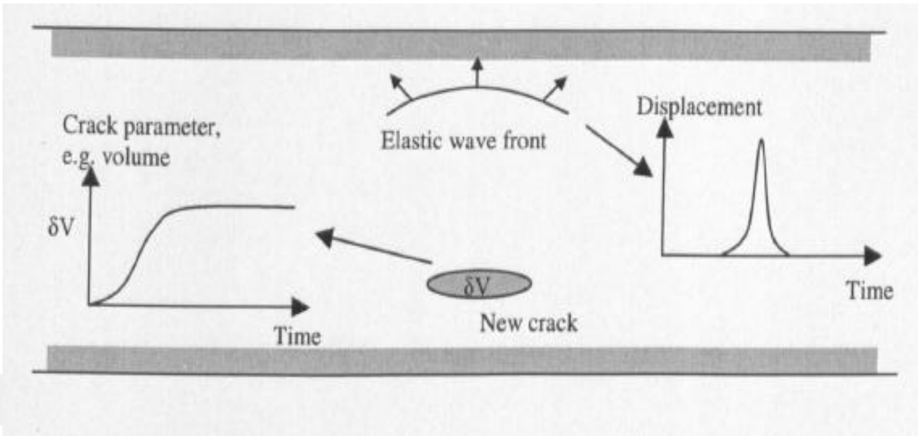

Figure 3.1 Illustrate an acoustic emission source as a crack growth [42].

3.3 Signal Processing and Data Analysis

Bearings faults identification involves the use of various signal processing algorithms to extract useful diagnostic information from measured vibration or AE signals. Traditionally analysis has been grouped into three classes; time domain, frequency domain and time-frequency domain. The statistical analysis techniques are commonly applied for time-domain signal analysis, in which descriptive statistics such as RMS, skewness, and kurtosis are used to detect the faults [41; 42]. A Fast Fourier Transform (FFT) is commonly used to obtain the frequency spectra of the signals. The detection of faults in the frequency domain is based on identification of certain frequencies which are known to be typical symptoms associated with bearing or gear faults. The time-frequency domain methods are composed of the short-time Fourier transform (STFT) [45], Wigner-Ville [43], and wavelet analysis [44; 45]. The use of these detection techniques are feasible for applications where a single component is being monitored. However, for applications that include several components, such as gearboxes, it is essential to employ separation algorithms. For this study, the vibration and AE signals acquired were processed.

3.3.1 Time Domain

Machine condition monitoring requires an easy-to-interpret and clear condition indicator that can be calculated from the extracted vibration characteristics. Useful indicators should allow for defect growth tracking and provide a way to define indicator levels that indicate acceptable and unacceptable machine conditions [27]. The statistical technique indicators (RMS, Crest factor, Kurtosis, skewness, etc) associated with a vibration or AE signature of bearings are observed most often in its time domain, where are used as condition monitoring indicators for bearing condition. Therefore, This study focuses on the RMS, CF, kurtosis, skewness, peak indicators.

3.3.1.1 Root Mean Square (RMS)

RMS is the most common statistical indicator. It has been used in some studies [46]. It can quickly reveal the status of the bearing and see if the operating conditions have changed since the last measurement [47].

$$\mathrm{RMS} = \sqrt[2]{\frac{1}{N}\sum(x_i - \mu)^2} \quad (3.1)$$

3.3.1.2 Peak Level

The Peak level of the discrete time signal is:

$$\text{Peak} = \text{maximum}\ (x_i) \quad (3.2)$$

3.3.1.3 Crest Factor (CF)

Crest Factor is the ratio of the peak value to the RMS value, which consider another factor used as a health indicator that gives a measure for the signal spikiness [27].

$$\mathrm{CF} = \frac{peak\ value}{RMS\ value} \quad (3.3)$$

3.3.1.4 Kurtosis

Kurtosis is an indicator of whether a data is peak or flat relative to a normal distribution, where a high kurtosis value represents a "peak" distribution and a low kurtosis value represents a "flat" distribution around the mean. It is a very low for the healthy bearing and very high value for a defective bearing because of the spiking behaviour of the signal [27]. The mathematical formula of kurtosis is as follows.

$$\text{Kurtosis} = \frac{\frac{1}{N}\sum_{i=1}^{n}(x_i-\mu)^4}{\sigma^4} \tag{3.4}$$

3.3.1.5 Skewness

Skewness is a measure of symmetry or, the absence of symmetry relative to its mean value. Where the distribution is symmetry if the left and right points of the distribution center appear identical. Negative skewness values indicate that the data is skewed to the left, and positive values are skewed to the right.

$$\text{Skewness} = \frac{\frac{1}{N}\sum_{i=1}^{n}(x_i-\mu)^3}{\sigma^3} \tag{3.5}$$

3.3.2 Frequency Domain

In addition to analyzing signals in the time domain, analysis in the frequency domain is one of the most widely used approach for analyzing antifriction bearing condition. In frequency domain analysis, the FFT analyzer is used to analyze the low and high frequency ranges of the signal. The study of the low and high range of frequency is important because of the complex behavior of ball bearing vibration signals.

The normal frequency of the whole system (bearing elements, structure, and housing) is excited when the defects interact with the rolling elements leading to the production of shock pulses. This leads to an increase in the vibrational energy at these frequencies. These frequencies can be calculated theoretically as stated at the end of this chapter, where each bearing has distinct frequencies. Frequency domain methods work best when the signals being monitored are periodic in nature, as is the case for vibration on a rotating shaft supported in bearings. Since a bearing defect produces a signal that is periodic at the characteristic defect frequency, frequency-domain analysis appears to be a suitable tool for condition monitoring. Examples of the frequency-domain techniques include spectrum analysis, cepstrum analysis, high frequency resonance technique (HFRT) and holospectrum. Among them, spectral analysis seems to be the most common and most important in fault diagnosis. One of the determinants of the use of spectrum analysis is the loss of frequency position relative to time. It is impossible to judge whether there is a certain frequency throughout life cycle of the time signal.

To achieve effective bearing condition monitoring, this requires the identification of transient frequency components and the time of their appearance. When the rolling element passes through local defect in the bearing, it creates a transient signal in the acquired signal, as in a machine with rapidly varying speed is an example of transient events, therefore methods that preserve both temporal and frequency perspectives are preferred. Spectral analysis can be used by analyzing the frequency components of the vibration signal using the Fourier transform of the function x(t), which represents an analogue signal with finite power [47].

$$F[x(t)] = X(f) = \frac{1}{2\pi} \int_{-\infty}^{+\infty} x(t)\; e^{-j2\pi ft}\, dt \qquad (3.6)$$

Since bearings components defects produce known characteristics vibration frequencies, some of which can be expressed as a multiple of the running speed of the machine. Therefore, by compared spectral peaks of calculated frequencies, cause of the defect can usually be determined using narrow-band spectral analysis. The deterioration of machine components generate an increase in vibration level at its characteristic defect frequencies. These frequencies are dependent on the dimensions of the bearing, the number of rolling elements and the speed of rotation [3].

3.3.2.1 Fast Fourier Transform (FFT Background)

The waveform is actually a collection of simple sine waves with different frequencies, phases and amplitudes. The Fourier series is a series of sine waves used to deconstruction the signal in its individual sine components. The result is an amplitude, where the vibration amplitude is a function of frequency. Fourier analysis works by “testing” for the presence of each frequency component. A discrete Fourier transform (DFT) multiplies the raw waveform by sine waves of discrete frequencies to determine if they match and what their corresponding amplitude and phase are.

A Fast Fourier transform (FFT) is just a DFT using a more efficient algorithm that takes advantage of the symmetry in sine waves. The FFT requires a signal length of some power of two for the transform and splits the process into cascading groups of 2 to exploit these symmetries. This dramatically improves processing speed; if N is the length of the signal, a DFT needs N^2 operations while an FFT needs $N*\log_2(N)$ operations. Although the execution time of an FFT will be fastest when the signal length is some power of 2, today's computing power and modern FFT algorithms make this time difference insignificant.

The number of discrete frequencies tested as part of the Fourier transform is proportional to the number of samples in the original waveform. N is the length of the signal, and the number of frequency lines or frequency segments is equal to N/2. The interval (Δf) of these frequency bins is equal to the sampling rate (Fs) of the original waveform divided by the number of samples (N), or it can be said that the frequency accuracy is equal to the reciprocal time (T) of the total acquisition amount. To improve the frequency accuracy, the recording time must be extended as shown below.

$$\Delta f = \frac{1}{T} = \frac{F_S}{N} \tag{3.7}$$

3.4 Bearing Kinematics

Impulses occur when a rolling element encounters a defect and touches the edge of the defect, generating periodic pulses at certain frequencies (characteristics frequencies of defects). These frequencies depend on the kinematics of the bearings (geometry and speed). The characteristic frequency of the bearing defect can be calculated as follows.

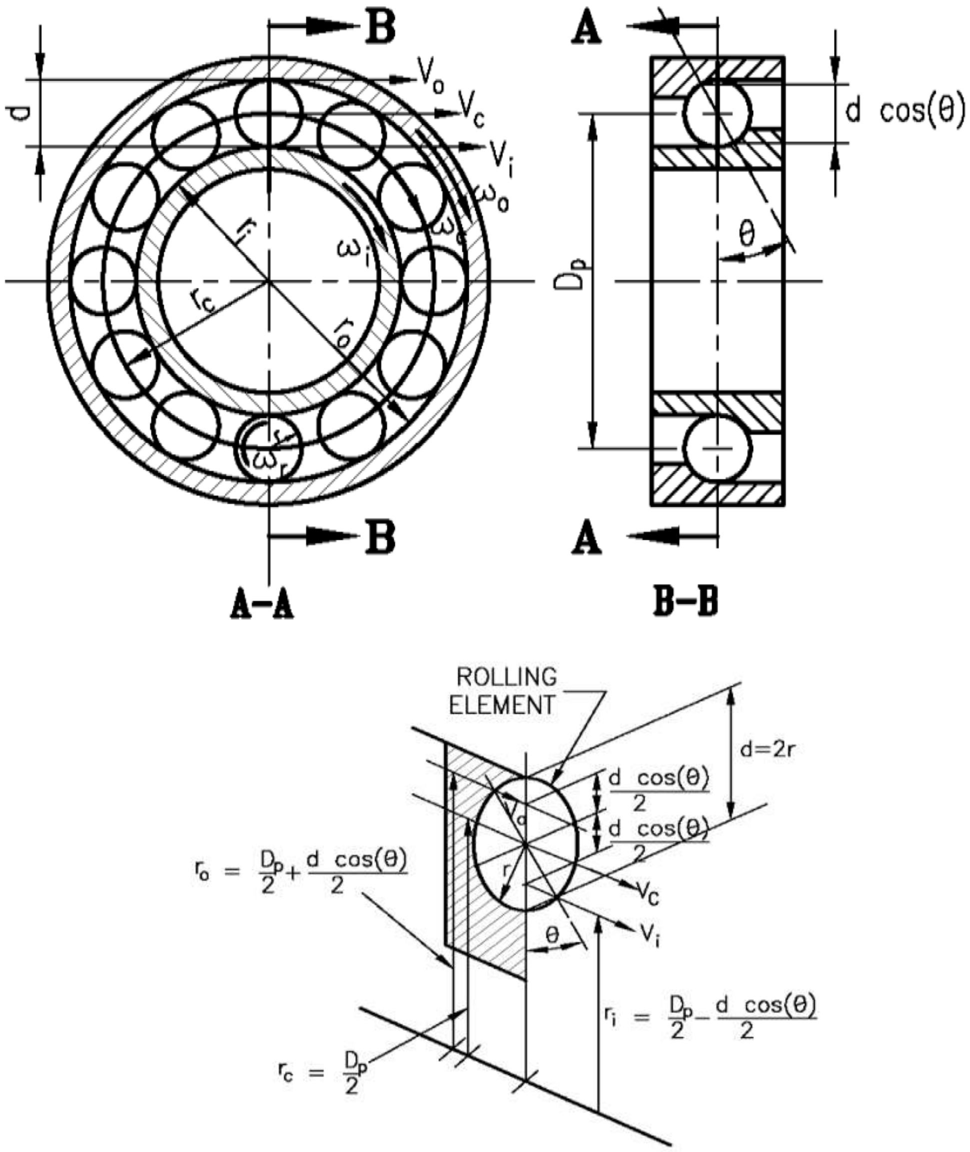

Figure 3.2 Bearing geometry [27].

Where (f, r, ω, ν, θ) refers to frequency, radius, angular speed, linear speed and angular contact of load in radial plane. Indices: (c, i, r, o) refers to the cage, inner race, rolling element and outer race. (D_P) Pitch diameter; (d) Diameter of the rolling element, (N_b) Number of rolling elements.

The linear velocity of the cage can be given as

$$v_c = \frac{v_i + v_o}{2} = \frac{w_i r_i + w_o r_o}{2} = \frac{f_i r_i + f_o r_o}{2} \tag{3.8}$$

$$r_c = \frac{D_P}{2} \tag{3.9}$$

$$r_i = \frac{D_P}{2} - \frac{d \cos\theta}{2} \tag{3.10}$$

$$r_o = \frac{D_P}{2} + \frac{d \cos\theta}{2} \tag{3.11}$$

Then, the angular speed of cage is

$$\omega_c = \frac{v_c}{r_c} \tag{3.12}$$

$$\omega_c = \frac{1}{2}\left[\omega_i \left(1 - \frac{d \cos\theta}{D_P}\right) + \omega_o \left(1 + \frac{d \cos\theta}{D_P}\right)\right] \tag{3.13}$$

$$\omega_c = 2\pi f_c \tag{3.14}$$

Then, the fundamental train frequency (FTF) can also be obtained from the above equations, as shown.

$$\text{FTF} = f_c = \frac{1}{2}\left[f_i \left(1 - \frac{d \cos\theta}{D_P}\right) + f_o \left(1 + \frac{d \cos\theta}{D_P}\right)\right] \tag{3.15}$$

The passage frequency (BPFO) of the ball in the outer ring can be obtained by multiplying the number of rolling elements (N_b) by the relative angular velocity between the cage and the outer ring.

$$\text{BPFO} = N_b (\omega_c - \omega_O) \tag{3.16}$$

$$\text{BPFO} = N_b \left[\frac{1}{2}\left\{f_i \left(1 - \frac{d \cos\theta}{D_P}\right) + f_o \left(1 + \frac{d \cos\theta}{D_P}\right)\right\} - f_o\right] \quad . \tag{3.17}$$

Similarly, can obtained the ball pass frequency of inner race (BPFI) by multiplying the number of rolling elements by the relative angular velocity between the cage and the inner ring:

$$\text{BPFI} = N_b (\omega_i - \omega_c) \tag{3.18}$$

$$\text{BPFI} = f_r = \frac{N_b}{2}(f_i - f_o)\left(1 + \frac{d \cos\theta}{D_P}\right) \tag{3.19}$$

The frequency of rolling elements that rotation around their axis, called the Ball Spin Frequency (BSF), it can be obtained as shown below. Taking into account the non-slip of the balls.

$$\omega_r = \frac{v_r}{r_r} \tag{3.20}$$

The tangential velocity of ball at the contact point with the inner race is:

$$v_r = N_b\,(\omega_i - \omega_c) r_r \tag{3.21}$$

$$\omega_r = \frac{(\omega_i - \omega_c)}{r_r} r_i \tag{3.22}$$

$$BSF = f_r = \frac{D_P}{2d}(f_i - f_o)\left[1 - \left(\frac{d\,\cos\theta}{D_P}\right)^2\right] \quad . \tag{3.23}$$

3.4.1 Simplified Model

Since the inner ring is to be the rotating part, it is possible to express mathematically the characteristic frequencies as shown.

$$FTF = f_c = \frac{f_i}{2}\left(1 - \frac{d\,\cos\theta}{D_P}\right) \tag{3.24}$$

$$BSF = f_r = \frac{D_P\,f_i}{2d}\left[1 - \left(\frac{d\,\cos\theta}{D_P}\right)^2\right] \tag{3.25}$$

$$BPFI = \frac{N_b f_i}{2}\left(1 + \frac{d\,\cos\theta}{D_P}\right) \tag{3.26}$$

$$BPFO = \frac{N_b f_i}{2}\left(1 - \frac{d\,\cos\theta}{D_P}\right) \tag{3.27}$$

CHAPTER 4

EXPERIMENTAL PROCEDURE AND RESULT

4.1 Experimental Setup

To measure vibration and AE signals at various loads and speeds, the test bench is designed as shown in Figure 4.1. It consists of a shaft driven by a three-phase AC motor that uses an electronic speed variator with an output speed in the range of 612 to 1495 rpm. The rotating shaft is simply supported between two self-lubricating standard ball bearings.

Three load levels (0, 5 and 10) kg were applied to the test bearings as required, with speed ranges of (612, 898, 1224, 1495) rpm. The load is applied using a disc load mounted on the free end of the shaft. The split housing is designed for easy installation and removal of test bearings. Four single row deep groove ball bearings are used as test bearings with zero contact angles. Three test bearings with different defects were used, one of them was not defective as a healthy bearing. The accelerometer is used to measure vibration data, mount it directly to the housing at the 12 o'clock position, and use a free-field array microphone to measure acoustic emission characteristics.

The nature of the sound and vibration to be measured may vary greatly. The sound may be "noisy" (roar or hiss-like), the machine emits constant noise under constant load, and the vibration of the machine is usually dominated by the frequency of rotation and its multiples.

The types of faults of the ball bearings in this research is formed artificially on the components of (ball, outer race, inner race), created using electro-discharge machining (EDM). The diameter of the defects is 0.7 mm.

A 4 channel data acquisition unit is used to obtain the vibration and AE signals and the recorded signals are post-processed in Labview environment. The digital data was collected at 1653 samples per second and 1357 Hz sample frequency.

The specification and dimension of bearings used in this test are listed in Table 4.1 and the theoretical characteristics frequencies are listed in Table 4.2.

Table 4.1 Dimensions of ORS 6206 TN1 C3 bearing.

Outer diameter D_o	62 mm
Inner diameter D_i	30 mm
Width b	16 mm
Ball diameter d	9.52 mm
Pitch diameter D_P	46.5 mm
Contact angle θ	0
No. of ball	9

Table 4.2 Theoretical characteristics defect frequencies at different speeds.

	RPM	612	898	1224	1495	Order
	Hz	10.17	14.97	20.4	24.92	
Defects Frequencies	FTF	242.55	357.30	486.7	594.46	0.397
		4.04	5.95	8.11	9.9	
	BSF	1427.31	2101.19	2863.99	3498.09	2.34
		22.22	35.01	47.73	58.49	
	BPFI	3306.98	4868.31	6635.65	8104.82	5.42
		55.11	81.13	110.59	135.08	
	BPFO	2183.01	3213.68	4380.34	5350.17	3.578
		36.38	53.56	73	89.16	

It is recommended that the sampling frequency be at least 2 times larger than the large expected characteristic frequency [48]. Therefore, in this study, the sampling frequency is 10 times the maximum expected frequency of defects.

Sample frequency = expected maximum frequency x 10

Then sample frequency = 1352.6 Hz

And the recording time $T=\frac{1}{f_s}=\frac{1}{1352.6}$ = 0.0007393 s (0.739 ms)

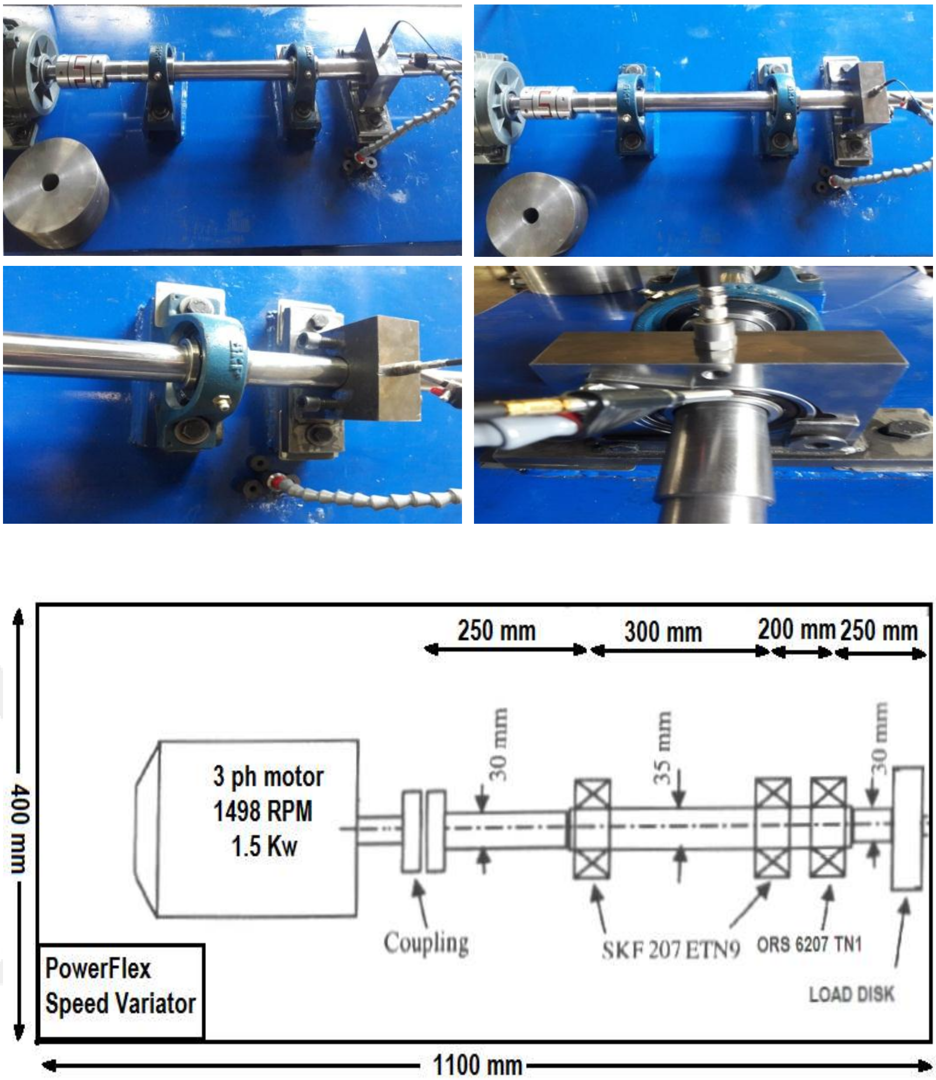

Figure 4.1 (a) Test rig and housing bearing (b) Sketch for test rig.

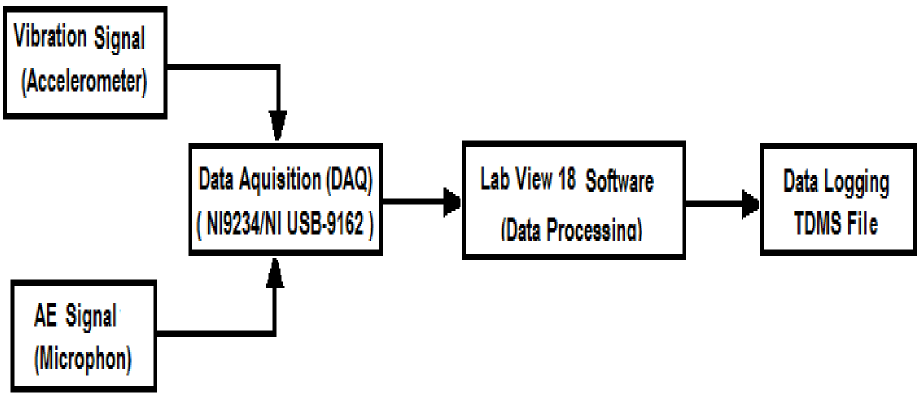

Figure 4.2 The schematic diagram of acquisition and data processing.

Figure 4.3 Artificial defects on the bearing components**.**

4.2 Instrumentation

The technical specifications of the equipment used in the collection and analysis of data.

1. General purpose Piezotronics PCB 352C04 Accelerometer (sensitivity: 10 mV/g).
2. Gras 40PH free field array microphone (sensitivity: 50 mV/g).
3. National instrument DAQ 9234 with USB-DAQ9162 chassis.
4. PowerFlex M4 speed variator.

The type of bearings used in experiment is ORS 6206 TN1 C3 (Glass Fibre Reinforced Polyamide 6.6 Plastic Cage).

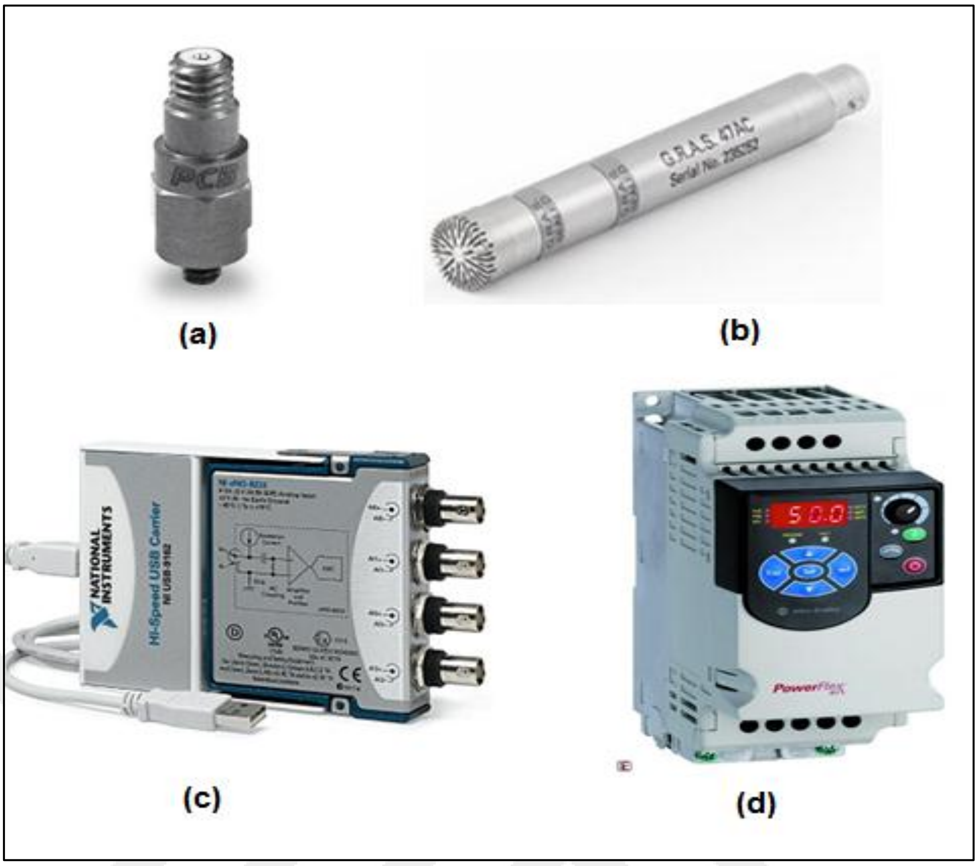

Figure 4.4 Measurement instrumentation (a) PCB 350C04 Accelerometer (b) 40PH free-field array microphone (c) National instrument DAQ 9234 with USB-DAQ9162 chassis (d) PowerFlex M4 speed variator.

4.3 Experimental Results

4.3.1 Waveform Signature in Time Domain

Overall condition monitoring of bearing can be done by studying statistical parameters extracted from a signal in the time domain. Figures 4.5 to 4.28 show the time signal generated from the healthy and defective bearings respectively. The temporal waveform of acoustic emission and vibration acceleration signals of the healthy and defective bearings are taken in different positions over 48 experiments (4 * 3 * 4), where 4 speeds (610 - 898 - 1224 - 1495) rpm, At 3 levels of load, where P0, P1 and P2 represents a 0 kg, 5.5 kg and 10 kg respectively. The root-mean-square value of signals is presented depending on each experiment with different speeds and loads.

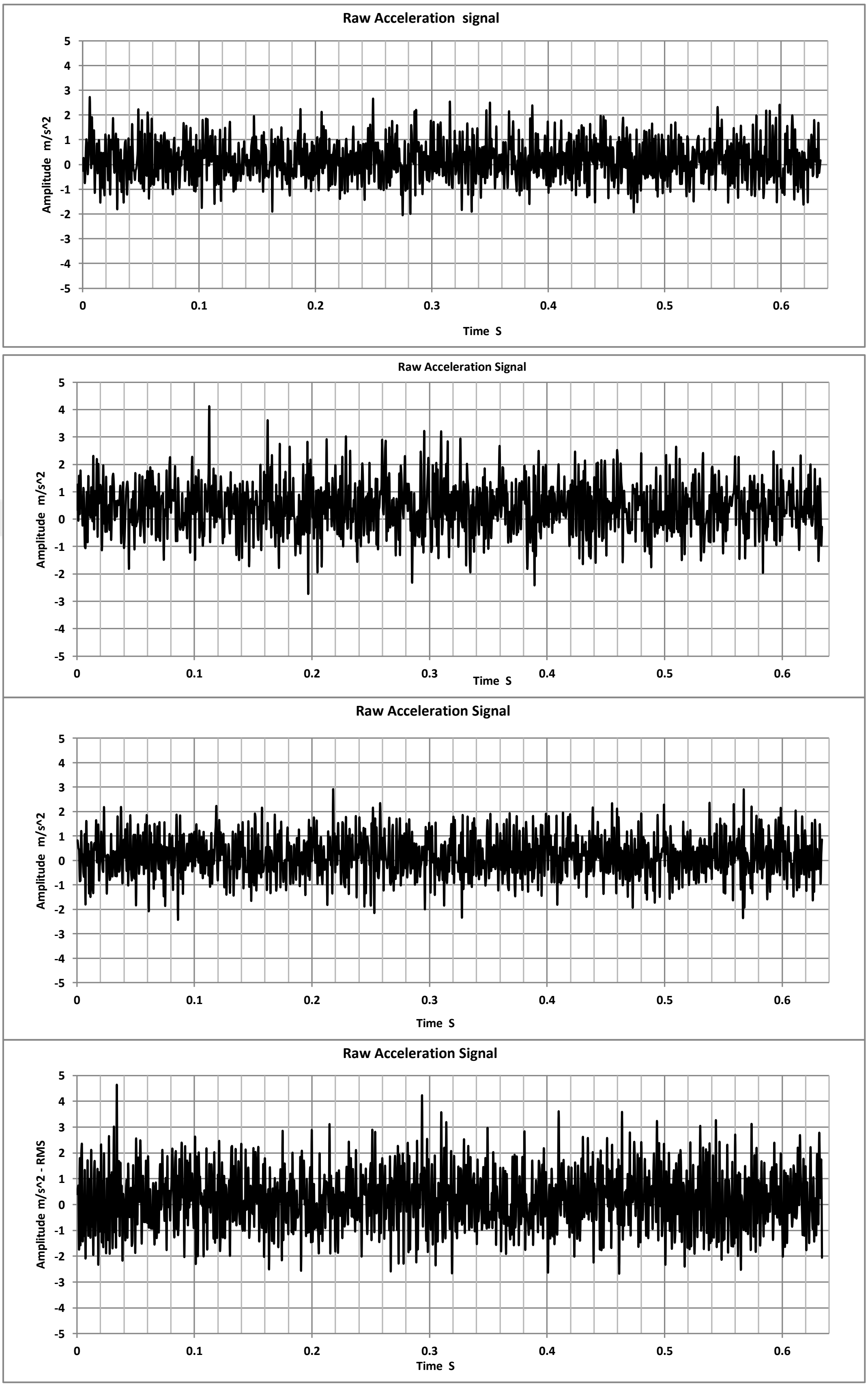

Figure 4.5 Vibration signature at load P0 & 610 rpm (a) Healthy bearing (b) Inner race defect (c) Outer race defect (d) Ball defect signature.

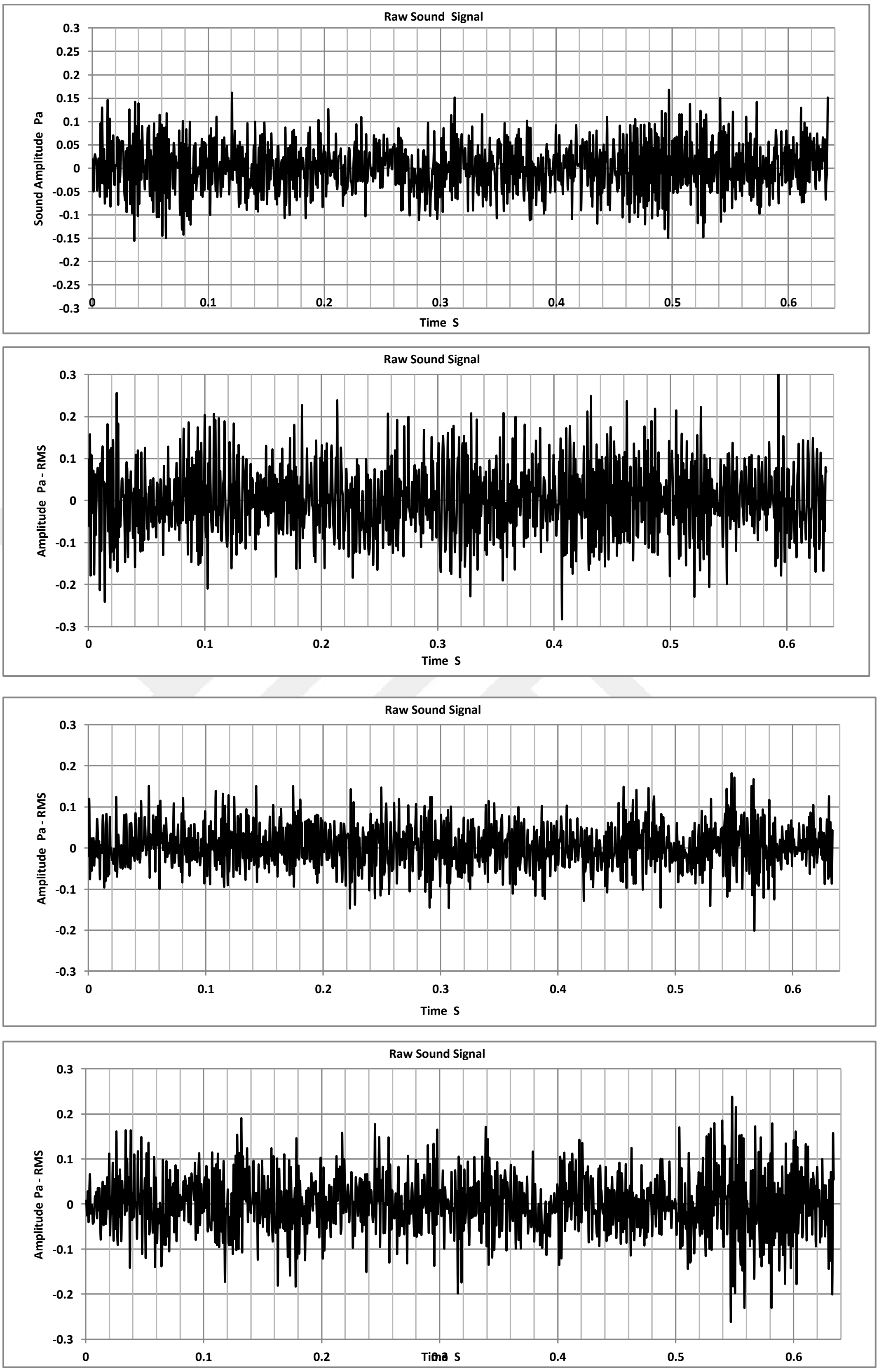

Figure 4.6 Sound signature at load P0 & 610 rpm (a) Healthy bearing signature (b) Inner race defect signature (c) Outer race defect signature (d) Ball defect signature.

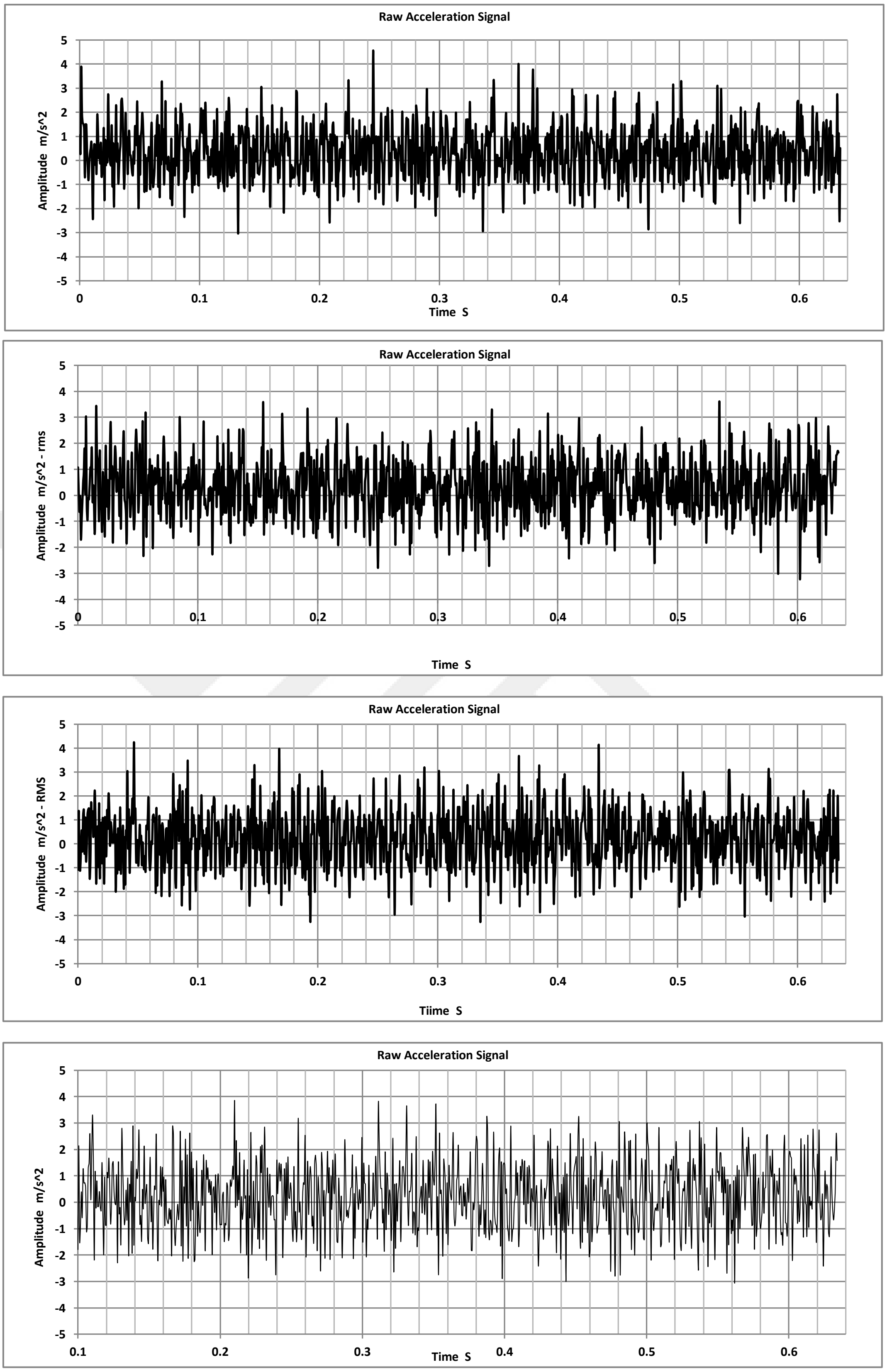

Figure 4.7 Vibration signature at load P0 & 898 rpm (a) Healthy bearing signature (b) Inner race defect signature (c) Outer race defect signature (d) Ball defect signature**.**

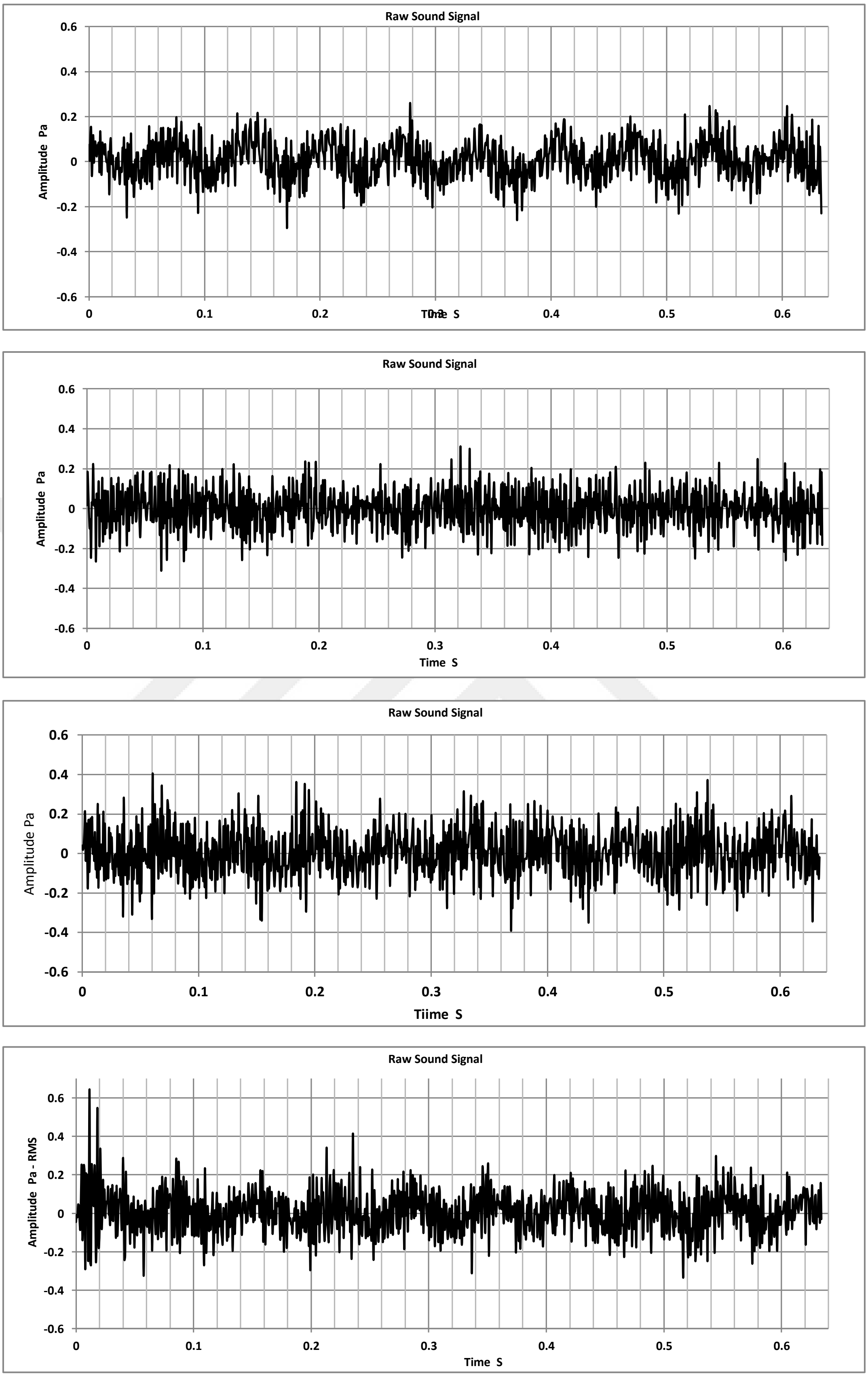

Figure 4.8 Sound signature at load P0 & 898 rpm (a) Healthy bearing signature (b) Inner race defect signature (c) Outer race defect signature (d) Ball defect signature.

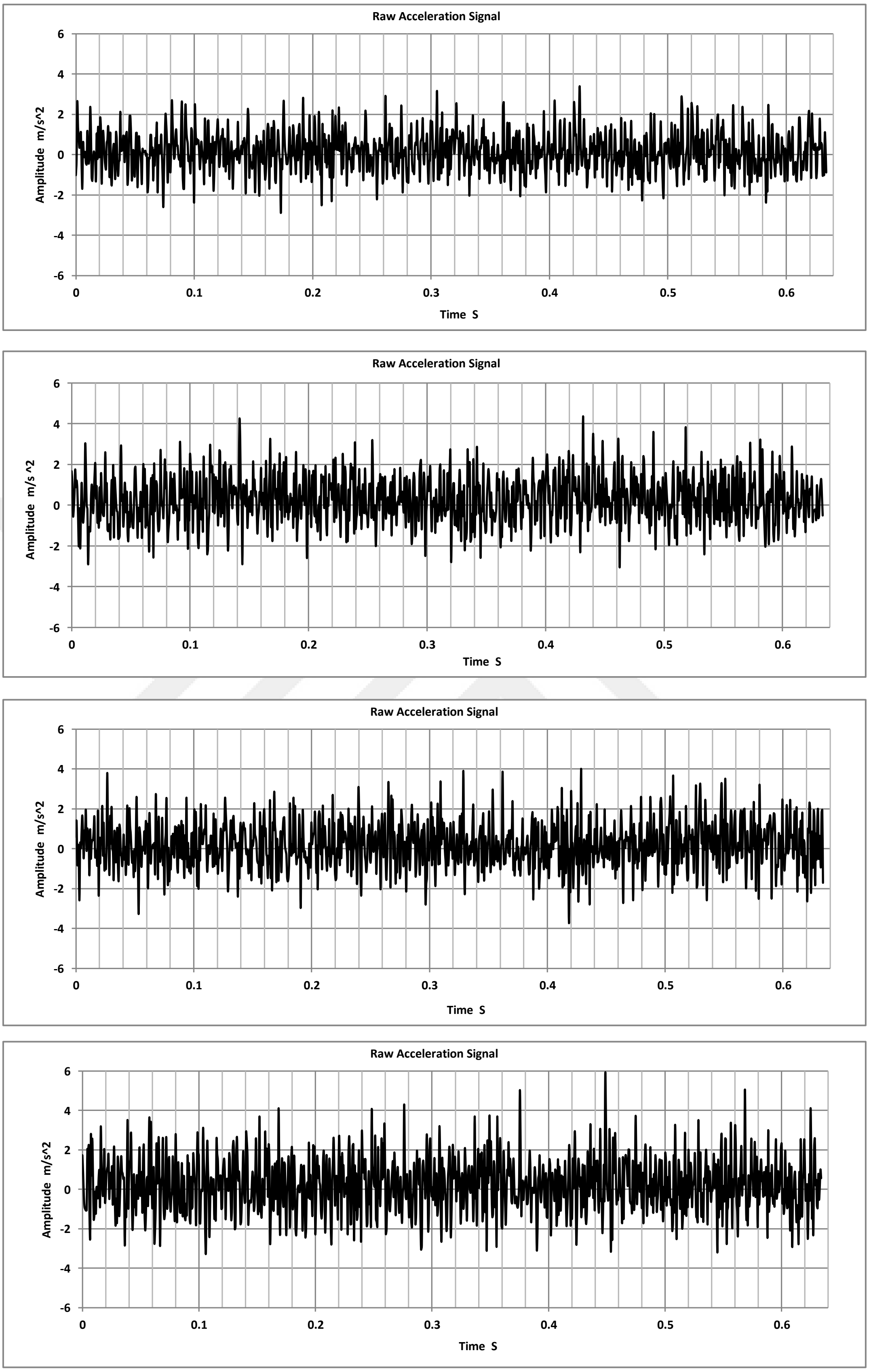

Figure 4.9 Acceleration signature at load P0 & 1224 rpm (a) Healthy bearing signature (b) Inner race defect signature (c) Outer race defect signature (d) Ball defect signature.

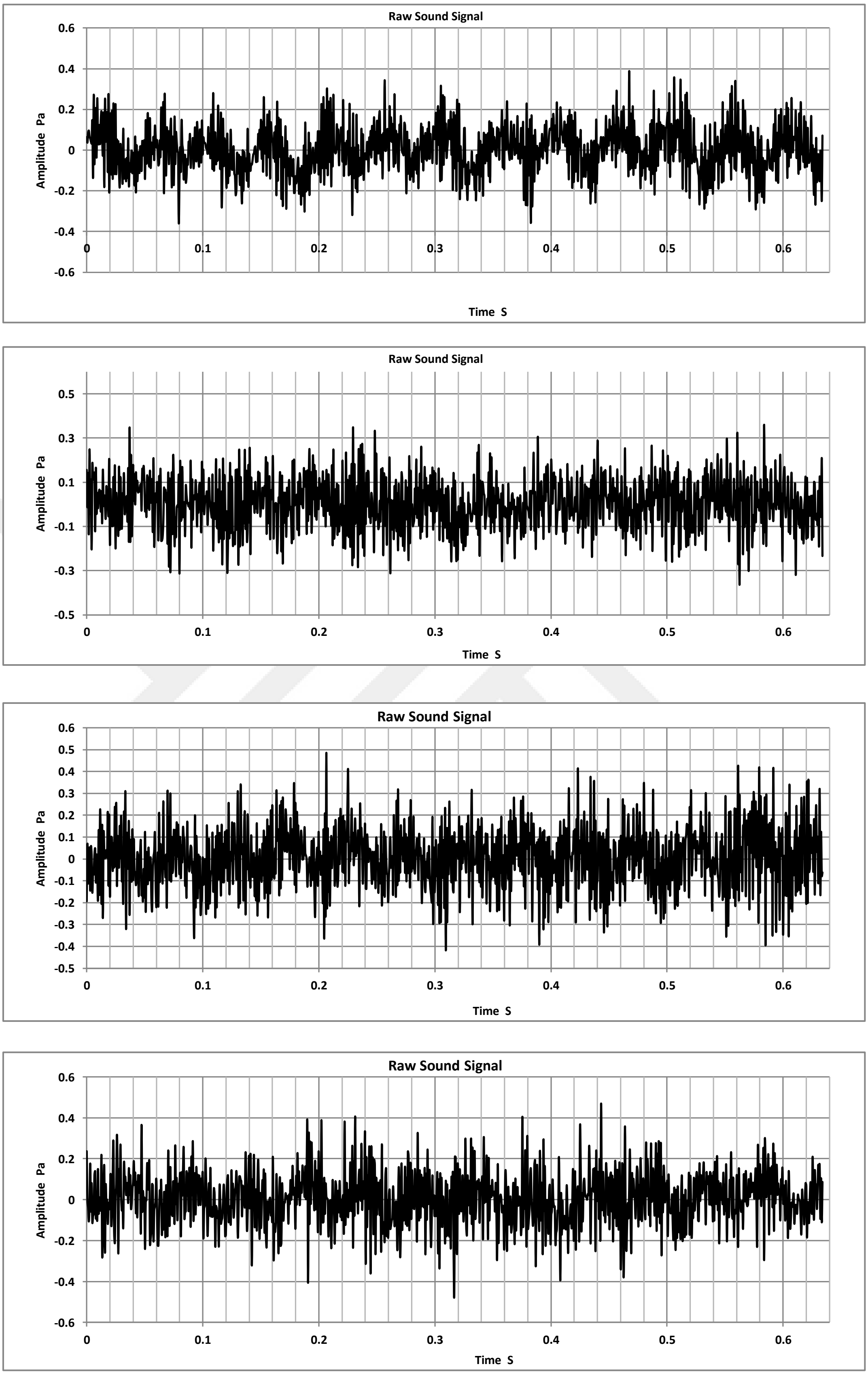

Figure 4.10 Sound signature at load P0 & 1224 rpm (a) Healthy bearing signature (b) Inner race defect signature (c) Outer race defect signature (d) Ball defect signature.

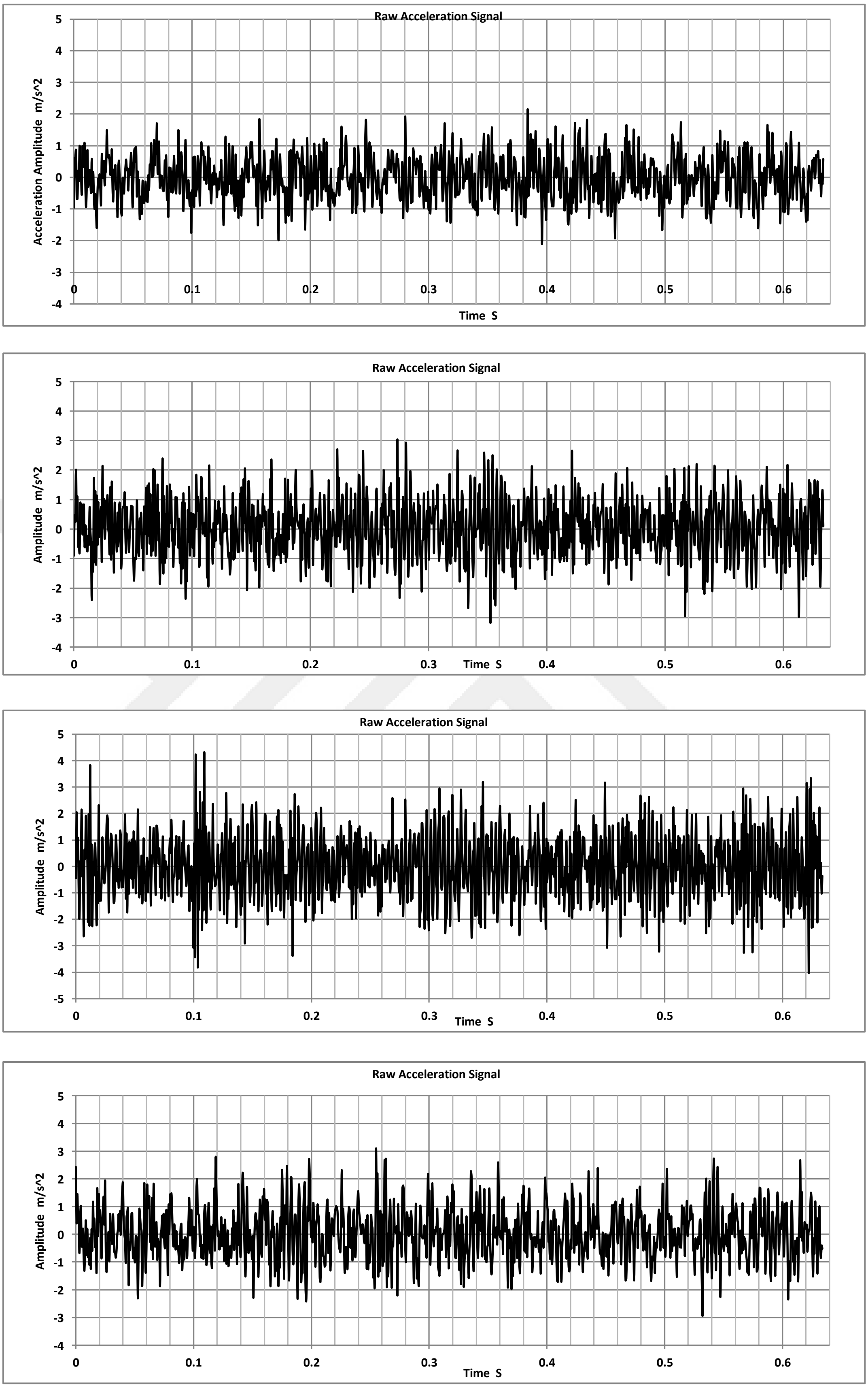

Figure 4.11 Acceleration signature at load P0 & 1495 rpm (a) Healthy bearing signature (b) Inner race defect signature (c) Outer race defect signature (d) Ball defect signature.

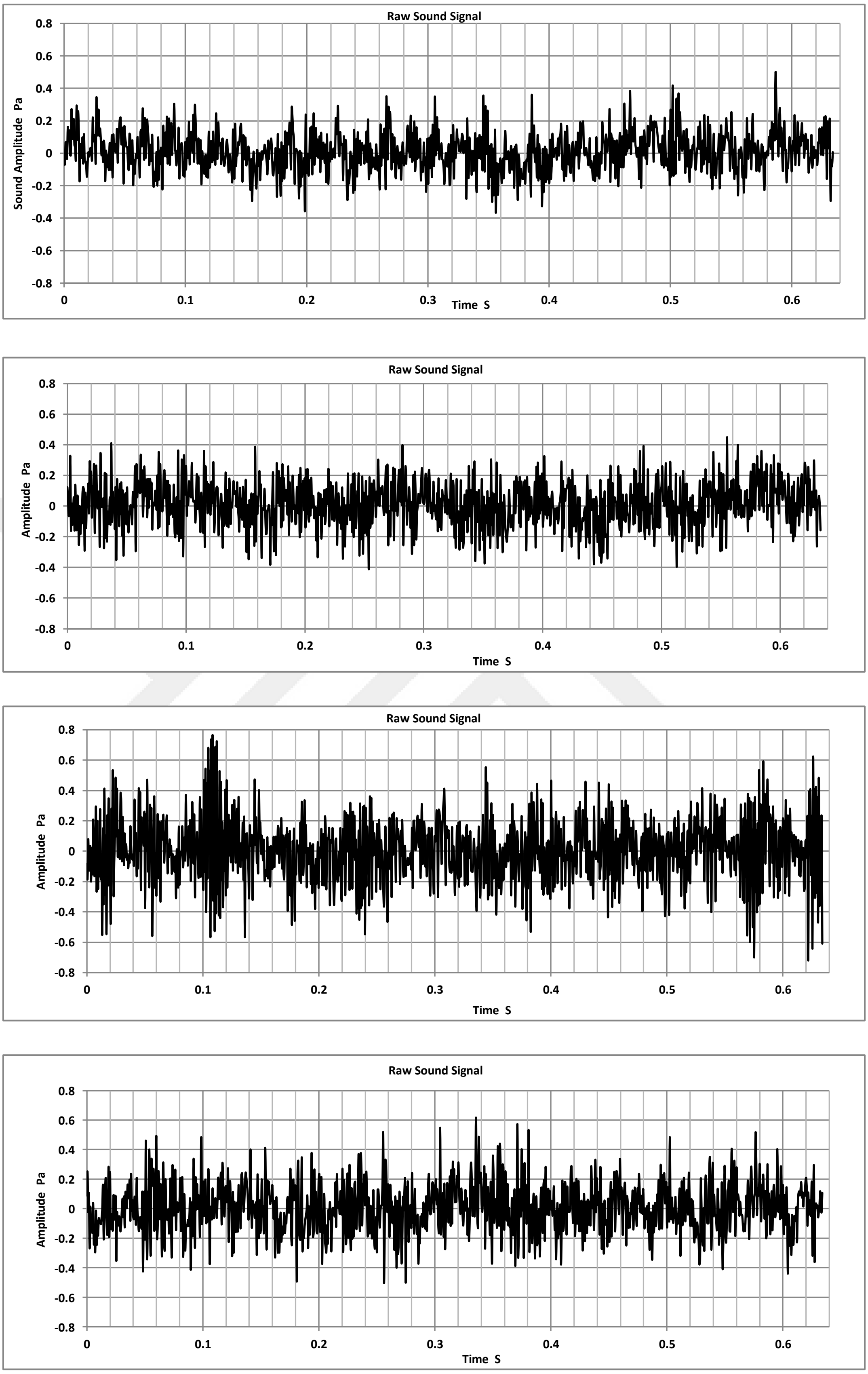

Figure 4.12 Sound signature at load P0 & 1495 rpm (a) Healthy bearing signature (b) Inner race defect signature (c) Outer race defect signature (d) Ball defect signature

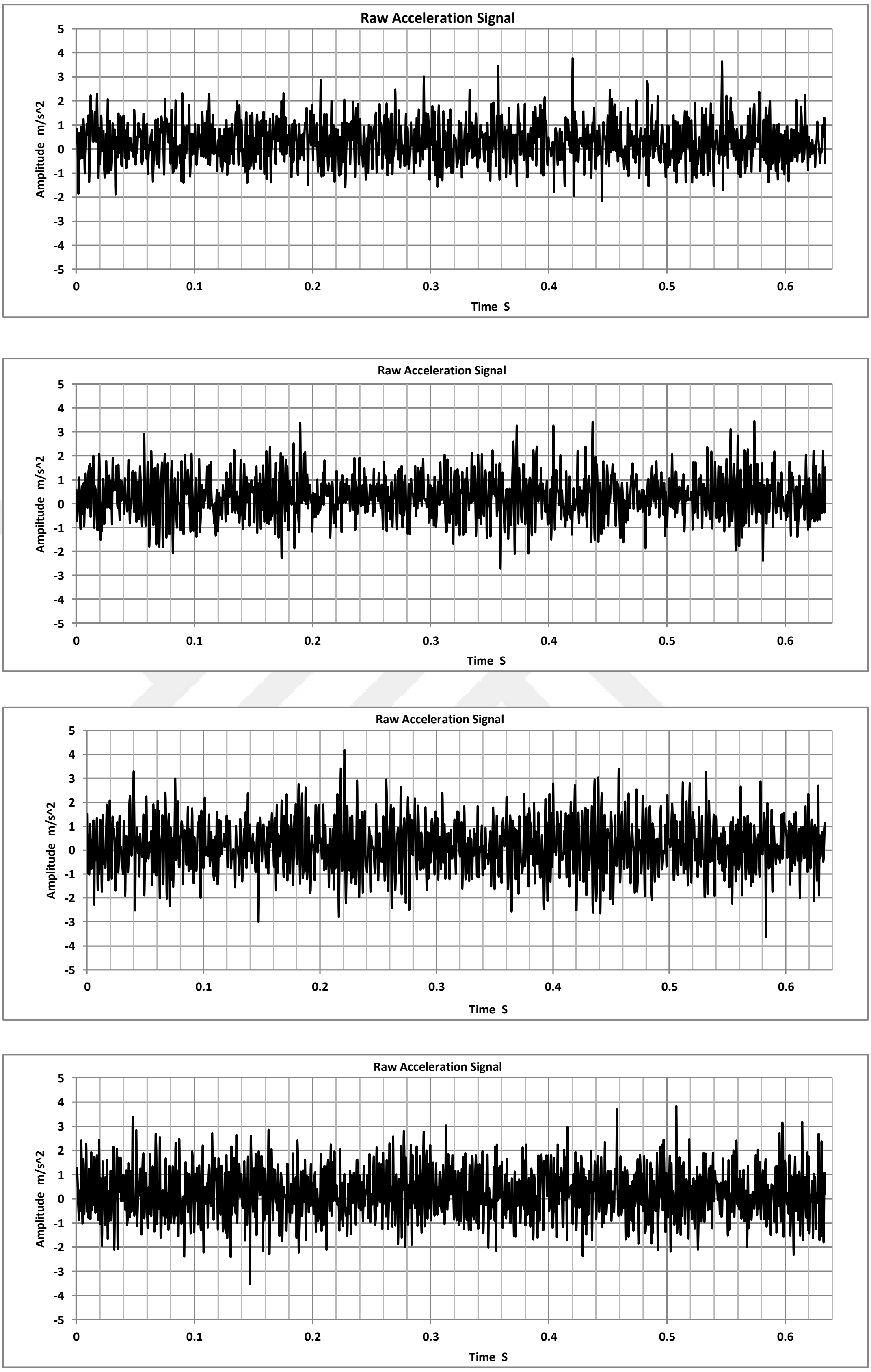

Figure 4.13 Acceleration signature at load P1 & 610 rpm (a) Healthy bearing signature (b) Inner race defect signature (c) Outer race defect signature (d) Ball defect signature.

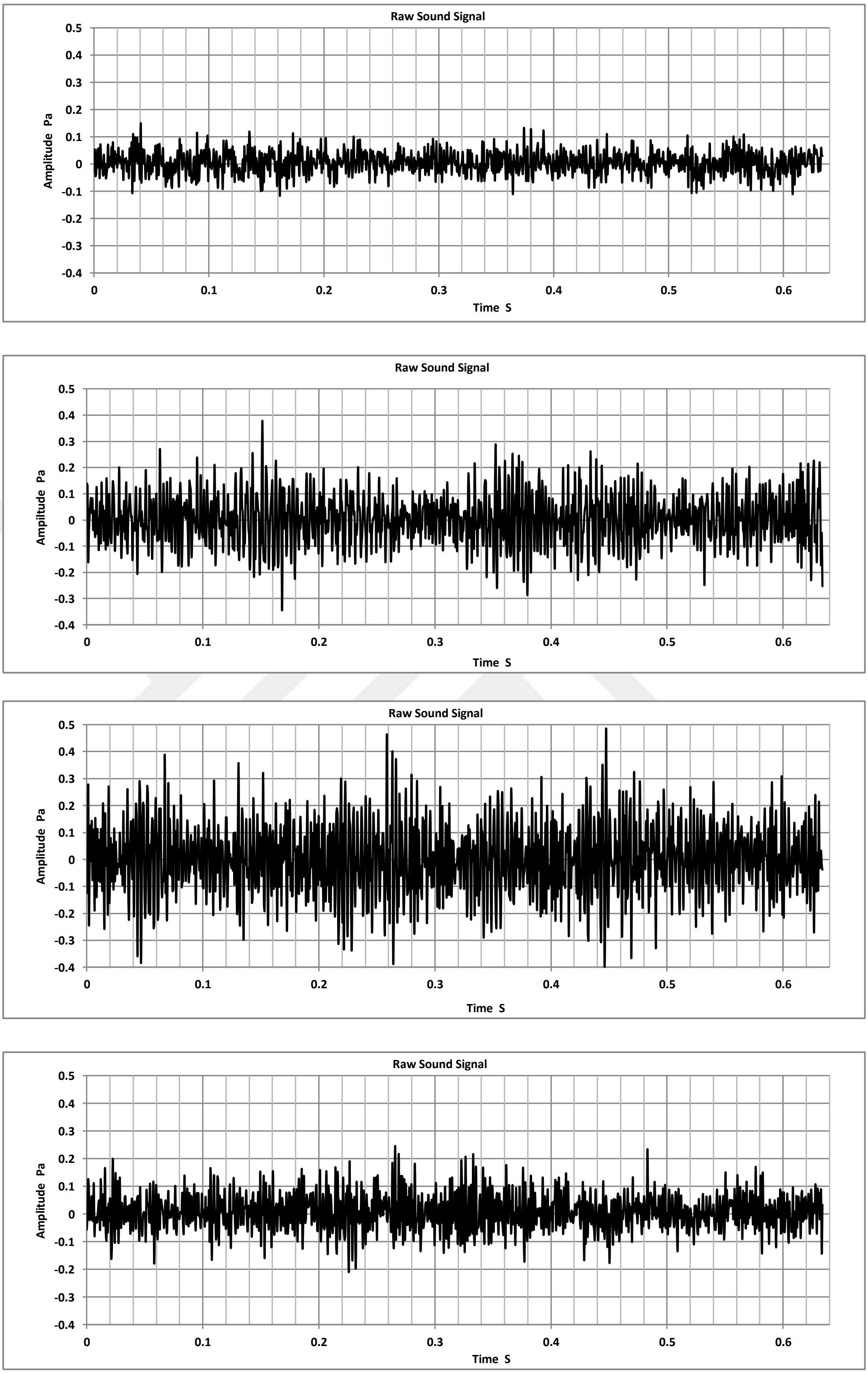

Figure 4.14 Sound signature at load P1 & 610 rpm (a) Healthy bearing signature (b) Inner race defect signature (c) Outer race defect signature (d) Ball defect signature.

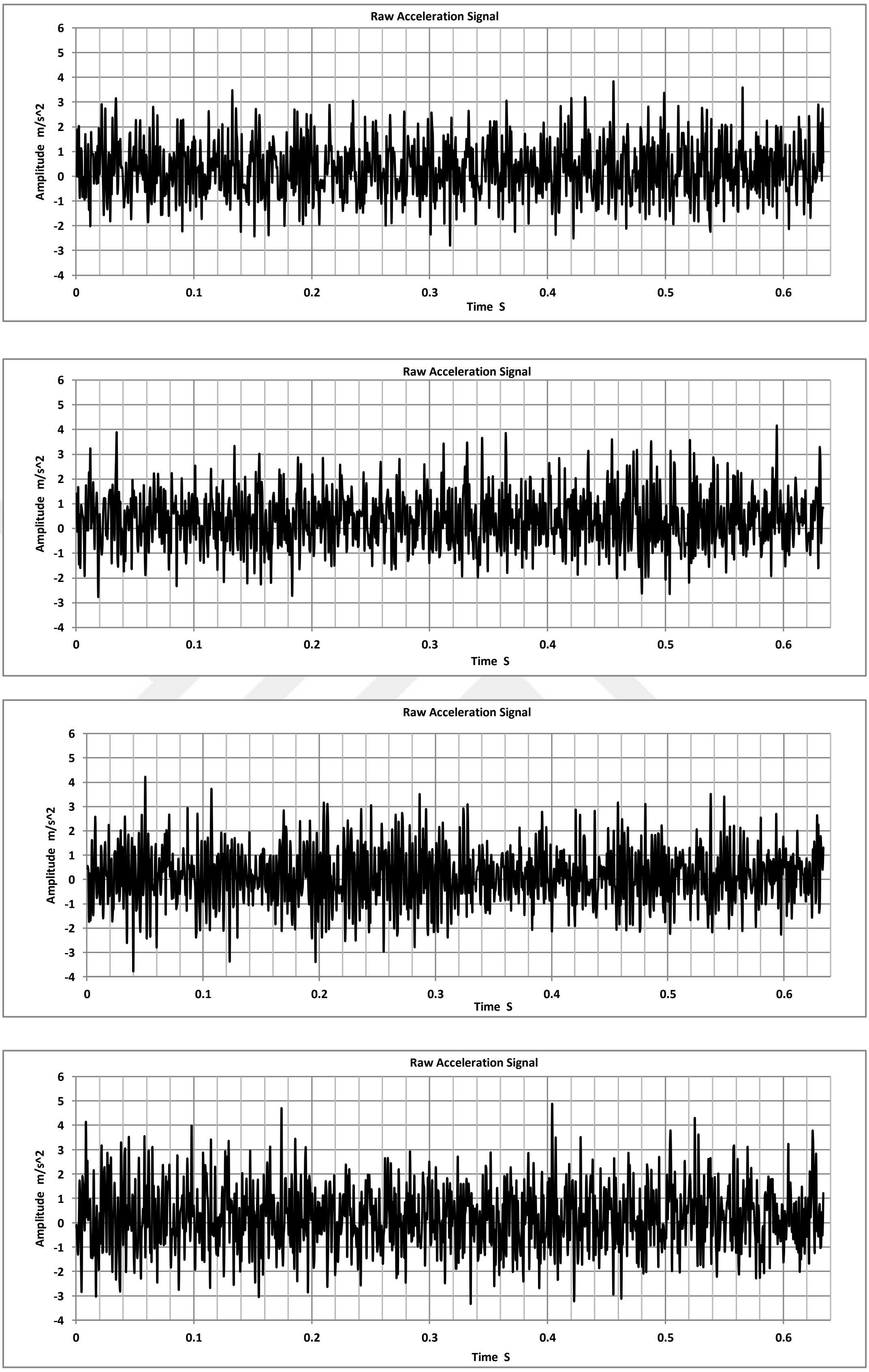

Figure 4.15 Acceleration signature at load P1 & 898 rpm (a) Healthy bearing signature (b) Inner race defect signature (c) Outer race defect signature (d) Ball defect signature.

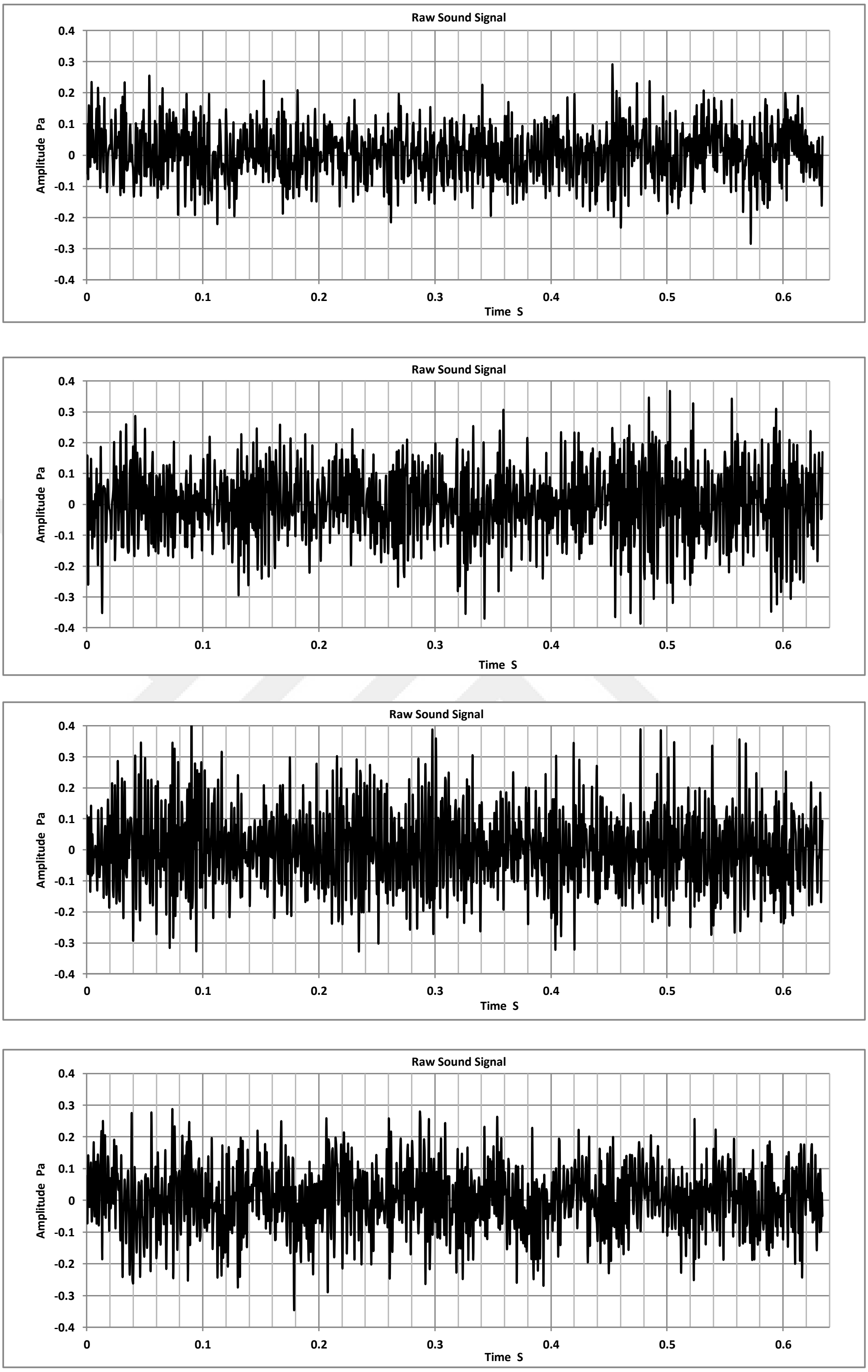

Figure 4.16 Sound signature at load P1 & 898 rpm (a) Healthy bearing signature (b) Inner race defect signature (c) Outer race defect signature (d) Ball defect signature.

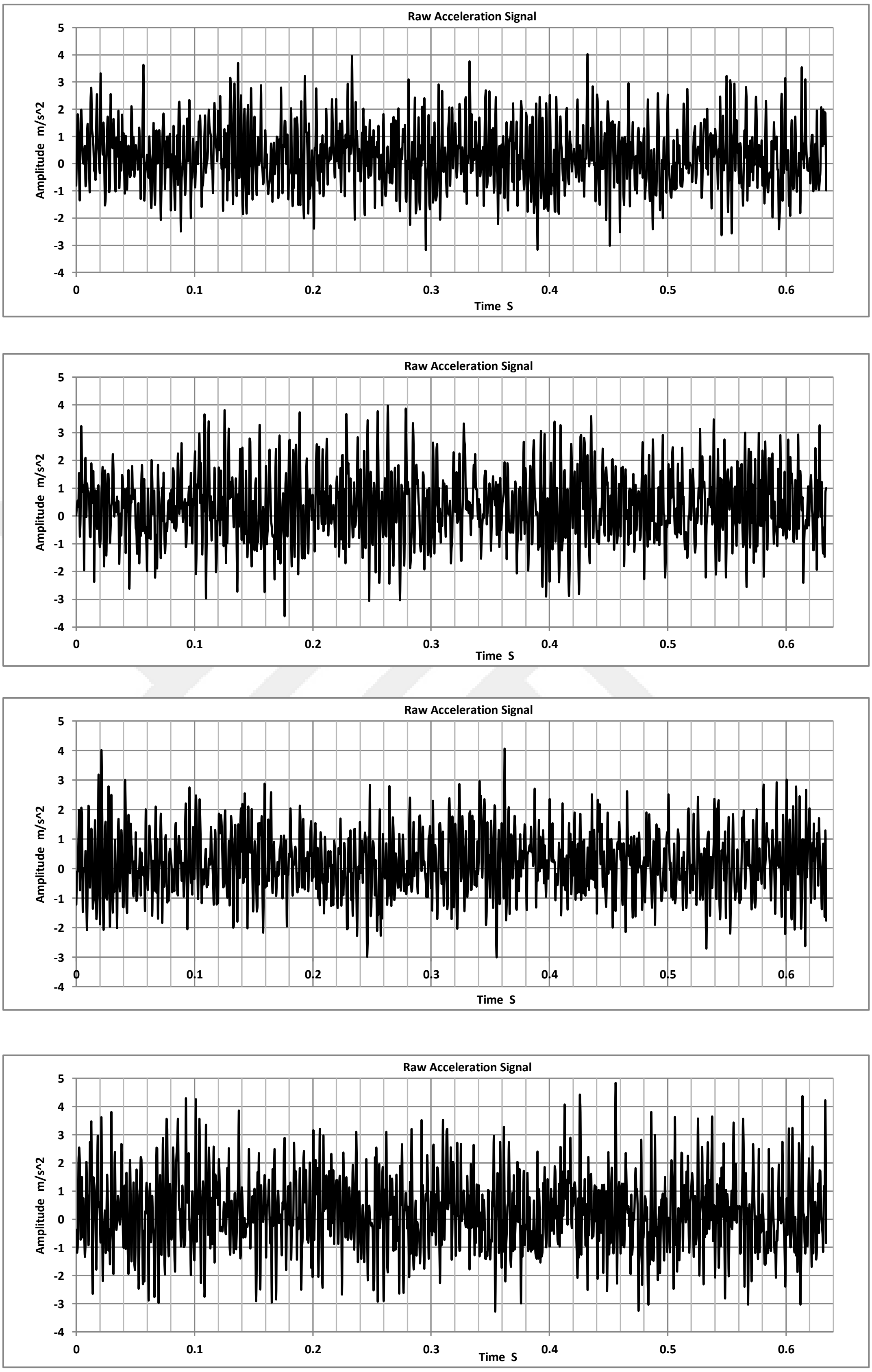

Figure 4.17 Acceleration signature at load P1 & 1224 rpm (a) Healthy bearing signature (b) Inner race defect signature (c) Outer race defect signature (d) Ball defect signature.

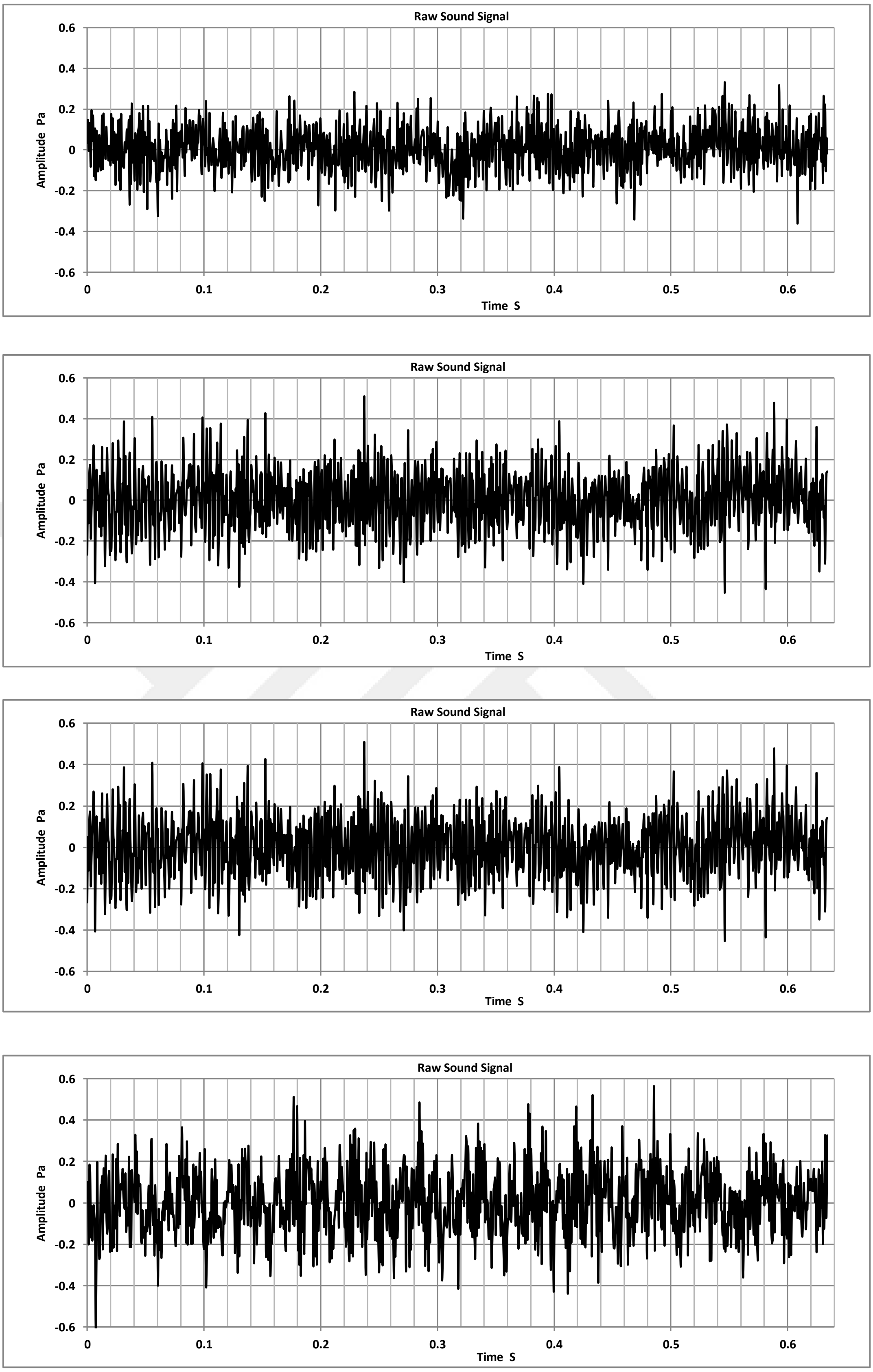

Figure 4.18 Sound signature at load P1 & 1224 rpm (a) Healthy bearing signature (b) Inner race defect signature (c) Outer race defect signature (d) Ball defect signature.

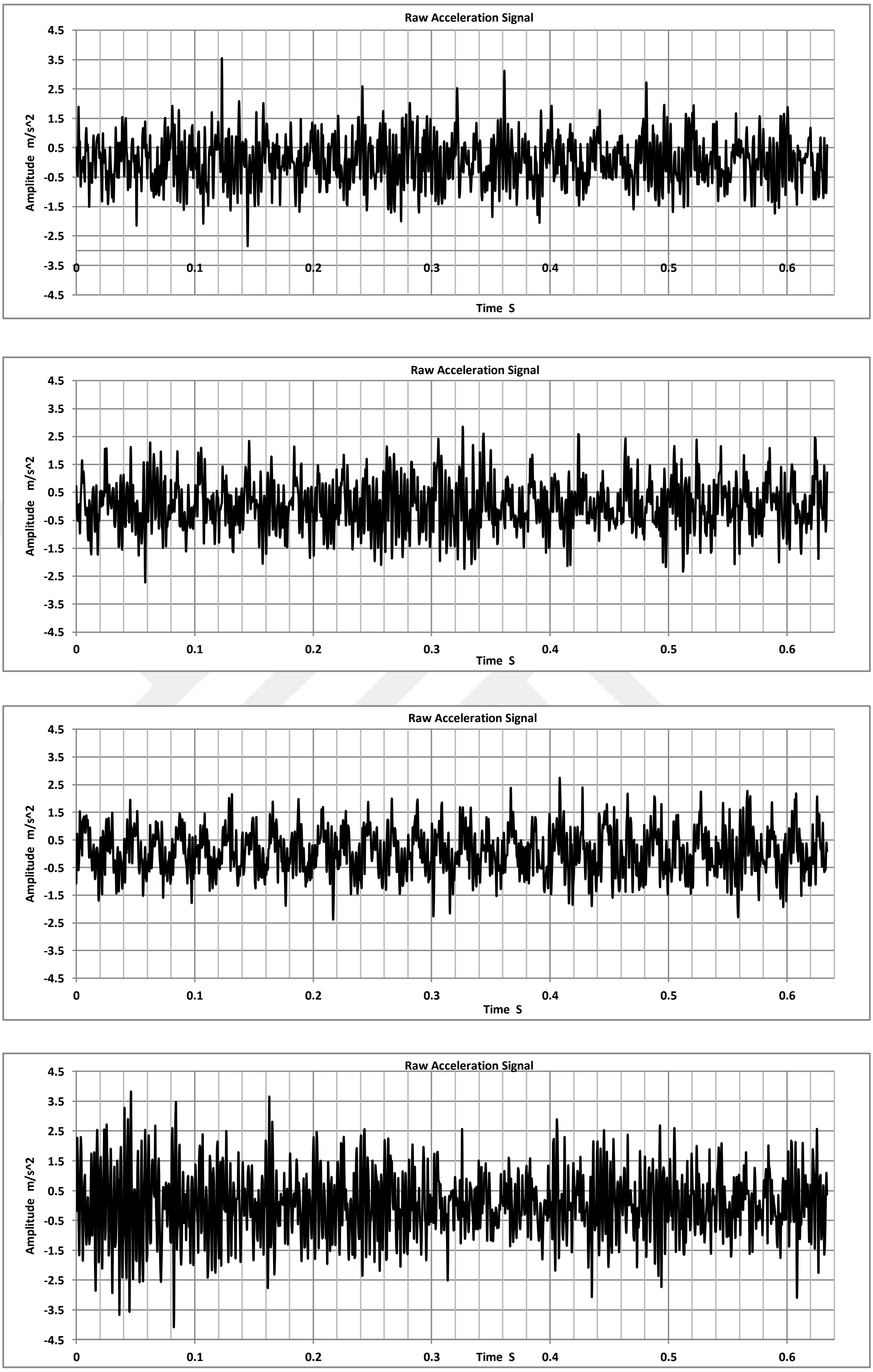

Figure 4.19 Acceleration signature at load P1 & 1495 rpm (a) Healthy bearing signature (b) Inner race defect signature (c) Outer race defect signature (d) Ball defect signature.

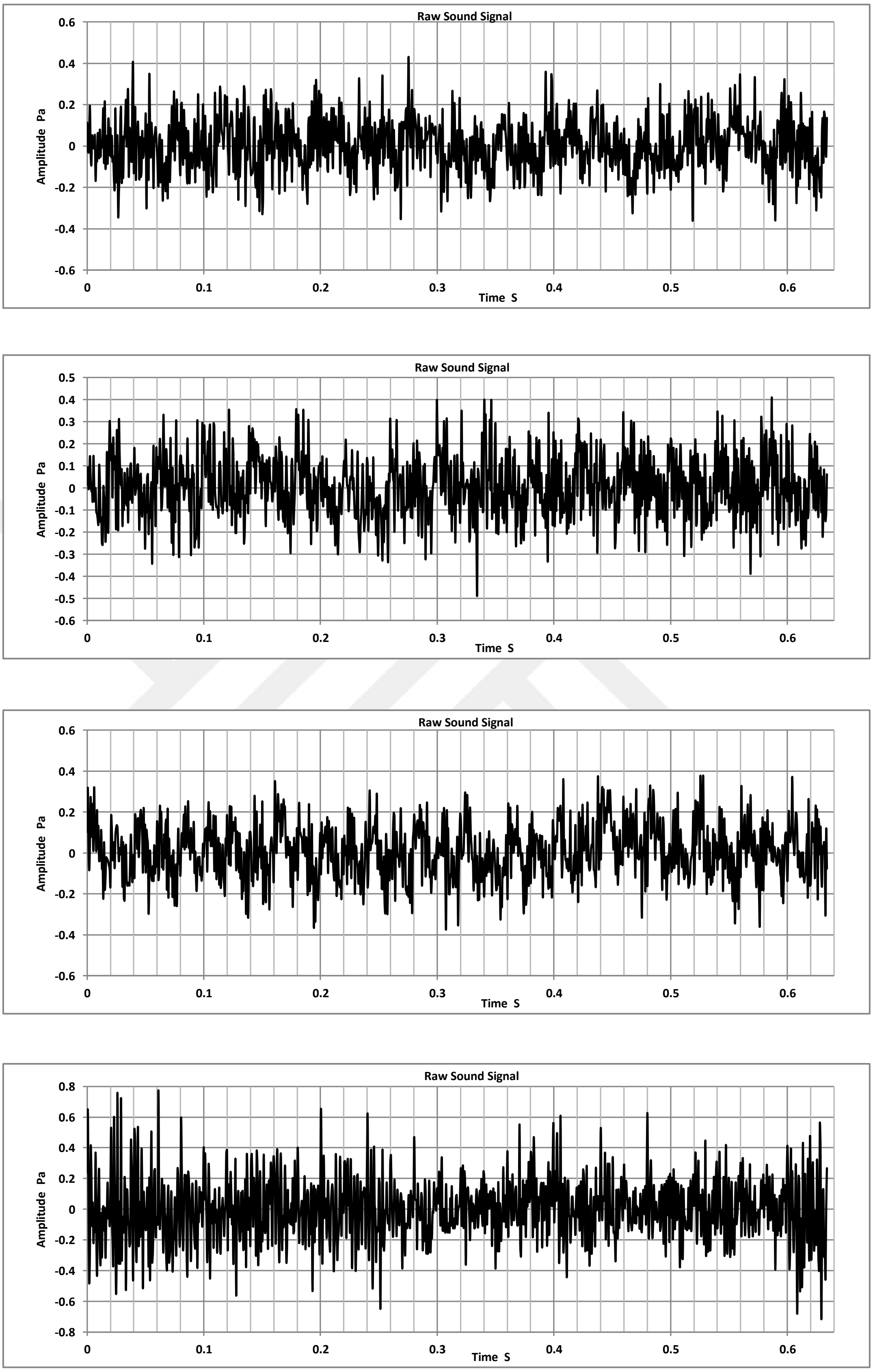

Figure 4.20 Sound signature at load P1 & 1495 rpm (a) Healthy bearing signature (b) Inner race defect signature (c) Outer race defect signature (d) Ball defect signature.

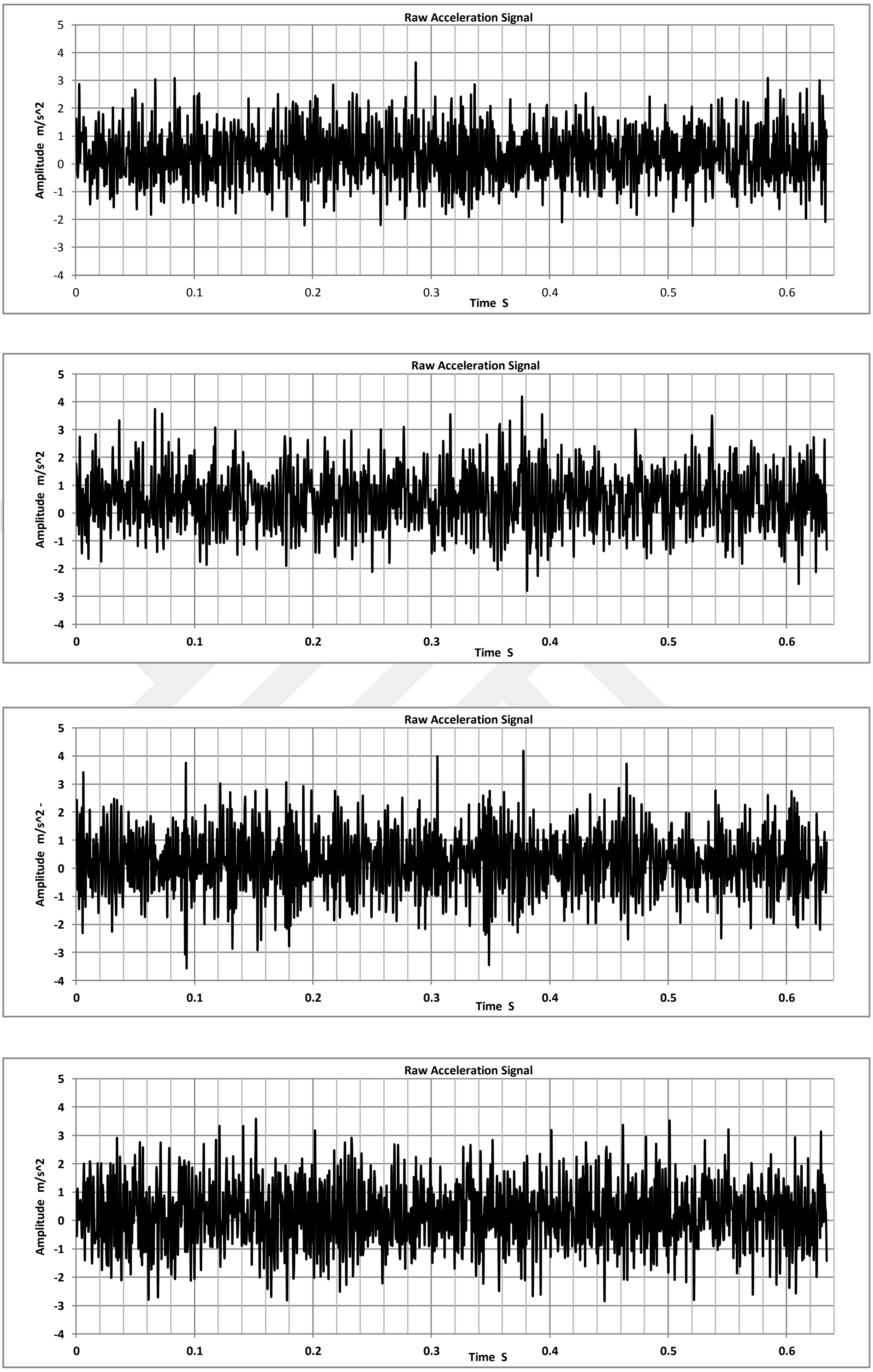

Figure 4.21 Acceleration signature at load P2 & 610 rpm (a) Healthy bearing signature (b) Inner race defect signature (c) Outer race defect signature (d) Ball defect signature.

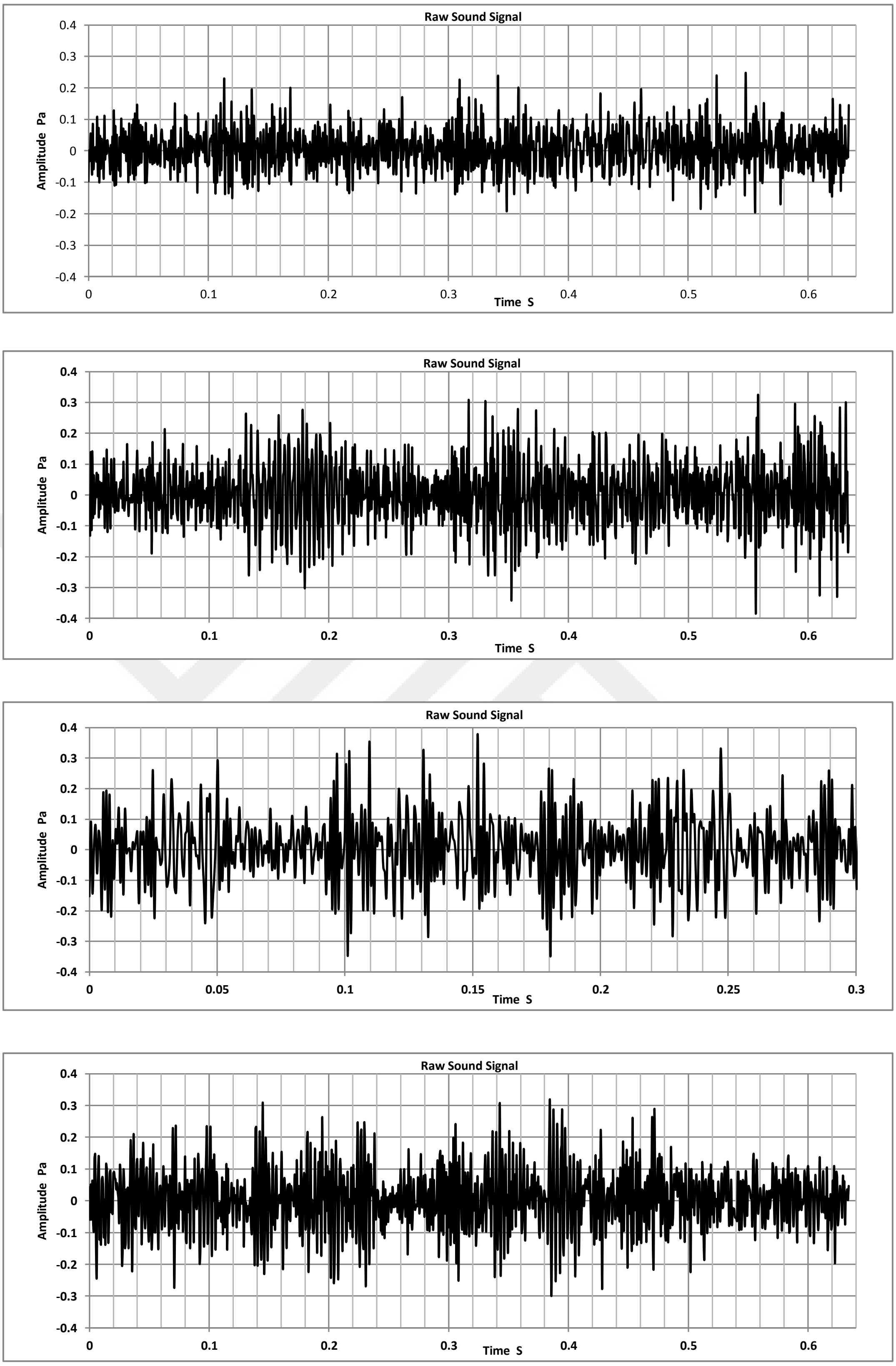

Figure 4.22 Sound signature at load P2 & 610 rpm (a) Healthy bearing signature (b) Inner race defect signature (c) Outer race defect signature (d) Ball defect signature.

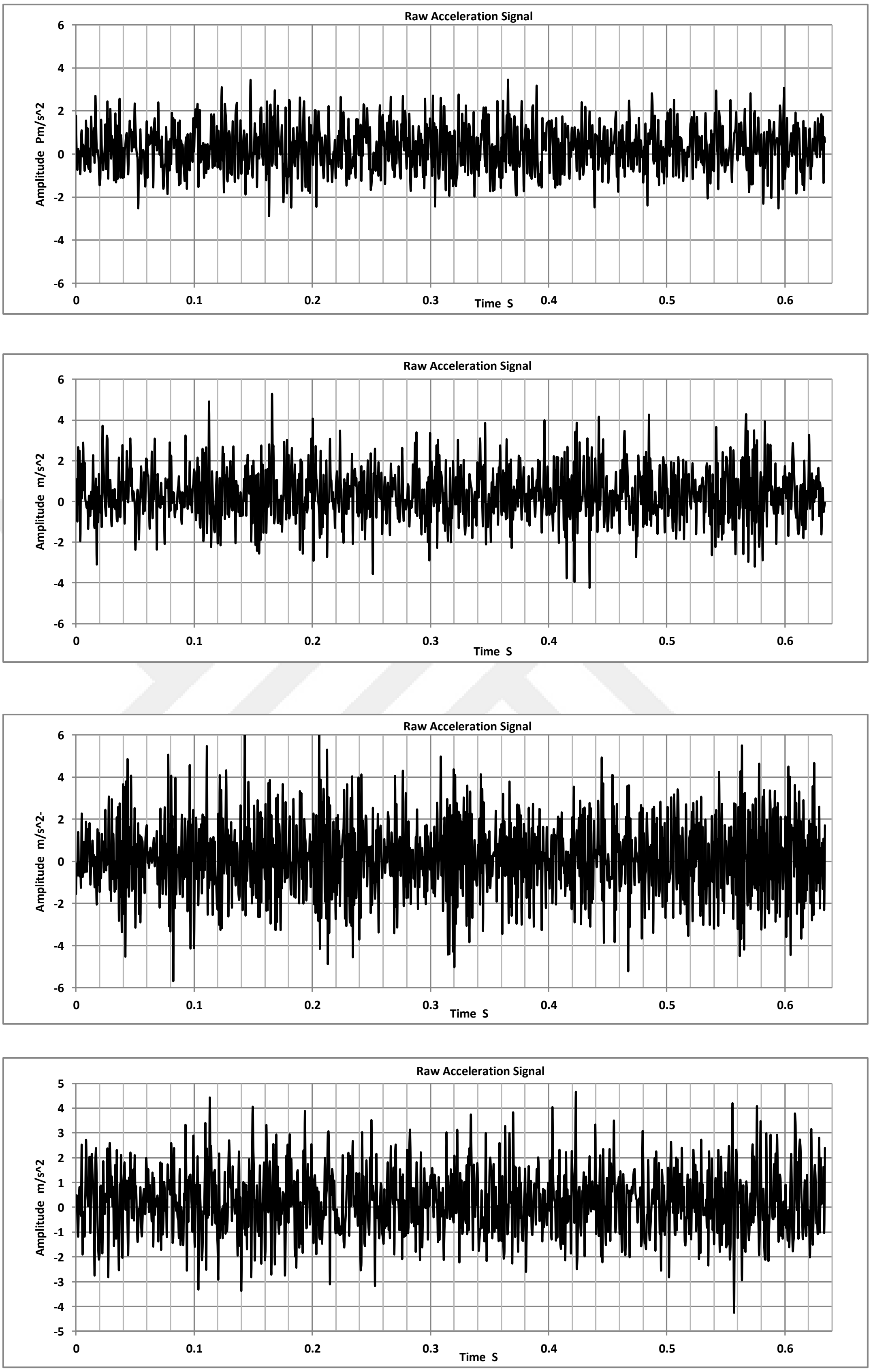

Figure 4.23 Acceleration signature at load P2 & 898 rpm (a) Healthy bearing signature (b) Inner race defect signature (c) Outer race defect signature (d) Ball defect signature.

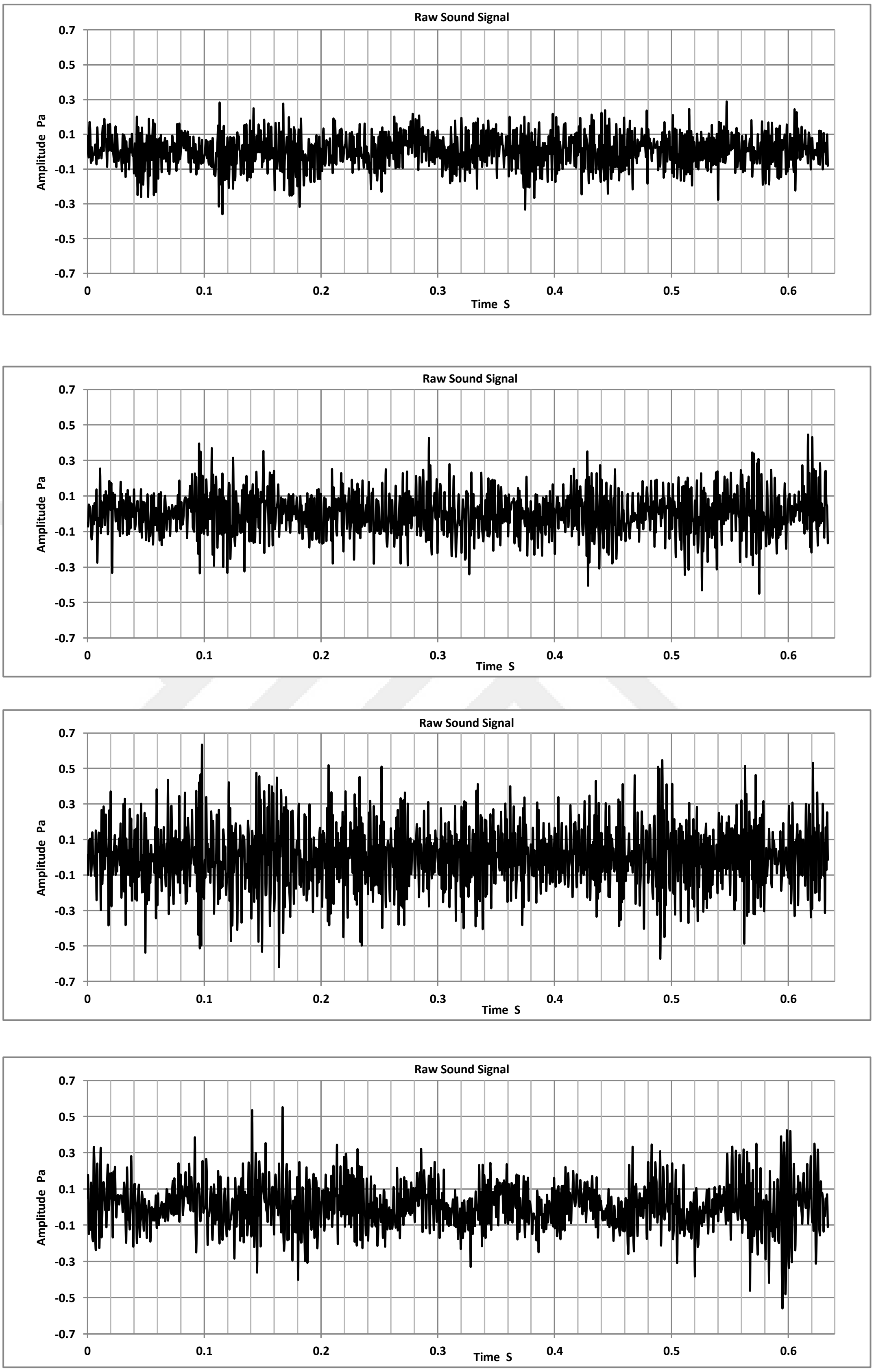

Figure 4.24 Sound signature at load P2 & 898 rpm (a) Healthy bearing signature (b) Inner race defect signature (c) Outer race defect signature (d) Ball defect signature.

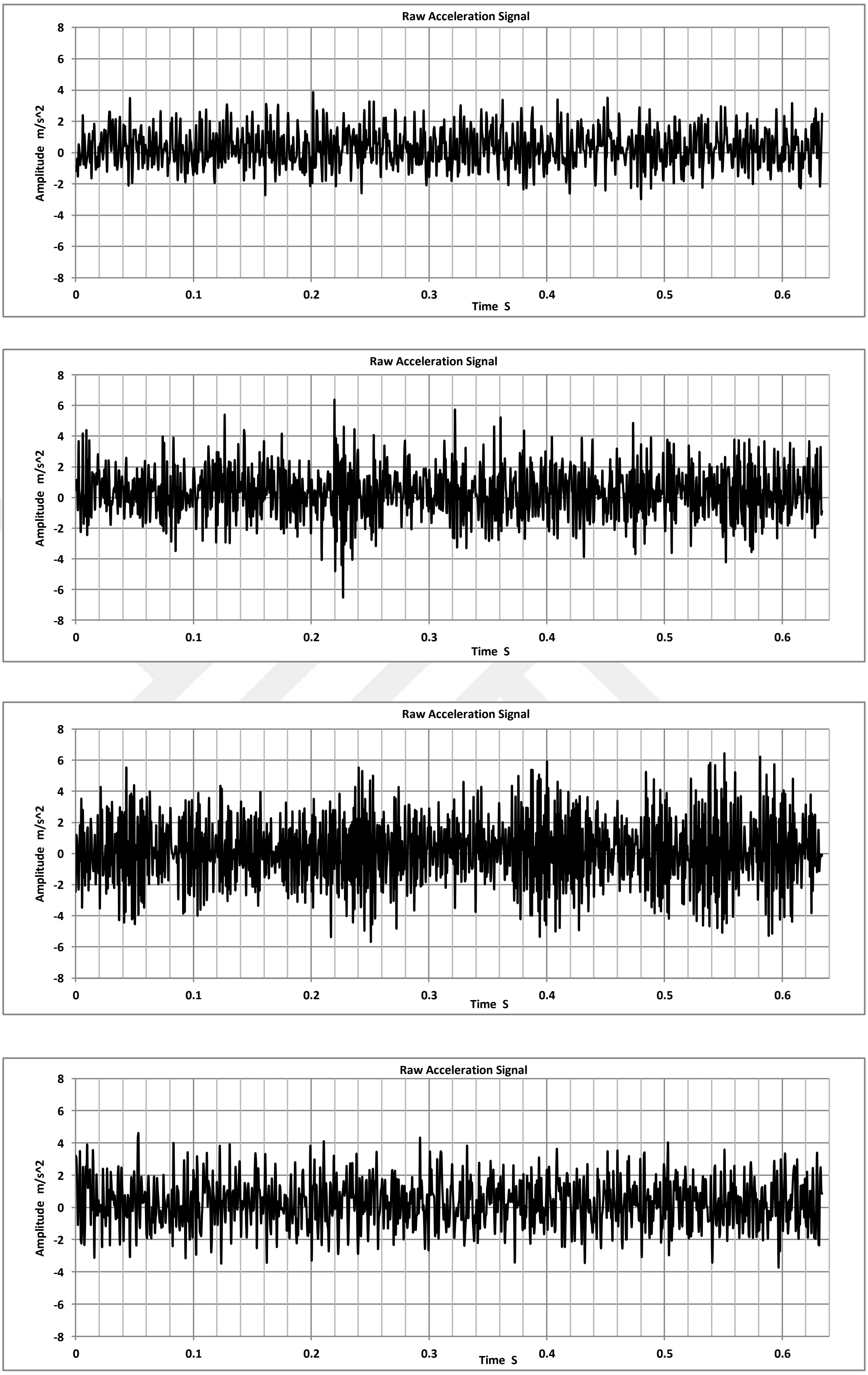

Figure 4.25 Acceleration signature at load P2 & 1224 rpm (a) Healthy bearing signature (b) Inner race defect signature (c) Outer race defect signature (d) Ball defect signature.

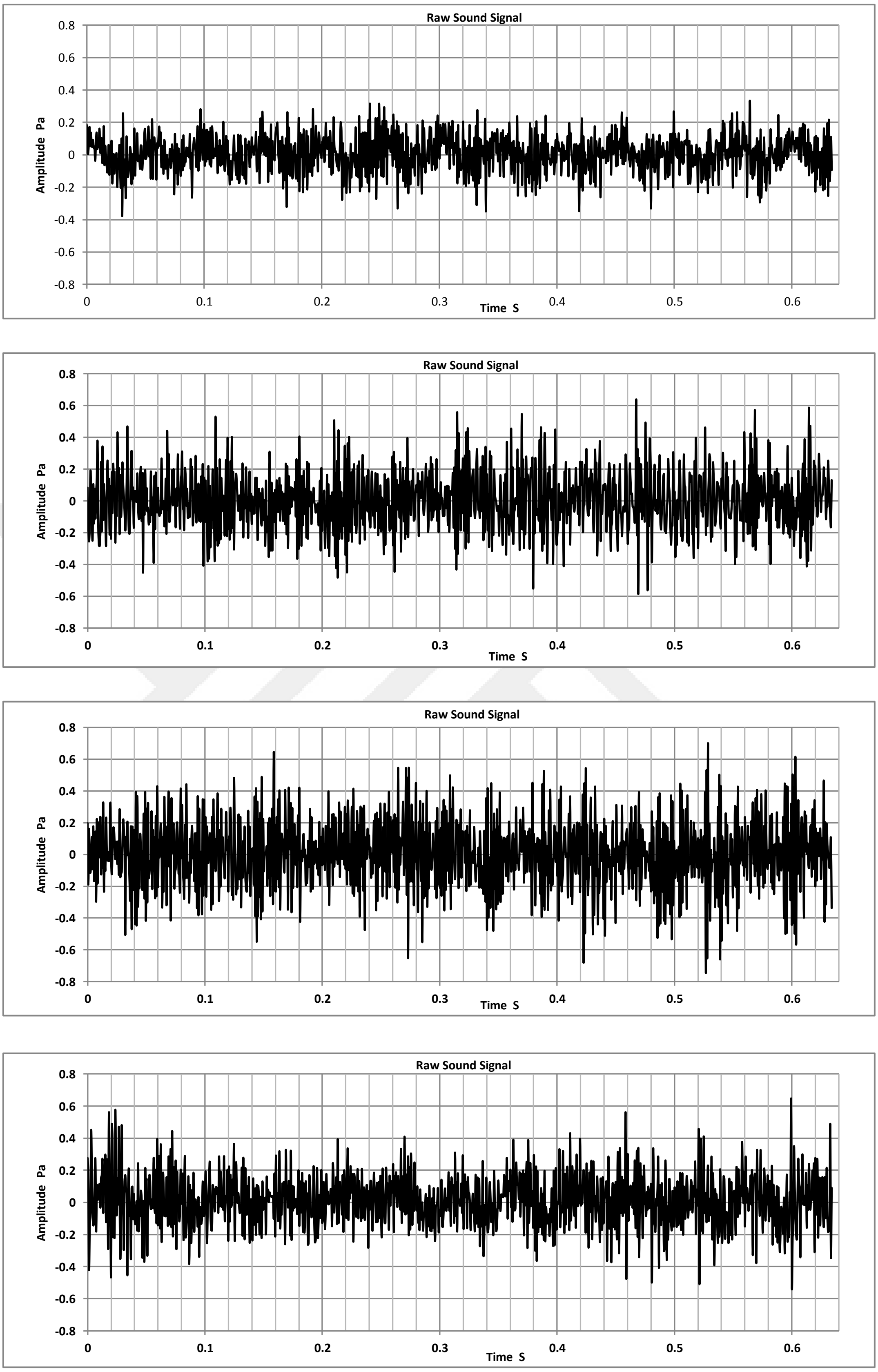

Figure 4.26 Sound signature at load P2 & 1224 rpm (a) Healthy bearing signature (b) Inner race defect signature (c) Outer race defect signature (d) Ball defect signature.

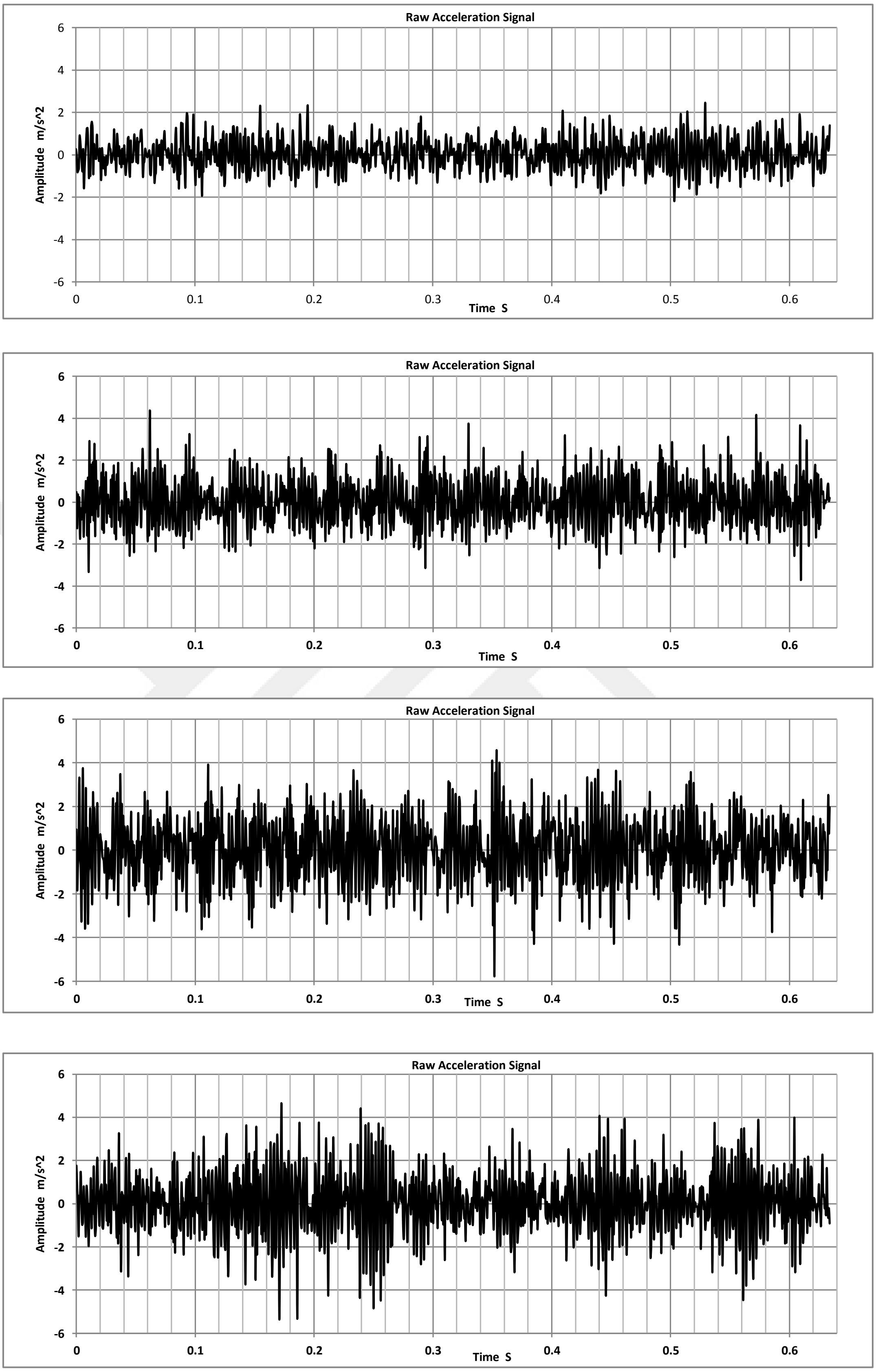

Figure 4.27 Acceleration signature at load P2 & 1495 rpm (a) Healthy bearing signature (b) Inner race defect signature (c) Outer race defect signature (d) Ball defect signature.

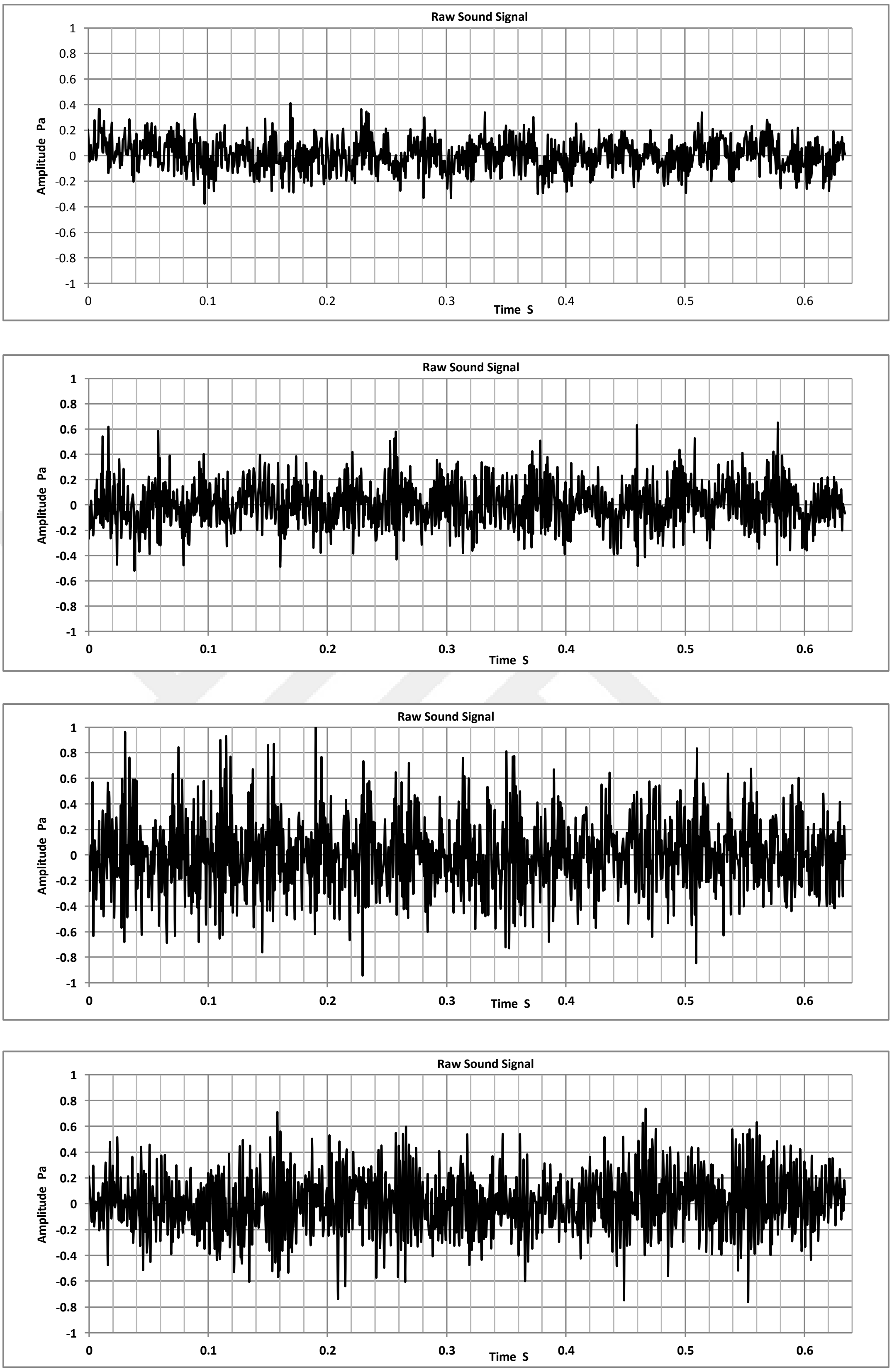

Figure 4.28 Sound signature at load P2 & 1495 rpm (a) Healthy bearing signature (b) Inner race defect signature (c) Outer race defect signature (d) Ball defect signature.

4.3.2 Statistical Analysis

Monitoring the general condition of the bearing can be done by examining the statistical parameters extracted from the acceleration and acoustic emission signals in the time domain. Figures 4.29 to 4.48 show the statistical parameters extracted from a fault-free bearing and a defective bearing, respectively. Time-domain statistical parameters are RMS, Crest Factor, Skewness, Kurtosis and Peak, etc.

4.3.2.1 RMS Results

One of the first ways to estimate the level of vibration is the root mean square value (RMS) of acceleration and the AE signature on the bearing housing. Figure 4.29 - 4.33 show measured RMS values for Acoustic emission and vibration signals for a and defective bearings.

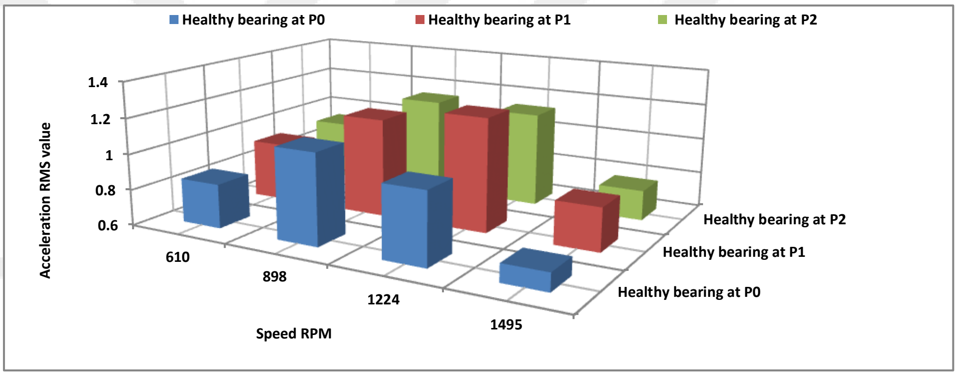

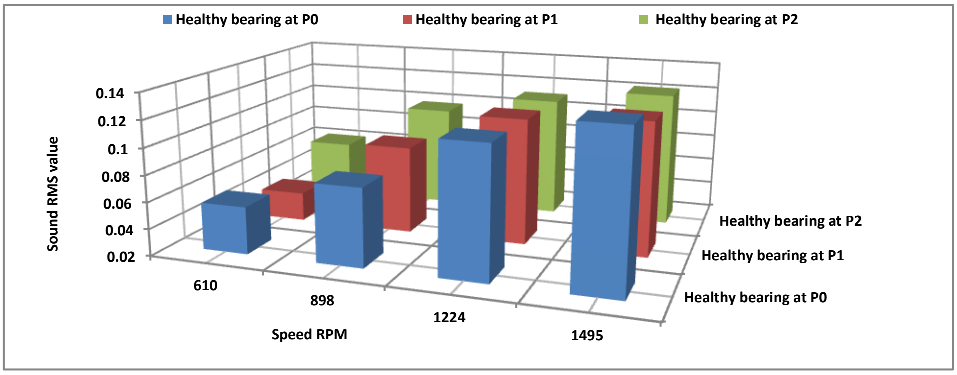

Figure 4.29 RMS value for healthy case signature at different load (a) Acceleration signal RMS (b) Sound signal RMS

Figures 4.29a and 4.29b show the RMS feature of the acceleration and acoustic emission signals for defective bearings at different loads and speeds. Figure 4.29a shows that the RMS of the AE signal increases with increasing speed and load, while

Figure 4.29b shows that the vibration signal also increases with speed and load, but reaches the maximum amplitude and then decreases at speed 1224 rpm.

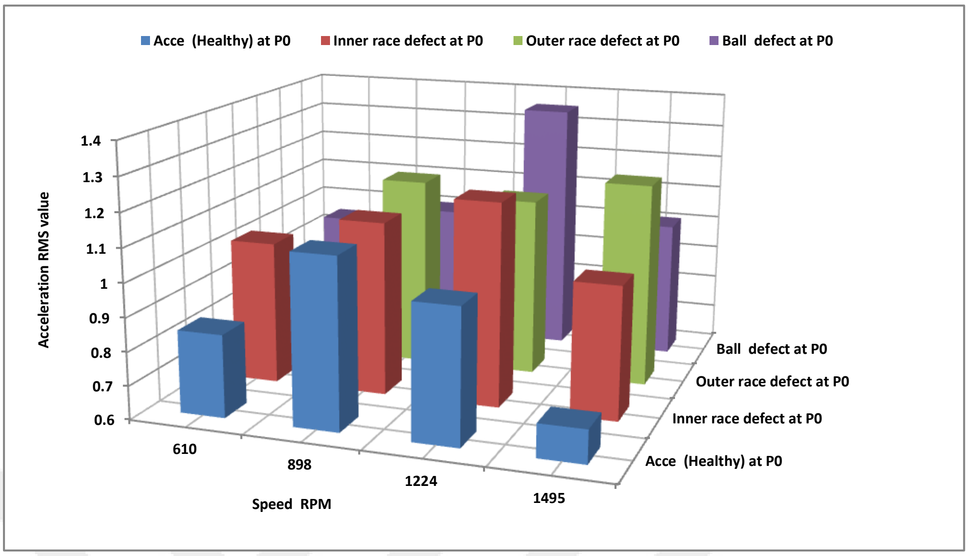

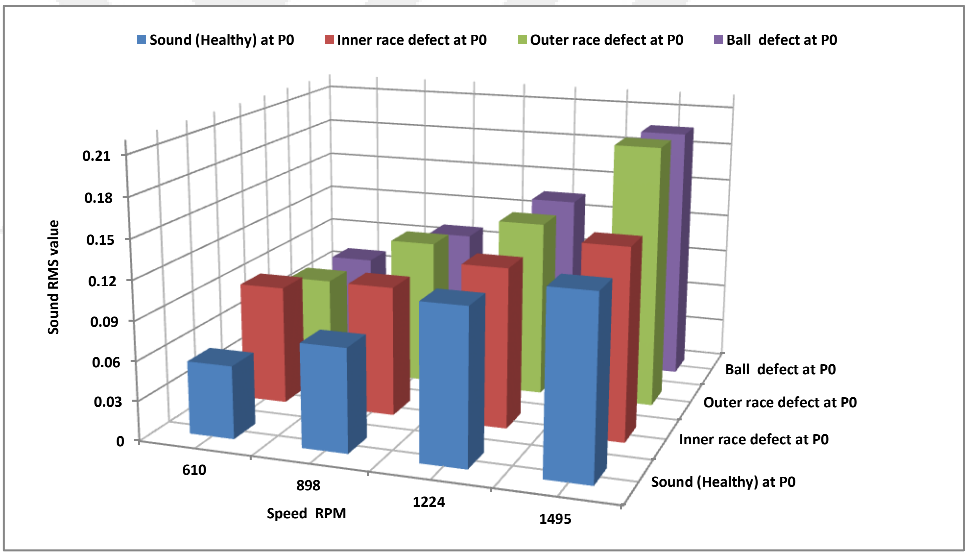

Figure 4.30 RMS feature for (a) Acceleration signal (b) Sound signal at load P0 and defect in different locations (ball, outer race, inner race).

Figures 4.30a and 4.3b show that the values of RMS is a good indicator for faults monitoring in all cases, except at 898 rpm for the ball defect, where the value decreases as shown in Figure 4.30a.

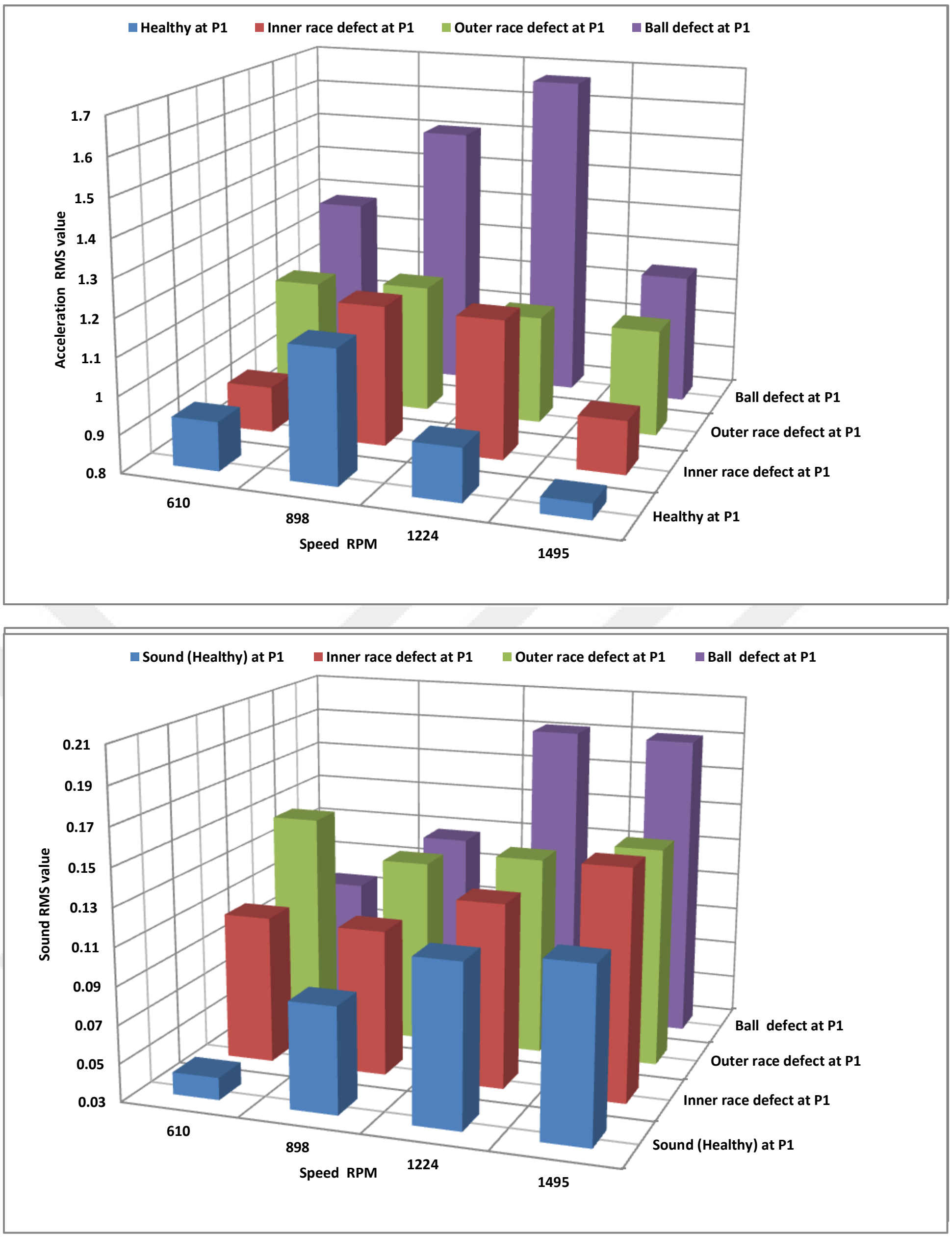

Figure 4.31 RMS feature for (a) acceleration signal (b) sound signal at load P1 and defect in different locations.

Figures 4.31a and 4.31b show that the values of RMS is a good indicator for faults monitoring in all cases especially for ball defect, except at low-frequency range of the inner race defect signature, where decreases below the RMS for healthy case as shown in Figure 4.31a.

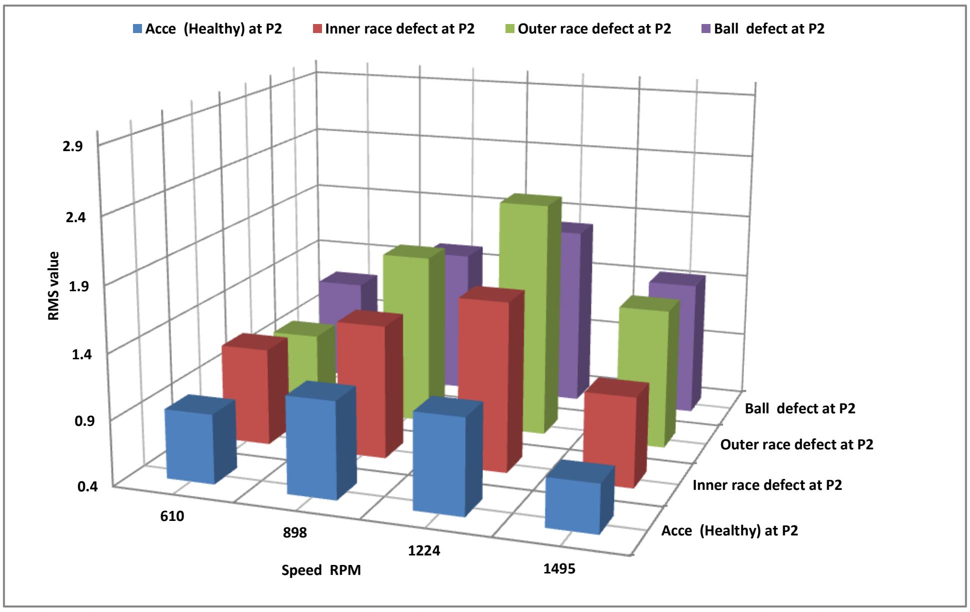

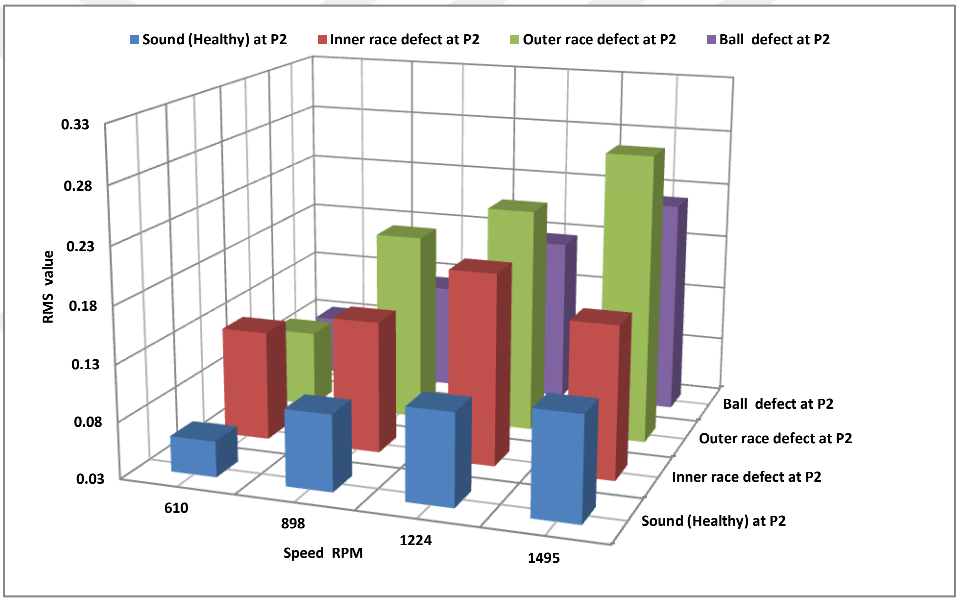

Figure 4.32 RMS feature for (a) acceleration signal (b) sound signal at load P2 and defect in different locations.

Figures 4.32a and 4.32b shows that RMS value is a good indicator for bearing faults monitoring in all cases.

4.3.2.2 Crest Factor Result

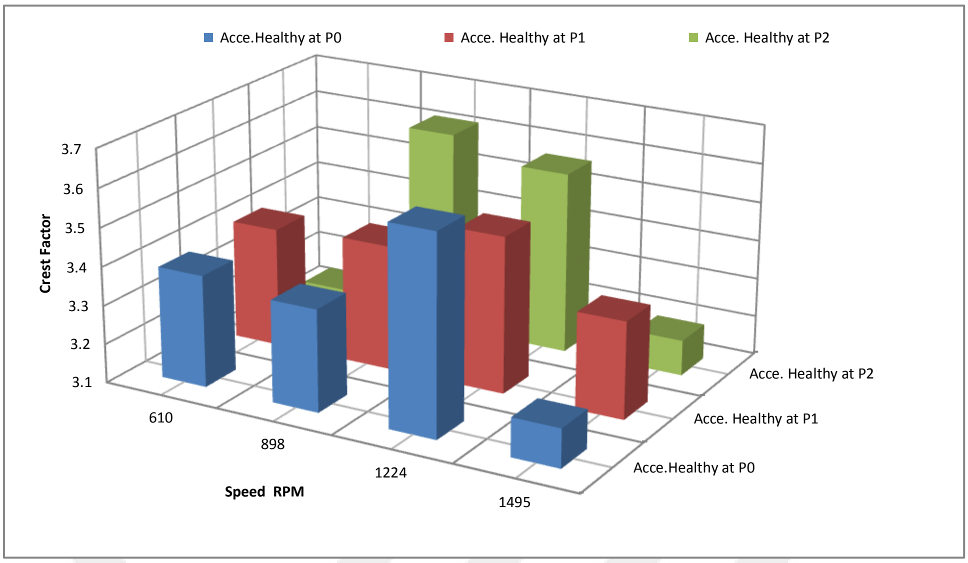

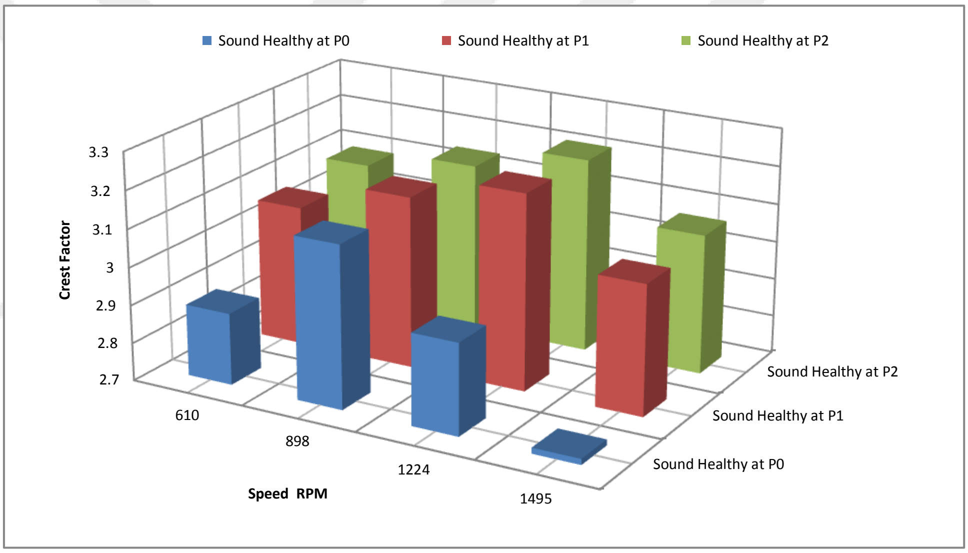

Figure 4.33 Crest factors for healthy case signature at different load (a) Acceleration Crest Factors (b) Sound Crest Factors.

Figure 4.33a shows that the crest factor of vibration signal that calculated from the fault-free bearing increases when the load increases, as in the load P1. While decreases in the case of P2 load, except for speed 1495 rpm. As for the acoustic emission signal, there is an increase in the crest factor value with the load increase for almost all speeds, except at 1495 rpm and at loading P1 as shown in Figure 4.33b.

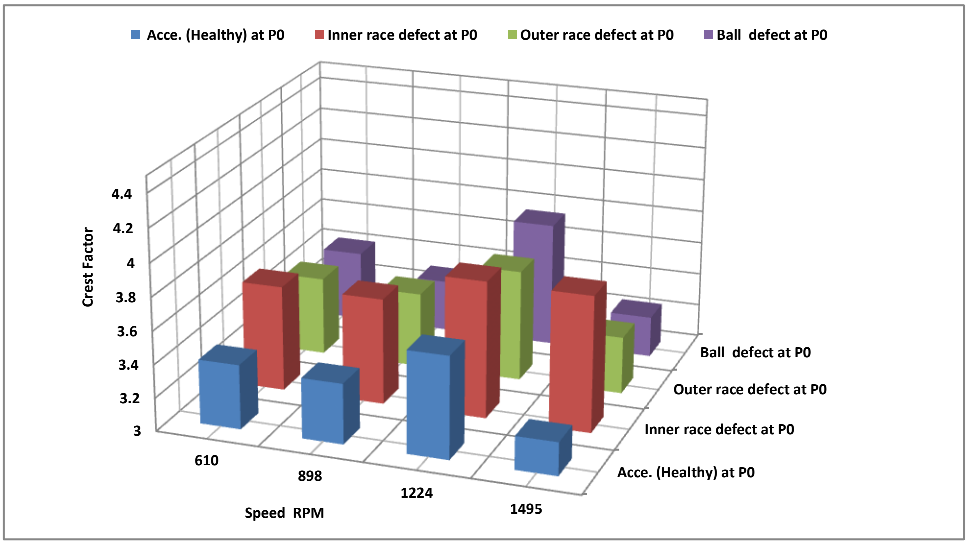

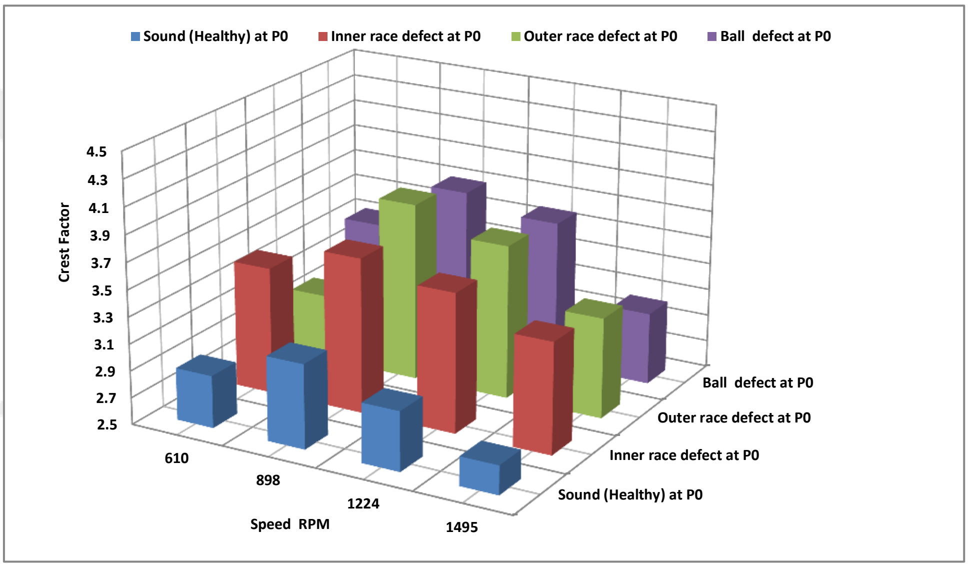

Figure 4.34 Crest factors feature for (a) Acceleration signal (b) Sound signal at load P0 and defects in different locations.

Figure 4.34 shows that crest factor of all defects, increases directly with speed at load level P0, except the case of a ball faulty, where the crest factor decreases at 898 RPM. For sound signals, it is worth noting that the crest factor is a very reliable indicator at most speeds, showing a relatively constant increase in each case compared with the fault-free bearing.

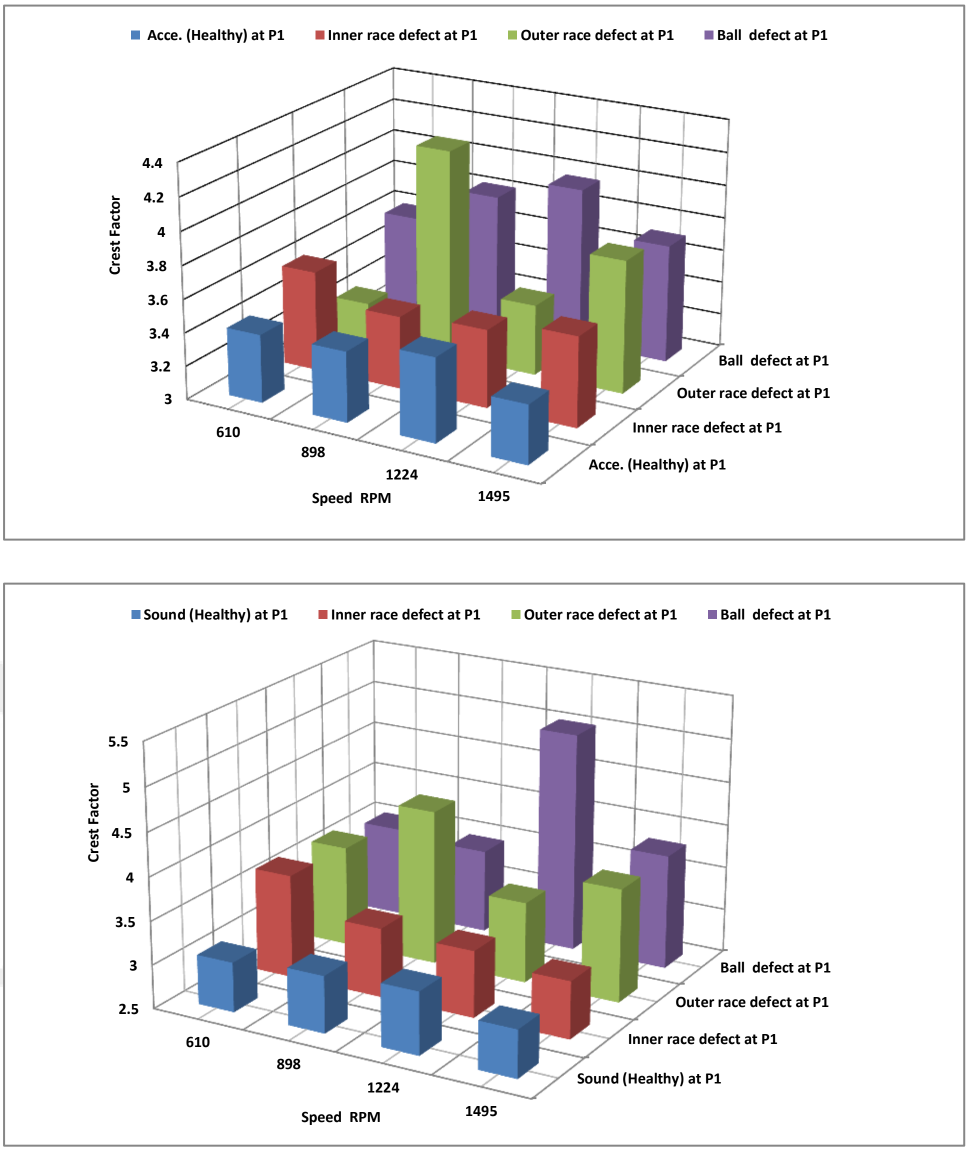

Figure 4.35 Crest factors feature for (a) Acceleration signal (b) Sound signal at load P1 and defects in different locations.

The acceleration signal crest factor is a good indicator for the defect of a defective ball bearing at all speeds, but for other defects, it is an indicator of some cases, for example at speed (898, 1495) rpm for defective bearing in the outer race, at speed (612, 1495) rpm in the inner race at load P1 as shown in Figure 4.35b. In all cases, the crest factor of acoustic emissions is a good indicator of bearing defects.

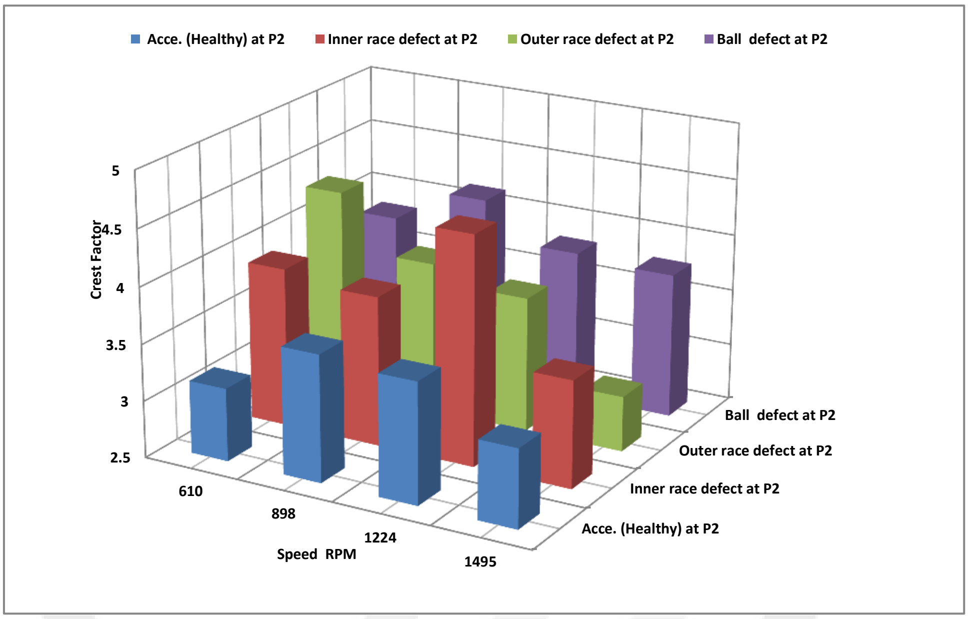

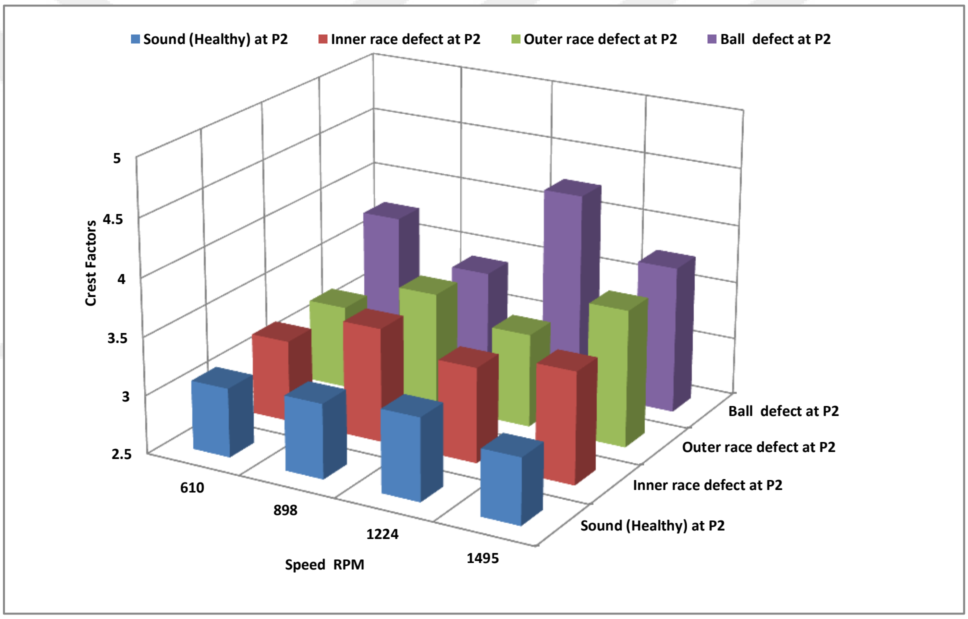

Figure 4.36 Crest factors feature for (a) Acceleration signal (b) Sound signal at load P2 and defects in different locations**.**

Figure 4.36a shows that in all defect cases, the crest factor of the acceleration signal increases significantly with speed, except the speed of 1495 rpm for the outer race defects. For sound signals, the crest factor is a good indicator of defects in all cases and all speeds, as shown in Figure 4.36b.

4.3.2.3 The Skewness Results

Skewness, in statistics, is a degree of distortion from the symmetrical, or a normal distribution, in a set of data. Skewness can be negative, positive, zero or undefined. A normal distribution has a zero deviation, while the other distributions show a degree of skewed to the right or left. In fact, the negative skewness means that the statistical distribution is skewed to the left and the tail on the left hand side is longer than the tail on the right hand side and in this condition, the mean is less than the mode. Once the right tail of the distribution is longer than its left tail, then the distribution is right skewed and in this condition the mean is greater than the mode. Such distribution result in positive skewness. Figures 4.37- 4.40 show the skewness feature calculated from 48 experiments related to three classes of faults compared with healthy case.

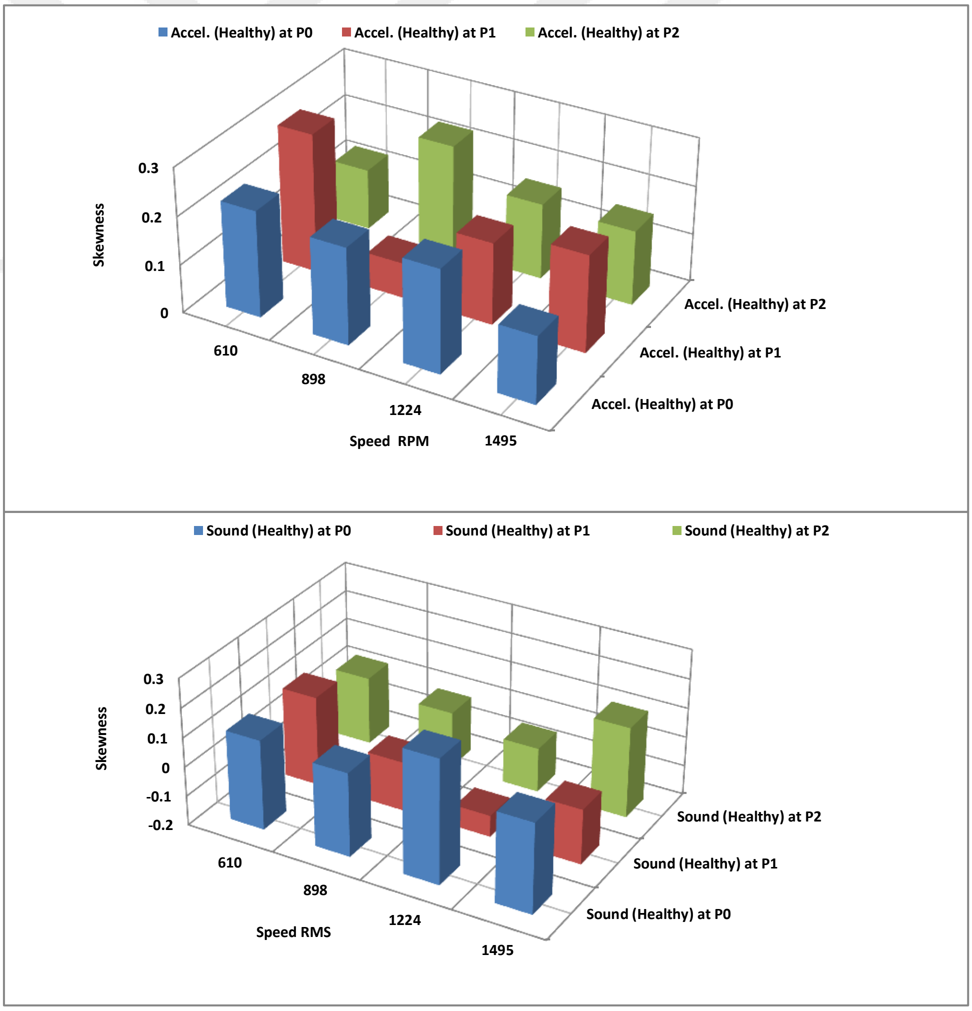

Figure 4.37 Skewness feature for healthy case signature at different load (a) Acceleration skewness (b) Sound skewness.

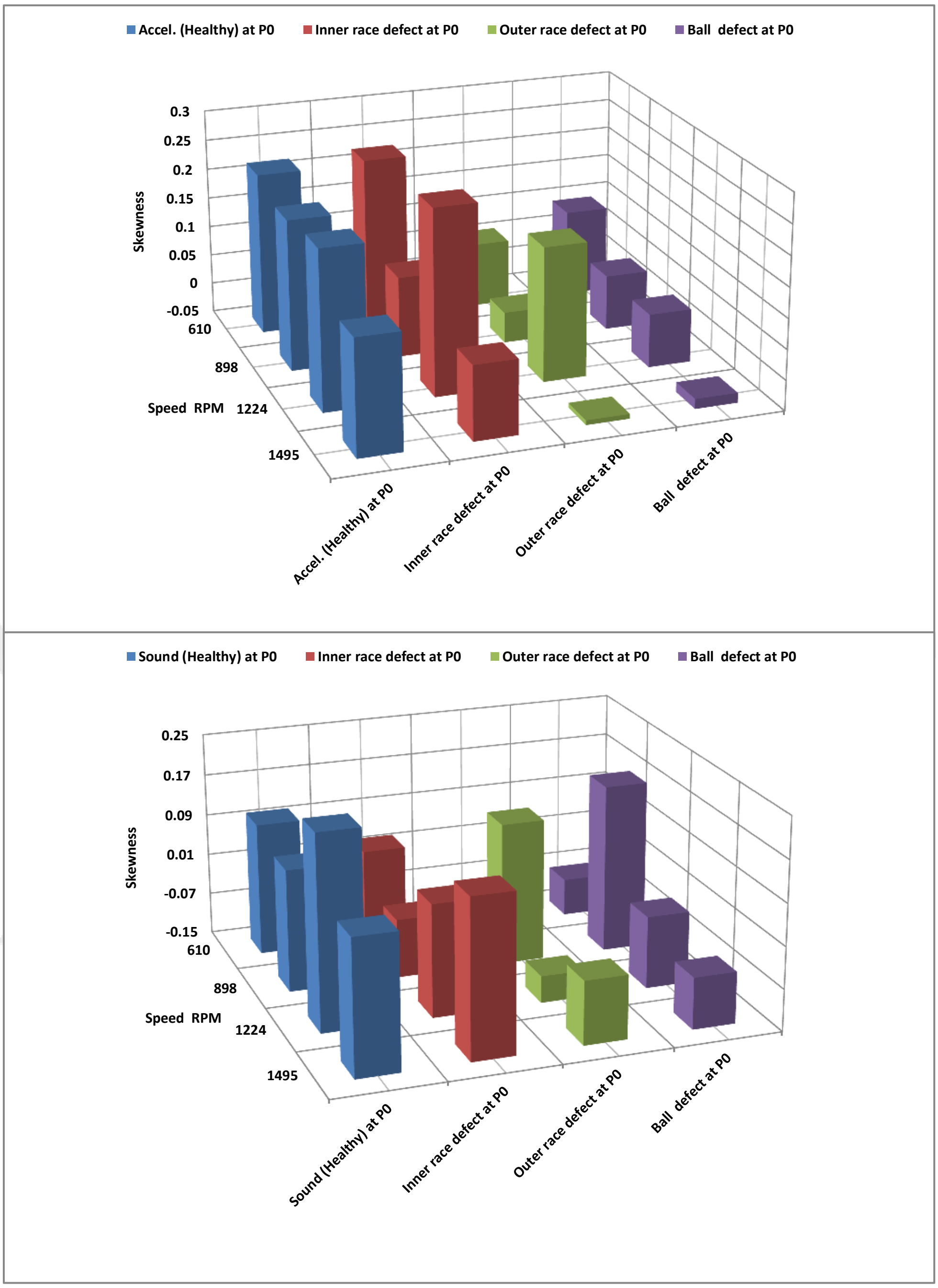

Figure 4.38 Skewness feature for (a) Acceleration signal (b) Sound signal at load P0 and defects in different locations.

Virtually all readings of skewness feature for both accelerometer signal and acoustic emission signal are lower than the healthy case values as shown in Figure 4.38.

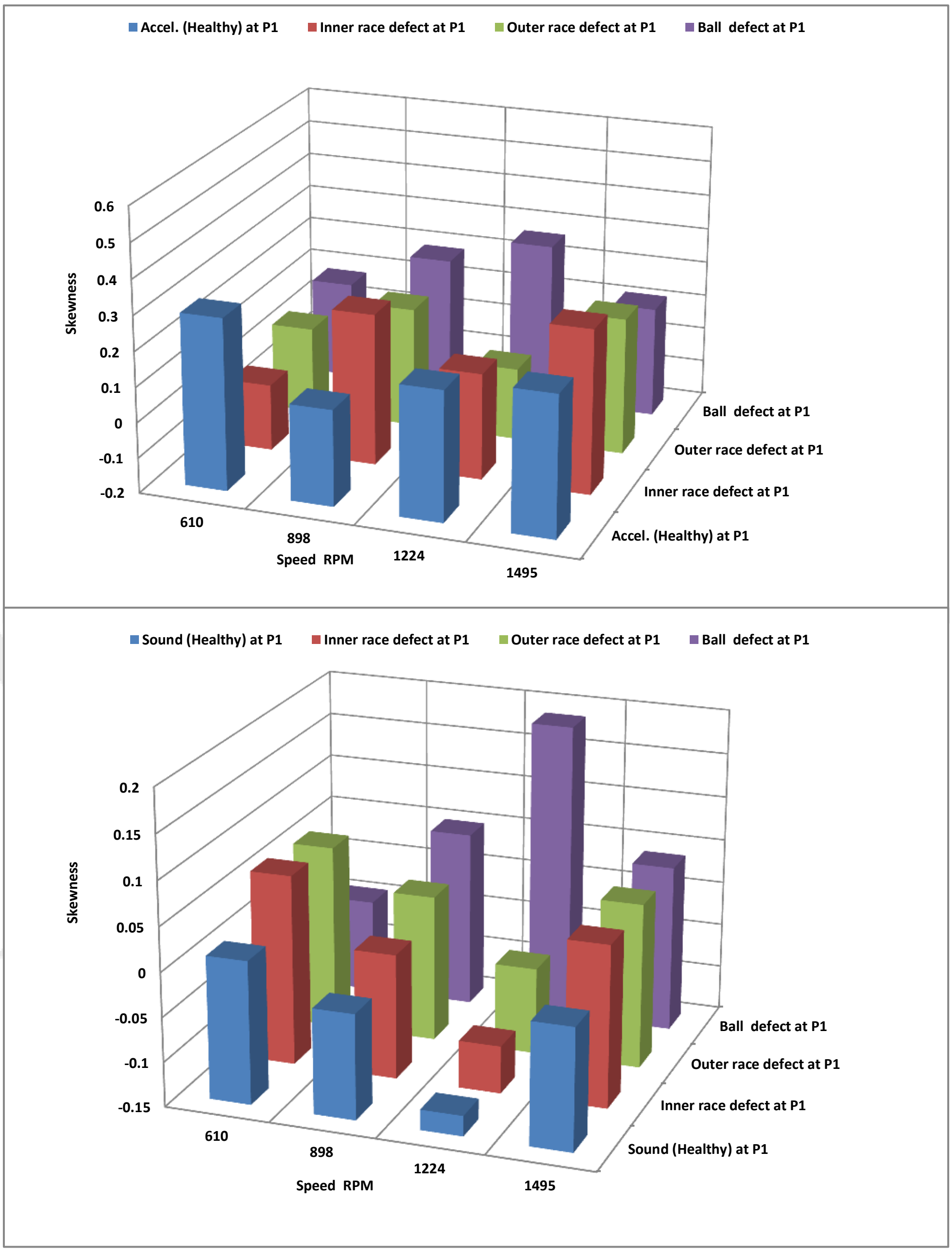

Figure 4.39 Skewness feature for (a) Acceleration signal (b) Sound signal at load P1 and defects in different locations.

It can be observed from Figure 4.39b that the skewness of sound signal at load P1 is a good indicator of the faults in bearings at all speeds, except at low speed of ball faulty bearing. In contrast, except for the (898, 1224) rpm speeds of the ball-defective bearing, skewness of the acceleration signal is not significant at most speeds as shown in Figure 4.39a.

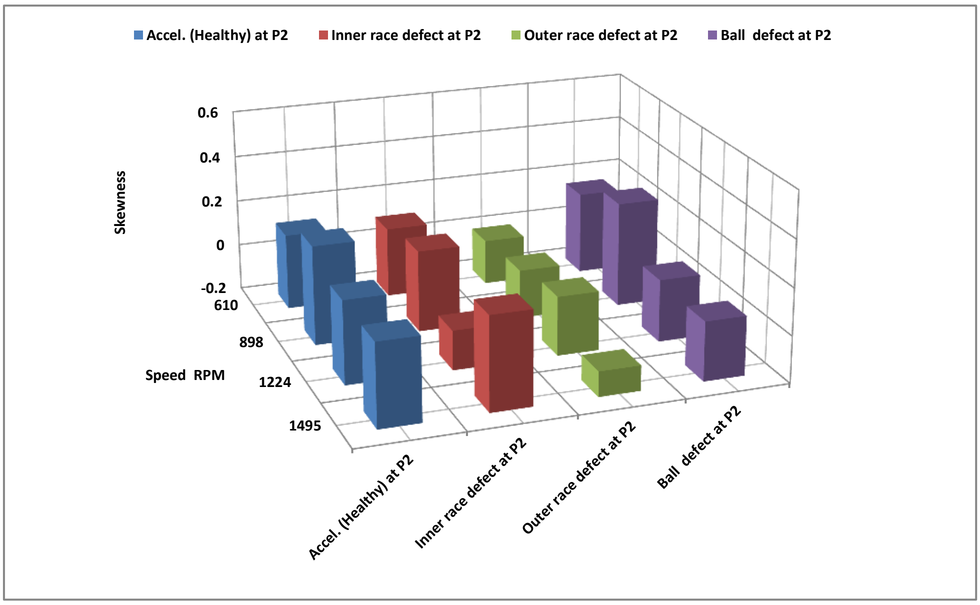

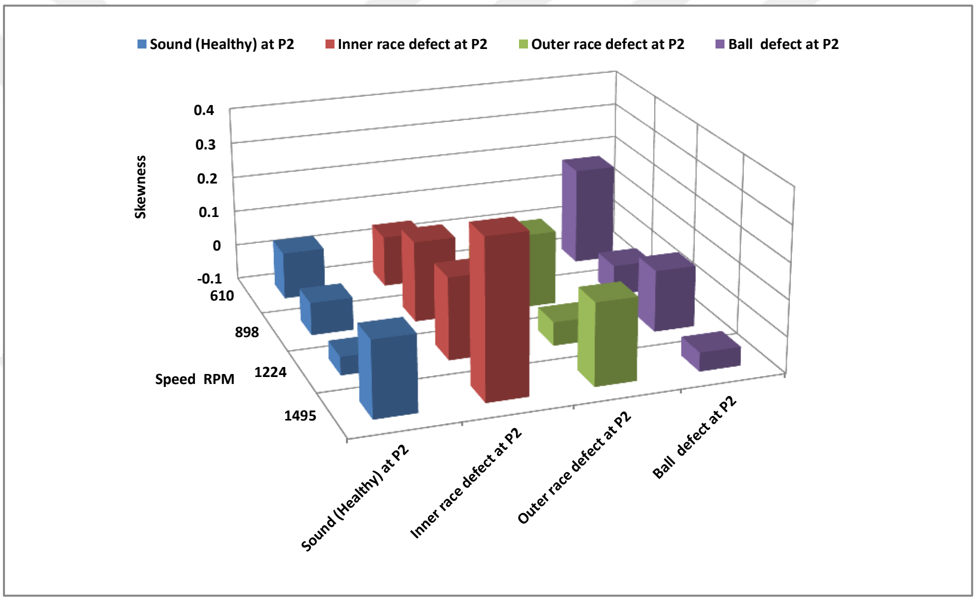

Figure 4.40 Skewness feature for (a) Acceleration signal (b) Sound signal at load P2 and defects in different locations.

The skewness value of the acceleration signal at load P2 is lower than skewness value of the faultless bearing, unless at the low speeds of bearings with defective balls, where skewness value appears to be an indicator of fault, while the skewness of sound signals indicates a fault in the bearings, especially for the case of the inner race defective bearing, due to the relative increase in the amplitude.

4.3.2.4 The Kurtosis Results

A signal with a Gaussian distribution has a kurtosis value equivalent to 3. But as the fault occurs on the ball bearings, the signal becomes noisy. The distribution changes, and the kurtosis characteristic value is higher than 3 [10].

Figures 4.41 - 4.44 show kurtosis feature that calculated for 48 experiments with three types of faults and health condition.

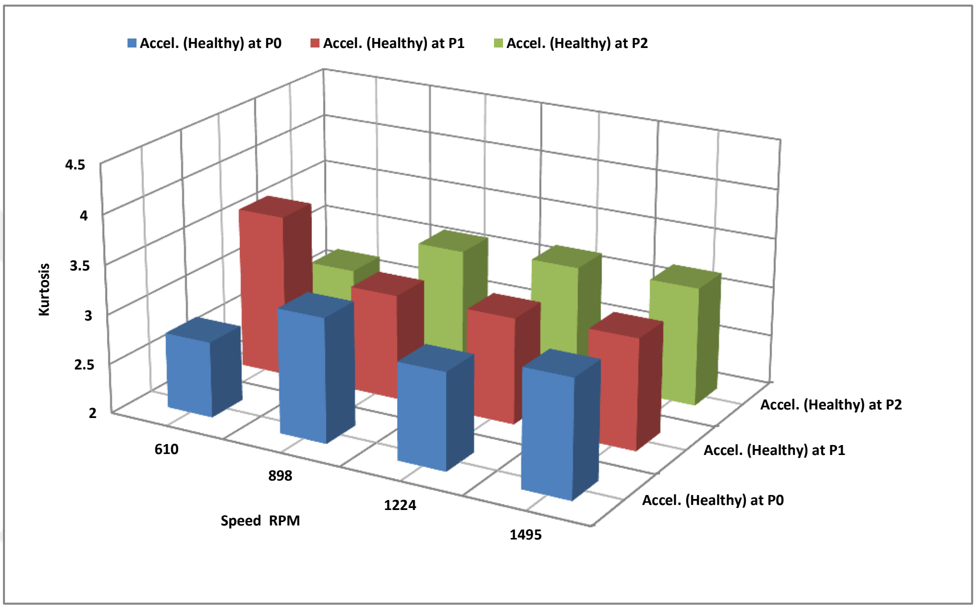

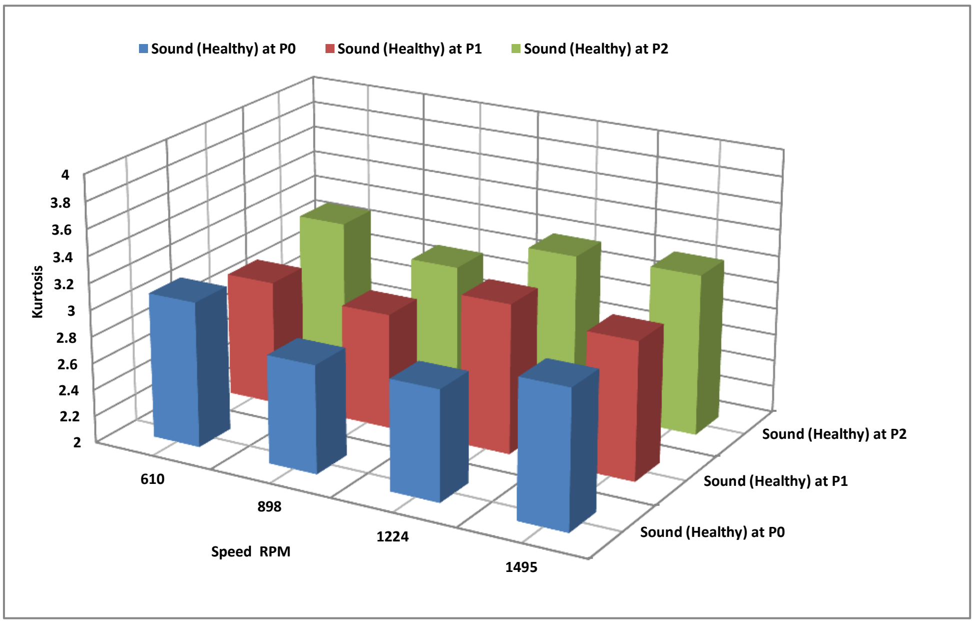

Figure 4.41 Kurtosis feature for healthy case signature at different load (a) Acceleration kurtosis (b) Sound kurtosis.

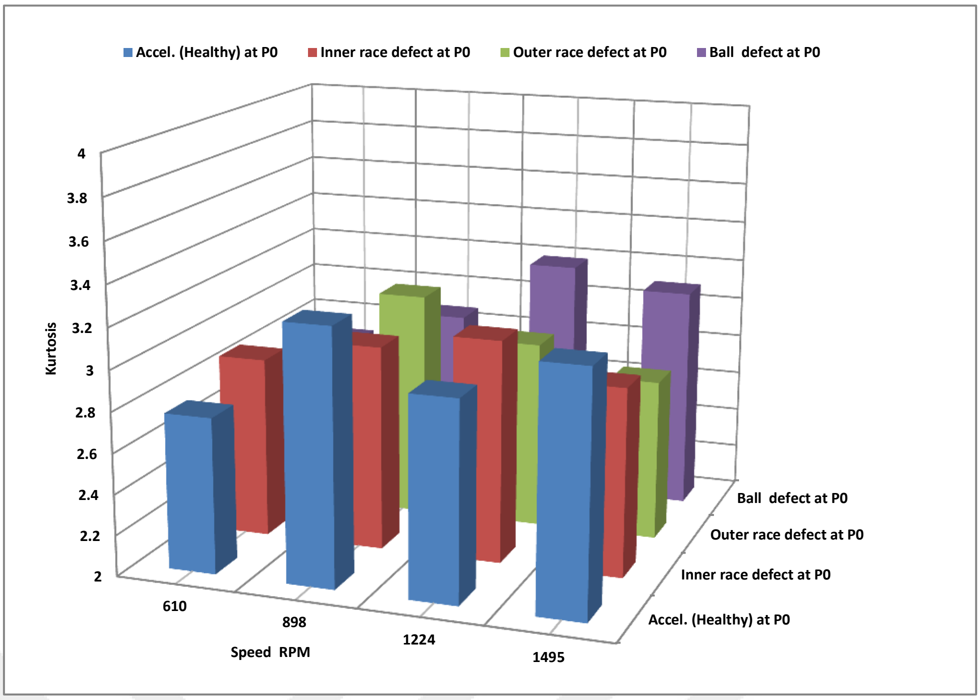

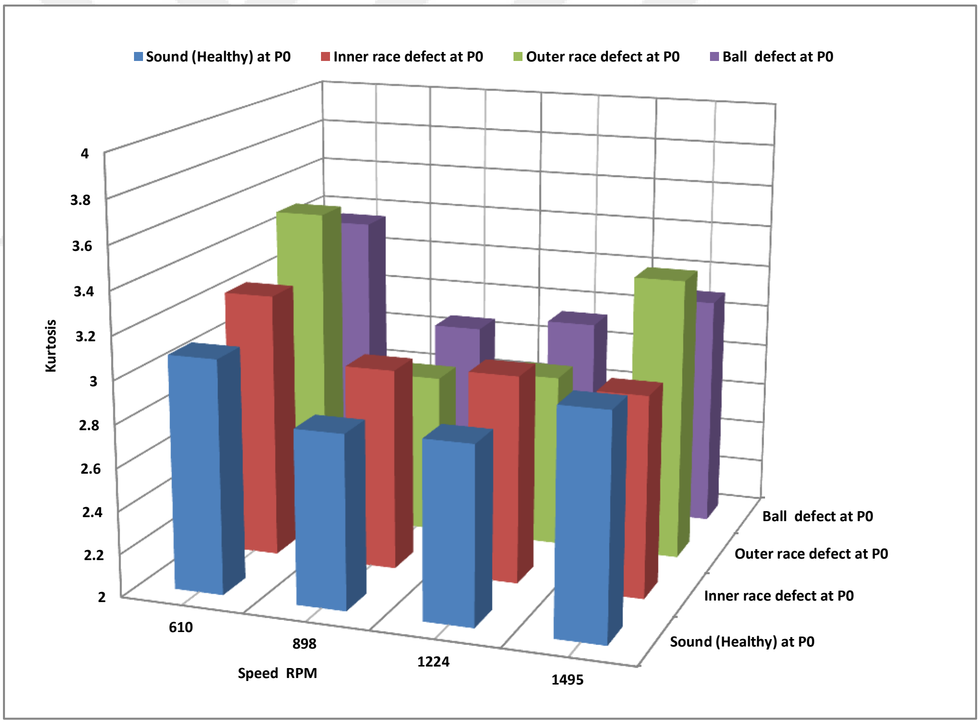

Figure 4.42 Kurtosis feature for (a) Acceleration signal (b) Sound signal at load P0 and defects in different locations.

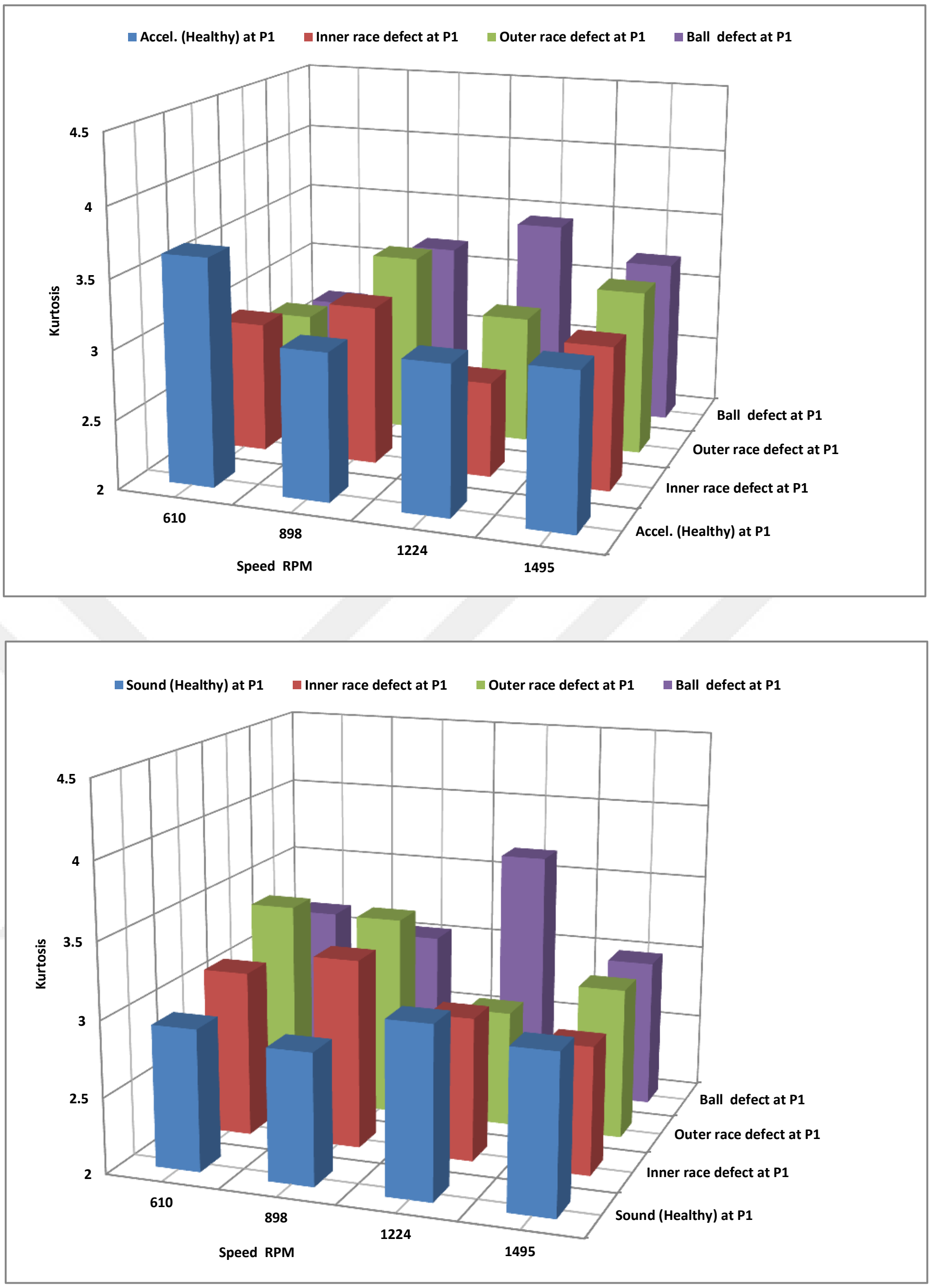

Figure 4.43 Kurtosis feature for (a) Acceleration signal (b) Sound signal at load P1 and defects in different locations.

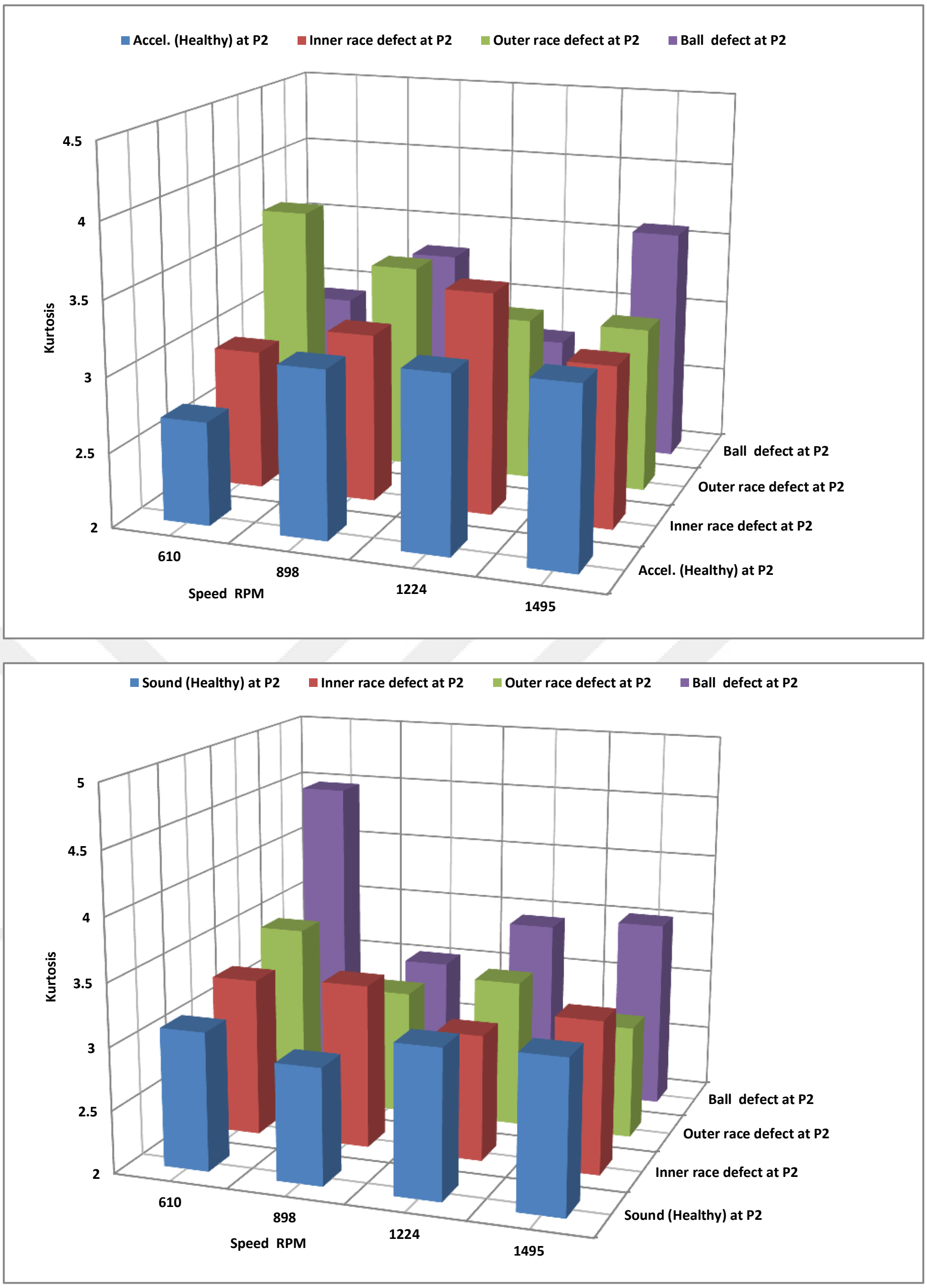

Figure 4.44 Kurtosis feature for (a) Acceleration signal (b) Sound signal at load P2 and defects in different locations.

As it can be seen from the Figures 4.41 - 4.44, the kurtosis feature of sound signal is a reliable indicator for monitoring bearing faults at the low speeds, unlike kurtosis feature of acceleration signal showing no significant trend in the speed range.

4.3.2.5 The Peak Results

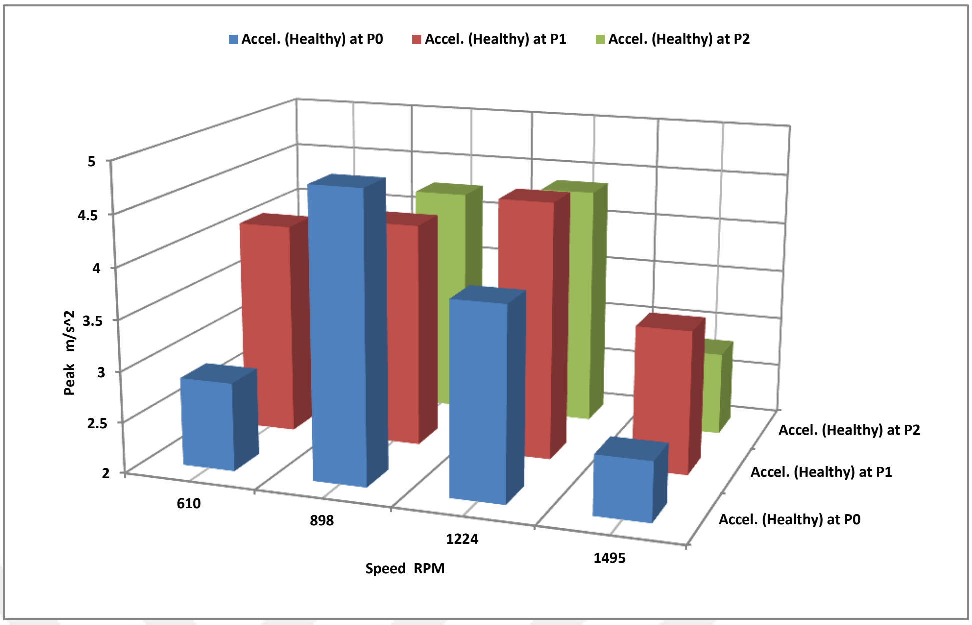

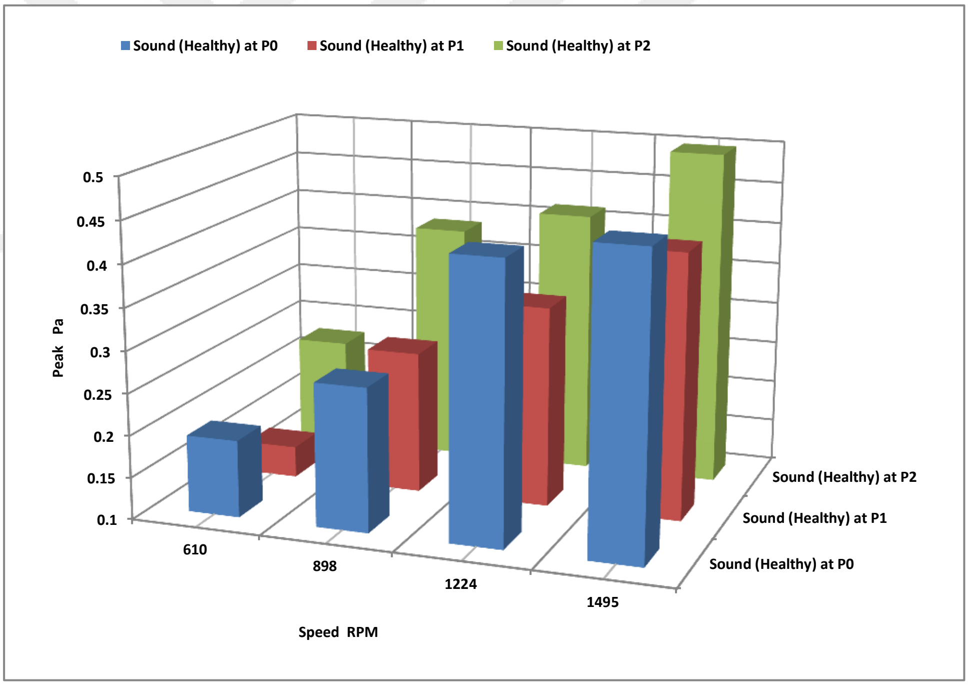

Figure 4.45 Peak feature for healthy case signature at different load (a) Acceleration peak value (b) Sound peak value.

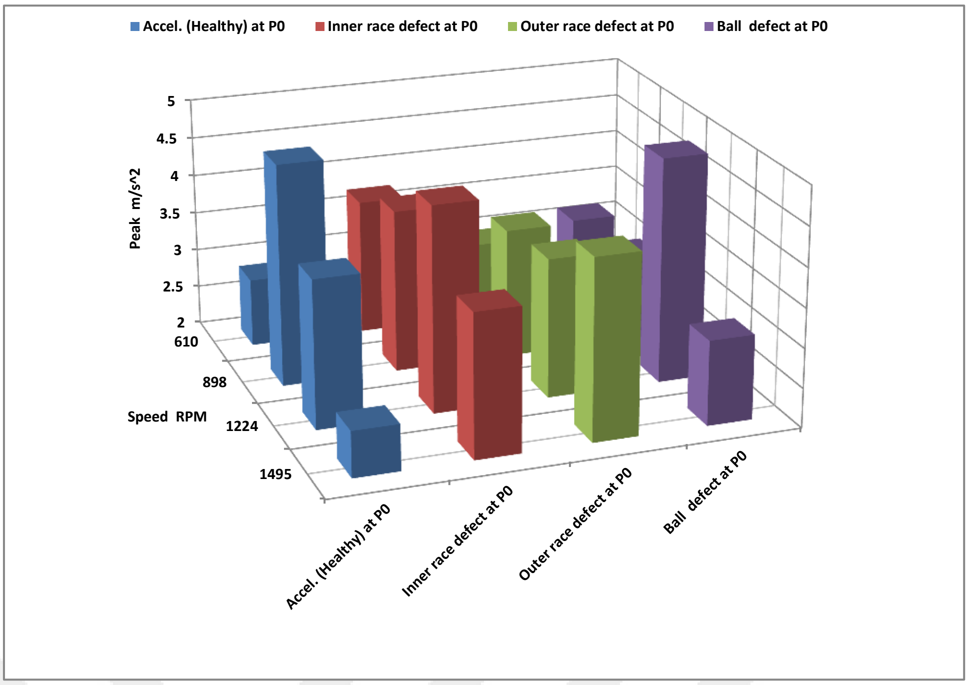

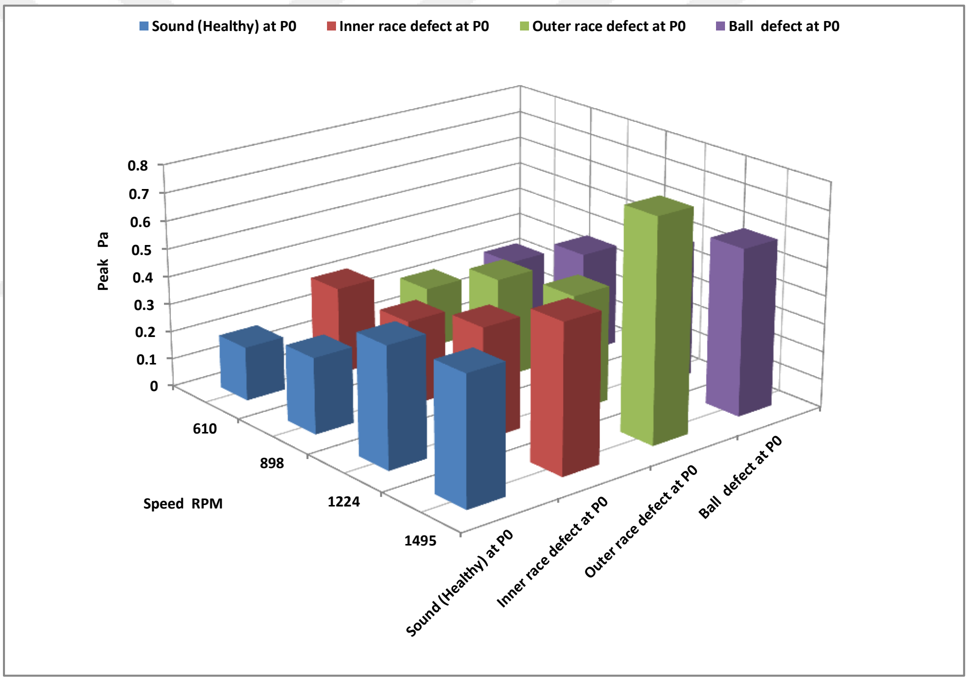

Figure 4.46 Peak feature for (a) Acceleration signal (b) Sound signal at load P0 and defects in different locations.

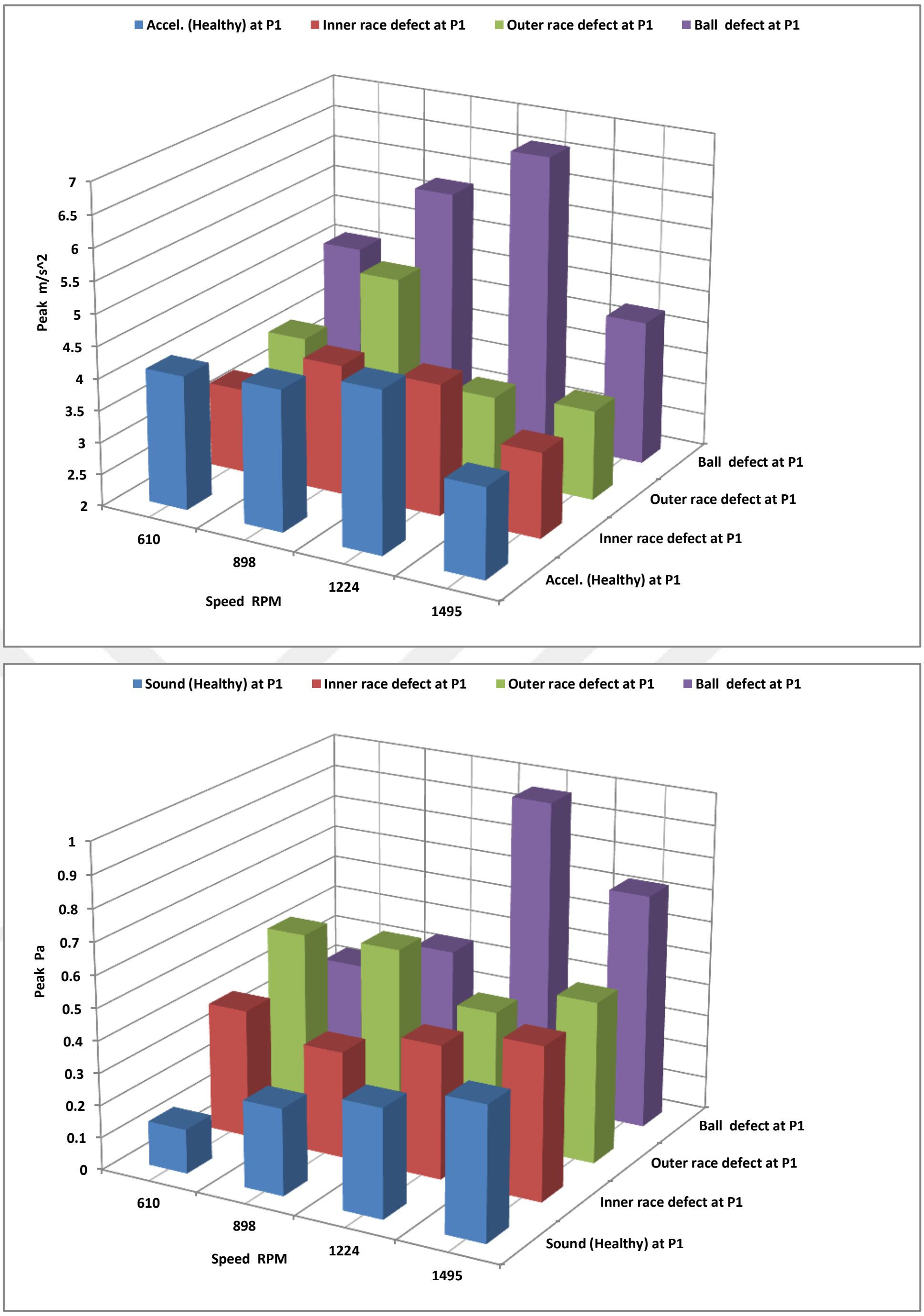

Figure 4.47 Peak feature for (a) Acceleration signal (b) Sound signal at load P1 and defects in different locations.

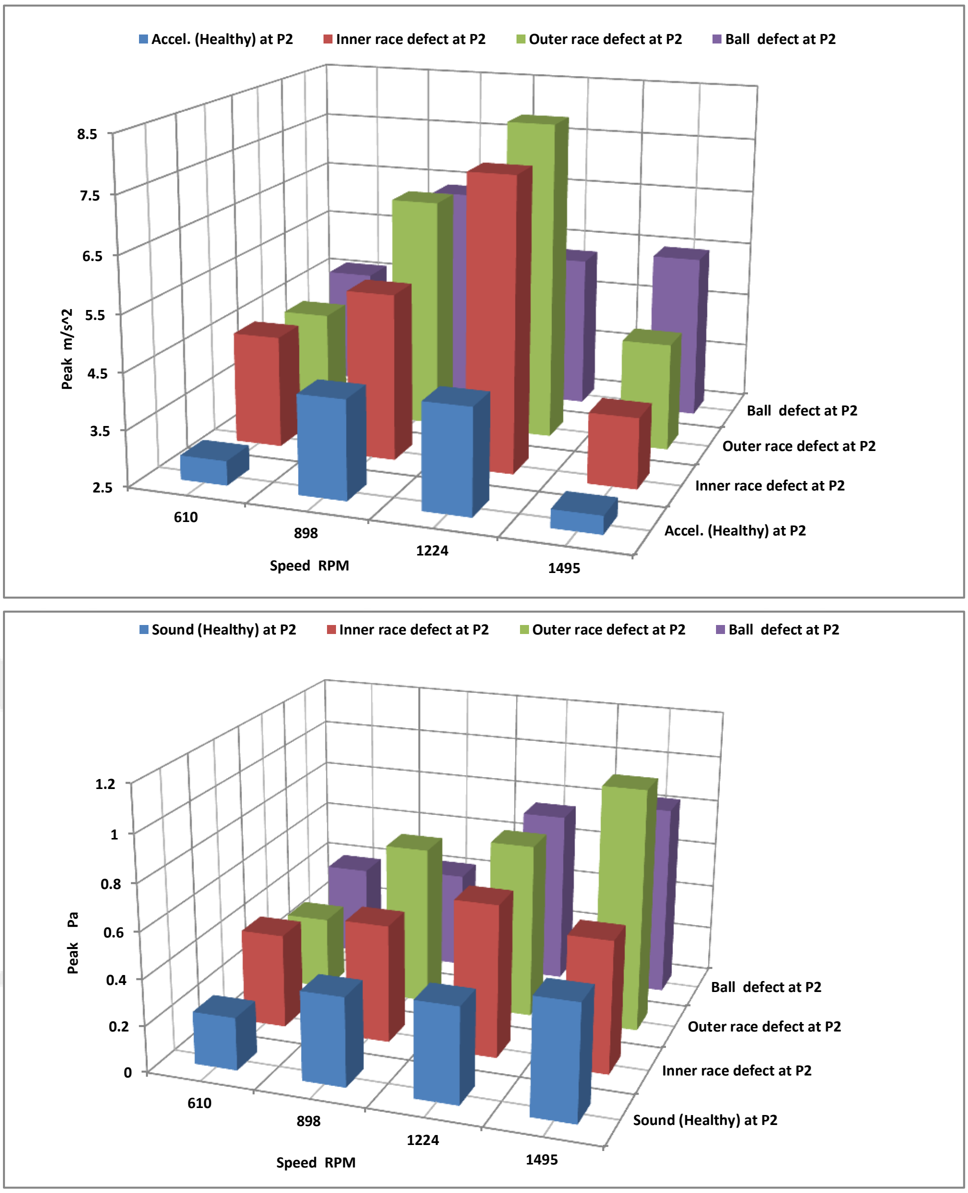

Figure 4.48 Peak feature for (a) Acceleration signal (b) Sound signal at load P2 and defects in different locations.

Under the P0 load, the peak feature of the acceleration signal shows interesting results only at high speeds, while the peak feature of the acoustic signal shows a reliable indicator of bearings faults at all speeds and cases, except at speed 1224 rpm for inner race defective bearing. However, when the load increases to P1 and P2 levels, the peak value increases, confirming that there is a clear indicator for condition monitor of bearings. Therefore the peak feature is a good indicator for the bearing defects. For acceleration and acoustic emission signals, the AE peak feature are better and more pronounced than the acceleration peak feature, as shown in Figure 4.46 - 4.48.

4.3.3 Results of Frequency Domain (Spectra Analysis)

In the spectra analysis (frequency domain), faults are quantified by measuring the magnitude of the vibration acceleration signal that is excited to the frequency of bearing defects (FTF, BPFO, BPFI, and BSF) or their harmonics [50]. The occurrence of a faults and their development in a faulty bearing result in an increase in the amplitude of the characteristics frequency of the defective bearing, as well as produces harmonics from these frequencies [1]. The waveform power spectrum for vibration and AE, will be analyzed. Where the health condition of bearing will be compared with each defective conditions.

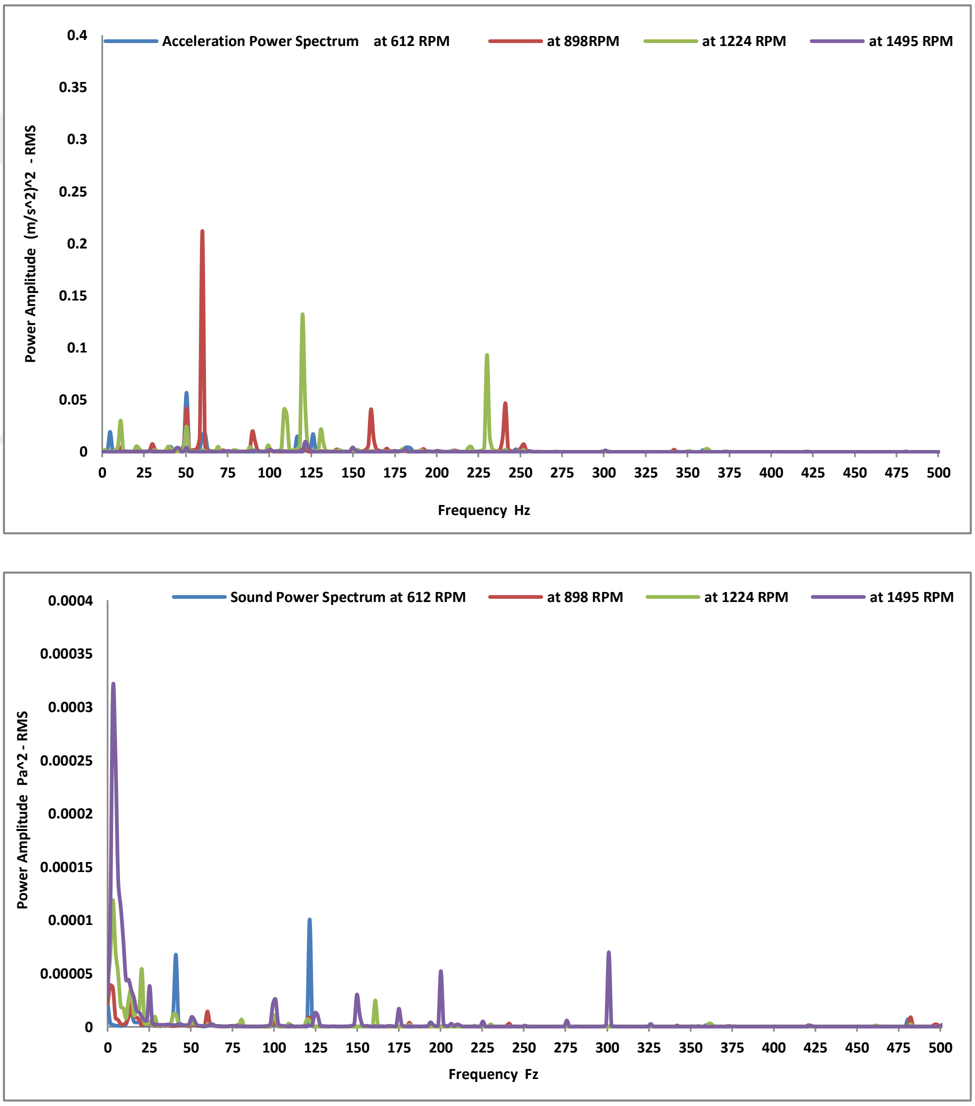

Figure 4.49 Power spectrum for free electrical motor of test rig at different speed (a) Acceleration power spectrum (b) Sound power spectrum

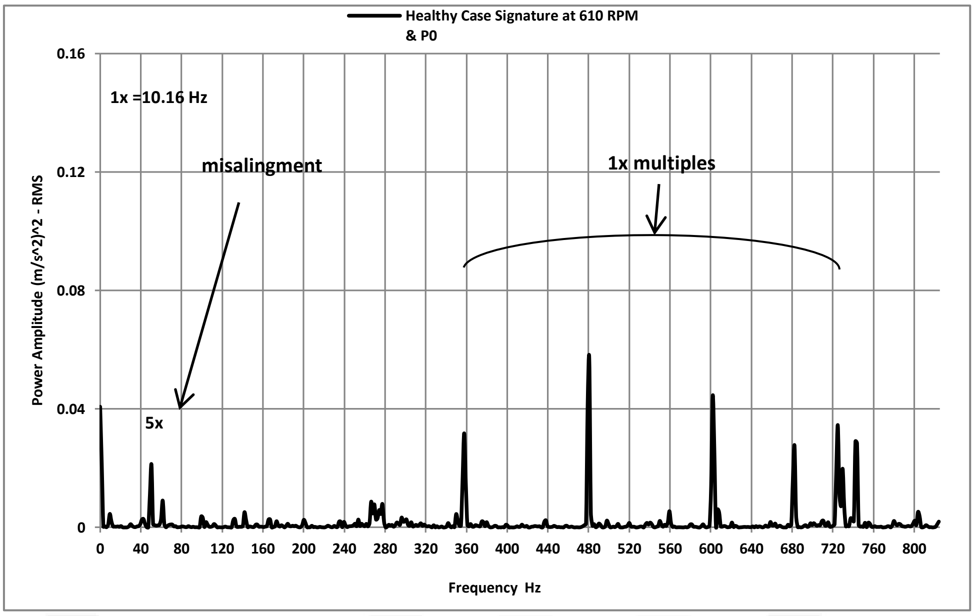

Figure 4.50 Acceleration power spectrum for fault-free bearing (Healthy case) at 610 RPM and load P0.

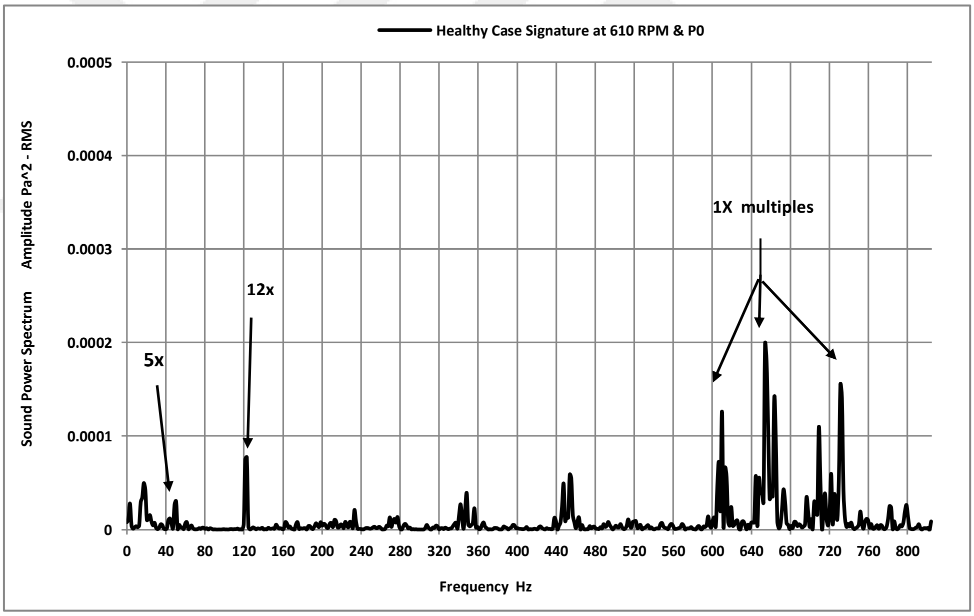

Figure 4.51 Sound power spectrum for fault-free bearing (Healthy case) at 610 RPM and load P0.

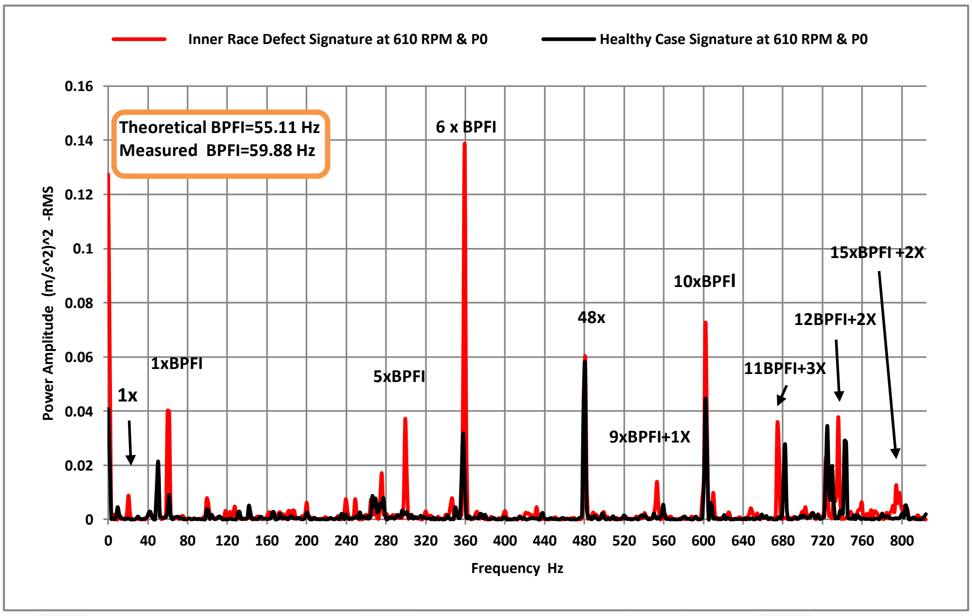

Figure 4.52 Acceleration power spectrum for healthy case vs inner race defect at 610 RPM and load P0.

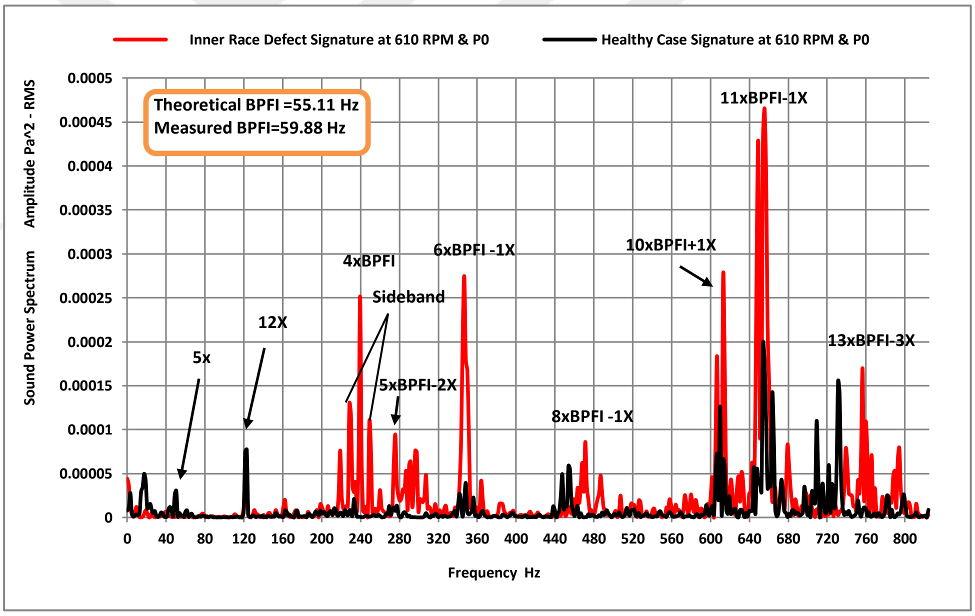

Figure 4.53 Sound power spectrum for healthy vs inner race defect at 610 RPM and load P0.

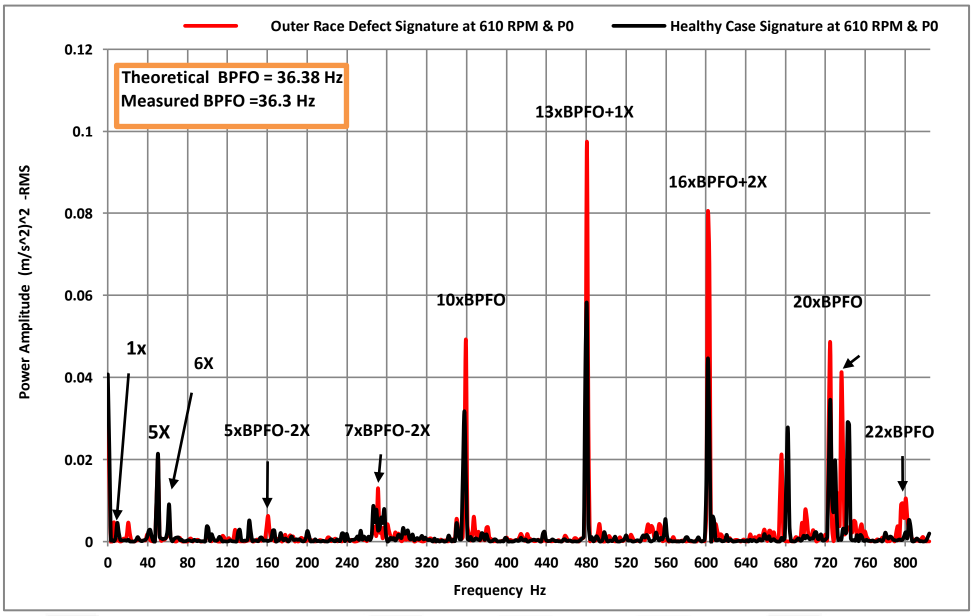

Figure 4.54 Acceleration power spectrum for healthy case vs outer race defect at 610 RPM and load P0.

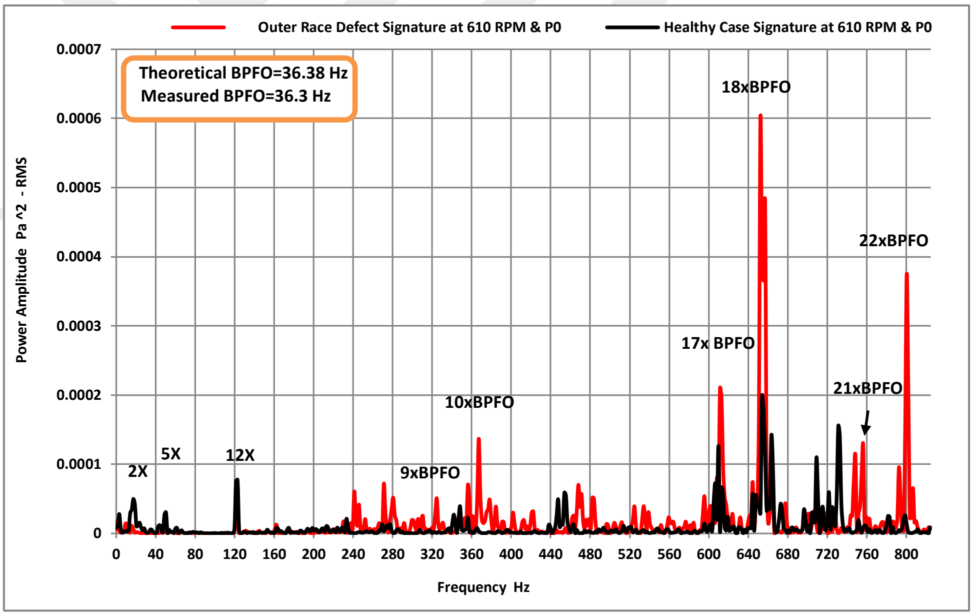

Figure 4.55 Sound power spectrum for healthy vs outer race defect at 610 RPM and load P0.

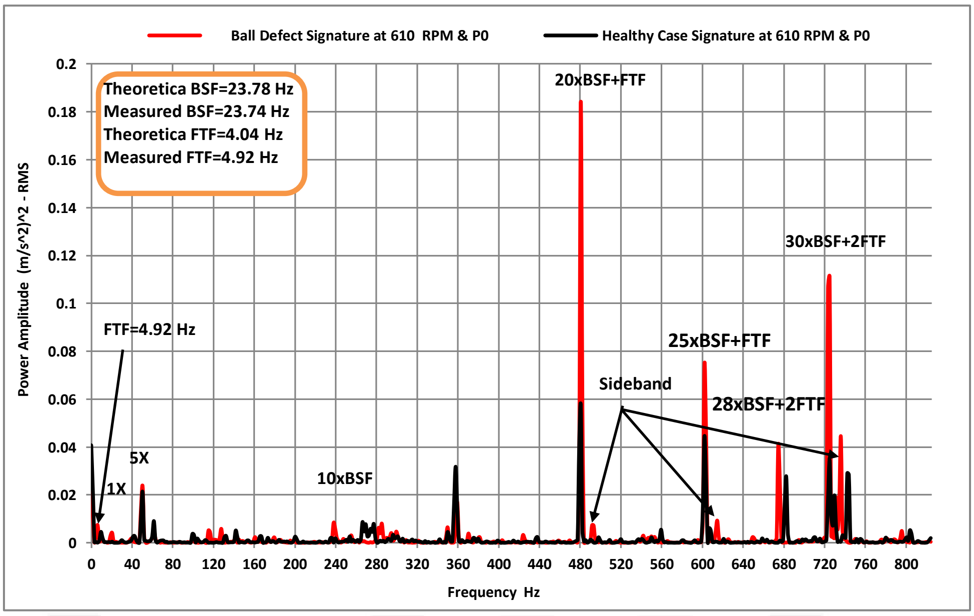

Figure 4.56 Acceleration power spectrum for healthy case vs ball defect at 610 RPM and load P0.

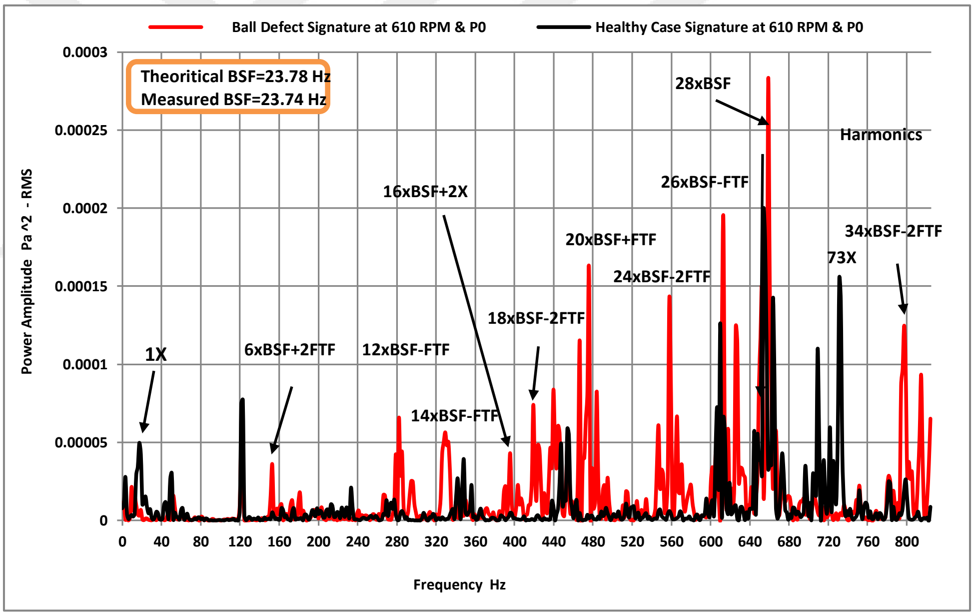

Figure 4.57 Sound power spectrum for healthy case vs ball defect at 610 RPM and load P0.

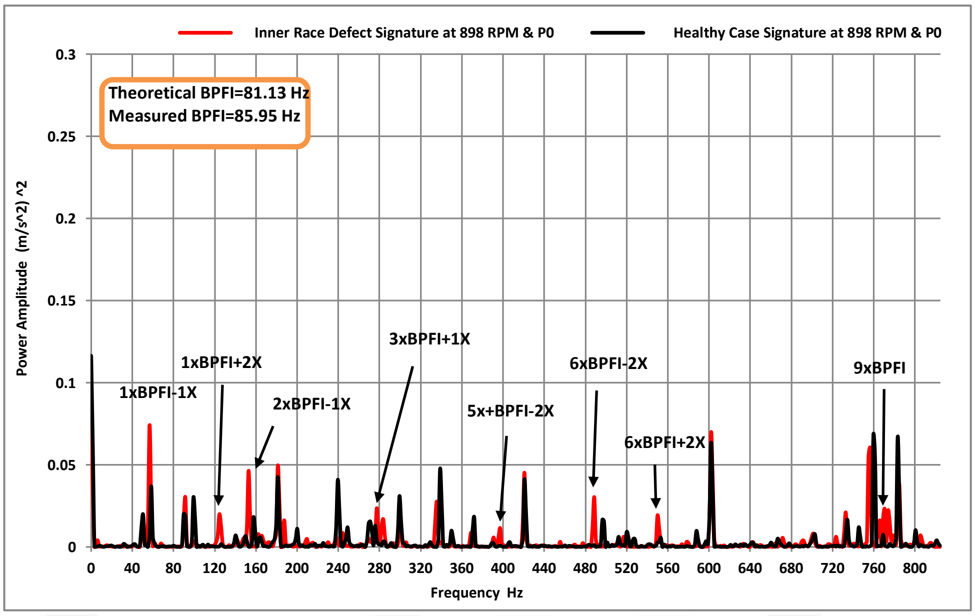

Figure 4.58 Acceleration power spectrum for healthy case vs inner race defect at 898 RPM and load P0.

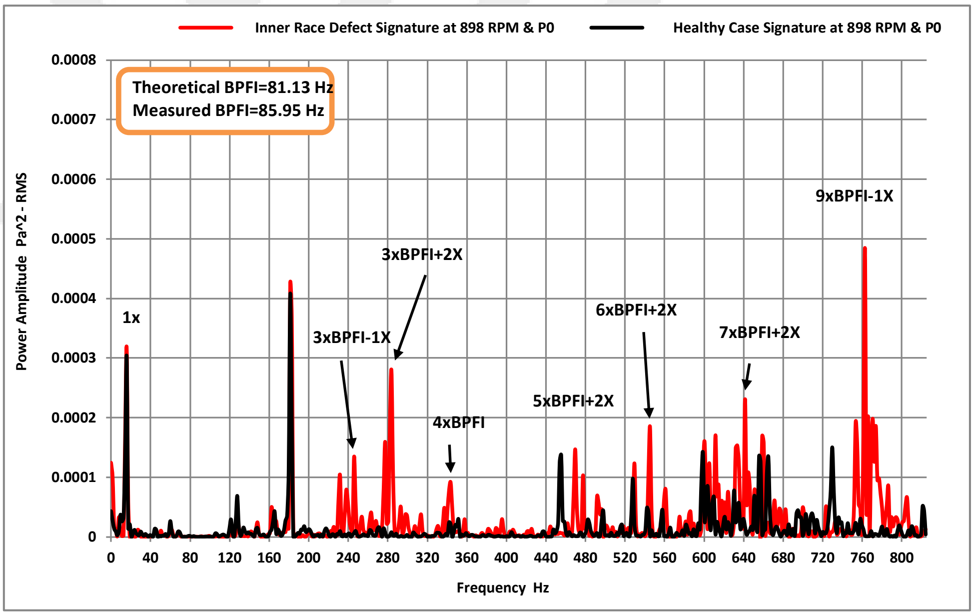

Figure 4.59 Sound power spectrum for healthy case vs inner race defect at 898 RPM and load P0.

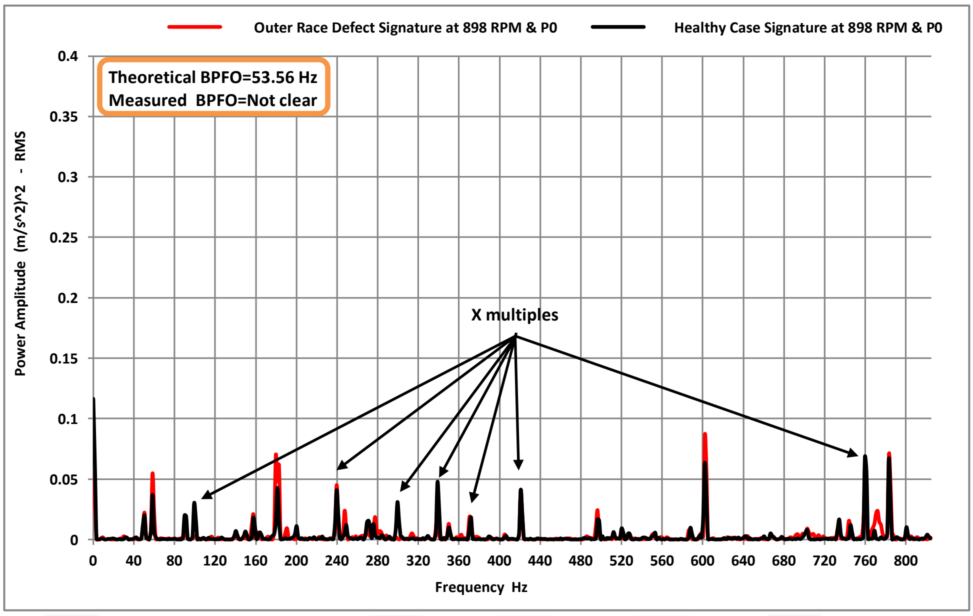

Figure 4.60 Acceleration power spectrum for healthy case vs outer race defect at 898 RPM and load P0.

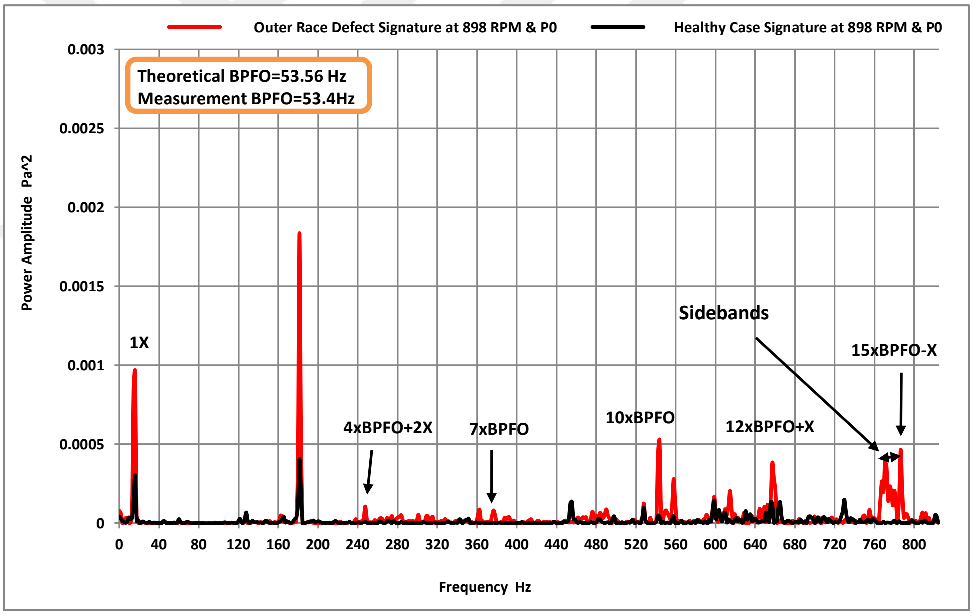

Figure 4.61 Sound power spectrum for healthy case vs outer race defect at 898 RPM and load P0.

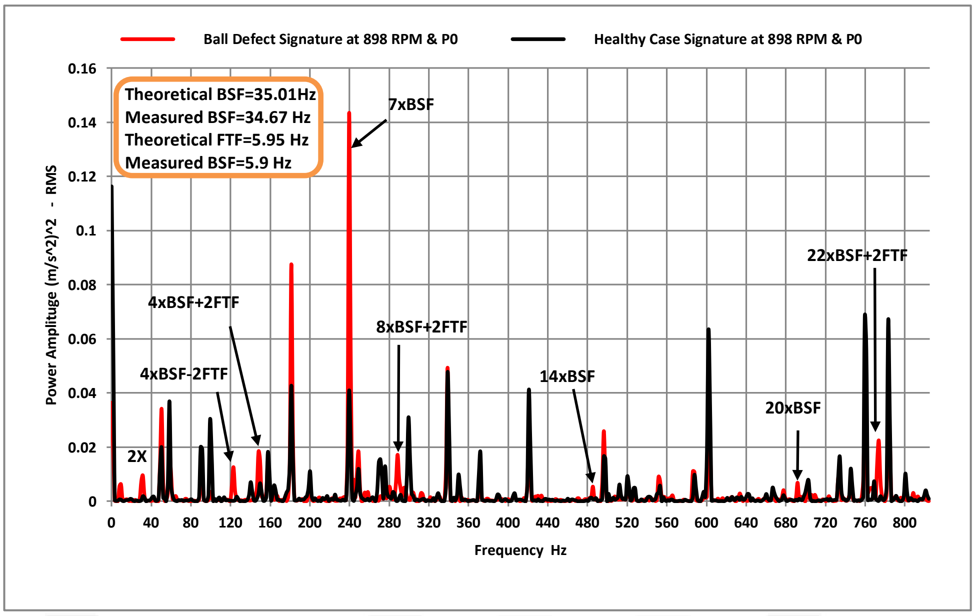

Figure 4.62 Acceleration power spectrum for healthy case vs ball defect at 898 RPM and load P0.

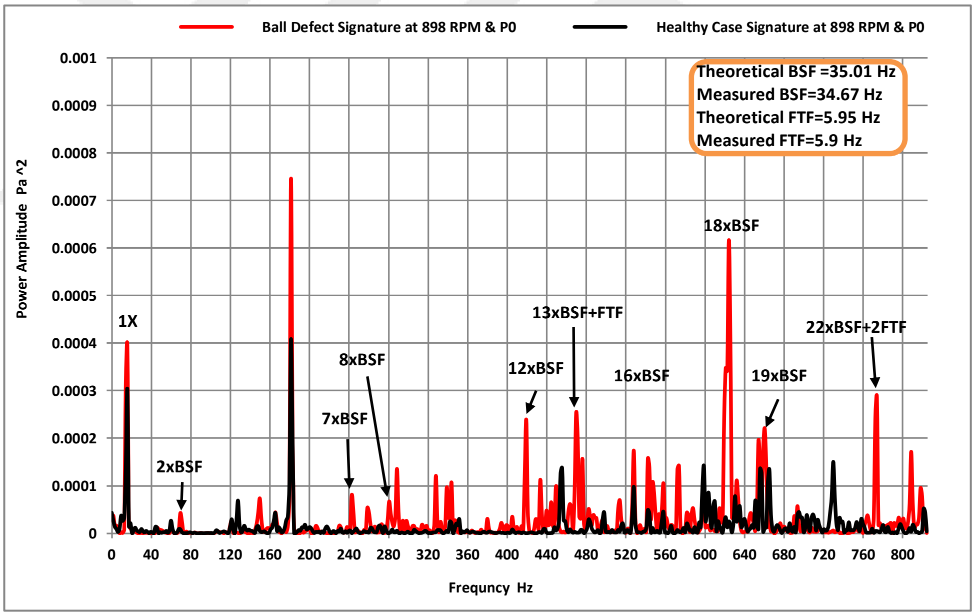

Figure 4.63 Sound power spectrum for healthy case vs ball defect at 898 RPM and load P0.

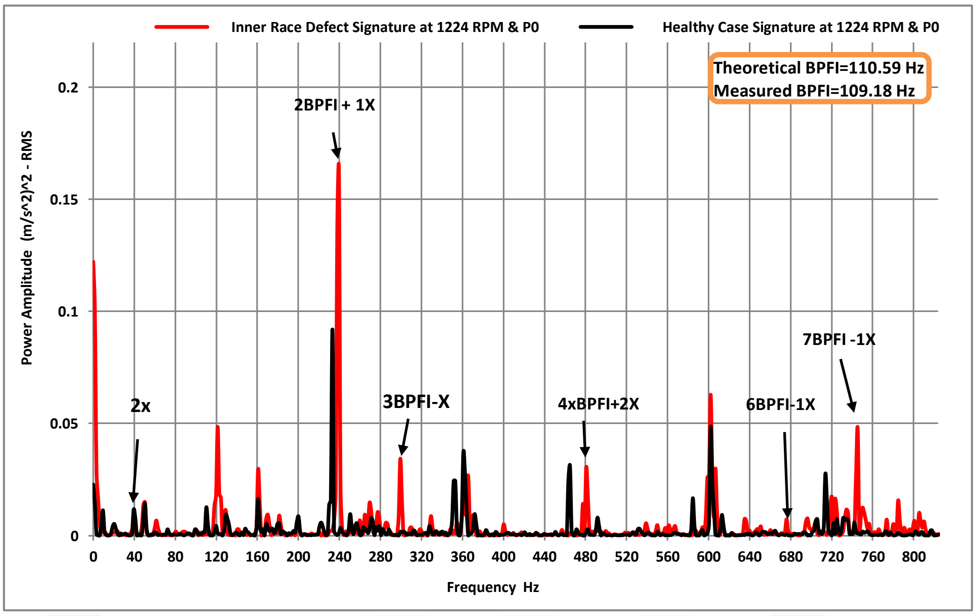

Figure 4.64 Acceleration power spectrum for healthy vs inner defect at 1224 RPM and load P0.

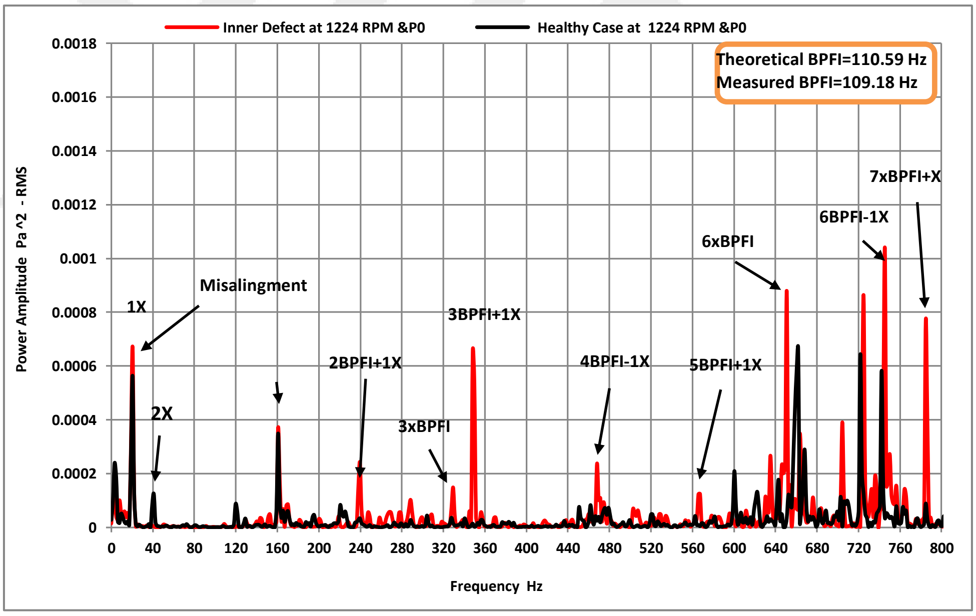

Figure 4.65 Sound power spectrum for healthy case vs inner defect at 1224 RPM and load P0.

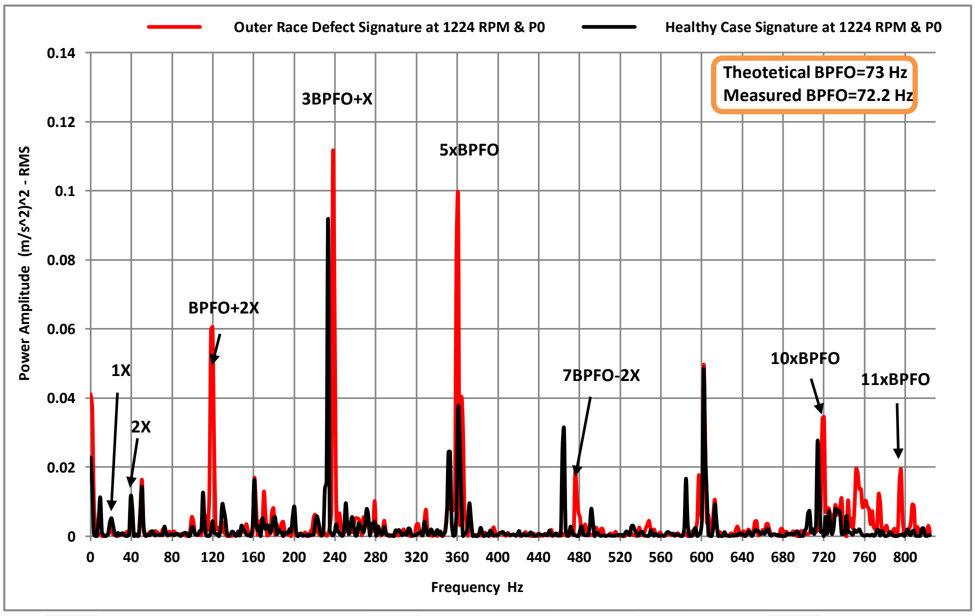

Figure 4.66 Acceleration power spectrum for healthy vs outer defect at 1224 RPM and load P0.

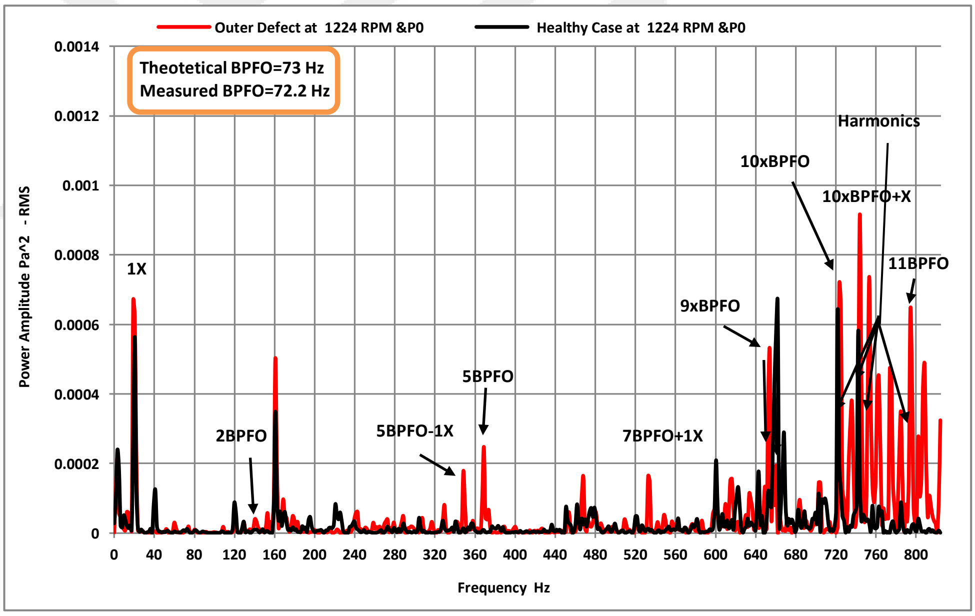

Figure 4.67 Sound power spectrum for healthy case vs outer defect at 1224 RPM and load P0.

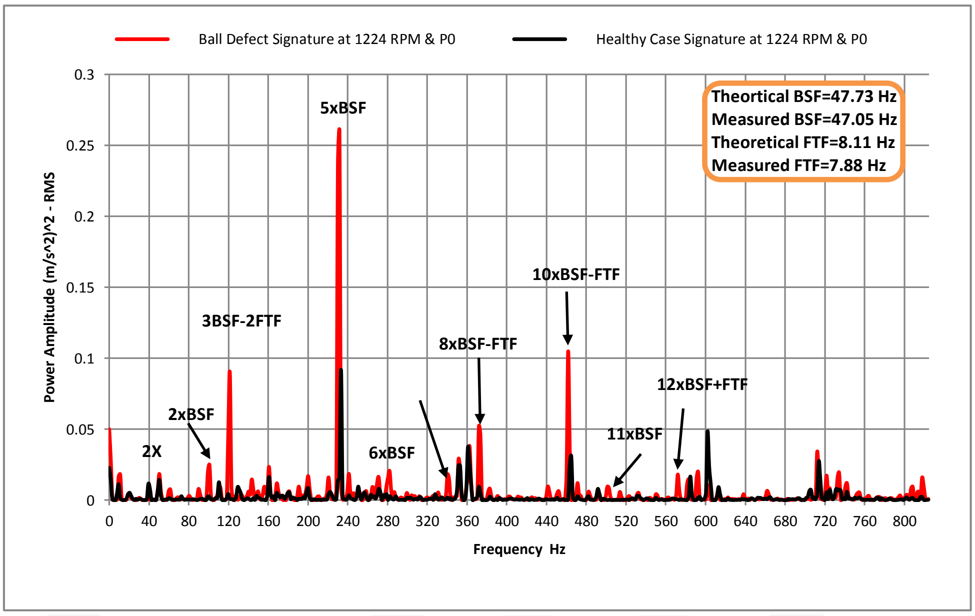

Figure 4.68 Acceleration power spectrum for healthy case vs ball defect at 1224 RPM and load P0.

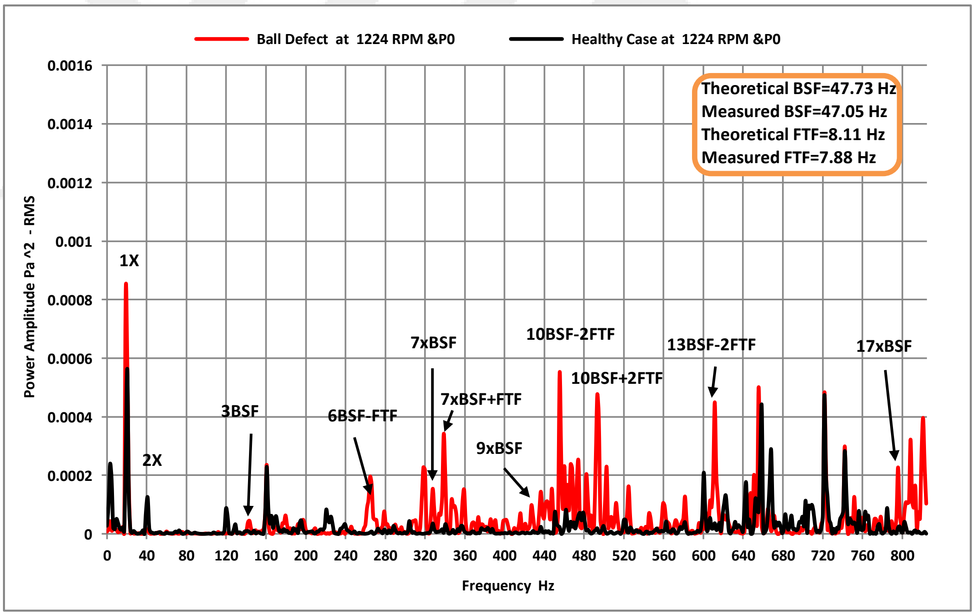

Figure 4.69 Sound power spectrum for healthy case vs ball defect at 1224 RPM and load P0.

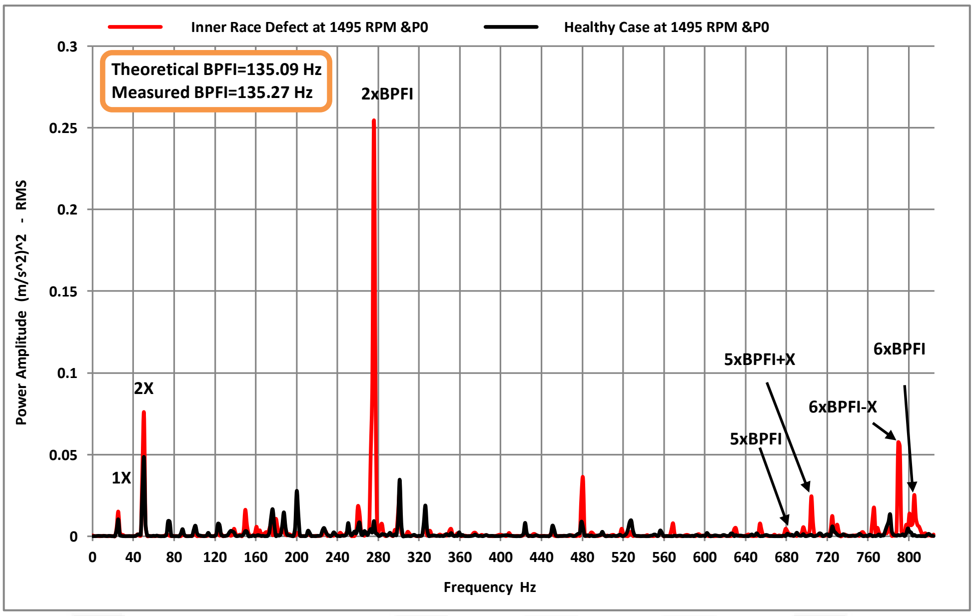

Figure 4.70 Acceleration power spectrum for healthy case vs inner race defect at 1495 RPM and load P0.

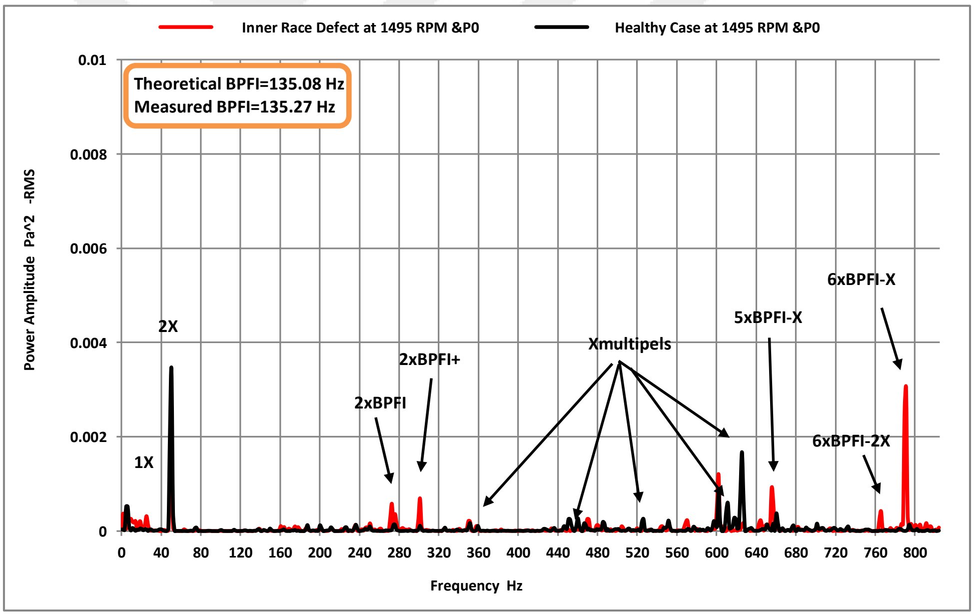

Figure 4.71 Sound power spectrum for healthy case vs inner race defect at 1495 RPM and load P0.

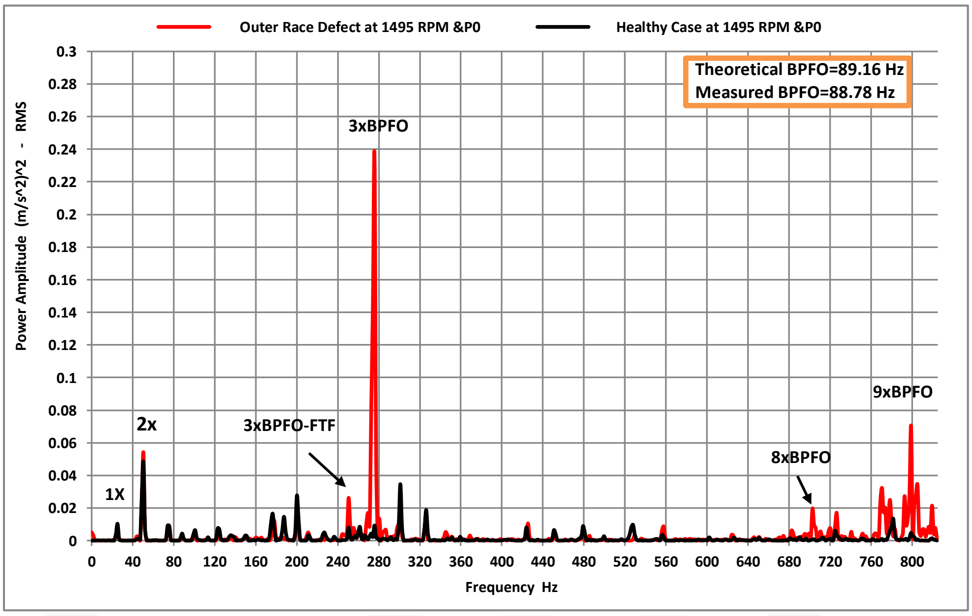

Figure 4.72 Acceleration power spectrum for healthy case vs outer race defect at 1495 RPM and load P0.

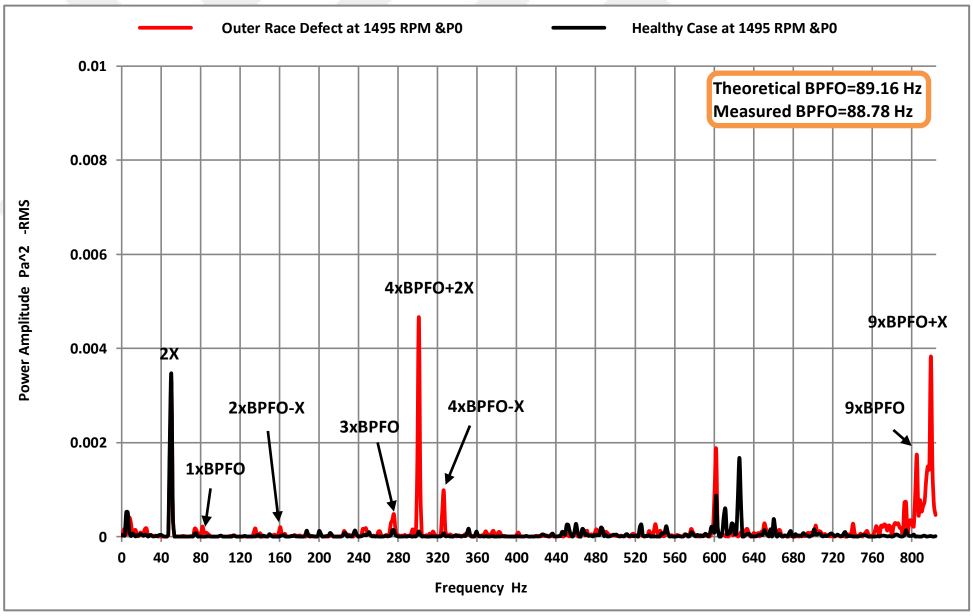

Figure 4.73 Sound power spectrum for healthy case vs outer race defect at 1495 RPM and load P0.

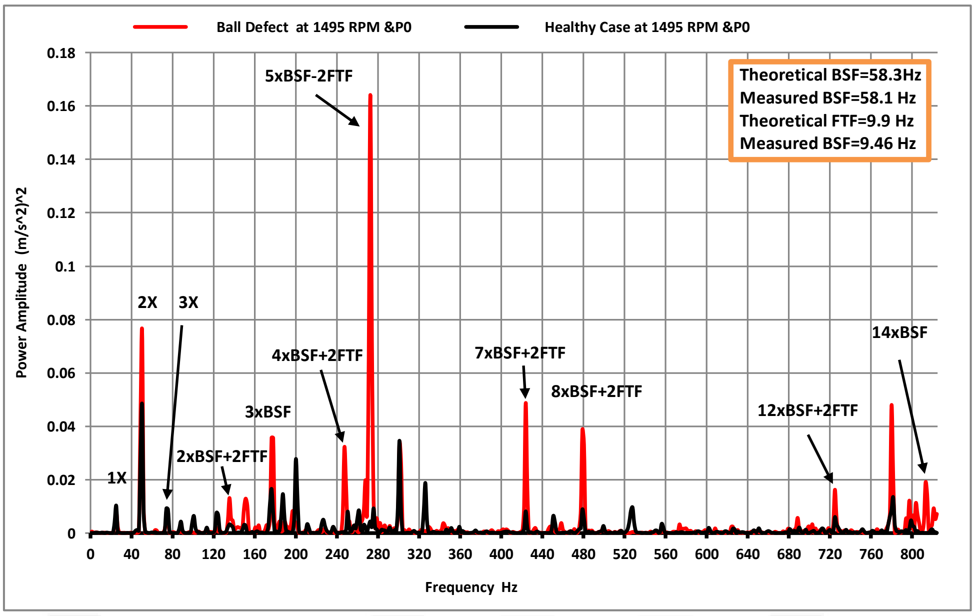

Figure 4.74 Acceleration power spectrum for healthy case vs ball defect at1495 RPM and load P0.

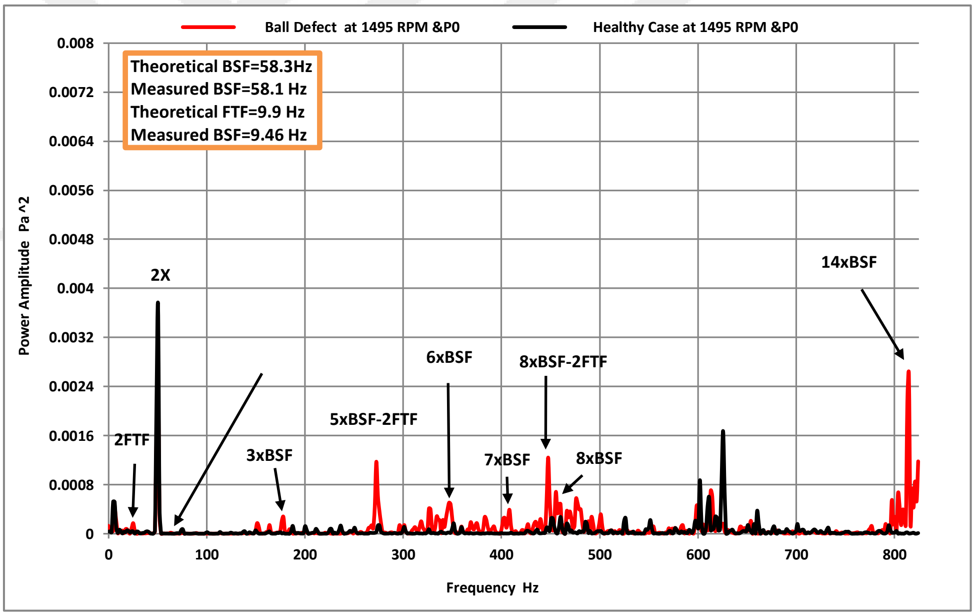

Figure 4.75 Sound power spectrum for healthy case vs ball defect at 1495 RPM and load P0.

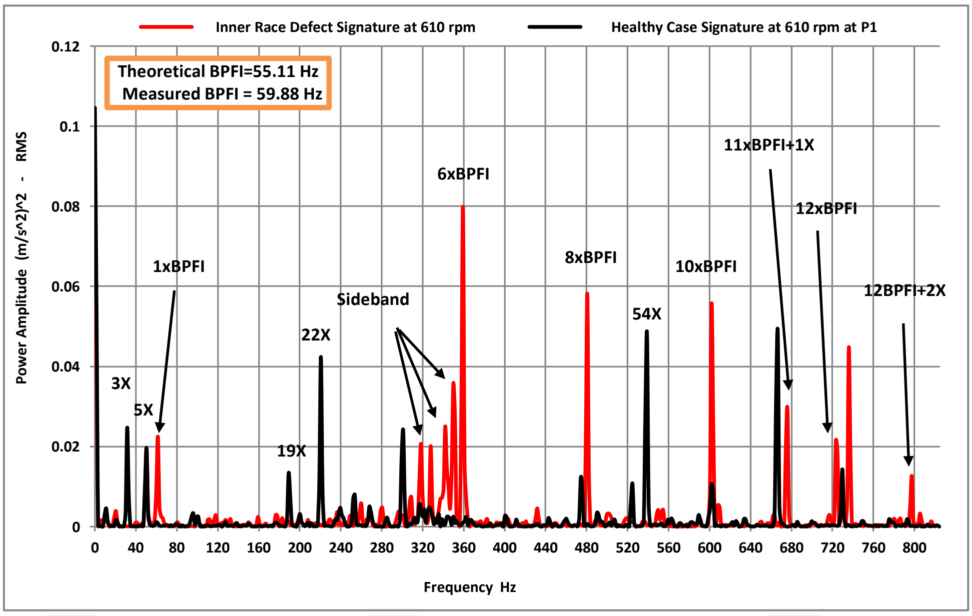

Figure 4.76 Acceleration power spectrum for healthy case vs inner race defect at 610 RPM and load P1.

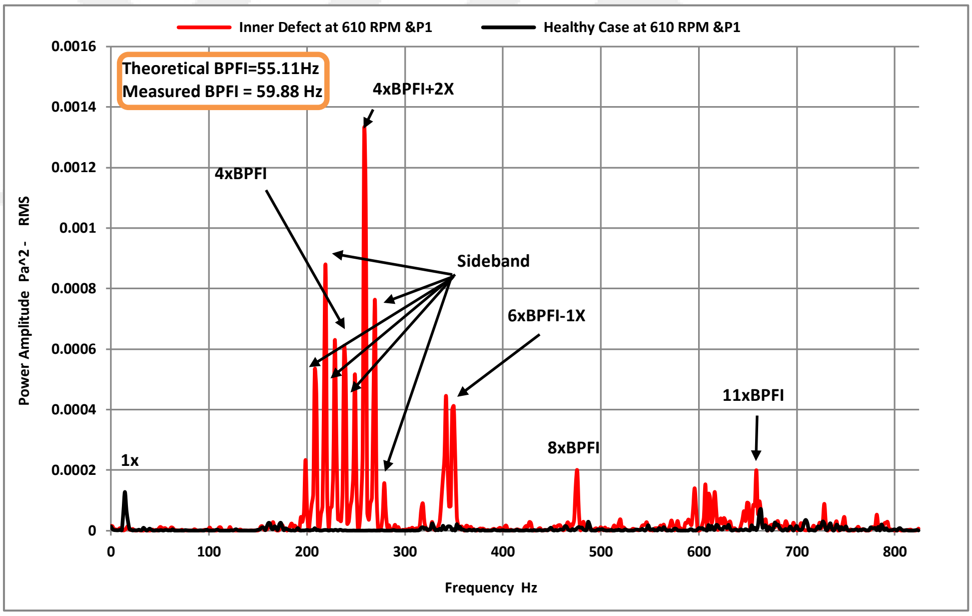

Figure 4.77 Sound power spectrum for healthy case vs inner race defect at 610 RPM and load P1.

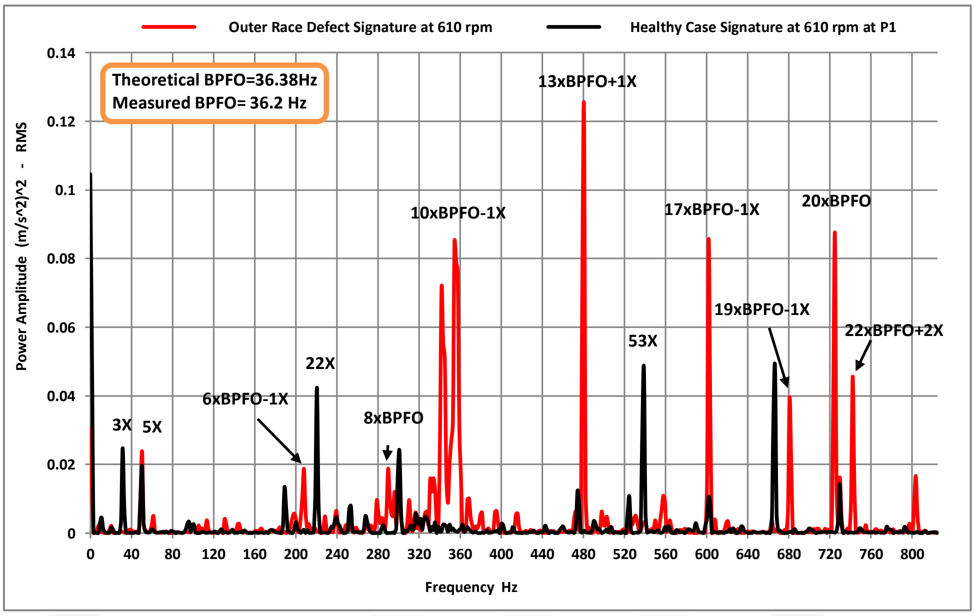

Figure 4.78 Acceleration power spectrum for healthy case vs outer race defect at 610 RPM and load P1.

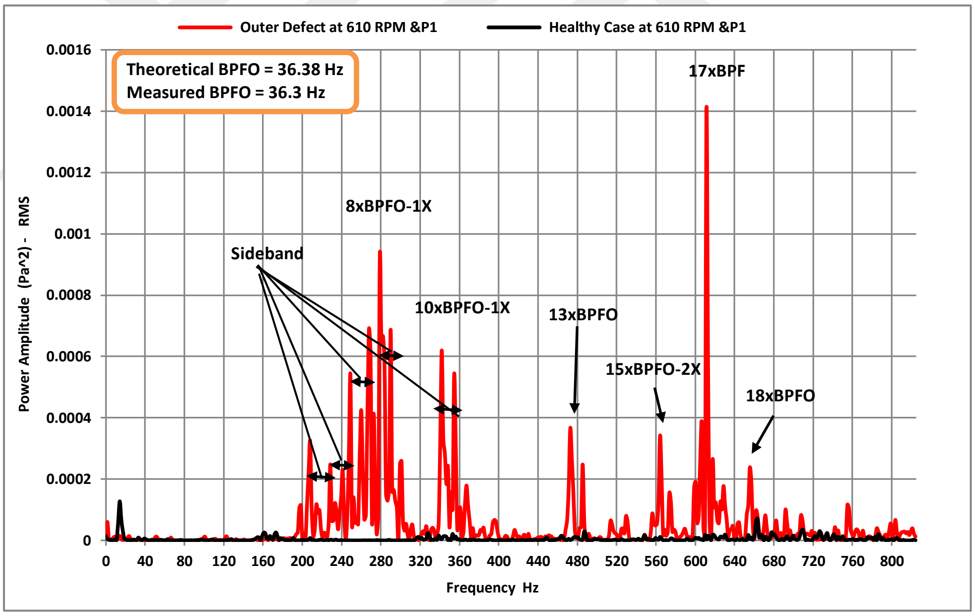

Figure 4.79 Sound power spectrum for healthy case vs outer race defect at 610 RPM and load P1.

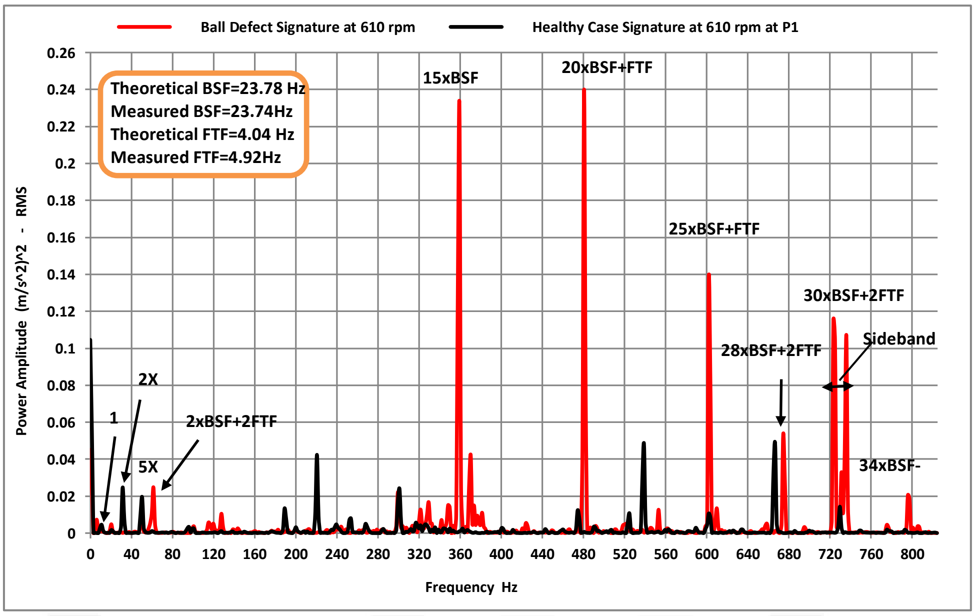

Figure 4.80 Acceleration power spectrum for healthy case vs ball race defect at 610 RPM and load P1.

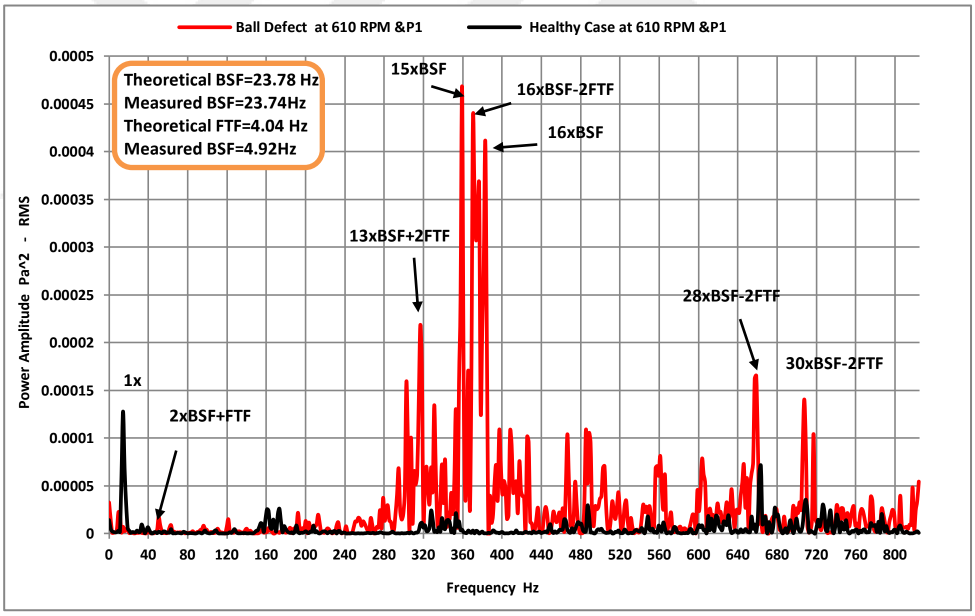

Figure 4.81 Sound power spectrum for healthy case vs ball race defect at 610 RPM and load P1.

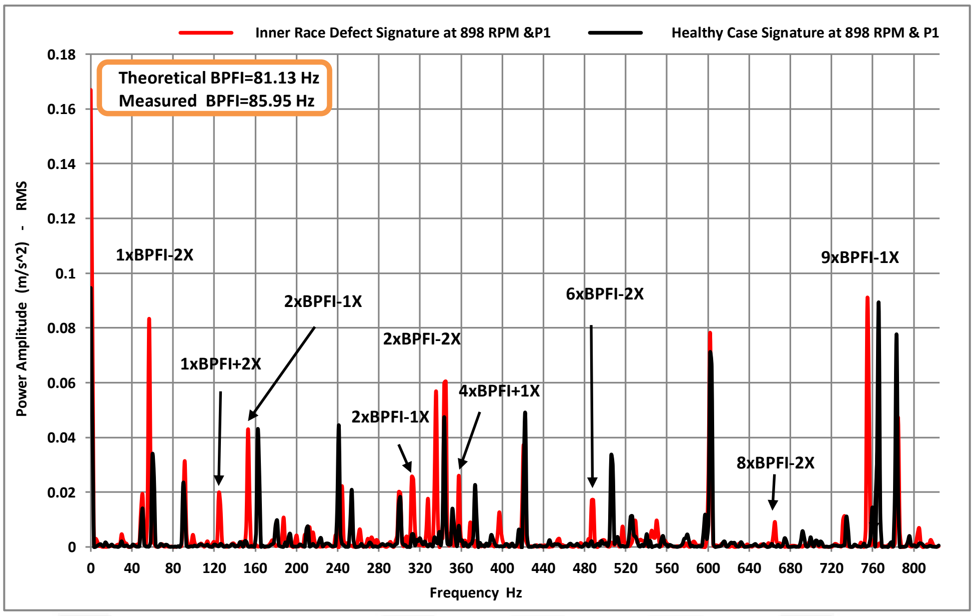

Figure 4.82 Acceleration power spectrum for healthy case vs inner race defect at 898 RPM and load P1.

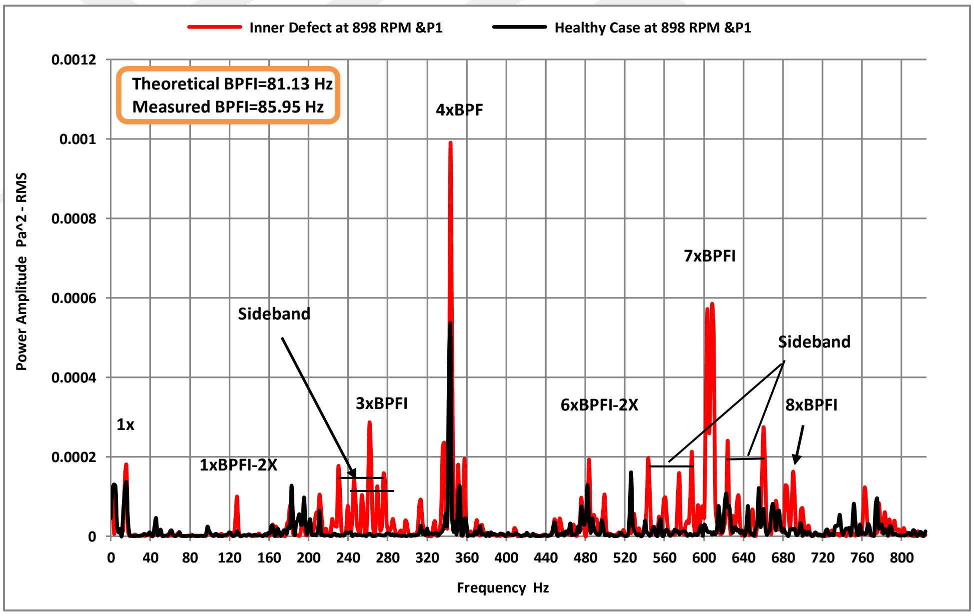

Figure 4.83 Sound power spectrum for healthy case vs inner race defect at 898 RPM and load P1.

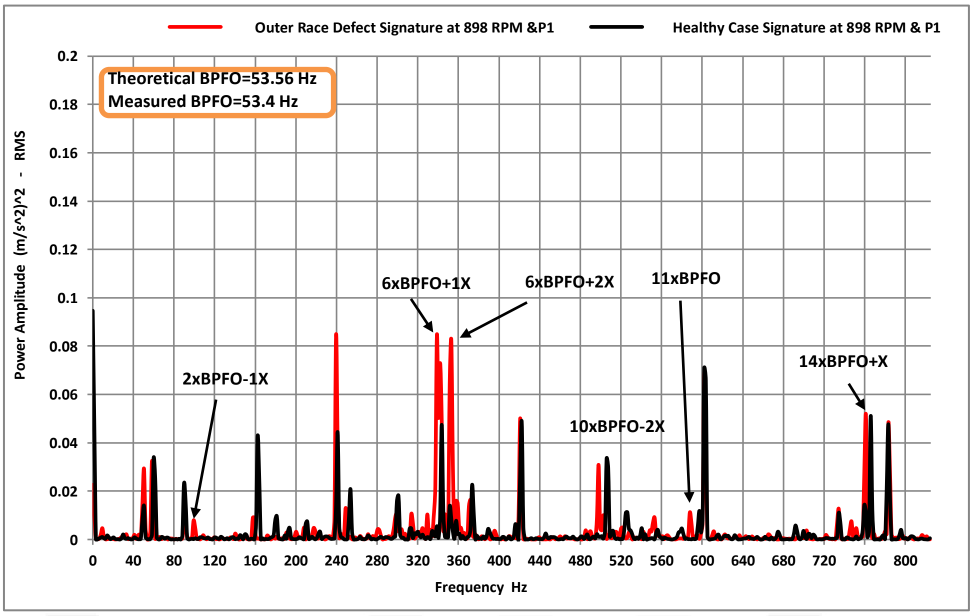

Figure 4.84 Acceleration power spectrum for healthy case vs outer race defect at 898 RPM and load P1.

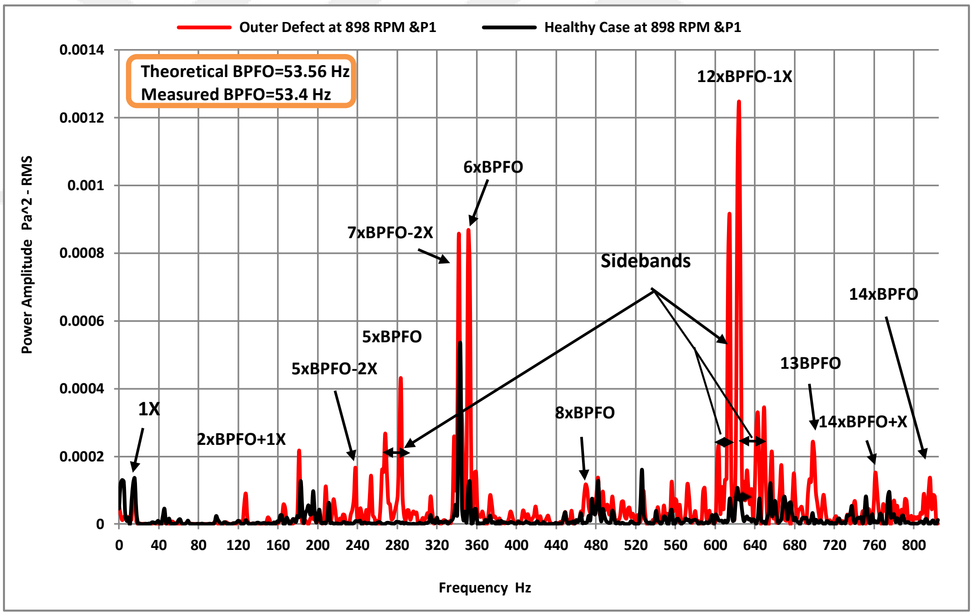

Figure 4.85 Sound power spectrum for healthy case vs outer race defect at 898 RPM and load P1.

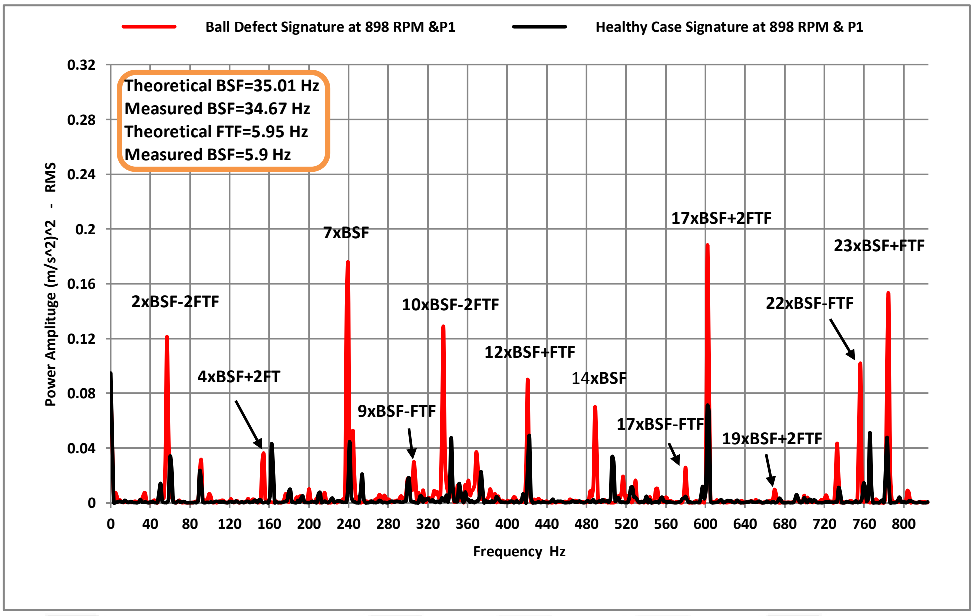

Figure 4.86 Acceleration power spectrum for healthy case vs ball defect at 898 RPM and load P1.

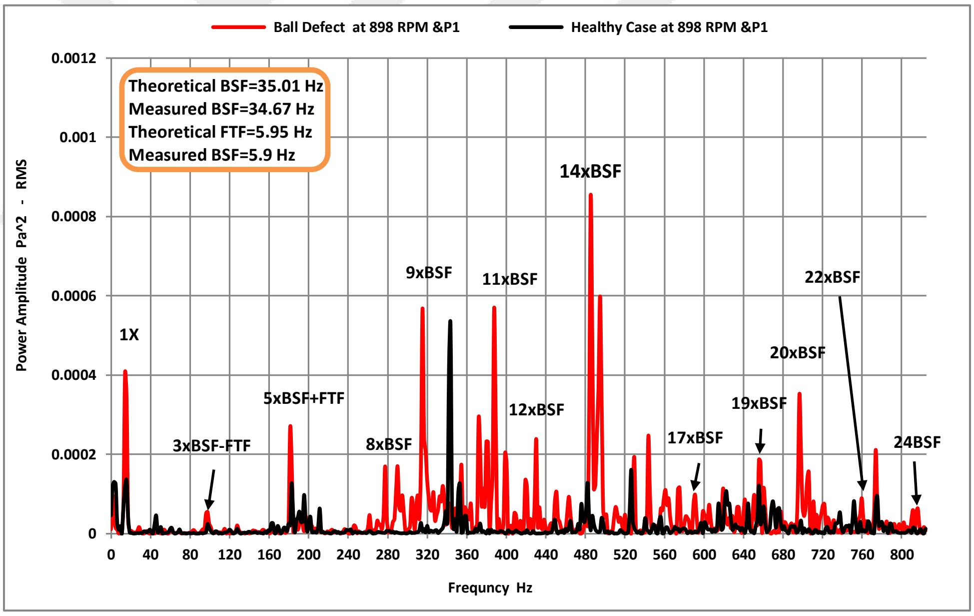

Figure 4.87 Sound power spectrum for healthy case vs ball defect at 898 RPM and load P1.

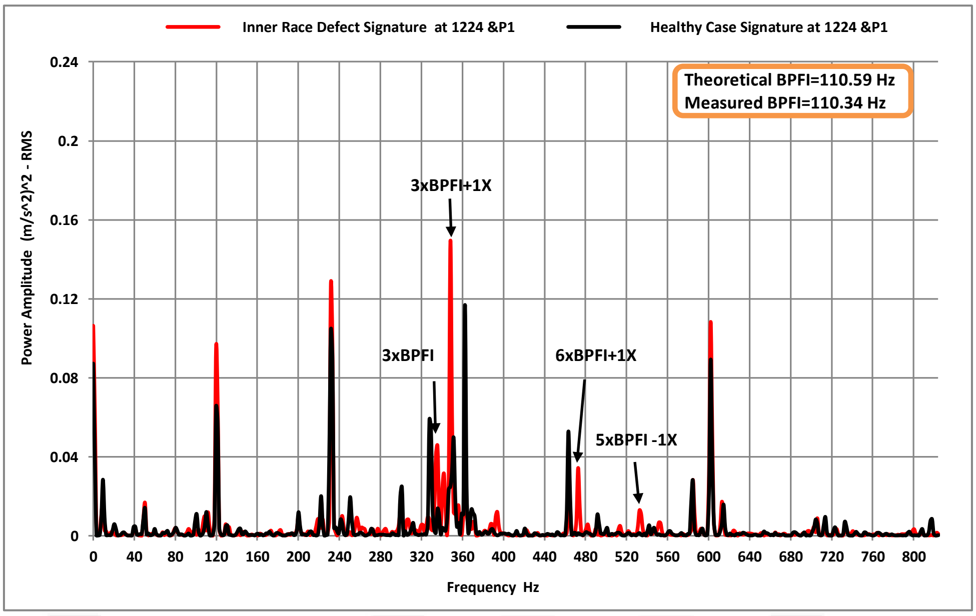

Figure 4.88 Acceleration power spectrum for healthy case vs inner defect at 1224 RPM and load P1.

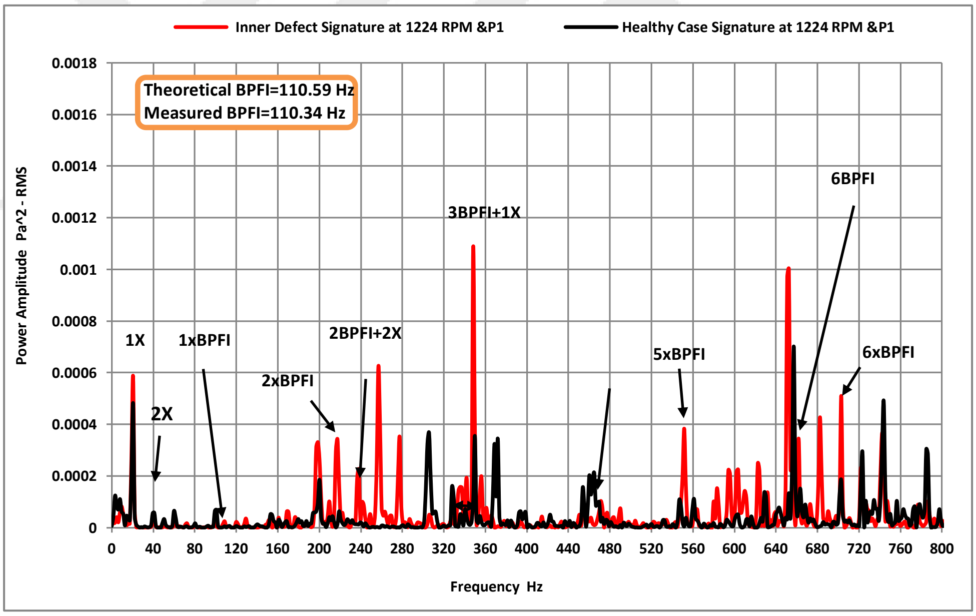

Figure 4.89 Sound power spectrum for healthy case vs inner defect at 1224 RPM and load P1.

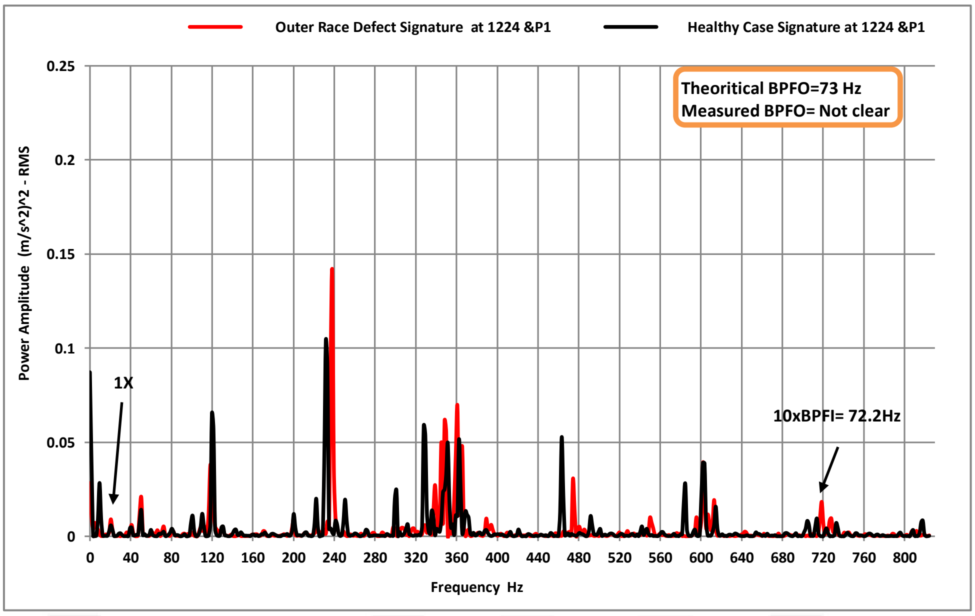

Figure 4.90 Acceleration power spectrum for healthy case vs outer defect at 1224 RPM and load P1.

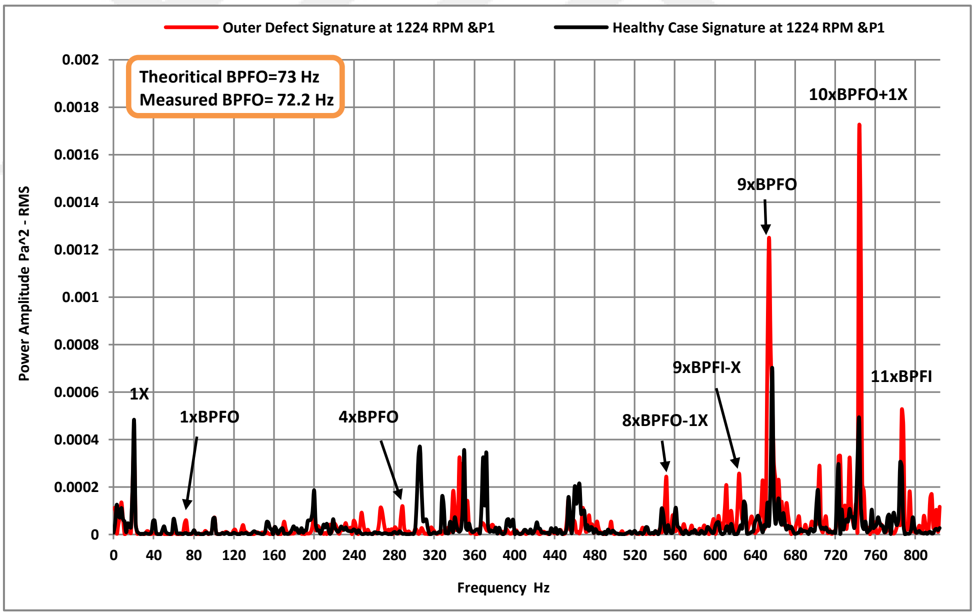

Figure 4.91 Sound power spectrum for healthy case vs outer defect at 1224 RPM and load P1.

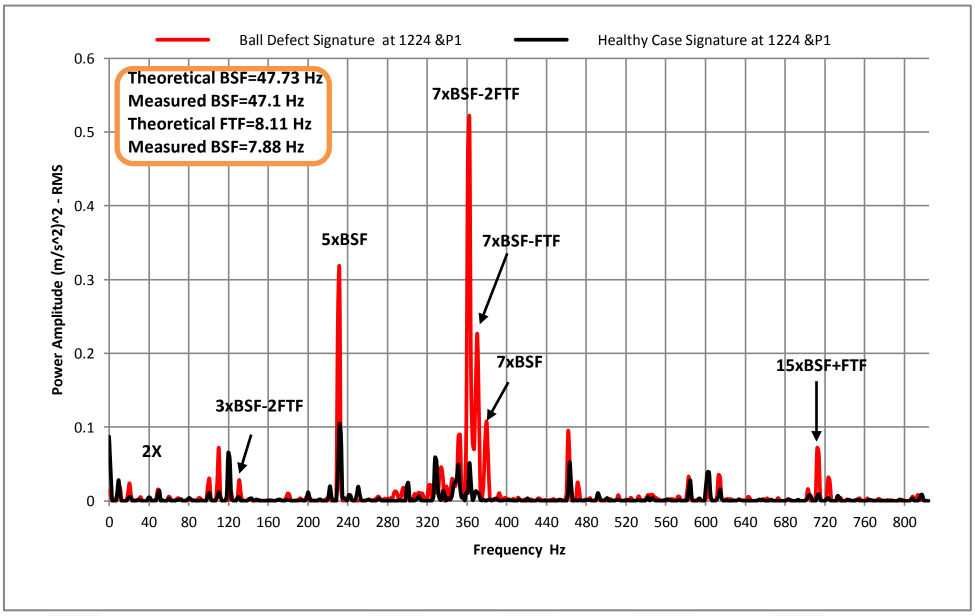

Figure 4.92 Acceleration power spectrum for healthy case vs ball defect at 1224 RPM and load P1.

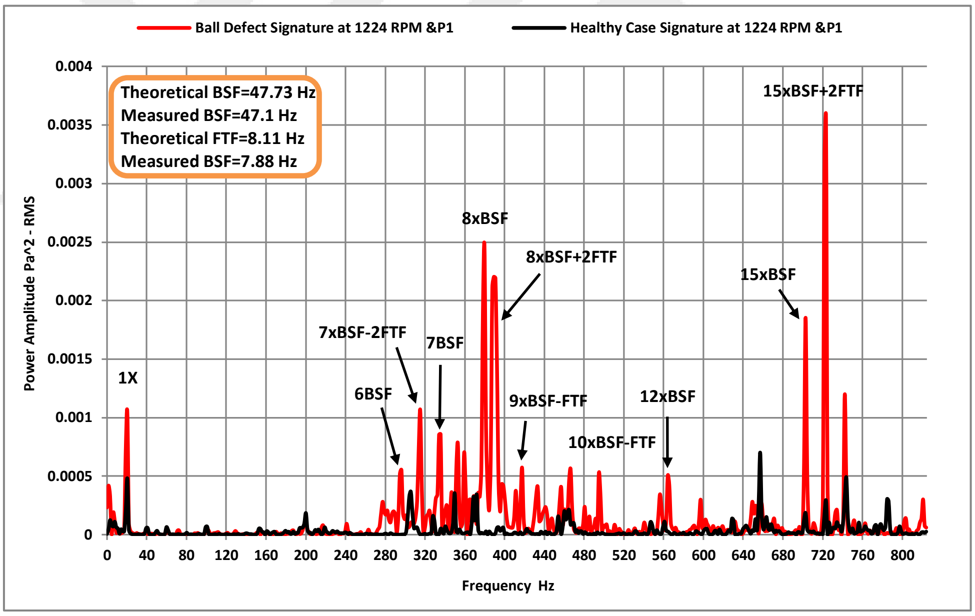

Figure 4.93 Sound power spectrum for healthy case vs ball defect at 1224 RPM and load P1.

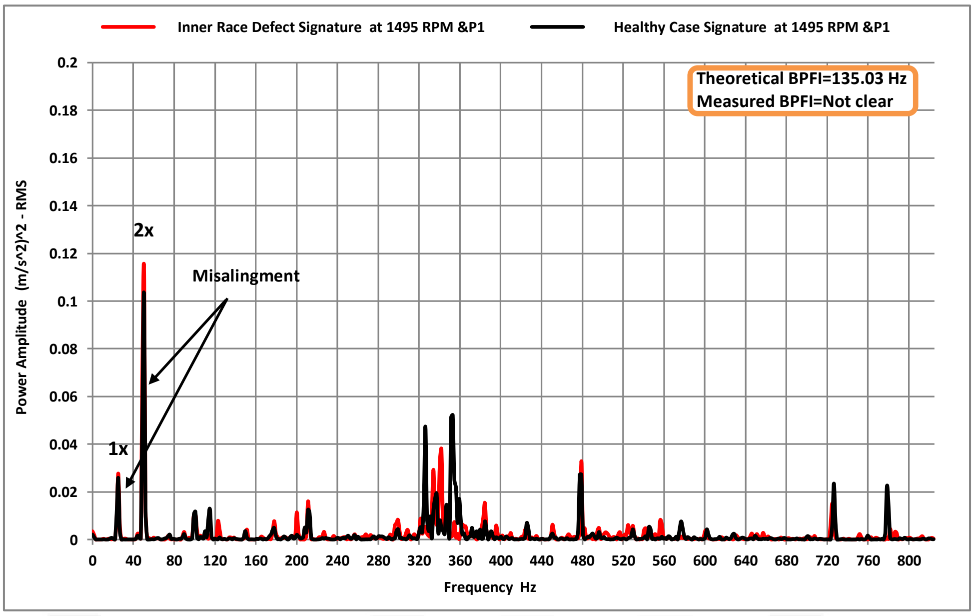

Figure 4.94 Acceleration power spectrum for healthy case vs inner race defect at 1495 RPM and load P1.

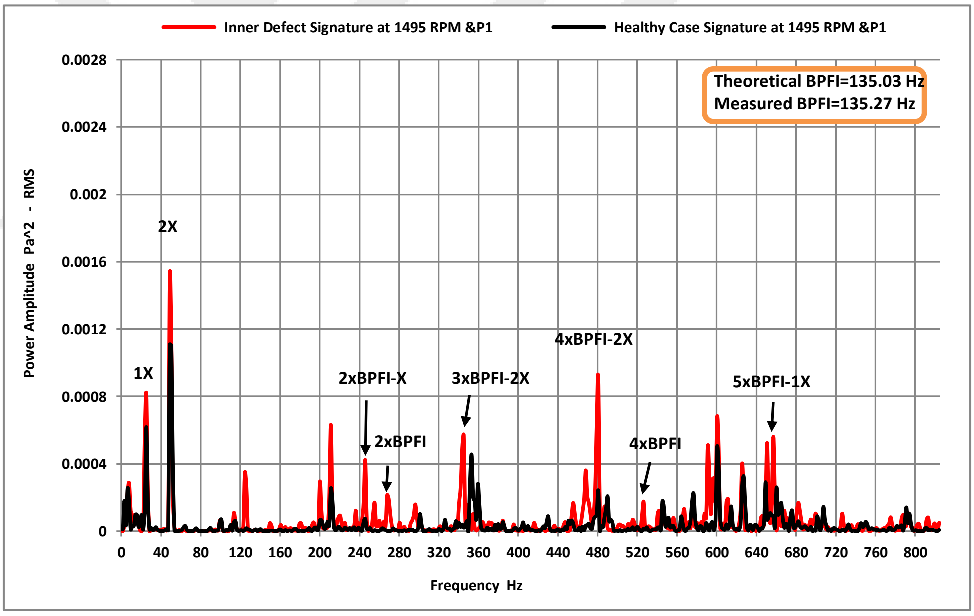

Figure 4.95 Sound power spectrum for healthy case vs inner race defect at 1495 RPM and load P1.

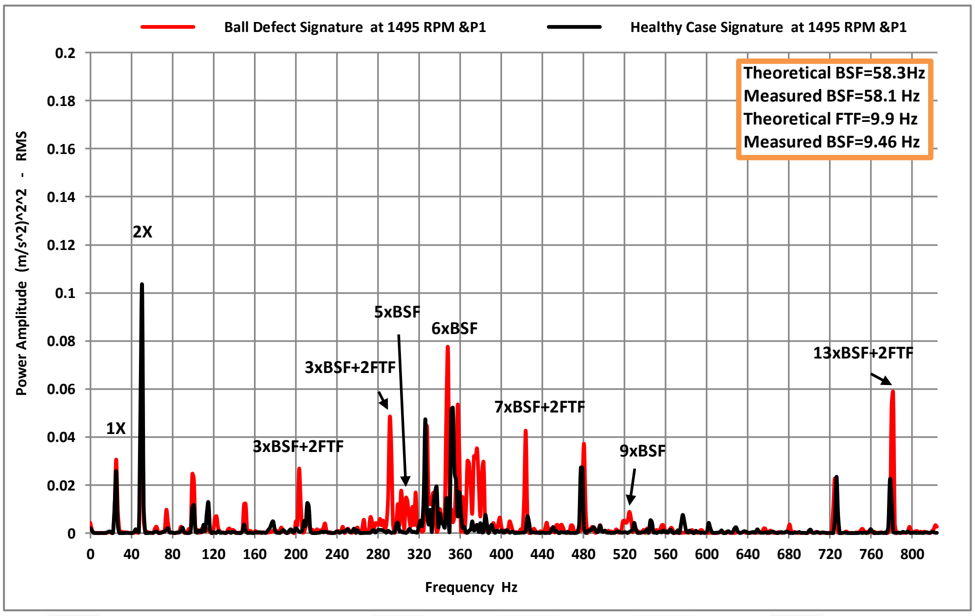

Figure 4.96 Acceleration power spectrum for healthy case vs ball defect at 1495 RPM and load P1.

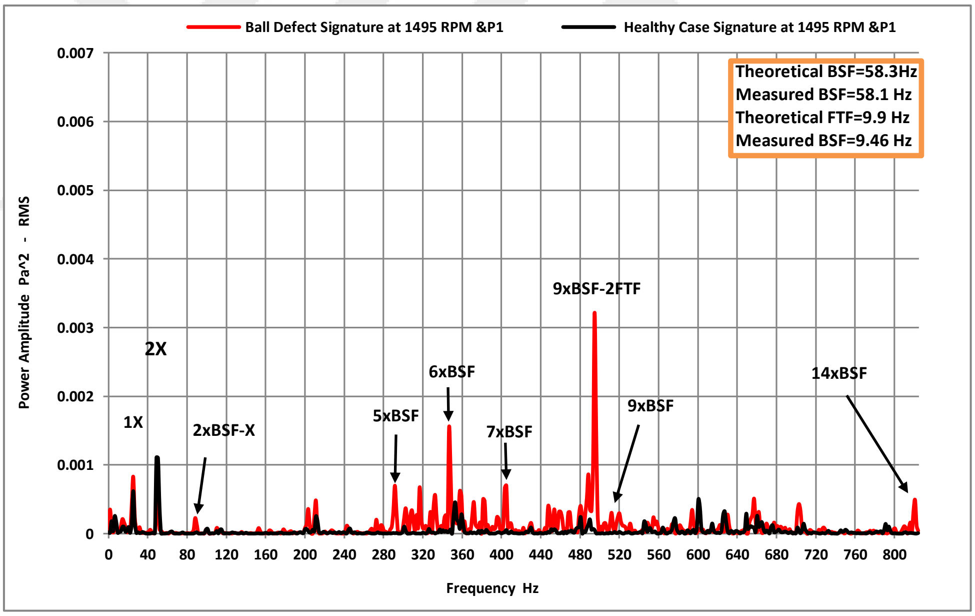

Figure 4.97 Sound power spectrum for healthy case vs ball defect at 1495 RPM and load P1.

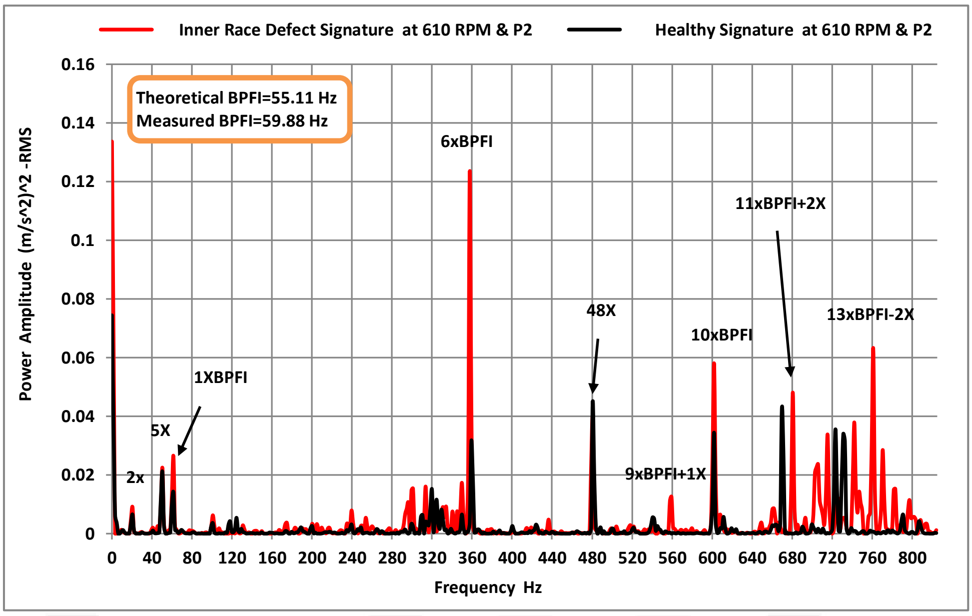

Figure 4.98 Acceleration power spectrum for healthy case vs inner race defect at 610 RPM and load P2.

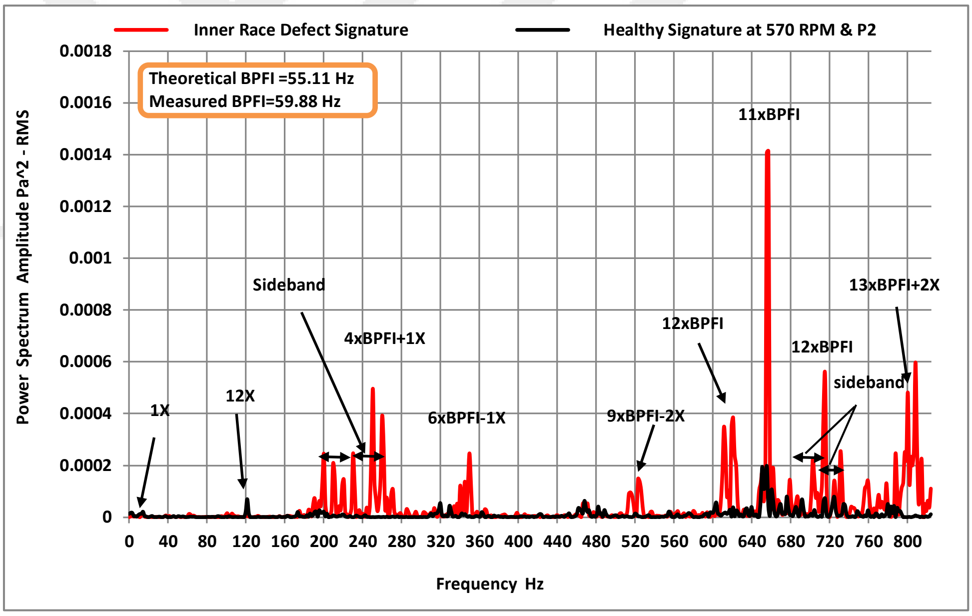

Figure 4.99 Sound power spectrum for healthy case vs inner race defect at 610 RPM and load P2.

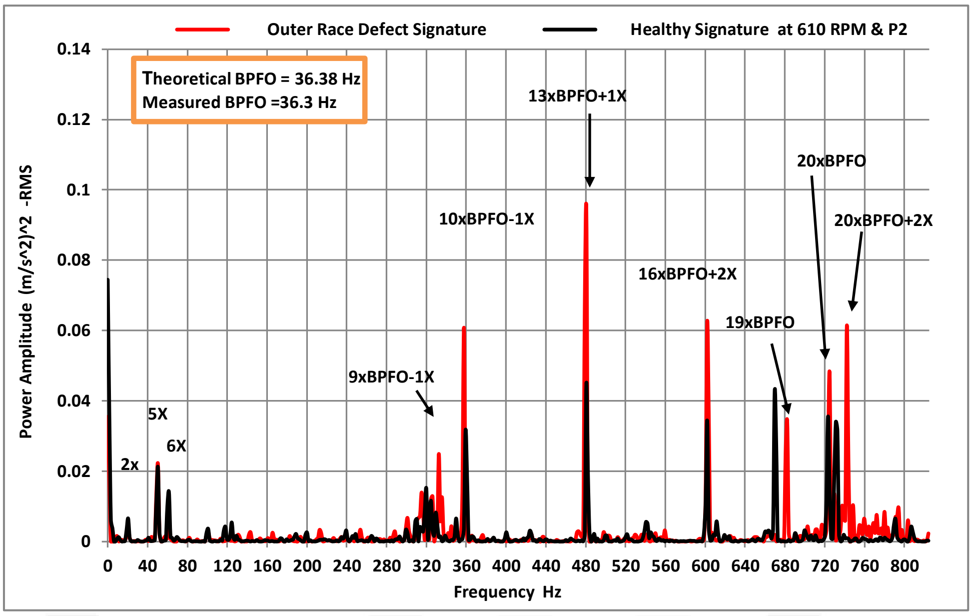

Figure 4.100 Acceleration power spectrum for healthy case vs outer race defect at 610 RPM and load P2.

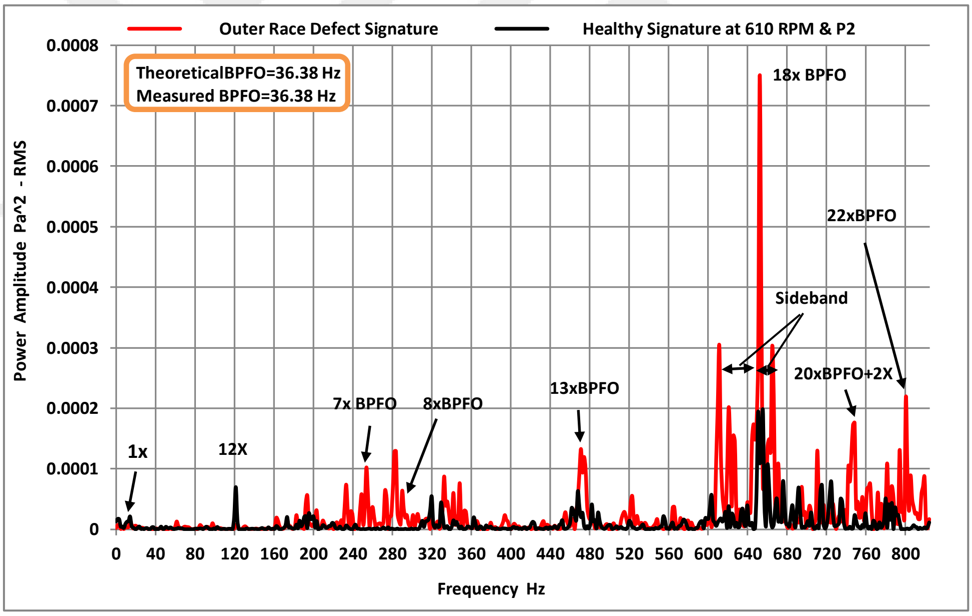

Figure 4.101 Sound power spectrum for healthy case vs outer race defect at 610 RPM and load P2.

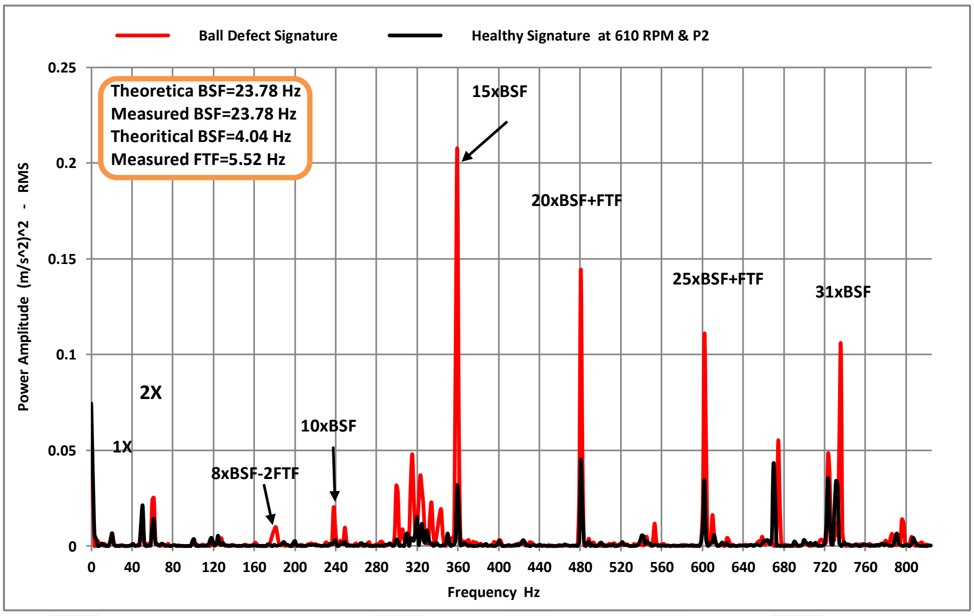

Figure 4.102 Acceleration power spectrum for healthy case vs ball defect at 610 RPM and load P2.

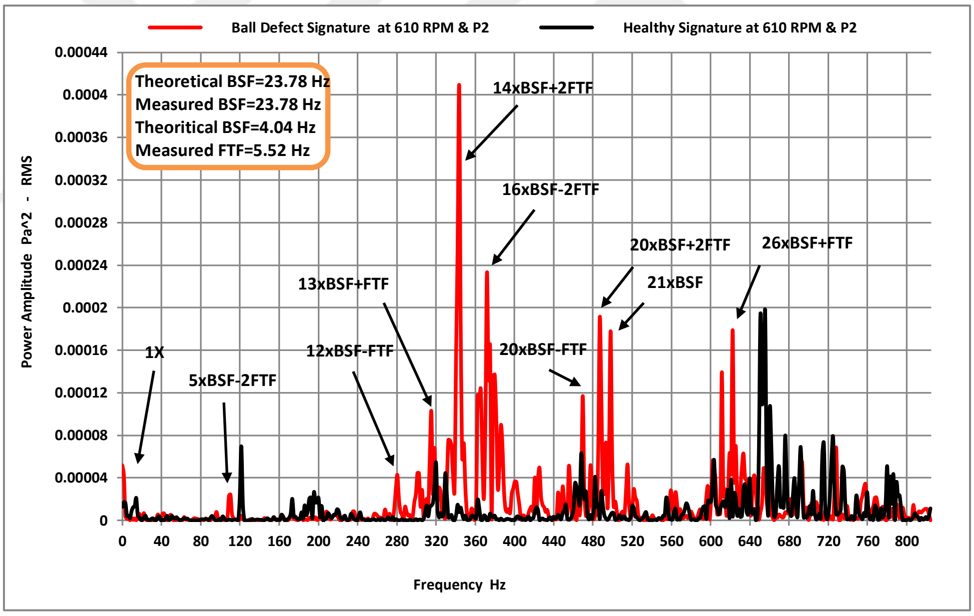

Figure 4.103 Sound power spectrum for healthy case vs ball defect at 610 RPM and load P2.

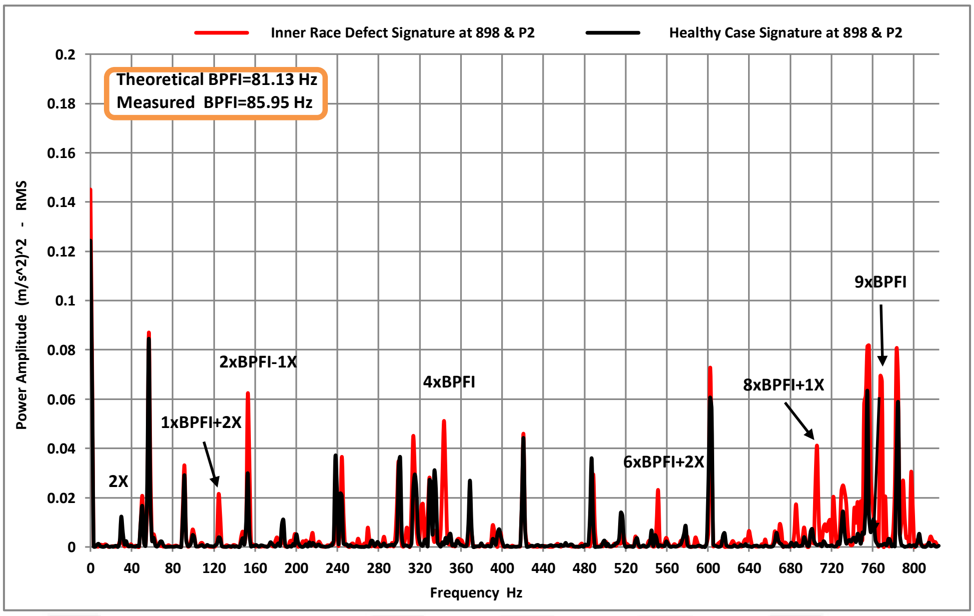

Figure 4.104 Acceleration power spectrum for healthy case vs inner race defect at 898 RPM and load P2.

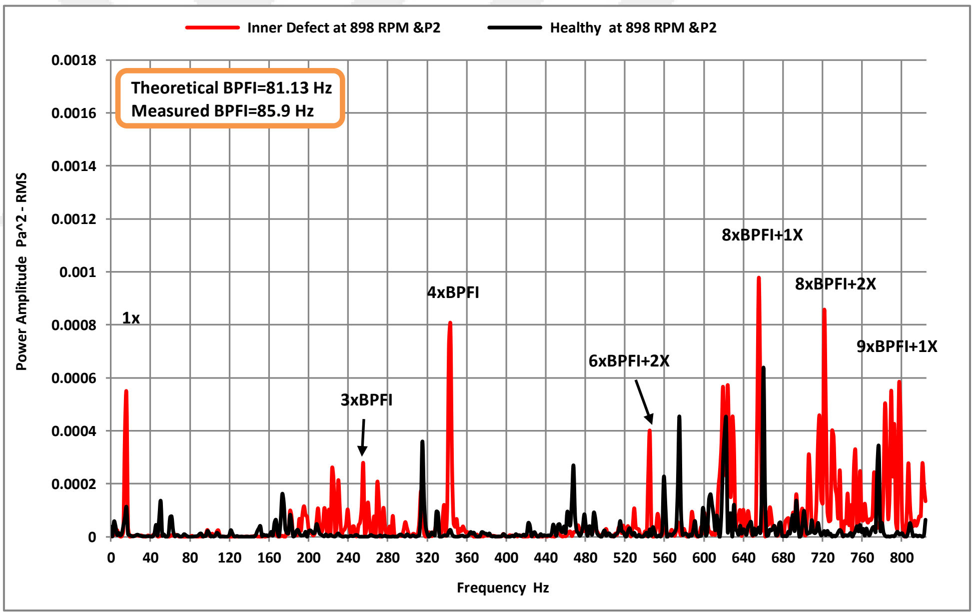

Figure 4.105 Sound power spectrum for healthy case vs inner race defect at 898 RPM and load P2.

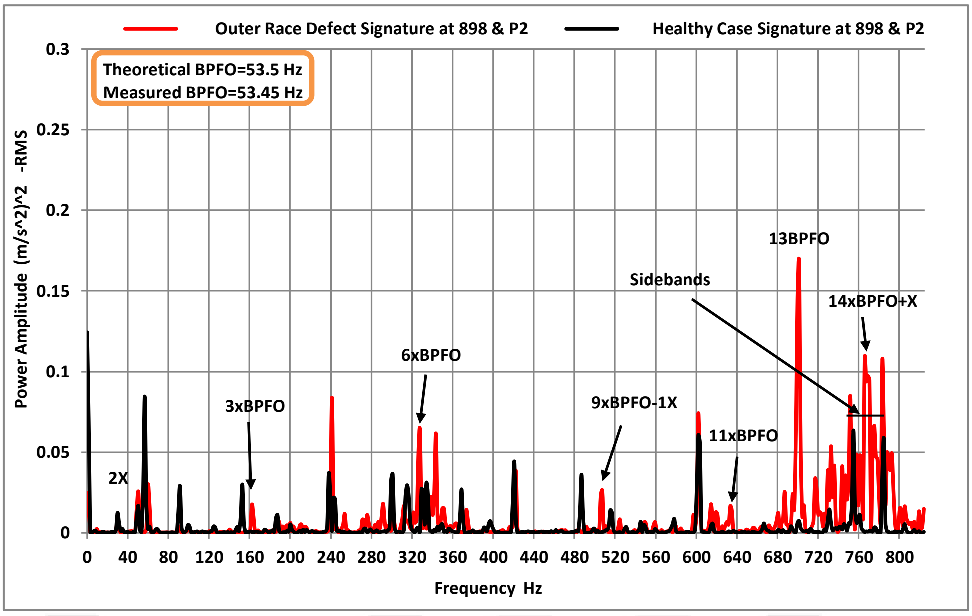

Figure 4.106 Acceleration power spectrum for healthy case vs outer race defect at 898 RPM and load P2.

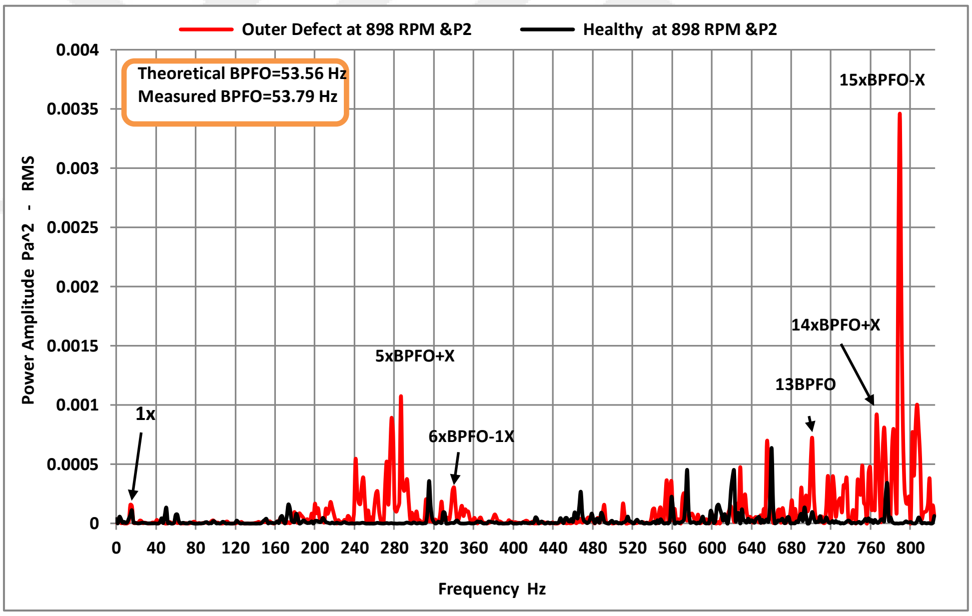

Figure 4.107 Sound power spectrum for healthy case vs outer race defect at 898 RPM and load P2.

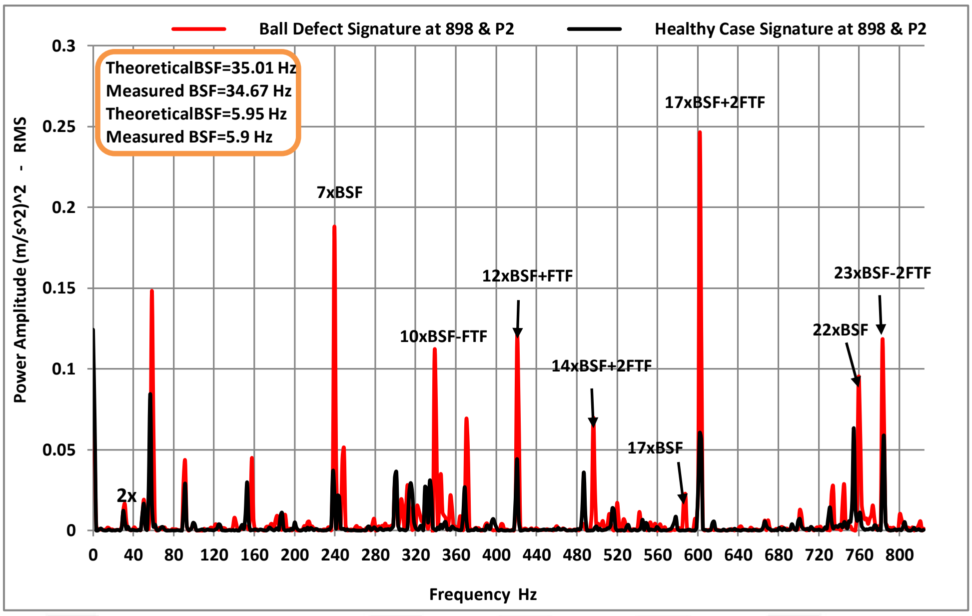

Figure 4.108 Acceleration power spectrum for healthy case vs ball defect at 898 RPM and load P2.

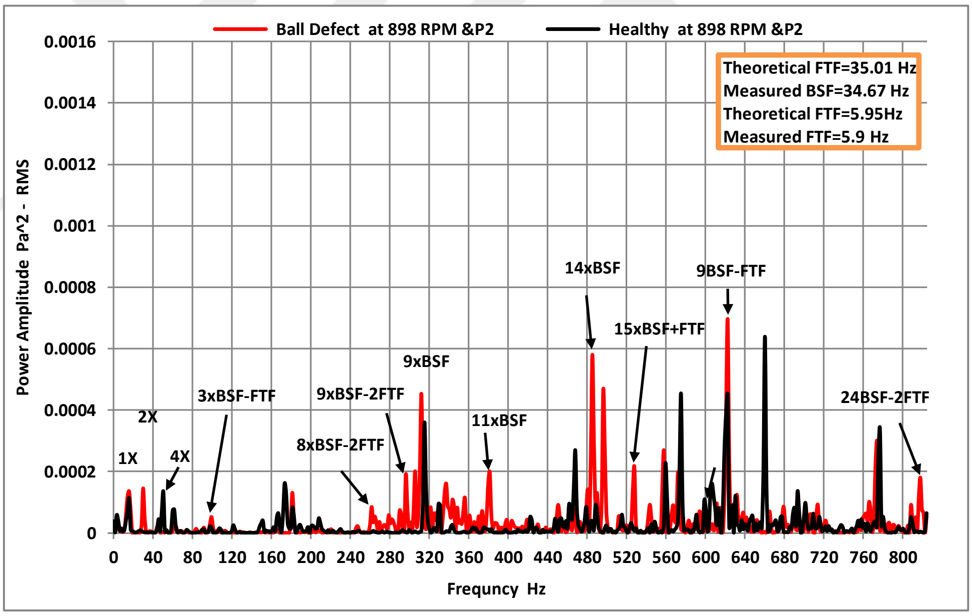

Figure 4.109 Sound power spectrum for healthy case vs ball defect at 898 RPM and load P2.

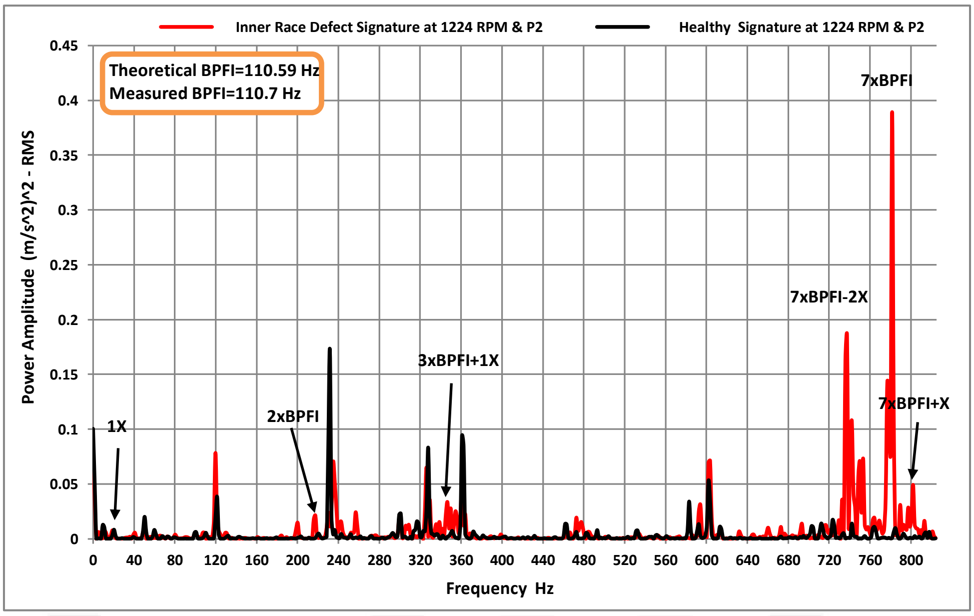

Figure 4.110 Acceleration power spectrum for healthy case vs inner defect at 1224 RPM and load P2.

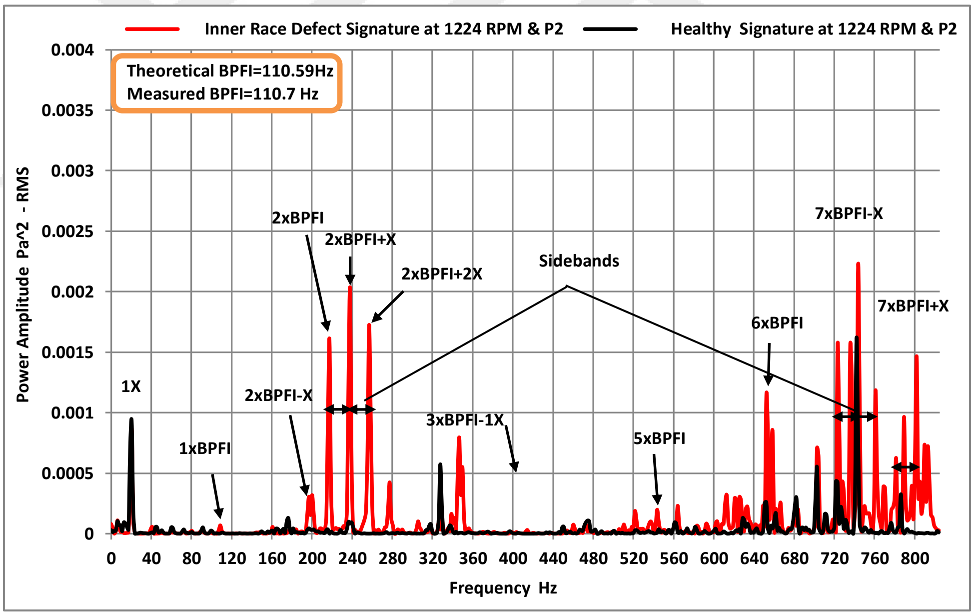

Figure 4.111 Sound power spectrum for healthy case vs inner defect at 1224 RPM and load P2.

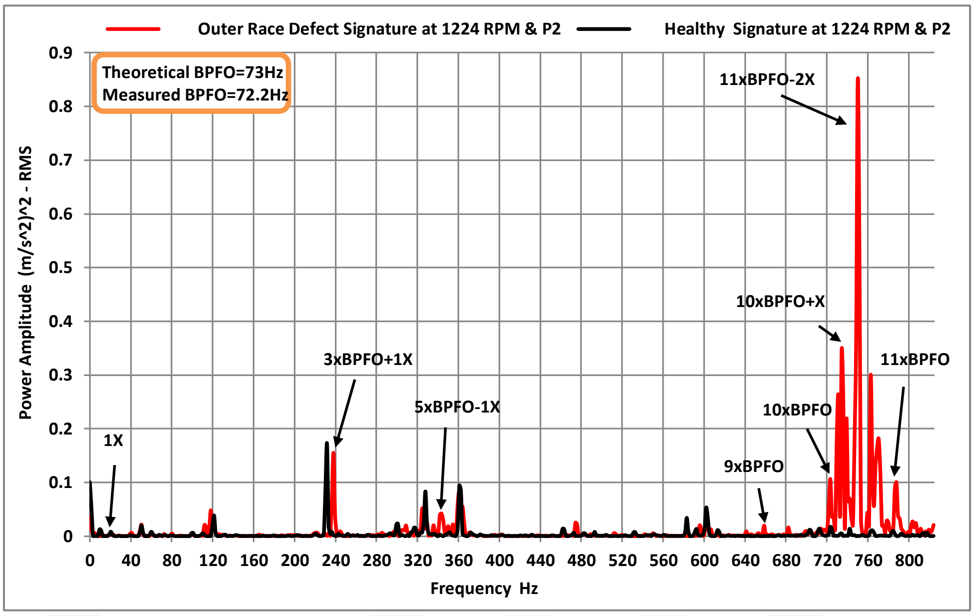

Figure 4.112 Acceleration power spectrum for healthy case vs outer defect at 1224 RPM and load P2.

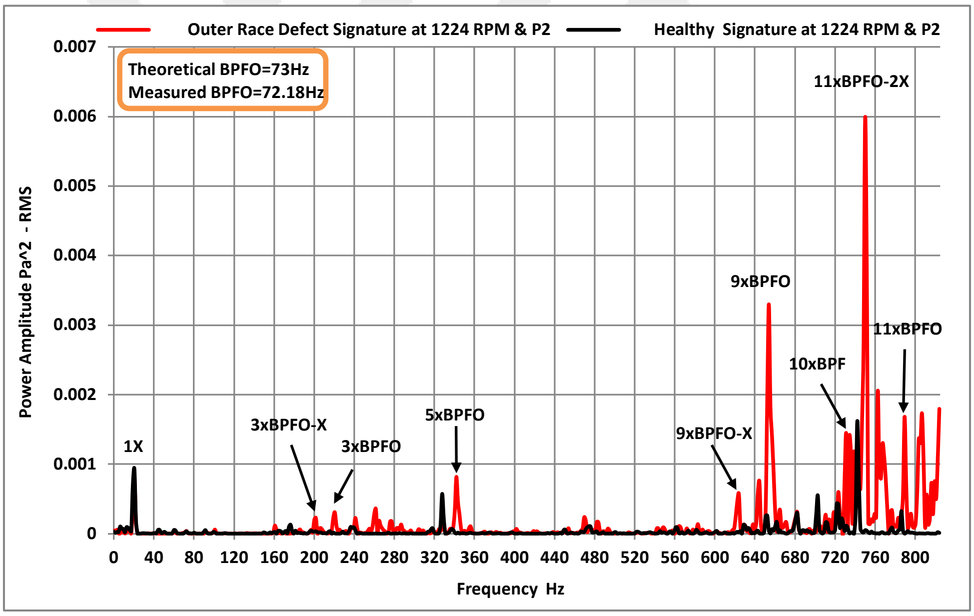

Figure 4.113 Sound power spectrum for healthy case vs outer defect at 1224 RPM and load P2.

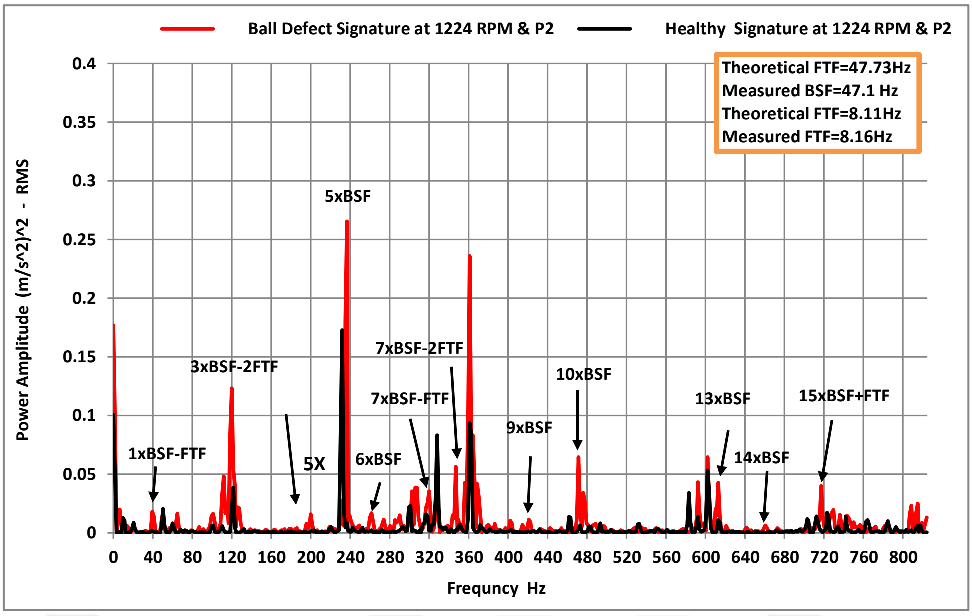

Figure 4.114 Acceleration power spectrum for healthy case vs ball defect at 1224 RPM and load P2.

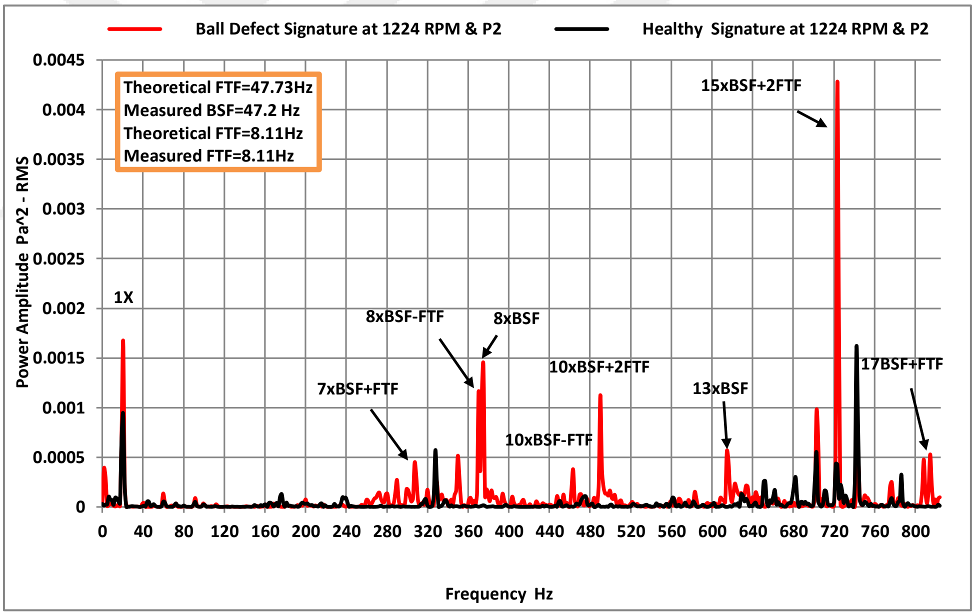

Figure 4.115 Sound power spectrum for healthy case vs ball defect at 1224 RPM and load P2.

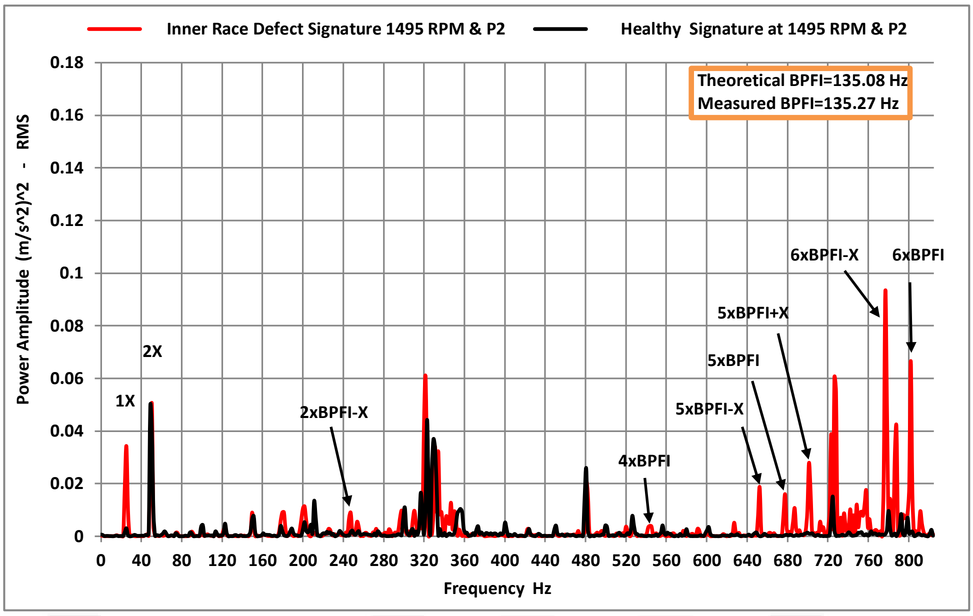

Figure 4.116 Acceleration power spectrum for healthy case vs inner race defect at 1495 RPM and load P2.

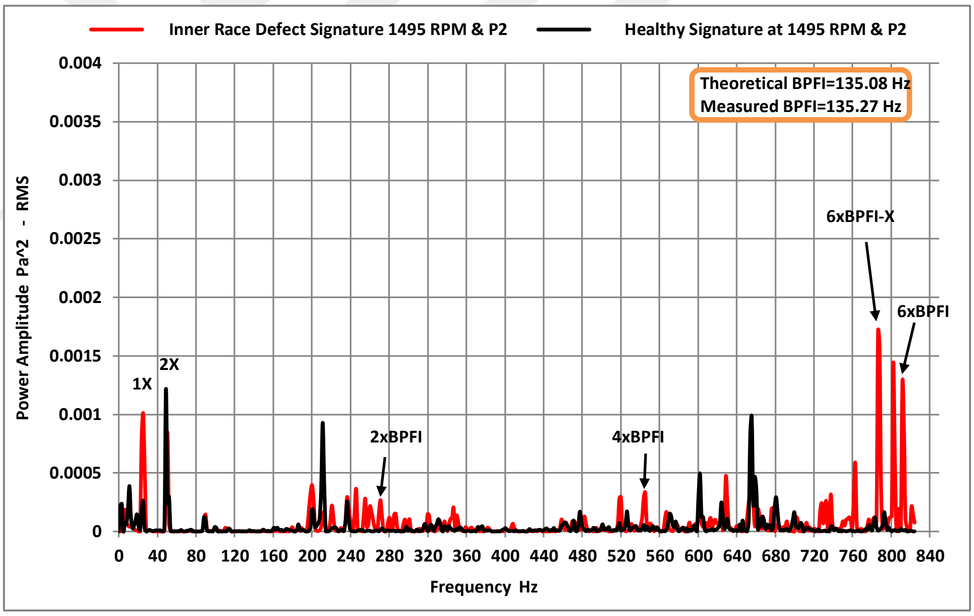

Figure 4.117 Sound power spectrum for healthy case vs inner race defect at 1495 RPM and load P2.

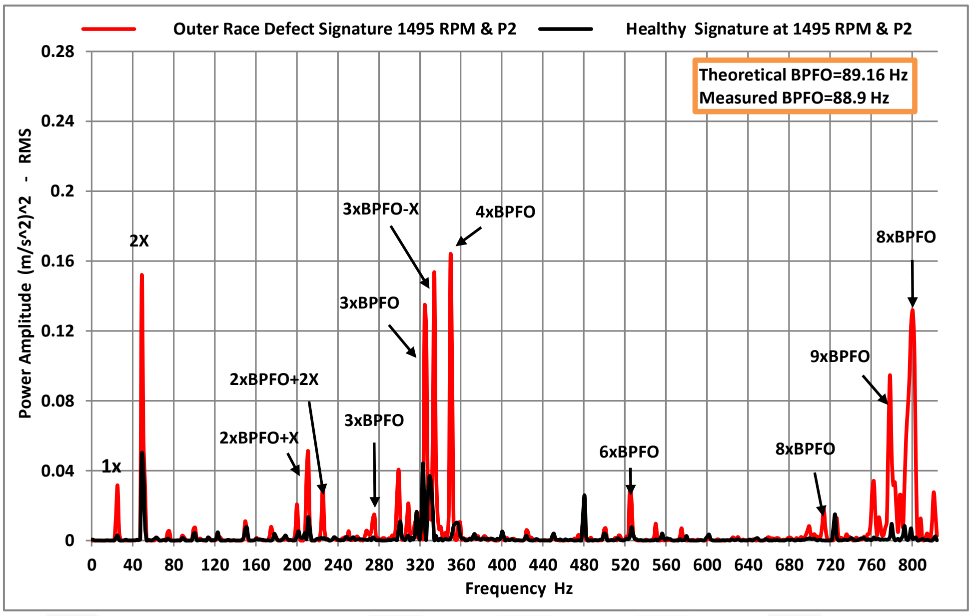

Figure 4.118 Acceleration power spectrum for healthy case vs outer race defect at 1495 RPM and load P2.

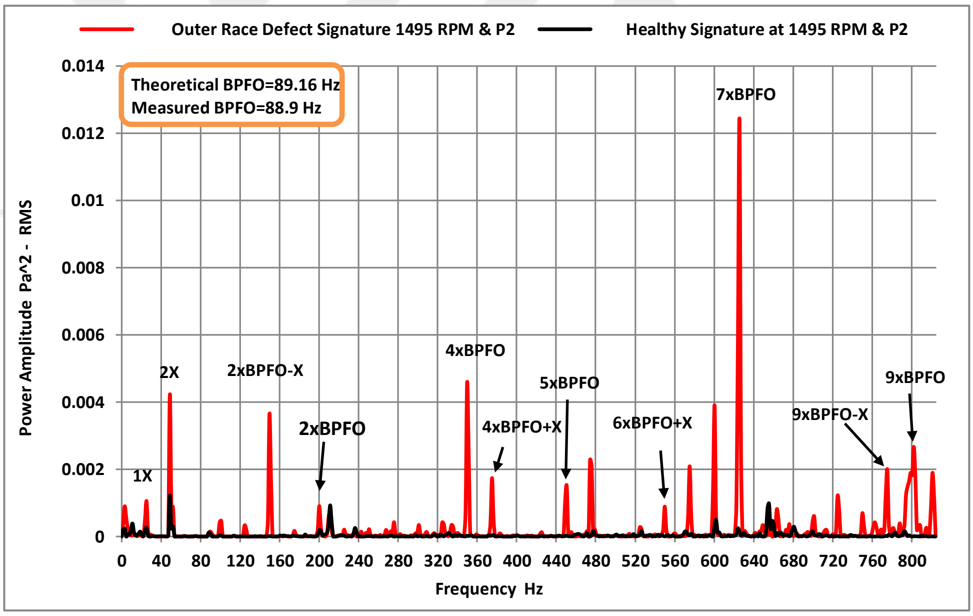

Figure 4.119 Sound power spectrum for healthy case vs outer race defect at 1495 RPM and load P2.

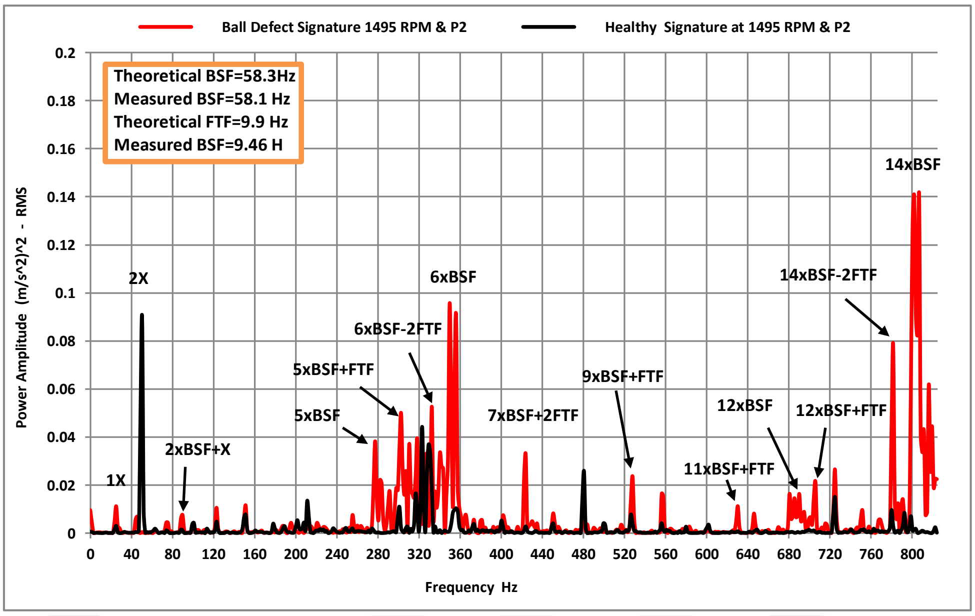

Figure 4.120 Acceleration power spectrum for healthy case vs ball defect at 1495 RPM and load P2.

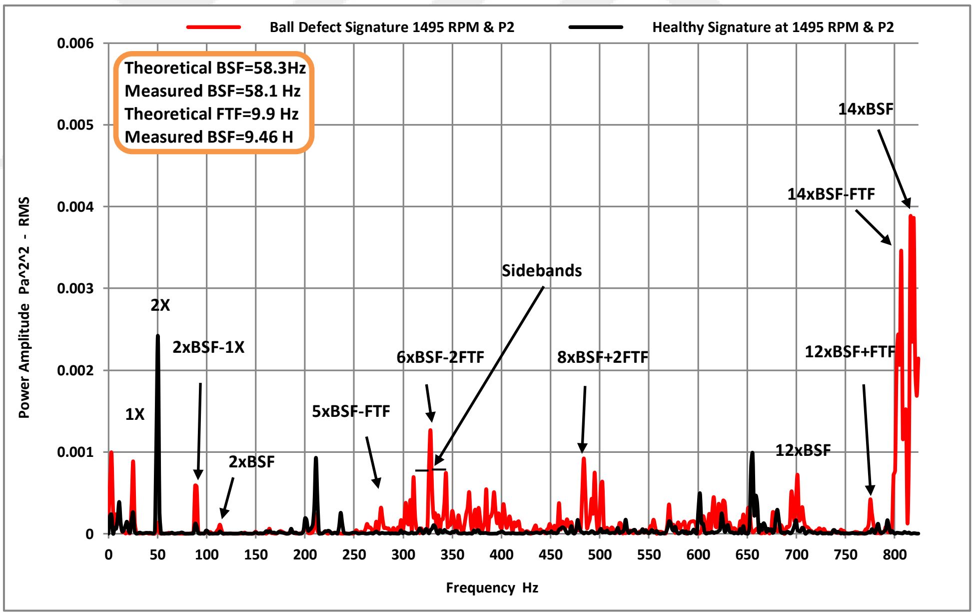

Figure 4.121 Sound power spectrum for healthy case vs ball defect at 1495 RPM and load P2.

CHAPTER 5

DISCUSSION AND CONCULUSION

5.1 Discussion

In this study, vibration signals and sound emissions from fault-free bearings were measured and compared with faulty bearings at speeds of 610, 898, 1224, and 1495 rpm. The purpose of this study is to measure the effectiveness of acoustic emission technique compared to vibration technique. The results of this paper focus on the comparison of two nondestructive testing methods. These tests are caused by bearings that have artificially induced defects on the outer ring, inner ring and balls. Therefore, three defective bearings and one healthy bearing are used. The vibration signal and the AE signal were recorded, compared and analyzed. This study was used to extract the following results.

5.1.1 Observations of Temporal Waveform

Figure 5.1 shows the time waveform segment of the acoustic emission signal, which is magnified from Figure 4.28 to compare normal bearing signals with faulty bearings. The signal amplitude of the faulty bearing is significantly increased compared to the faultless bearing, and also shows fluctuations and bursts due to defects. Therefore, the bearing waveform signal can be considered as a fast and initial method for diagnosing bearing conditions based on the bearing's operating history.

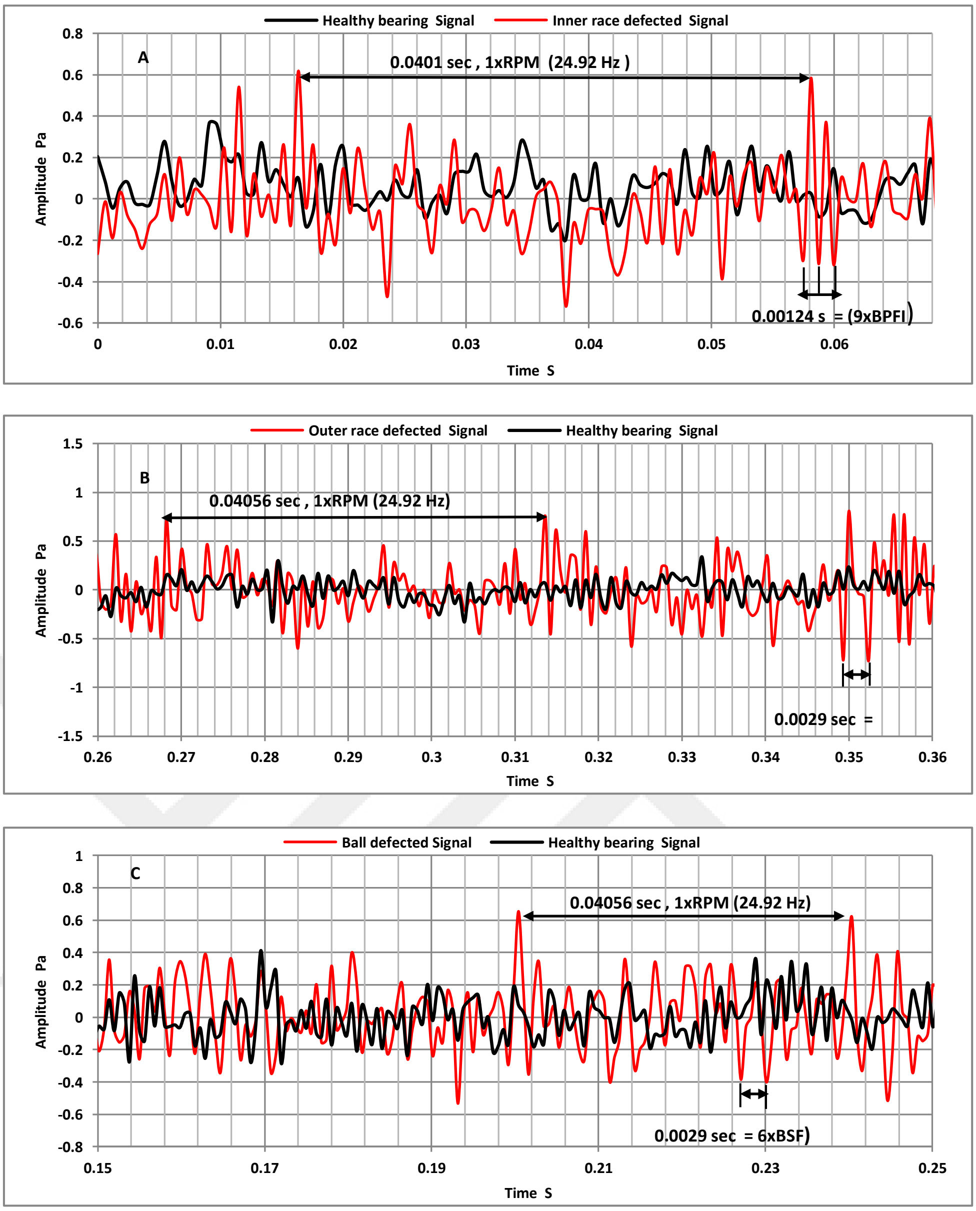

Figure 5.1 Segment of sound signal for healthy bearing vs (a) Inner race defect (b) Outer race defect (c) Ball defect bearing at load P2 & 1495 rpm (Zoomed from figure 4.28).

5.1.2 Observations of Statistical Analysis

Figures 4.5 - 4.28 show a sample plots of the parameters extracted from the AE and vibration acceleration signals, for both healthy and defective bearings. Tables 5.3 - 5.5 show the acoustic emission parameters of the experimental time-domain signal, indicating that most of the faulty bearing parameter values are fluctuate upward compared to healthy bearing parameters, such as RMS, crest factor, peak value. The amplitude increases significantly when speed increases at all loads, which show the presence of faults in the bearings. Except for the kurtosis feature, there is a significant increase in amplitude just at low speeds for all bearing defects, while follows a random increment at high speeds. Localized defects in the bearing increase the pulse content of the signal, therefore, kurtosis value, which is a measure of the peakedness waveform, will also increase. Healthy bearing signal shows an ideal Gaussian behavior at the time domain, hence the value of kurtosis feature of bearing should be around 3 [50; 51].

At all load levels, especially at speeds (612 and 898) rpm, the kurtosis feature values for faulty bearings are greater than 3, as shown in Tables 5.7 and 5.9. This is an indication of a fault in the defective bearings. Skewness is an important scalar parameter for signal behaviour, but in this study, it did not reflect a clear trend of degradation of bearing conditions.

For the statistical parameters of the acceleration signal, tables 5.6 -5.8 show that the amplitude values of most parameters increased to the maximum at speed of 1224 rpm then decreased at speed of 1495 rpm, where most parameters exhibit the behaviour of the curve, which peaked at speed of 1224 rpm. RMS, crest factor and peak value parameters indicate that there are an indication of the defects in bearings in different ratio, especially at the high speeds. While the skewness and kurtosis feature in this study did not reflect the apparent degradation of bearing conditions, except limited cases at different speeds as in Figures 4.41 and 4.44. The kurtosis amplitude of the ball defective bearings increases at the P1 load, speed higher than 612 rpm and the P2 load level at speeds lower than 612 rpm.

Based on the above, statistical analysis of vibration and acoustic emission signature is very useful for determining bearing conditions. Moreover, it turns out that RMS and peaks are more effective at identifying faulty bearings at all speeds. The crest factor also shows significant efficiency in determining the state of a defective bearing compared to a healthy bearing, but kurtosis feature of acoustic emission more efficient at low-frequency range, as opposed to vibration technique that appears to be more effective in the high frequency range.

Table 5.1 Estimation of acceleration statistical parameters in the time domain at load P0.

Parameters	RMS				Crest Factor				Skewness				Kurtosis				Peak value			
Speed	S1	S2	S3	S4	S1	S2	S3	S4	S1	S2	S3	S4	S1	S2	S3	S4	S1	S2	S3	S4
Healthy	0.846	1.105	0.999	0.699	3.388	3.363	3.614	3.211	0.220	0.201	0.214	0.139	2.764	3.253	2.977	3.179	2.868	4.826	3.880	2.579
Inner race defect	1.027	1.119	1.205	0.997	3.634	3.638	3.823	3.818	0.226	0.083	0.257	0.071	2.889	3.006	3.092	2.922	3.733	4.071	4.611	3.809
Outer race defect	0.895	1.170	1.134	1.209	3.469	3.452	3.669	3.344	0.057	0.001	0.172	-0.042	2.745	3.117	2.924	2.790	2.981	3.655	3.770	4.286
Ball defect	0.950	1.002	1.354	1.009	3.423	3.311	3.751	3.245	0.095	0.041	0.038	-0.033	2.698	2.873	3.186	3.096	3.157	3.130	4.865	3.074

Table 5.2 Estimation of acceleration statistical parameters in the time domain at load P1.

Parameters	RMS				C.F				Skewness				Kurtosis				Peak value			
Speed	S1	S2	S3	S4	S1	S2	S3	S4	S1	S2	S3	S4	S1	S2	S3	S4	S1	S2	S3	S4
Healthy	0.929	1.152	0.94	0.841	3.408	3.421	3.502	3.350	0.288	0.073	0.169	0.200	3.639	3.062	3.072	3.118	4.096	4.207	4.529	3.410
Inner race defect	0.922	1.172	1.168	0.941	3.600	3.436	3.467	3.541	-0.011	0.231	0.102	0.267	2.943	3.148	2.686	3.035	3.319	4.030	4.051	3.334
Outer race defect	1.123	1.141	1.088	1.082	3.223	4.262	3.425	3.811	0.046	0.142	0.005	0.189	2.783	3.308	2.925	3.2	3.620	4.865	3.293	3.5
Ball defect	1.277	1.505	1.667	1.147	3.594	3.822	3.961	3.712	0.079	0.188	0.266	0.115	2.672	3.187	3.435	3.202	4.591	5.756	6.603	4.259

Table 5.3 Estimation of acceleration statistical parameters in the time domain at load P2.

Parameters	RMS				Crest Factor				Skewness				Kurtosis				Peak value			
Speed	S1	S2	S3	S4	S1	S2	S3	S4	S1	S2	S3	S4	S1	S2	S3	S4	S1	S2	S3	S4
Healthy	0.933	1.141	1.130	0.768	3.143	3.619	3.567	3.191	0.126	0.228	0.157	0.154	2.693	3.122	3.178	3.199	2.934	4.257	4.372	2.820
Inner race defect	1.152	1.431	1.702	1.089	3.905	3.821	4.522	3.445	0.102	0.151	-0.030	0.200	2.939	3.130	3.482	3.083	4.501	5.469	7.701	3.753
Outer race defect	1.004	1.732	1.732	1.480	4.327	3.835	3.835	2.986	-0.004	0.011	0.011	-0.092	3.723	3.395	3.395	3.111	4.348	6.643	6.643	4.419
Ball defect	1.202	1.533	1.802	1.446	3.836	4.151	3.816	3.776	0.158	0.254	0.068	0.053	2.912	3.303	2.742	3.584	4.614	6.365	5.256	5.464

Table 5.4 Estimation of acoustic emission statistical parameters in the time domain at load P0.

Parameters	RMS				Crest Factor				Skewness				Kurtosis				Peak value			
Speed	S1	S2	S3	S4	S1	S2	S3	S4	S1	S2	S3	S4	S1	S2	S3	S4	S1	S2	S3	S4
Healthy	0.055	0.078	0.117	0.135	2.889	3.129	2.942	2.715	0.106	0.085	0.222	0.106	3.089	2.811	2.828	3.034	0.192	0.271	0.43	0.454
Inner race defect	0.09	0.099	0.122	0.145	3.444	3.655	3.541	3.33	0.029	-0.036	0.066	0.151	3.239	2.943	2.972	2.939	0.313	0.303	0.396	0.528
Outer race defect	0.074	0.112	0.135	0.2	2.994	3.828	3.648	3.248	-0.108	0.124	-0.098	-0.028	3.508	2.756	2.813	3.323	0.222	0.363	0.412	0.791
Ball defect	0.071	0.099	0.135	0.196	3.326	3.704	3.593	3.035	-0.077	0.175	-0.011	-0.051	3.351	2.861	2.932	3.09	0.236	0.368	0.485	0.595

Table 5.5 Estimation of acoustic emission statistical parameters in the time domain at load P1.

Parameters	RMS				Crest Factor				Skewness				Kurtosis				Peak value			
Speed	S1	S2	S3	S4	S1	S2	S3	S4	S1	S2	S3	S4	S1	S2	S3	S4	S1	S2	S3	S4
Healthy	0.041	0.086	0.114	0.120	3.069	3.152	3.217	3.045	0.01	-0.031	-0.127	-0.013	2.933	2.866	3.124	3.036	0.137	0.269	0.338	0.415
Inner race defect	0.107	0.106	0.126	0.150	3.685	3.292	3.264	3.157	0.064	-0.009	-0.096	0.032	3.095	3.249	2.945	2.841	0.397	0.33	0.414	0.475
Outer race defect	0.147	0.127	0.134	0.145	3.651	4.276	3.427	3.8	0.058	0.015	-0.052	0.036	3.363	3.338	2.77	3	0.536	0.546	0.408	0.5
Ball defect	0.095	0.127	0.191	0.190	3.531	3.459	5.026	3.815	-0.044	0.05	0.187	0.038	3.147	3.034	3.66	2.987	0.337	0.44	0.964	0.727

Table 5.6 Estimation of acoustic emission statistical parameters in the time domain at load P2.

Parameters	RMS				Crest Factor				Skewness				Kurtosis				Peak value			
Speed	S1	S2	S3	S4	S1	S2	S3	S4	S1	S2	S3	S4	S1	S2	S3	S4	S1	S2	S3	S4
Healthy	0.061	0.097	0.111	0.122	3.093	3.143	3.211	3.067	0.031	-0.008	-0.048	0.109	3.105	2.928	3.183	3.209	0.228	0.385	0.414	0.499
Inner race defect	0.127	0.147	0.199	0.165	3.201	3.479	3.318	3.461	0.043	0.126	0.128	0.335	3.265	3.31	3.005	3.216	0.408	0.511	0.66	0.571
Outer race defect	0.098	0.197	0.229	0.285	3.215	3.494	3.304	3.679	-0.054	0.108	-0.034	0.127	3.455	3.003	3.18	2.9	0.317	0.691	0.759	1.051
Ball defect	0.083	0.124	0.177	0.220	3.75	3.405	4.243	3.764	0.174	-0.014	0.072	-0.048	4.475	3.024	3.428	3.515	0.396	0.423	0.751	0.831

5.1.3 Observations of Frequency Domain Analysis (Spectra Analysis)

This section summarizes the frequency domain results obtained from experimental data. Therefore, typical results for each specific type of faults are discussed. The frequency and amplitude plots 4.49 - 4.121 show the characteristic frequencies of defective bearings, according to location of defect.

The power spectrum analysis of the inner race defected signature has been carried out, on which defect frequency of inner race (BPFI) and its harmonics can be seen, as well as each harmonic sidebands. These sidebands are separated by approximately equal distances equal to the rotation frequency of the inner ring.

These sidebands are due to the fact that the inner ring rotates, so the entry of the defect into the loading zone and leaving it leads to a change in the contact force between the rolling element and the inner race, can cause a deflection. The impact size will be higher at load zone, and will decrease while leaving the defect to this area. This behaviour results in a modified signal (amplitude-modulation) with the inner race frequency (rotation speed). The corresponding time signal in Figure 4.29 shows the impacts occurring in the rolling bearing, where the time between the highest peaks corresponds to the inner race rotation.

The analysis of the outer race defect frequency (BPFO) can be observed through the figures that illustrated in the previous chapter. The defect frequency of the outer ring and its harmonics have been determined. There are no sidebands with these defects. This is due to the type of bearing that is fixed to the housing bearing, the outer ring has a rigid constraint and therefore no amplitude modulation.

As for the characteristic frequency of the ball defect, due to the amplitude modulation, it can be seen that this frequency and its harmonics appear in the sideband, and the distance of the sideband is equal to a new frequency, called the fundamental train frequency (FTF) [52].

Finally, Tables 5.9 -5.11 shows that the outer ring defect and the defective ball are measured at a lower frequency than the theoretical frequency. However, the measurement frequency of the inner ring defect is higher than the theoretical value.

Table 5.7 Theoretical and measured characteristics frequency of vibration at load P0.

Frequency	Inner race defect (BPFI)				Fundamental (FTF)				Outer race defect (BPFO)				Ball defect (BSF			
Speed	S1	S2	S3	S4	S1	S2	S3	S4	S1	S2	S3	S4	S1	S2	S3	S4
Theoretical	55.11	81.13	110.59	135.08	4.04	5.95	8.11	9.9	36.38	53.56	73	89.16	23.78	35.01	47.73	58.3
Measured	59.88	85.95	109.18	135.27	4.92	5.9	8.11	9.46	36.3	-	72.2	88.78	23.74	34.67	47.05	58.1

Table 5.8 Theoretical and measured characteristics frequency of vibration at load P1.

Frequency	Inner race defect (BPFI)				Fundamental (FTF)				Outer race defect (BPFO)				Ball defect (BSF			
Speed	S1	S2	S3	S4	S1	S2	S3	S4	S1	S2	S3	S4	S1	S2	S3	S4
Theoretical	55.11	81.13	110.08	135.08	4.04	5.95	8.11	9.9	36.38	53.56	73	89.16	23.78	35.01	47.73	58.3
Measured	59.88	85.95	110.34	-	4.92	5.9	7.88	9.46	36.2	53.4	-	87.46	23.74	34.67	47.1	58.1

Table 5.9 Theoretical and measured characteristics frequency of vibration at load P2.

Frequency	Inner race defect (BPFI)				Fundamental (FTF)				Outer race defect (BPFO)				Ball defect (BSF			
Speed	S1	S2	S3	S4	S1	S2	S3	S4	S1	S2	S3	S4	S1	S2	S3	S4
Theoretical	55.11	81.13	110.08	135.08	4.04	5.95	8.11	9.9	36.38	53.56	73	89.16	23.78	35.01	47.73	58.3
Measured	59.88	85.95	110.7	135.27	5.52	5.9	8.16	9.46	36.3	53.45	72.2	88.9	23.78	34.67	47.1	58.1

Table 5.10 Theoretical and measured characteristics frequency of AE at load P0.

Frequency	Inner race defect (BPFI)				Fundamental (FTF)				Outer race defect (BPFO)				Ball defect (BSF			
Speed	S1	S2	S3	S4	S1	S2	S3	S4	S1	S2	S3	S4	S1	S2	S3	S4
Theoretical	55.11	81.13	110.59	135.08	4.04	5.95	8.11	9.9	36.38	53.56	73	89.16	23.78	35.01	47.73	58.3
Measured	59.88	85.95	109.18	135.27	4.92	5.9	7.88	9.46	36.3	53.4	72.2	88.78	23.74	34.67	47.05	58.1

Table 5.11 Theoretical and measured characteristics frequency of AE at load P1.

Frequency	Inner race defect (BPFI)				Fundamental (FTF)				Outer race defect (BPFO)				Ball defect (BSF			
Speed	S1	S2	S3	S4	S1	S2	S3	S4	S1	S2	S3	S4	S1	S2	S3	S4
Theoretical	55.11	81.13	110.08	135.08	4.04	5.95	8.11	9.9	36.38	53.56	73	89.16	23.78	35.01	47.73	58.3
Measured	59.88	85.95	110.34	135.27	4.92	5.9	7.88	9.46	36.3	53.4	72.2	88.78	23.74	34.67	47.1	58.1

Table 5.12 Theoretical and measured characteristics frequency of AE at load P2.

Frequency	Inner race defect (BPFI)				Fundamental (FTF)				Outer race defect (BPFO)				Ball defect (BSF			
Speed	S1	S2	S3	S4	S1	S2	S3	S4	S1	S2	S3	S4	S1	S2	S3	S4
Theoretical	55.11	81.13	110.08	135.08	4.04	5.95	8.11	9.9	36.38	53.56	73	89.16	23.78	35.01	47.73	58.3
Measured	59.88	85.95	110.7	135.27	5.52	5.9	8.11	9.46	36.38	53.79	72.18	88.9	23.78	34.67	47.2	58.1

5.2 Conclusion

In summary, this study showed that:

1. Acoustic emission technique is as good as vibration measurements for detecting bearings faults. More specifically, AE is more sensitive than vibration technology in all frequency bands, especially in low bands, where it is highly effective in detecting incipient faults, either by statistically analyzing signals to extracting appropriate features or through spectral analysis of the signal in the frequency band.
2. The frequency domain analysis accurately gives the fault location. The time domain and its statistical analysis only predict failures.

In conclusion, we can conclude from this study that there is an integration between these techniques to monitor the condition of bearings and diagnose defects and incipient defects, at a wide range of speeds.

5.3 Future Work

1. Automatic recognition of faults
2. Further experiments with finer resolution in rotational speeds and even lower speeds.
3. Selection of best sampling frequency and initial filter guess based on rotational speed and other known properties of the system.

REFERENCES

[1] El Anouar, B. A., Elamrani, M., Elkihel, B., Delaunois, F., Manssouri, I. (2017). A Comparative Experimental Study Of Different Methods In Detection And Monitoring Bearing Defects. *International Journal Of Advanced Scientific And Technical Research*, **1**(7), 409-423.

[2] Kahirdeh, A. (2014). *A Diagnosis Feature Space For Condition Monitoring And Fault Diagnosis Of Ball Bearings* (Published Doctoral Dissertation). Louisiana State University, Louisiana, USA.

[3] Kaewkongka, T. (2002). *Bearing Condition Monitoring Using Acoustic Emission And Vibration: The Systems Approach* (Published Doctoral Dissertation). Brunel University School Of Engineering And Design, London, United Kingdom.

[4] KSB Pump. (2019). Rolling Element Bearing. https://www.ksb.com/centrifugal-pump-lexicon/rolling-element-bearing/191386/. 22-6-2019.

[5] Nippon Bearing. (2018). The Difference Between A Roller Bearing And A Ball Bearing. https://www.nbcorporation.com/difference-roller-bearing-ball-bearing/. 22-6-2019.

[6] Palmgren, A. (1959). *Ball And Roller Bearing Engineering*. 3rd edition. Philadelphia, PA. USA: SKF Industries. Inc.

[7] Nisbet, T. S., Mullett, G. W. (1978). *Rolling Bearings In Service*; *Interpretation of Types of Damage*. London: Hutchinson Benham

[8] Raison, B., Rostaing, G., Butscher, O., Maroni, C. S. (2002). Investigations Of Algorithms For Bearing Fault Detection In Induction Drives. *In IECON 02 Industrial Electronics Society, IEEE 2002 28th Annual Conference Of The. Vol. 2,* (Pp. 1696-1701). *IEEE.*

[9] Whittle, M. (2013). *Wind Turbine Generator Reliability: An Exploration of The Root Causes of Generator Bearing Failures* (Published Doctoral Dissertation). Durham University, North Carolina, UK.

[10] Fiixsoftware, “Preventative Maintenance (PM).” [Online]. https://www.fiixsoftware.com/maintenance-strategies/preventative-maintenance., 10-02-2017.

[11] Messer A., 2015, Mechanical Remote Monitoring with Ultrasound. http://www.bearing-news.com/mechanical-remote-monitoring-with-ultrasound., 12-04-2018

[12] Balderston, H. L. (1969). The Detection Of Incipient Failure In Bearings. *Mater Evaluation*, **27**(6), 121-128.

[13] Yoshioka, T., Fujiwara, T. (1984). Application Of Acoustic Emission Technique To Detection Of Rolling Bearing Failure. *American Society Of Mechanical Engineers*, **14**(1), 55-76.

[14] Bagnoli, S., Capitani, R., Citti, P. (1988). Comparison Of Accelerometer And Acoustic Emission Signals As Diagnostic Tools In Assessing Bearing. *In Proceedings of 2nd International Conference on Condition Monitoring* (pp. 117-125).

[15] Rao, V. V., Ratnam, C. (2015). A Comparative Experimental Study On Identification Of Defect Severity In Rolling Element Bearings Using Acoustic Emission And Vibration Analysis. *Tribology in Industry*, **37**(2). 176-185

[16] Mba, D. (2003). Acoustic Emissions And Monitoring Bearing Health. *Tribology Transactions*, **46**(3), 447-451.

[17] Tandon, N., Choudhury, A. (1999). A Review Of Vibration And Acoustic Measurement Methods For The Detection Of Defects In Rolling Element Bearings. *Tribology International*, **32**(8), 469-480.

[18] Butler, D. E. (1973). The Shock-Pulse Method For The Detection Of Damaged Rolling Bearings. *Non-Destructive Testing*, **6**(2), 92-95.

[19] Tandon, N., Nakra, B. C. (1992). Comparison Of Vibration And Acoustic Measurement Techniques For The Condition Monitoring Of Rolling Element Bearings. *Tribology International*, **25**(3), 205-212.

[20] Collacott, R. (2012). *Mechanical Fault Diagnosis And Condition Monitoring*. Landon: Springer Science & Business Media.

[21] Dyer, D., Stewart, R. M. (1978). Detection Of Rolling Element Bearing Damage By Statistical Vibration Analysis. *Journal Of Mechanical Design*, **100**(2), 229-235.

[22] White, M. F. (1984). Simulation And Analysis Of Machinery Fault Signals. *Journal of Sound And Vibration*, **93**(1), 95-116.

[23] Rush, A. A. (1979). Kurtosis-Crystal Ball For Maintenance Engineers. *Iron And Steel International,* **52**(1), 23.

[24] Springer, C. W. (1988). Dont Forget The Time Domain In Analyzing Bearings-A Case-Study. *Tappi Journal*, **71**(8), 190-193.

[25] Gustafsson, O. G., Tallian, T. (1962). Detection Of Damage In Assembled Rolling Element Bearings. *Asle Transactions*, **5**(1), 197-209.

[26] Kim, P. Y. (1984). A Review Of Rolling Element Bearing Health Monitoring. III- Preliminary test results on eddy current proximity transducer technique. *In International Conference on Vibrations in Rotating Machinery, 3rd ed., Heslington, England* (pp. 119-125).

[27] Bhende, A. R., Awari, G. K., Untawale, S. P. (2014). Comprehensive Bearing Condition Monitoring Algorithm For Incipient Fault Detection Using Acoustic Emission. *Jurnal Tribologi*, **2**, 1-30.

[28] Rogers, L. M. (1979). The Application Of Vibration Signature Analysis And Acoustic Emission Source Location To On-Line Condition Monitoring Of Anti-Friction Bearings. *Tribology International*, **12**(2), 51-58.

[29] Heng, R. B. W., Nor, M. J. M. (1998). Statistical Analysis Of Sound And Vibration Signals For Monitoring Rolling Element Bearing Condition. *Applied Acoustics*, **53**(1-3), 211-226.

[30] Al-Ghamd, A. M., Mba, D. (2006). A Comparative Experimental Study On The Use of Acoustic Emission and Vibration Analysis For Bearing Defect Identification and Estimation of Defect Size. *Mechanical Systems And Signal Processing*, **20**(7), 1537-1571.

[31] Kim, E. Y., Tan, A. C., Mathew, J., Yang, B. S. (2008). Condition Monitoring Of Low Speed Bearings: A Comparative Study Of The Ultrasound Technique Versus Vibration Measurements. *Australian Journal Of Mechanical Engineering*, **5**(2), 177-189.

[32] Roque, A. A., Silva, T. A. N., Calado, J. M. F., Dias, C. Q. (2009). An Approach To Fault Diagnosis Of Rolling Bearings. *WSEAS Transactions on Systems and Control*, **4**(4), 188-197.

[33] Saruhan, H., Saridemir, S., Qicek, A., Uygur, I. (2014). Vibration Analysis Of Rolling Element Bearings Defects. *Journal Of Applied Research And Technology*, **12**(3), 384-395.

[34] Van Hecke, B., Qu, Y., He, D., Bechhoefer, E. (2014). A New Spectral Average-Based Bearing Fault Diagnostic Approach. *Journal Of Failure Analysis And Prevention*, **14**(3), 354-362.

[35] Freitas, C., Cuenca, J., Morais, P., Ompusunggu, A., Sarrazin, M., Janssens, K. (2016). Comparison Of Vibration And Acoustic Measurements For Detection Of Bearing Defects. *In International Conference On Noise And Vibration Engineering And International Conference On Uncertainty In Structural Dynamics* (Vol. 1). Leuven, Belgium

[36] Praveenkumar, T., Saimurugan, M., Ramachandran, K. I. (2017). Comparison Of Vibration, Sound And Motor Current Signature Analysis For Detection Of Gear Box Faults. *International Journal of Prognostics and Health Management*, **8**(2).

[37] Caesarendra, W., Tjahjowidodo, T. (2017). A Review Of Feature Extraction Methods In Vibration-Based Condition Monitoring And Its Application For Degradation Trend Estimation Of Low-Speed Slew Bearing. *Machines*, **5**(4), 21.

[38] Kim, D. H., Kim. Y. H., Lee, S. B. (2019). Advanced Condition Monitoring System Using Acoustic Emission And Vibration Analysis Technique. EWGAE (Eds.), *Proceedings of the European Conference On Acoustic Emission Testing,* 33rd , Selins, France.

[39] Hebrard, Y. (2019). Combination Of Vibration Analysis And Acoustic Emission Measurements To Better Characterize Damage And Mechanical Behaviour Of Aerospace High Speed Rolling Bearing. EWGAE (Eds.), *Proceedings of the European Conference On Acoustic Emission Testing,* 33rd , Selins, France.

[40] Swindlehurst, W. (1973). Acoustic Emission-1 Introduction. *Non-Destructive Testing*, **6**(3), 152-158.

[41] Holroyd, T. J., Randall, N. (1993). Use Of Acoustic Emission For Machine Condition Monitoring. *British Journal Of Non-Destructive Testing*, **35**(2), 75-78.

[42] Scruby, C. B. (1987). An Introduction To Acoustic Emission. *Journal Of Physics E: Scientific Instruments*, **20**(8), 946.

[43] Sait, A. S., Sharaf-Eldeen, Y. I. (2011). A Review Of Gearbox Condition Monitoring Based On Vibration Analysis Techniques Diagnostics And Prognostics. *In Rotating Machinery, Structural Health Monitoring, Shock And Vibration*, Volume 5 (Pp. 307-324). Springer, New York, NY.

[44] Martin, H. R. (1989, January). Statistical Moment Analysis As A Means Of Surface Damage Detection. *In Proceedings Of The 7th International Modal Analysis Conference* (Pp. 1016-1021). Las Vegas, USA: Society For Experimental Mechanics.

[45] Mehala, N., Dahiya, R. (2008). A Comparative Study Of FFT, STFT And Wavelet Techniques For Induction Machine Fault Diagnostic Analysis. *In Proceedings Of The 7th WSEAS International Conference On Computational Intelligence, Man-Machine Systems And Cybernetics*, Cairo, Egypt (Vol. 2931).

[46] Mathew, J., Alfredson, R. J. (1984). The Condition Monitoring Of Rolling Element Bearings Using Vibration Analysis. *Journal Of Vibration, Acoustics, Stress, And Reliability In Design*, **106**(3), 447-453.

[47] Harris, C. M., Piersol, A. G. (2002). *Harris' Shock And Vibration Handbook* (Vol. 5). New York: Mcgraw-Hill.

[48] Goldman, S. (1999). *Vibration Spectrum Analysis: A Practical Approach* (2nd Eds.). New York NY, USA: Industrial Press Inc.

[49] M. Kedadouche, M. Thomas and A. Tahan. (2012). Monitoring Bearings By Acoustic Emission: A Comparative Study With Vibration Techniques For Early Detection. *Proceedings of the 30th Seminar on machinery vibration, Canadian Machinery Vibration Association*, Niagara Falls, Canada, p17.

[50] Singh, S. K. (2007). Acoustics Based Condition Monitoring. *Research Scholar, Dept. Of Mech. Engg., IITG,* 1-07.

[51] Mobley, R. K. (1999). *Vibration Fundamentals* (2nd ed.). Oxford, UK: Butterworth-Heinemann, Elsevier

[52] Roque, A. A., Silva, T. A. N., Calado, J. M. F., Dias, C. Q. (2009). An Approach To Fault Diagnosis Of Rolling Bearings. *WSEAS Transactions on Systems and Control*, **4**(4), 188-197.

APPENDICES

A. LabVIEW Environment Program

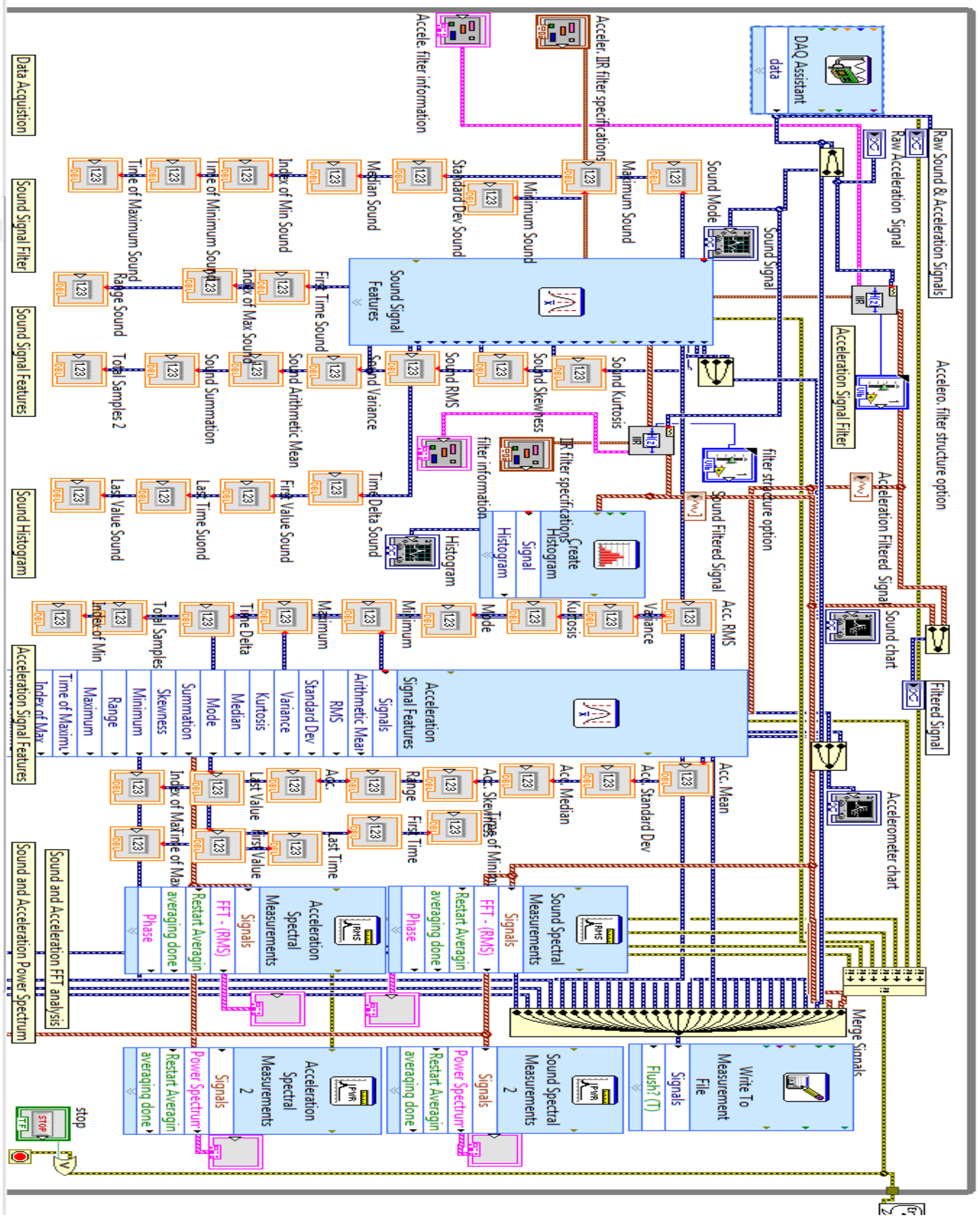

B. Technical Specification of Instruments

Model Number 352C04	ICP® ACCELEROMETER	Revision: D ECN #: 25274

Performance	ENGLISH	SI	
Sensitivity (± 10 %)	10 mV/g	1.02 mV/(m/s²)	
Measurement Range	± 500 g pk	± 4900 m/s² pk	
Frequency Range (± 5 %)	0.5 to 10,000 Hz	0.5 to 10,000 Hz	
Frequency Range (± 10 %)	0.3 to 15,000 Hz	0.3 to 15,000 Hz	
Resonant Frequency	≥ 50 kHz	≥ 50 kHz	
Broadband Resolution (1 to 10,000 Hz)	0.0005 g rms	0.005 m/s² rms	[1]
Non-Linearity	≤ 1 %	≤ 1 %	[4]
Transverse Sensitivity	≤ 5 %	≤ 5 %	
Environmental			
Overload Limit (Shock)	± 5000 g pk	± 49,000 m/s² pk	
Temperature Range (Operating)	-65 to +250 °F	-54 to +121 °C	
Temperature Response	See Graph	See Graph	[1][3]
Base Strain Sensitivity	0.003 g/με	0.029 (m/s²)/με	[1]
Electrical			
Excitation Voltage	18 to 30 VDC	18 to 30 VDC	
Constant Current Excitation	2 to 20 mA	2 to 20 mA	
Output Impedance	≤ 100 ohm	≤ 100 ohm	
Output Bias Voltage	7 to 12 VDC	7 to 12 VDC	
Discharge Time Constant	1.0 to 2.5 sec	1.0 to 2.5 sec	
Settling Time (within 10% of bias)	<10 sec	<10 sec	
Spectral Noise (1 Hz)	110 μg/√Hz	1080 (μm/s²)/√Hz	[1]
Spectral Noise (10 Hz)	25 μg/√Hz	245 (μm/s²)/√Hz	[1]
Spectral Noise (100 Hz)	8 μg/√Hz	78 (μm/s²)/√Hz	[1]
Spectral Noise (1 kHz)	4 μg/√Hz	39 (μm/s²)/√Hz	[1]
Physical			
Sensing Element	Ceramic	Ceramic	
Sensing Geometry	Shear	Shear	
Housing Material	Titanium	Titanium	
Sealing	Hermetic	Hermetic	
Size (Hex x Height)	0.44 in x 0.88 in	11.2 mm x 22.4 mm	
Weight	0.20 oz	5.8 gm	[1]
Electrical Connector	10-32 Coaxial Jack	10-32 Coaxial Jack	
Electrical Connection Position	Top	Top	
Mounting Thread	10-32 Female	10-32 Female	
Mounting Torque	10 to 20 in-lb	113 to 226 N-cm	

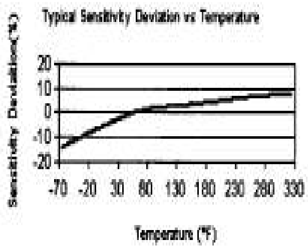

CE [5]

All specifications are at room temperature unless otherwise specified.
In the interest of constant product improvement, we reserve the right to change specifications without notice.

ICP® is a registered trademark of PCB Group, Inc.

OPTIONAL VERSIONS

Optional versions have identical specifications and accessories as listed for the standard model except where noted below. More than one option may be used.

HT - High temperature, extends normal operation temperatures [3]

Excitation Voltage	22 to 30 VDC	22 to 30 VDC	
Frequency Range (± 5 %)	5 to 10,000 Hz	5 to 10,000 Hz	
Frequency Range (± 10 %)	3 to 15,000 Hz	3 to 15,000 Hz	
Temperature Range (Operating)	-65 to +325 °F	-54 to +163 °C	
Discharge Time Constant	0.1 to 0.3 sec	0.1 to 0.3 sec	
Spectral Noise (1 Hz)	200 μg/√Hz	1962 (μm/s²)/√Hz	[1]
Spectral Noise (10 Hz)	30 μg/√Hz	294 (μm/s²)/√Hz	[1]
Output Bias Voltage	10 to 15 VDC	10 to 15 VDC	[2]

Supplied Accessory : Model ACS-68 Single Axis Amplitude Response Calibration from 5 Hz to upper 5% plotted on dB scale replaces Model ACS-1

J - Ground Isolated

Frequency Range (5 %)	9 kHz	9 kHz
Frequency Range (10 %)	14 kHz	14 kHz
Resonant Frequency	≥ 40 kHz	≥ 40 kHz
Electrical Isolation (Base)	>10⁸ ohm	>10⁸ ohm
Size - Hex x Height	0.44 in x 0.93 in	11.2 mm x 23.6 mm
Weight	0.21 oz	6.0 gm

T - TEDS Capable of Digital Memory and Communication Compliant with IEEE P1451.4
TLA - TEDS LMS International - Free Format
TLB - TEDS LMS International - Automotive Format
TLC - TEDS LMS International - Aeronautical Format

Excitation Voltage	20 to 30 VDC	20 to 30 VDC
Temperature Range (Memory Access)	-10 to +250 °F	-23 to +121 °C
Output Bias Voltage	7.5 to 13 VDC	7.5 to 13 VDC

TLD - TEDS Capable of Digital Memory and Communication Compliant with IEEE 1451.4

Excitation Voltage	20 to 30 VDC	20 to 30 VDC
Output Bias Voltage	7.5 to 13 VDC	7.5 to 13 VDC
Temperature Range (Memory Access)	-10 to +250 °F	-23 to +121 °C

W - Water Resistant Cable

Electrical Connector	Sealed Integral Cable
Electrical Connection Position	Top

NOTES:
[1] Typical.
[2] TEDS option adds 1.0 VDC to bias voltage.
[3] 250° F to 325° F data valid with HT option only.
[4] Zero-based, least-squares, straight line method.
[5] See PCB Declaration of Conformance PS023 for details.

SUPPLIED ACCESSORIES:
Model 080A Adhesive Mounting Base (1)
Model 080A109 Petro Wax (1)
Model 081B05 Mounting Stud (10-32 to 10-32) (1)
Model ACS-1 NIST traceable frequency response (10 Hz to upper 5% point).
Model M081B05 Mounting Stud 10-32 to M6 X 0.75 (1)

Entered: [signature]	Engineer: [signature]	Sales: [signature]	Approved: [signature]	Spec Number:
Date: 11/09/06	Date: 11/9/06	Date: 11/9/6	Date: 11/9/6	16921

PCB PIEZOTRONICS
VIBRATION DIVISION
3425 Walden Avenue, Depew, NY 14043
Phone: 716-684-0001
Fax: 716-685-3886
E-Mail: vibration@pcb.com

degree of interchangeability; a major advantage when used in multiples forming arrays and matrices.

The low cost of the 40PH is a key consideration when setting up measurements requiring a multiplicity of concurrent transient and spatial data.

Calibrating the 40PH with a G.R.A.S. pistonphone, e.g. G.R.A.S. 42AA, is as straight forward as calibrating any other G.R.A.S. 1/4-inch microphone.

All G.R.A.S. microphones are individually checked and calibrated before leaving the factory. An individual calibration chart is supplied with each microphone.

Specifications

Frequency range (±1 dB)	Hz	50 to 5 k
Frequency range (±2 dB)	Hz	5k to 20 k
Frequency range (±3 dB)	Hz	10 to 50
Dynamic range lower limit (microphone thermal noise)	dB(A)	< 32
Dynamic range upper limit	dB	135
Set sensitivity @ 250 Hz (±2 dB)	mV/Pa	50
Power supply (Constant Current Power)	mA	2 to 20
Microphone venting		Front
Output impedance	Ω	< 50
Temperature range, operation	°C / °F	-10 to 50 / -50 to 122
Temperature range, storage	°C / °F	-40 to 85 / -40 to 185
Influence of axial vibration @1 m/s²	dB re 20 µPa	50
TEDS UTID (IEEE 1451.4)		27 v. 1.0
Connector type		SMB
CE/RoHS compliant/WEEE registered		Yes / Yes / Yes
Weight	g / oz	5.50 / 0.20

Headquarters Skovlytoften 33 • DK-2840 Holte • Denmark • Tel: +45 45 66 40 46 • Fax: +45 45 66 40 47 • E-mail: gras@gras.dk • www.gras.dk

Figure 3. AC Cutoff Frequency Response

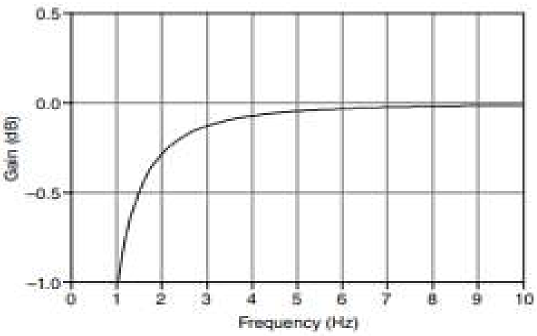

Input range	±5 V
AC voltage full-scale range	
Minimum	±5 Vpk
Typical	±5.1 Vpk
Maximum	±5.2 Vpk
Common-mode voltage range (AI- to earth ground)	±2 V maximum
IEPE excitation current (software-selectable on/off)	
Minimum	2.0 mA
Typical	2.1 mA
Power-on glitch	90 µA for 10 µs
IEPE compliance voltage	19 V maximum

If you are using an IEPE sensor, use the following equation to make sure your configuration meets the IEPE compliance voltage range.

$(V_{common\text{-}mode} + V_{bias} \pm V_{full\text{-}scale})$ must be 0 to 19

Where

$V_{common\text{-}mode}$ is the common-mode voltage applied to the NI 9234

V_{bias} is the bias voltage of the IEPE sensor

$V_{full\text{-}scale}$ is the full-scale voltage of the IEPE sensor

Overvoltage protection (with respect to chassis ground)	
For a signal source connected to AI+ and AI-	±30 V
For a low-impedance source connected to AI+ and AI-	-6 V to 30 V
Input delay	$(40 + 5/512)/f_s + 2.6$ µs

Table 1. Accuracy

Measurement Conditions		Percent of Reading (Gain Error)	Percent of Range[2] (Offset Error)
Calibrated	Maximum (-40 °C to 70 °C)	0.34%, ±0.03 dB	±0.14%, 7.1 mV
	Typical (25 °C ±5 °C)	0.05%, ±0.005 dB	±0.006%, 0.3 mV
Uncalibrated[3]	Maximum (-40 °C to 70 °C)	1.9%, ±0.16 dB	±0.27%, 13.9 mV
	Typical (25 °C ±5 °C)	0.48%, ±0.04 dB	±0.04%, 2.3 mV

Phase nonlinearity (f_s = 51.2 kS/s)	±0.45° maximum
Stopband	
Frequency	0.55 * f_s
Rejection	100 dB
Alias-free bandwidth	0.45 * f_s
Oversample rate	64 * f_s
Crosstalk (1 kHz)	-110 dB
CMRR (f_{in} ≤ 1 kHz)	
Minimum	40 dB
Typical	47 dB
SFDR (f_{in} = 1 kHz, -60 dBFS)	120 dB

Table 2. Idle Channel Noise and Noise Density

Idle Channel	51.2 kS/s	25.6 kS/s	2.048 kS/s
Noise	97 dBFS	99 dBFS	103 dBFS
	50 μVrms	40 μVrms	25 μVrms
Noise density	310 nV/√Hz	350 nV/√Hz	780 nV/√Hz

Input impedance	
Differential	305 kΩ
AI- (shield) to chassis ground	50 Ω

Table 3. Total Harmonic Distortion (THD)

Input Amplitude	1 kHz	8 kHz
-1 dBFS	-95 dB	-87 dB
-20 dBFS	-95 dB	-80 dB

Intermodulation distortion (-1 dBFS)	
DIN 250 Hz/8 kHz 4:1 amplitude ratio	-80 dB
CCIF 11 kHz/12 kHz 1:1 amplitude ratio	-93 dB
MTBF	390,362 hours at 25 °C; Bellcore Issue 2, Method 1, Case 3, Limited Part Stress Method
Gain drift	
Typical	0.14 mdB/°C (16 ppm/°C)
Maximum	0.45 mdB/°C (52 ppm/°C)
Offset drift	
Typical	19.2 μV/°C
Maximum	118 μV/°C
Channel-to-channel matching	
Phase (f_{in} in kHz)	(f_{in} * 0.045° + 0.04 maximum)
Gain	
Typical	0.01 dB
Maximum	0.04 dB
Passband	
Frequency	0.45 * f_s
Flatness (f_s = 51.2 kS/s)	40 mdB (pk-to-pk maximum)

[2] Range = 5.1 Vpk

[3] Uncalibrated accuracy refers to the accuracy achieved when acquiring in raw or unscaled modes where the calibration constants stored in the module are not applied to the data.

Power Requirements

Power consumption from chassis	
Active mode	900 mW maximum
Sleep mode	25 μW maximum
Thermal dissipation (at 70 °C)	
Active mode	930 mW maximum
Sleep mode	25 μW maximum

Physical Characteristics

If you need to clean the module, wipe it with a dry towel.

Weight	173 g (6.1 oz)

Safety Voltages

Connect only voltages that are within the following limits:

Channel-to-earth ground	±30 V maximum, Measurement Category I
Isolation	
Channel-to-channel	None
Channel-to-earth ground	None

Measurement Category I is for measurements performed on circuits not directly connected to the electrical distribution system referred to as *MAINS* voltage. MAINS is a hazardous live electrical supply system that powers equipment. This category is for measurements of voltages from specially protected secondary circuits. Such voltage measurements include signal levels, special equipment, limited-energy parts of equipment, circuits powered by regulated low-voltage sources, and electronics.

⚠ **Caution** Do not connect the NI 9234 to signals or use for measurements within Measurement Categories II, III, or IV.

Hazardous Locations

U.S. (UL)	Class I, Division 2, Groups A, B, C, D, T4; Class I, Zone 2, AEx nA IIC T4
Canada (C-UL)	Class I, Division 2, Groups A, B, C, D, T4; Class I, Zone 2, Ex nA IIC T4
Europe (ATEX) and International (IECEx)	Ex nA IIC T4 Gc

NI USB-9162 SPECEFICATION

Portable Bus-Powered USB Carrier for NI C Series I/O Modules

The following specifications are typical for the range 0 to 60 °C unless otherwise noted.

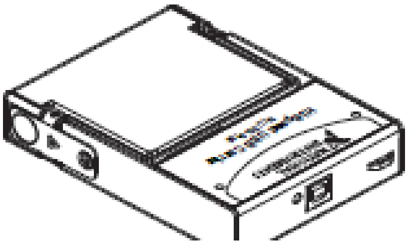

Figure 1. NI USB-9162 and C Series I/O Module

Power Requirements

Caution The protection provided by the NI USB-9162 carrier can be impaired if it is used in a manner not described in this document.

Current consumption from USB .... 500 mA, max

Suspend mode .... 2.5 mA, max

Bus Interface

USB specification .... USB 2.0 Hi-Speed

Physical Characteristics

Weight .... 101 g (3.5 oz)

Dimensions .... 114.6 mm × 85.7 mm × 25.1 mm (4.51 in. × 3.37 in. × 0.99 in.)

If you need to clean the module, wipe it with a dry towel.

Safety Voltages

Connect only voltages that are within these limits.

Isolation

- Channel-to-channel
  - Continuous .... 250 VAC, Measurement Category II
  - Withstand .... 1500 VAC, verified by a 5 s dielectric withstand test
- Channel-to-earth ground
  - Continuous .... 250 VAC, Measurement Category II
  - Withstand .... 3000 VAC, verified by a 5 s dielectric withstand test

Measurement Category II is for measurements performed on circuits directly connected to the electrical distribution system. This category refers to local-level electrical distribution, such as that provided by a standard wall outlet, for example, 115 V for U.S. or 230 V for Europe. Do *not* connect the NI USB-9162 to signals or use for measurements within Measurement Categories III or IV.

Environmental

Operating temperature
(IEC 60068-2-1, IEC 60068-2-2)......................0 to 60 °C

Storage temperature
(IEC 60068-2-1, IEC 60068-2-2)......................-40 to 85 °C

Operating humidity (IEC 60068-2-56) ....10 to 90% RH, noncondensing

Storage humidity (IEC 60068-2-56) ....5 to 95% RH, noncondensing

Maximum altitude..2,000 m

Pollution Degree (IEC 60664) 2

Indoor use only.

Hazardous Locations

The NI USB-9162 is not certified for use in hazardous locations.

Safety

This product is designed to meet the requirements of the following standards of safety for electrical equipment for measurement, control, and laboratory use:

- IEC 61010-1, EN 61010-1
- UL 61010-1, CSA 61010-1

Note For UL and other safety certifications, refer to the product label or the *Online Product Certification* section.

Electromagnetic Compatibility

This product meets the requirements of the following EMC standards for electrical equipment for measurement, control, and laboratory use:

- EN 61326-1 (IEC 61326-1): Class A emissions; Basic immunity
- EN 55011 (CISPR 11): Group 1, Class A emissions
- AS/NZS CISPR 11: Group 1, Class A emissions
- FCC 47 CFR Part 15B: Class A emissions
- ICES-001: Class A emissions

Note In the United States (per FCC 47 CFR), Class A equipment is intended for use in commercial, light-industrial, and heavy-industrial locations. In Europe, Canada, Australia and New Zealand (per CISPR 11) Class A equipment is intended for use only in heavy-industrial locations.

Note Group 1 equipment (per CISPR 11) is any industrial, scientific, or medical equipment that does not intentionally generate radio frequency energy for the treatment of material or inspection/analysis purposes.

PowerFlex® 4M AC Drive

Allen-Bradley

Cost Effective Motor Control in a Compact Package

Providing powerful motor speed control in a compact, space saving design, the Allen-Bradley® PowerFlex 4M AC drive is the smallest and most cost effective member of the PowerFlex family of drives.

- Power ratings of 0.2...11 kW / 0.25...15 Hp at 120V, 240V and 480V to meet a wide range of applications
- Volts per hertz and slip compensation to meet application demands
- Help reduce energy costs and mechanical wear and tear
- An integral RS485/DSI port supports multi-drive networking
- A wide range of communication option cards including DeviceNet™, EtherNet/IP™, ControlNet™, PROFIBUS™ DP, BACnet®, LonWorks® and Bluetooth® adapters
- Flexible, time-saving installation using DIN rail mounting with A and B frame drives
- Feed-through wiring for simple retrofitting into applications requiring variable speed motor control
- Side-by-side mounting in ambient temperatures up to 40°C (104°F), saving valuable panel space
- Drives operate in ambient temperatures from -10°C (14°F) to 50°C (122°F)

When your application requires a compact drive ideal for machine level speed control, take advantage of the PowerFlex 4M AC drive. PowerFlex 4M AC drives provide the application versatility to meet the demands of global OEMs and end users who require space savings and flexibility with DIN rail mounting, feed-through wiring and ease of programming.

Flexible Installation

PowerFlex 4M AC drives offer flexible, time-saving installation using DIN rail mounting with A and B frame drives. PowerFlex 4M AC drives can be stacked side-by-side in ambient temperatures up to 40°C (104°F), saving valuable panel space. These drives operate in ambient temperatures up to 50°C (122°F) with minimal spacing between drives. Feed-through wiring provides simple variable speed motor control with minimal installation and retrofitting time.

Ease of Configuration

Connected Components Workbench™ software can help you get your drives up and running with an intuitive interface and startup wizards. This free software uses Rockwell Automation and Microsoft® Visual Studio® technologies for fast and easy drive configuration. Connected Components Workbench software can help minimize your machine design and development time and is ideal for standalone applications.

LISTEN. THINK. SOLVE.

Allen-Bradley · Rockwell Software

Rockwell Automation

Specifications

Power Ratings	100 - 120V: 0.2...1.1 kW / 0.25...1.5 Hp 200 - 240V: 0.2...7.5 kW / 0.25...10 Hp 380 - 480V: 0.4...11 kW / 0.5...15 Hp	
Motor Control	Volts per hertz	Slip compensation
Application	Open loop speed regulation	
Overload Capability	Heavy duty application: 150% for 60 seconds, 200% for 3 sec	
Input Specifications	1 phase voltage: 100 … 120V/200 … 240V 3 phase voltage: 200 … 240V/380 … 480V Frequency: 50 to 60 Hz Voltage: adjustable 0V to rated motor voltage; -10% / +10% voltage tolerance Logic control ride through: >0.5 seconds, 2 seconds typical Maximum short circuit rating: 100,000 amps symmetrical	
Output Voltage Range	Adjustable 0V to rated motor voltage	Intermittent current: 150% for 60 seconds, 200% for 3 secs
Frequency Range	Max output frequency 400 Hz	Input frequency variation 47 to 63 Hz
Ambient Operating Temperatures	-10 °C to 50 °C (-14 °F to 122 °F)	
Altitude	1000 m (3280 ft)	
Enclosures	IP20 NEMA/Open IP30 NEMA/UL Type 1 (with conduit kit)	
Mounting	DIN rail (frames A and B) Zero Stacking (side-by-side mounting) 120 mm (4.7 in) air-flow gap at the top and bottom	
Configuration	Integral keypad with a 4-digit display Local potentiometer Connected Components Workbench software	10 additional LED indicators Studio 5000 Logix Designer™ application
Control I/O	5 digital inputs (24V DC, 2 programmable) 1 analog input (unipolar voltage or current) 1 relay (form C)	
Dynamic Braking	Internal IGBT – Available only in 5.5...7.5kW/7.5...15 Hp drives (C Frame)	
Carrier Frequency	2 to 10 kHz. 4 kHz default	
EMC Filtering	Embedded 1 ph 240V and 3 ph 480V. Available as an external option for all voltages	
Communications	Integral RS485 with Modbus RTU/DSI Optional: DeviceNet, LonWorks, Bluetooth, EtherNet/IP, PROFIBUS DP, ControlNet, BACnet (Optional networks for use only with external DSI communications kit)	
Protection	Fault history log	
Standards	UL C-Tick RoHS CE cUL KCC	
Control Features	Flying start V/F ratio Bus regulator Process PID Multi-drive connectivity (requires communication option card) 4 preset speeds	
Accessories	NEMA/UL Type 1 kits Line reactors Dynamic brake resistors for 5.5 to 7.5 kW/7.5 to 15 Hp drive ratings	EMC line filters DSI cable accessories/HIMs
Dimensions	A Frame: 174 (6.85) H x 72 (2.83) W x 136 (5.35) D B Frame: 174 (6.85) H x 100 (3.94) W x 136 (5.35) D C Frame: 260 (10.24) H x 130 (5.12) W x 180 (7.09) D	

www.rockwellautomation.com

Power, Control and Information Solutions Headquarters
Americas: Rockwell Automation, 1201 South Second Street, Milwaukee, WI 53204-2496 USA, Tel: (1) 414.382.2000, Fax: (1) 414.382.4444
Europe/Middle East/Africa: Rockwell Automation NV, Pegasus Park, De Kleetlaan 12a, 1831 Diegem, Belgium, Tel: (32) 2 663 0600, Fax: (32) 2 663 0640
Asia Pacific: Rockwell Automation, Level 14, Core F, Cyberport 3, 100 Cyberport Road, Hong Kong, Tel: (852) 2887 4788, Fax: (852) 2508 1846

Publication [illegible] - August 2013
[illegible]